THE CHEMISTRY OF NEW CYCLIC PHOSPHORUS(III) LIGANDS

By

Allen Tobin Ekubo

A Doctoral Thesis submitted in partial fulfilment of the requirements for the award of

Doctor of Philosophy

Loughborough University

2009

Department of Chemistry

ABSTRACT

A range of new aniline derivatives of tetrakis(hydroxymethyl)phosphonium chloride represented as $[P(CH_2NHR)_4]Cl$, where R = phenyl or a substituted phenyl group were synthesised by reacting tetrakis(hydroxymethyl)phosphonium chloride with different aniline precursors in EtOH. Similarly, new phenylenediamine derivatives of tetrakis(hydroxymethyl)phosphonium chloride $[P\{(CH_2NH)_2R\}_2]Cl$, [R = C_6H_4, C_6H_3Me, C_6H_3COPh, $C_6H_2C_4H_4$] were synthesised by reacting tetrakis(hydroxymethyl)phosphonium chloride with phenylenediamine precursors. Selected aniline derivatives of tetrakis(hydroxymethyl)phosphonium chloride were reacted with triethylamine in acetone at room temperature to give the corresponding diazaphosphorinane ligands cyclo-$\{CH_2N(R)CH_2N(R)CH_2\text{-}P\}\text{-}CH_2N(H)R$, where R = phenyl or a substituted phenyl group. Some of the diazaphosphorinane ligands were reacted with Ru(II), Rh(III), Ir(III), Pd(II) and Pt(II) precursors to form new transition metal complexes.

New tertiary phosphine ammonium chlorides, [cyclo-$\{CH_2N(R')CH_2N(R')CH_2\text{-}P\}\text{-}CH_2N(H_2)R']^+Cl^-$, [R' = $C_6H_5CH_2$, 4-$FC_6H_4CH_2$, 4-$ClC_6H_4CH_2$, 4-$MeC_6H_4CH_2$, 4-$MeOC_6H_4CH_2$] were synthesised by reacting benzylamine precursors with tetrakis(hydroxymethyl)phosphonium chloride in ethanol. A range of new tertiary phosphine ammonium salts were also prepared by anion metathesis of four of the chlorides with $Na[BPh_4]$, $Na[SbF_6]$ or $K[PF_6]$ in methanol at room temperature under aerobic conditions to give the corresponding colourless tertiary phosphine ammonium salts in high yields: [cyclo-$\{CH_2N(R')CH_2N(R')CH_2\text{-}P\}\text{-}CH_2N(H_2)R']^+X^-$, [R' = $C_6H_5CH_2$, 4-$FC_6H_4CH_2$, 4-$ClC_6H_4CH_2$, 4-$MeC_6H_4CH_2$; X = BPh_4, SbF_6, PF_6]. Selected tertiary phosphine ammonium salts were reacted with Ru(II), Rh(I), Rh(III), Ir(III), Pd(II), Pt(II) and Au(I) precursors to form the corresponding transition metal complexes. Novel Pd(II) and Pt(II) Zwitterionic dimers have also been structurally characterised.

The phosphonium salts, diazaphosphorinane ligands, tertiary phosphine ammonium salts and metal complexes were characterised by a combination of conventional techniques: MS, microanalysis, FT–IR, NMR [^1H and $^{31}P\{^1H\}$], and in several cases by single crystal X-ray crystallography. The tertiary phosphine ammonium salts were shown to be charged variants of the well-known 1,3,5-triaza-7-phosphaadamantane ligand and their metal complexes were found to have similar stereoelectronic properties to those of analogous complexes with 1,3,5-triaza-7-phosphaadamantane.

DEDICATION

To my dear wife, Lucky and our beloved children, Timi, Womotimi, Iyenimi, Ayibaifie and Ebiemi.

ACKNOWLEDGEMENTS

I would like to thank the Niger Delta University and the Bayelsa State Government of Nigeria, for the Award of a Study Fellowship and funding. I am also grateful to the Department of Chemistry, Loughborough University for the Laboratory facilities used in this research.

I wish to use this medium to express my profound gratitude to my supervisors- Drs M. B. Smith, S. E. Dann and P. F. Kelly for their thorough guidance and supervision throughout the period of this work. I am especially indebted to Dr M. B. Smith who has painstakingly led me through this research. His moral support, supervision and teaching, group meetings, constructive criticisms and corrections made the research very interesting and encouraging. I am also grateful to Dr Mark R. J. Elsegood, Andrew Lake and Noelia Sanchez-Ballester for all their time and help with completing the X-ray crystal structures. My thanks also go to Professors J. C. Buseri and W-A. L. Izonfuo both of the Niger Delta University, Nigeria for their support and encouragement throughout the period of my research.

My sincere thanks also go to the technicians especially Mrs Pauline King as well as my colleagues and friends in the Inorganic Research Laboratories especially, Gavin, Andrew, Paul, Anna, Noelia, Amy, John, Olga, Rob, Leanne, Lee, Chris, Jenna and Rafal for useful discussions. I would also like to thank my friends, Evans Osaisai for sorting out my computer questions as well as Cornelius Odigi and Nizoloman Odual for lively jokes. The moral support from my relations and well-wishers especially, Ala, Ayibatari, Dickson, Bies, Ebakumo, Elizabeth, Innocent, Loveday, Simon, Patrick, Kontei, Famous, Festus, Atoru, Paulinah, Macaulay, Diseimokumo, Kimisuotei, Samuel, Miebi, Bara, Adi, John, Jackson, Amos, Diepreye, Temi, Ibiba, Onoriode, Fanny, Thulani and all others who spurred me through phone calls and E-mails, is also gratefully acknowledged. I would also like to thank my cousin, Dr Franklin E. Osaisai for his enormous support and encouragement. I thank the Pastors and entire congregation of God's Vineyard Church, Loughborough, especially Pastor Akin Oluwole and family for their support and prayers.

Finally, I am indebted to my wife, children and mother for their patience and encouragement throughout the period of my stay in Loughborough.

TABLE OF CONTENTS

LIST OF FIGURES

LIST OF TABLES

SYMBOLS AND ABBREVIATIONS

Acac	Acetylacetonate
Ar	Aryl
bp	boiling point
BP	British Petroleum
Butyl	Butyl
COD	Cycloocta-1,5-diene
Cp	Cyclopentadienyl, C_5H_5
Cp*	pentamethylcyclopentadienyl, C_5Me_5
Cy	Cyclohexyl
δ	chemical shift (NMR)
DCM	Dichloromethane
dmba	N,C-chelating 2-(dimethylaminomethyl)phenyl
DMF	Dimethylformamide
DMSO	Dimethylsulfoxide
ESMS	Electrospray mass spectrometry
Et	Ethyl
FAB-MS	Fast atomic bombardment mass spectrometry
FT-IR	Fourier transform infrared spectroscopy
h	hours
HPLC	High Performance Liquid Chromatography
Hz	Hertz
i	iso
IR	Infrared spectroscopy
LSI-MS	Liquid secondary ionisation mass spectrometry
m-	Meta
m	medium
Me	Methyl
Min	minutes
MS	Mass Spectrometry
n	normal
NMP	*N*-methylpyrrolidone
NMR	Nuclear Magnetic Resonance

o-	Ortho
OAc	Acetate
OTf	Triflate, $CF_3SO_3^-$
OTs	Tosylate, *p*-CH_3–C_6H_4–SO_3^-
p-	Para
Ph	Phenyl
ppm	parts per million
Pr	Propyl
PR_3	Phosphine
PTA	1,3,5-Triaza-7-phosphaadamantane
s	strong
THF	Tetrahydrofuran
THP	Tris(hydroxymethyl)phosphine
THPC	Tetrakis(hydroxymethyl)phosphonium chloride
THPS	Tetrakis(hydroxymethyl)phosphonium sulfate
THT	Tetrahydrothiophene
TMEDA	Tetramethylethylenediamine
TMS	Tetramethylsilane, $(CH_3)_4Si$
ν	stretching frequency (cm^{-1})
vs	very strong
w	weak

CHAPTER ONE

1.0 INTRODUCTION

The design and development of new ligands and or transition metal complexes for specific purposes is of immense importance in the fields of organometallic and coordination chemistry. Organometallic complexes which were originally defined as metal complexes with one or more metal-carbon bonds nowadays include metal complexes with ligands such as phosphines, hydrides and amines. Transition metal complexes are useful in organic synthesis, catalysis,[1] and medicine (as therapeutic and diagnostic agents)[2] among other uses.

The concern for the environment has led to the rise of "green chemistry", and the concept of *atom economy* the purpose of which is to minimise the production of chemical waste in industry and commerce by using catalysts rather than stoichiometric reagents in chemical transformations. This has led to the development of many organotransition metal complexes as catalysts. For example in the rhodium catalyst-based Monsanto Process as well as the new and more efficient iridium-based Cativa™ Process by BP Chemicals for the production of acetic acid, by the carbonylation of methanol, atom economy is achieved where CH_3OH and CO are converted to CH_3COOH with no loss of atoms.[3] In all the synthetic protocols for transition metal complexes, the trend is to be guided by the '12 Principles of Green Chemistry',[4] because of environmental concerns.

The application of organotransition metal complexes as homogeneous catalysts for the synthesis and production of multifunctional, more complex molecules such as agrochemicals and pharmaceuticals is of importance in the field of organometallic chemistry. Areas where the application of homogeneous catalysts has proven fruitful for the synthesis of relatively complex fine chemicals include enantioselective catalysis, C–C coupling and carbonylation reactions. Although homogeneous catalysis has the advantage of high reactivity and high selectivity, it has the problem of separation (purity of the products), recovery and regeneration of the catalysts. In small scale synthesis these problems are solved by purification using chromatography accompanied by the loss of the catalyst, but for synthesis of industrial interest the cost of the catalyst materials are of importance. In addition to the separation problems, homogeneous catalysts usually suffer from deactivation, thus there is increasing desire to heterogenise homogeneous catalysts

to improve recovery and recyclability. In this context, the immobilisation of cationic ligands on solid supports with cation exchange sites, amongst other alternatives is an attractive strategy.[5]

1.1 PHOSPHONIUM SALTS

Phosphonium salts can be regarded as derived from the tetrahedral phosphonium (PH_4^+) ion and can be represented as shown in Figure 1.1. The simplest and best established phosphonium salts are the tetraalkylphosphonium halides, $R_4P^+X^-$ where X = halide or another anionic group. These are colourless salt-like solids with fairly high melting points which are soluble in water and stable to oxidation.

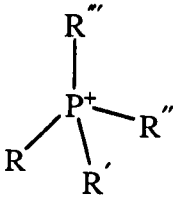

Figure 1.1 Phosphonium ion, where R, R′, R″, R‴ = halogen, alkyl, aryl, H, etc.

Several methods of preparing phosphonium salts are known,[6] for example phosphonium salts can be prepared from tertiary phosphines by reacting with the appropriate organic halide under anhydrous conditions (Equation 1.1).[6]

$$MeI + Me_3P \longrightarrow [Me_4P]^+I^-$$

Equation 1.1.

Recently Rao *et al.*[7] have found a general method of preparing 2-(N-disubstituted amino)ethyltriphenyphosphonium bromides by reacting $[MeOCH_2CH_2PPh_3]Br$ with secondary amines (R_2NH) under aqueous conditions.

Uziel *et al.*[8] have found a short and convenient "one pot" procedure to prepare chiral and achiral phosphonium salts from the relatively easily handled phosphine borane adducts. This involves reacting phosphine borane adduct with an alkyl (or aryl) halide in the presence of an olefin under mild conditions (Equation 1.2). This is a decomplexation-quaternisation reaction that proceeds with retention of configuration at the P centre. This

is an alternative protocol for the synthesis of optically active quaternary phosphonium salts usually prepared by resolution of the racemic form.

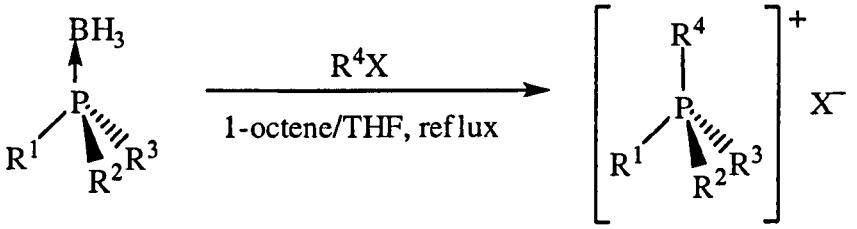

Where R^1, R^2, R^3, R^4 = alkyl, aryl

Equation 1.2

Phosphonium salts show a much wider range of reactions than the corresponding tetraalkylammonium salts. This might be attributed to the larger size of the phosphorus atom, compared to the nitrogen, and the participation of *d*-orbitals or σ* orbitals in the bonding to phosphorus.[6,9]

With alkalis, phosphonium halides are first converted to hydroxides which then undergo hydrolysis to phosphine oxide and hydrocarbon (Equation 1.3).[6]

$$[Et_4P]^+I^- + NaOH \longrightarrow [Et_4P]^+OH^- \longrightarrow Et_3PO + EtH + NaI$$

Equation 1.3

Acylphosphonium salts are hydrolysed to phosphine oxides and aldehydes (Equation 1.4),[6] while tetrakis(hydroxymethyl)phosphonium chloride (THPC) gives tris(hydroxymethyl)phosphine oxide and hydrogen (Equations 1.5).[6]

$$[R_3PC(O)R]X + NaOH \longrightarrow R_3PO + RCHO + NaX$$

Equation 1.4

$$[P(CH_2OH)_4]Cl + NaOH \longrightarrow (HOCH_2)_3PO + H_2 + HCHO + NaCl$$

Equation 1.5

Phosphonium salts are usually stable to oxidation, but can be reduced electrolytically or by lithium aluminium hydride to phosphines. Alkyl phosphonium halides are

decomposed on strong heating to give tertiary phosphines, while phosphonium hydroxides easily give phosphine oxide and hydrocarbon.[6]

Double decomposition or metathesis reactions can be used to change the anion of phosphonium salts if one of the products is insoluble in a second solvent (Equation 1.6).[6]

$$[PPh_4]Cl + KNO_3 \longrightarrow KCl + [PPh_4]NO_3$$

Equation 1.6

The hydroxyl groups in phosphonium salts can be removed by condensation reactions leading to other useful products (Equation 1.7).[6]

$$[P(CH_2OH)_4]Cl + 4RNH_2 \longrightarrow [P(CH_2NHR)_4]Cl + 4H_2O$$

Equation 1.7

For example Frank *et al.*[10] reported the reaction of THPC with aniline which gave a well-defined crystalline phosphonium salt as an aniline derivative of THPC which subsequently reacts with Et_3N or NH_3 to give potential phosphorus(III) ligands as shown in Scheme 1.1. Aniline reacts readily with THPC in ethanol at room temperature, displacing all four hydroxyl groups to form $[P(CH_2NHPh)_4]Cl$.

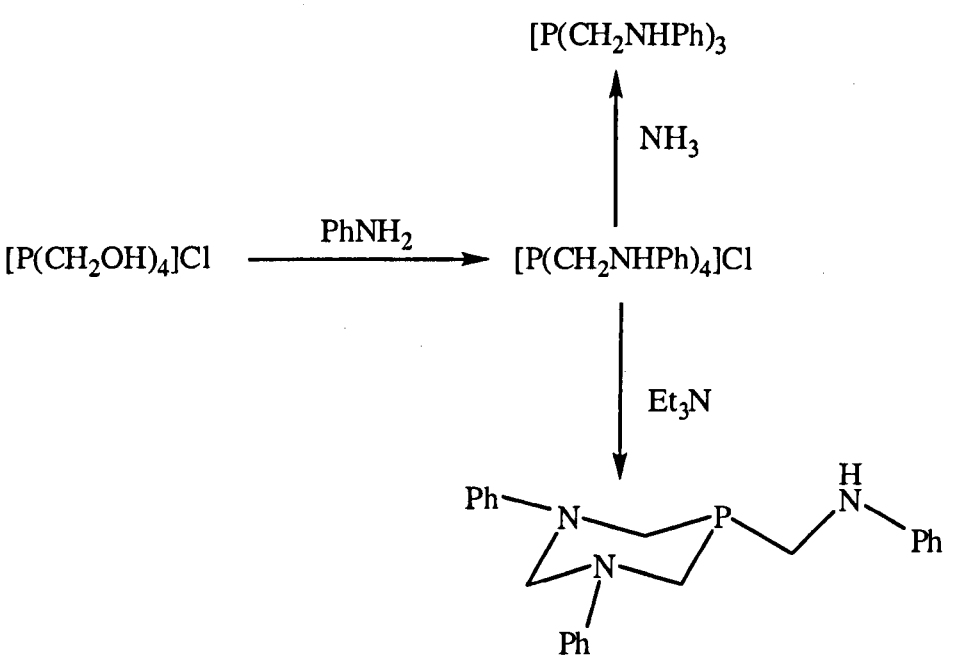

Scheme 1.1

When NH_3 was bubbled into a slurry of $[P(CH_2NHPh)_4]Cl$ in acetone, ammonium chloride was formed as a finely divided white precipitate. The ammonium chloride was filtered off and the resulting pale yellow oil on work-up gave a white crystalline solid, $P(CH_2NHPh)_3$.

When stirred with a slight excess of triethylamine for 1 h at room temperature, $[P(CH_2NHPh)_4]Cl$ gave triethylamine hydrochloride as a solid which was filtered off. The filtrate was concentrated under reduced pressure and upon stiring with absolute ethanol gave a white crystalline solid cyclo-$\{CH_2N(Ph)CH_2N(Ph)CH_2\text{-}P\}\text{-}CH_2N(H)Ph$. The product contains a diazaphosphorinane ring (six-membered P–C–N–C–N–C ring) and an aminomethyl group evidently formed by displacement of aniline and HCl from $[P(CH_2NHPh)_4]Cl$, perhaps *via* an intramolecular mechanism shown in Scheme 1.2.[10] This is a useful reaction for the synthesis of cyclic phosphorus(III) ligands as will be indicated in Chapters Two and Three.

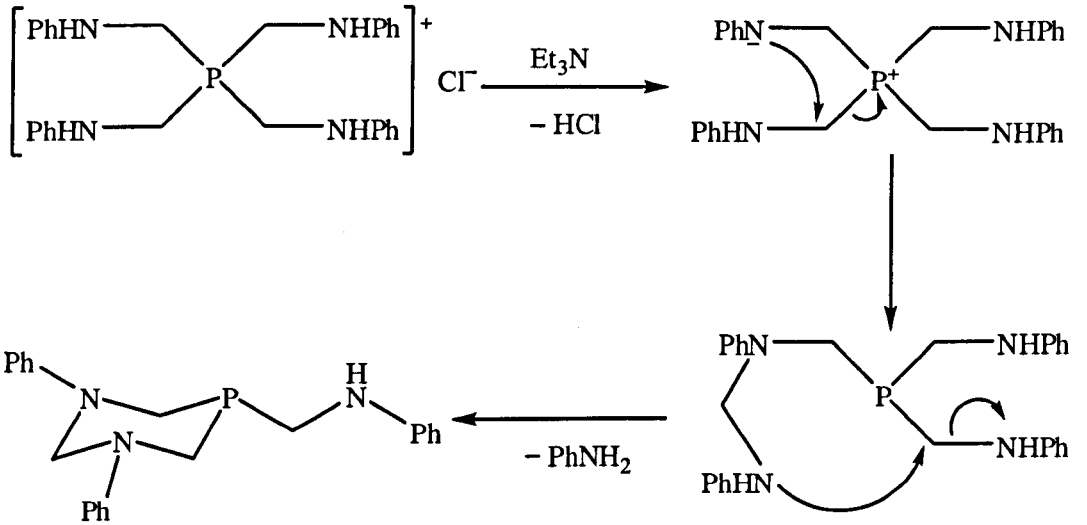

Scheme 1.2

Apart from the formation of a diazaphosphorinane ring, $[P(CH_2NHPh)_4]Cl$ has been reported to form a novel biphosphetidine, **1** consisting of two four-membered P–C–N–C rings linked together through a P–P bond by disproportionation in ethanol.[11]

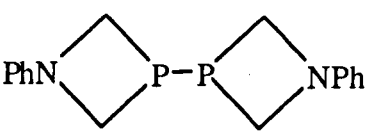

1

The transformation of cyclo-{$CH_2N(R)CH_2N(R)CH_2$-P}-$CH_2N(H)R$, R = 4-MeC_6H_4, which is an analogue of cyclo-{$CH_2N(Ph)CH_2N(Ph)CH_2$-P}-$CH_2N(H)Ph$ mentioned previously, by electrochemical oxidation at a mercury electrode into a new diphosphine ligand and its coordination chemistry with Pt(II), Pd(II) and Hg(II) have been reported (Equations 1.8a and 1.8b).[12]

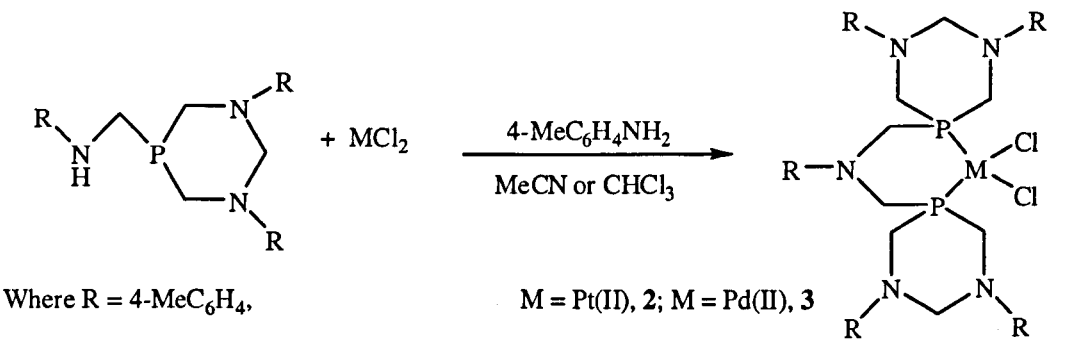

Where R = 4-MeC_6H_4, M = Pt(II), **2**; M = Pd(II), **3**

Equation 1.8a

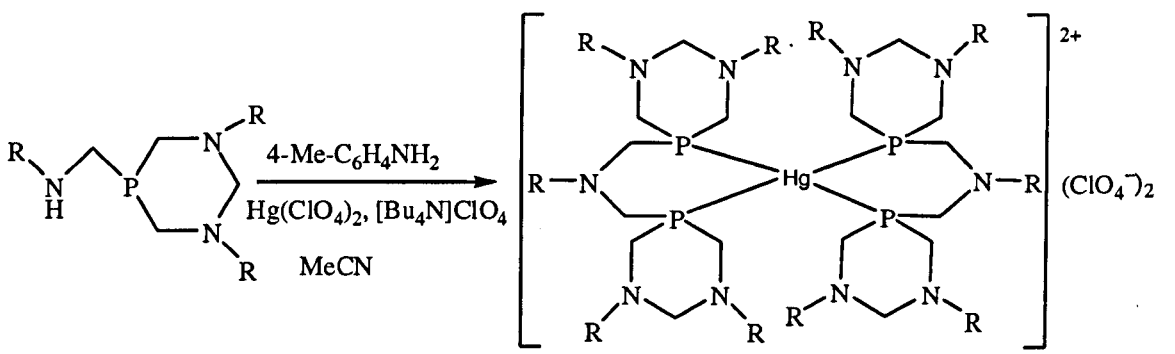

Where R = 4-MeC_6H_4 **4**

Equation 1.8b

Similarly, the transformation of cyclo-{$CH_2N(R)CH_2N(R)CH_2$-P}-$CH_2N(H)R$, R = 4-MeC_6H_4 by electrochemical oxidation at a glassy carbon electrode, resulted in the new unusual organophosphorus compounds **5** and **6** (Equation 1.9).[13]

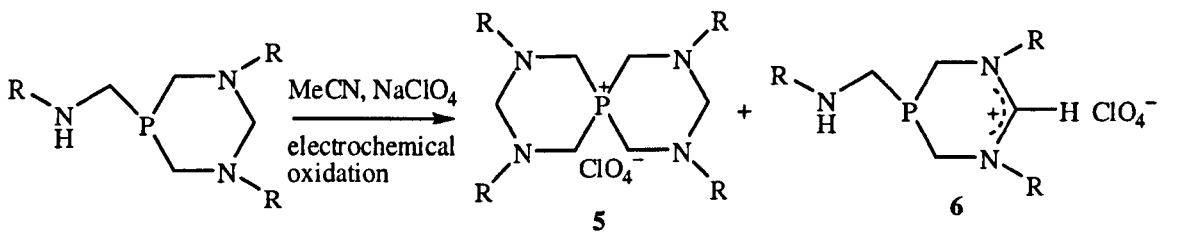

5 **6**

Where R = 4-MeC_6H_4

Equation 1.9

Compound **6** has been shown to have a carbocation between the two N atoms in the ring.[13] Reaction of **6** with $PtCl_2(COD)$ gave a complex **7**, incorporating a new six-membered diphosphine ligand (Equation1.10).[13]

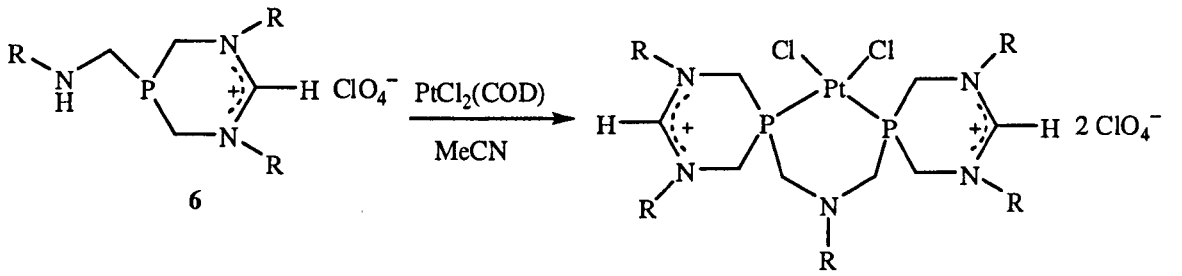

Where R = 4-MeC_6H_4

6 **7**

Equation 1.10

The synthesis of new cyclic phosphorus(III) ligands from THPC and their coordinaion chemistry are discussed in Chapters Two and Three.

Phosphonium halides can be reduced to phosphines by some metals and metal phosphides (Equations 1.11 and 1.12),[6] and phosphoranes can be formed when some aromatic phosphonium salts react with organometallic compounds (Equation 1.13),[6] while others may form ylides (Equation 1.14).[6]

$$[PR_4]X + 2Na \longrightarrow R_3P + RNa + NaX$$

Equation 1.11

$$[PPh_4]Cl + Ph_2PNa \longrightarrow 2Ph_3P + NaCl$$

Equation 1.12

$$[PPh_4]Cl + PhLi \longrightarrow PPh_5 + LiCl$$

Equation 1.13

$$[Ph_3PMe]Br + MeLi \longrightarrow Ph_3P{=}CH_2 + LiBr + CH_4$$

Equation 1.14

Phosphonium salts are useful as a source of ylides for the synthesis of alkenes,[6] they are also precursors for the synthesis of phosphines. Reduction of phosphonium salts is one of the methods used in the preparation of phosphines. The use of simple palladium salts such as $PdCl_2$ or $Pd(OAc)_2$ in the presence of tetraphenylphosphonium salts, $[Ph_4P]X$, (X

= Cl, Br, I) as a new catalyst system for the Heck reaction of unreactive aryl halides has been reported. This resulted in unexpectedly high catalytic activities.[14] Similarly, Teiwari *et al.*[15] have reported a novel catalytic system using alkyl-di-(1-adamantyl)phosphonium salts as practical ligand precursors for the palladium-catalysed amination (C-N bond formation) of aryl chlorides. For example, these salts can be prepared *via* alkylation of di-(1-adamantyl)phosphines (Figure 1.2) with alkyl or benzyl halides.

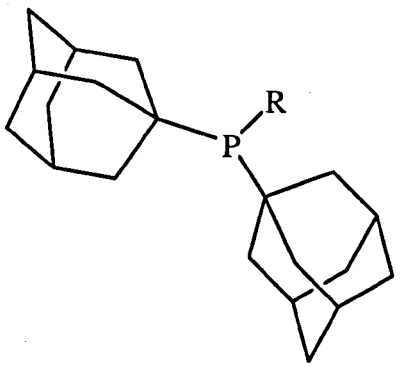

R = *n*-butyl, **8**; R = *i*-butyl, **9**;

R = methyl, **10**; R = allyl, **11**;

R = 2-methoxyethyl, **12**; R = benzyl, **13**

Figure 1.2 Selected examples of alkyl-di-(1-adamantyl)phosphines.

Phosphonium salts are also now being used as ionic liquids,[16] although tetraalkylphosphonium salts have long been used as phase transfer catalysts.[17] One of the most important benefits of using an ionic liquid in catalysis as solvents is that it allows recyclable use of the catalyst. Karodia *et al.*[18] have investigated the application of phosphonium tosylates as ionic solvents for Diels-Alder reactions, whilst Gerristsma *et al.*[19] have shown that judicious choice of phosphonium salt ionic liquids provide an economical recyclable media for the Heck reaction. This class of ionic solvent has been successfully utilised in catalytic hydroformylation reactions[20] and hydrogen transfer reactions[21] as well as co-catalyst for the Baylis-Hillman reaction.[22] Phosphonium salts are also useful as insecticides and fungicides.[6] Phosphonium salts also find use as anti-static[6] and softening agents for textiles, as corrosion inhibitors[6] and as photographic chemicals.[6] The use of tetraarylphosphonium salts as soluble supports for the synthesis of small molecules has also been reported.[23] The use of the commercially available THPC and the analogous THPS, $[P(CH_2OH)_4]_2SO_4$ and related compounds as flame retardants is also well known.[6]

It has been established that phosphonium salts of double long-chain type exhibit superior antibacterial activity to their quaternary ammonium analogues.[24] They are thus excellent

cationic biocides. This might be due to the fact that the phosphorus cations have strong interaction and high affinity with bacteria, since there are many phosphoric acid derivatives present in tissues such as the cytoplasmic membrane of bacterial cells. In the past few years, many cationic phosphonium salts have been synthesised and shown to possess anticancer activity, but the mechanism in the anticancer process has remained unclear.[25–28] Recently, Xie *et al.*[25] have synthesised hexadecyltriphenylphosphonium bromide and demonstrated that it is an anticancer therapeutic reagent and the anticancer activity is related to its interaction with DNA.

Another area where phosphonium salts have been put to use is organocatalysis. Organocatalysis is currently being vigorously pursued because of its attractive features such as metal-free conditions, experimental simplicity and the ease by which organocatalysts can be recovered. Wang *et al.*[29] have demonstrated that benzyltriphenylphosphonium chloride is a highly effective organocatalyst to promote the cyanosilylation of a wide variety of unconjugated and conjugated, acylic and cyclic ketones. This protocol not only presents a new organocatalytic synthesis of cyanohydrin silyl ethers, but also adds a synthetically useful entry into the catalysis with phosphonium salts.

Phosphonium salts have also been used as chemosensors.[30,31] A ditriphenylphosphonium calix[4]arene derivative has been demonstrated as a novel receptor for anions by anion complexation.[30] Similarly, Yeo *et al.*[31] have synthesised a novel phosphonium derivative of naphthalene by the reaction of 1,8-dibromomethylnaphthalene with triphenylphosphine which showed a distinct colour change when treated with fluoride ions. Receptor compounds for fluoride ions are known but reports on selective naked eye chemosensors for fluoride ions are scarce. This is the first report of a colorimetric chemosensor based on phosphonium ions.

1.1.1 TETRAKIS(HYDROXYMETHYL)PHOSPHONIUM CHLORIDE

Tetrakis(hydroxymethyl)phosphonium chloride (THPC), Figure 1.3, is a white crystalline phosphonium salt, usually marketed in concentrated aqueous solutions at approximately 80% by weight.

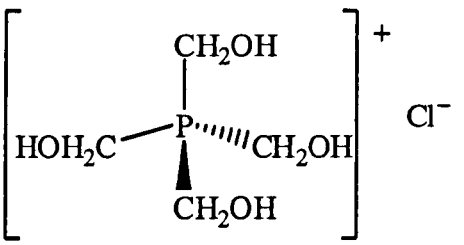

14

Figure 1.3 Tetrakis(hydroxymethyl)phosphonium chloride (THPC).

It has a relative molecular weight of 190.56 and the molecular formula is $C_4H_{12}O_4PCl$. It is hygroscopic and a useful material for making important organophosphorus compounds such as $P(CH_2OH)_3$, tris(hydroxymethyl)phosphine, (THP).[32]

THPC is made by reacting phosphine, formaldehyde and hydrogen chloride (Equation 1.15).

$$PH_3 + 4HCHO + HCl \longrightarrow [P(CH_2OH)_4]Cl$$

Equation 1.15

Without hydrogen chloride, the water soluble phosphine, THP is formed (Equation 1.16).

$$PH_3 + 3HCHO \longrightarrow P(CH_2OH)_3$$

Equation 1.16

THPC is a hydroxyalkyl-containing organophosphorus compound of industrial interest. It is used as a flame retardant,[10] and bleaching and brightness-stabilising agent for mechanical and chemical pulps.[33] THPC is a precursor to notable water-soluble phosphine ligands such as THP[32,33] and 1,3,5-triaza-7-phosphaadamantane (PTA).[32,34,35]

1.1.2 TETRAKIS(HYDROXYMETHYL)PHOSPHONIUM SULFATE

Like the analogous THPC, tetrakis(hydroxymethyl)phosphonium sulfate (THPS) is of industrial significance and marketed in concentrated solutions at approximately 75% by weight and is mainly used as a biocide. The relative molecular mass of THPS is 406.28 and has a chemical formula of $C_8H_{24}O_{12}P_2S$. THPS is produced by reacting phosphine, formaldehyde and sulfuric acid, (Equation 1.17).

$$2PH_3 + 8HCHO + H_2SO_4 \longrightarrow [P(CH_2OH)_4]_2SO_4$$

Equation 1.17

Jeffery *et al.*[36] were able to explain how $[P(CH_2OH)_4]_2SO_4$ aids the dissolution of FeS by proposing the self assembly of $[P(CH_2OH)_4]_2SO_4$ and $[Fe(NH_4)_2(SO_4)_2]$ in the presence of NaOH, forming a red novel water-soluble iron(II) macrocyclic phosphine complex, $[Fe(H_2O)_2\{RP(CH_2N(CH_2PR_2)CH_2)_2PR\}]SO_4$ as shown in Equation 1.18.

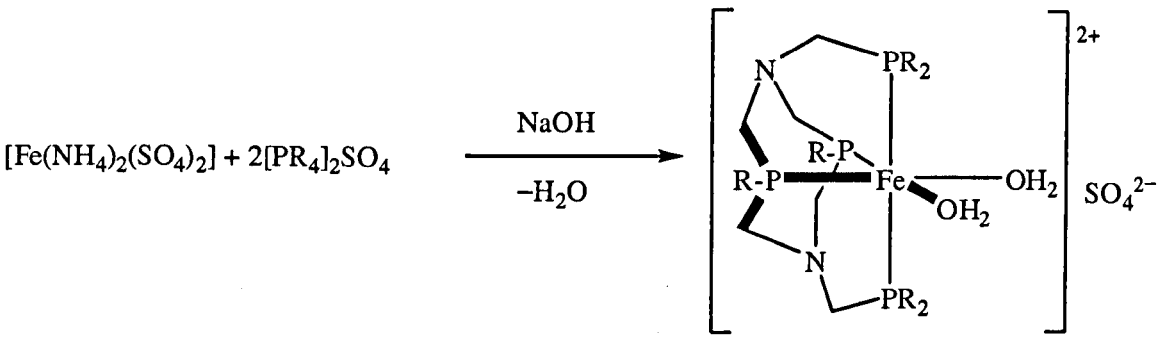

15

Where R = CH_2OH

Equation 1.18

The crystallographic structure of this complex reveals a cationic octahedral Fe(II) complex with a remarkable tetradentate phosphine ligand in which alternating phosphorus and nitrogen atoms are linked by CH_2 spacers to form an eight-membered macrocyclic ring which functions as a *cis* bound tetradentate phosphine donor to iron. The presence of the nitrogen atoms enhances water solubility due to hydrogen-bonding interactions with water.

Whilst the original intention was not to prepare new water-soluble catalysts, the novel tetradentate macrocyclic phosphine ligand has obvious potential in this context because it imposes facial octahedral coordination leaving two *cis* sites free for potential catalytic transformations.[36] Thus such complexes are potential water-soluble catalysts and might also be good materials for waste clean-up procedures, since such self assembled ligands strongly bind to transition metals.

1.2 PHOSPHINE LIGANDS

Phosphine ligands have the general formula PR_3 where R = alkyl, aryl, H, halide etc. Phosphite ligands are closely related to phosphines and have the general formula $P(OR)_3$. Both phosphines and phosphites are neutral two electron donors. Phosphines are

classified as primary, secondary and tertiary depending on the number of organic groups - PR_3 (tertiary), PHR_2 (secondary) and PH_2R (primary).

The chemistry of phosphorus(III) compounds are centred on the lone pair of electrons and its availability for forming new bonds to phosphorus. Structurally, phosphines are different from their nitrogen congeners- the amines. Both phosphines and amines have pyramidal geometry as would be expected, but whereas pyramidal inversion is rapid in amines at room temperature, it is sometimes slow in phosphines, therefore predominantly they have fixed pyramidal structures.[6]

Important methods used in the preparation of phosphines have been given by McAuliffe,[37] Gilheany and Mitchell[38] and Quin.[39] The main methods used are: *via* organometallic reagents and halophosphines, nucleophilic substitutions using metal phosphides, or reduction of phosphonium salts or tertiary phosphine oxides. The preparation of these ligands usually involve an inert atmosphere as the majority of phosphines are air and moisture sensitive, although some are neither air nor moisture sensitive, hence prepared under aerobic conditions which is an added advantage to be chosen as a potential candidate in coordination chemistry, catalysis, and medical applications. A variety of chiral phosphine transition metal complexes have been synthesised, these phosphine-metal complexes are stereogenic and function as stereospecific catalysts in enantioselective catalysis.[40–42]

1.2.1 METAL COMPLEXES

The bonding in metal complexes basically involves the donation of electron pairs from a ligand to a metal atom or ion to form a coordination compound. Important uses of metal complexes are in the field of catalysis and medicine among others. Phosphorus compounds like the phosphines are among the most useful ligands in the coordination chemistry of metals. When the donor strengths are considered, phosphorus is one of the strongest coordinating atoms and also has multiple coordination numbers (1 to 6) and valencies 3 and 5 hence its coordination patterns with metals can be modified, unlike carbon. Carbon monoxide and cyanide are the strongest but they cannot be modified and so the next strongest modifiable phosphorus ligands become most important. Phosphorus ligands can form strong bonds with transition metals in low oxidation states. This is very useful in the area of catalysis and many metal complexes of phosphorus ligands like the

phosphines are used as catalysts in industry to produce chemicals in a better way. In the coordination to metals, the phosphorus acts as an electron donor to the metal and takes back some of the electrons through a vacant 3*d*-orbital/a σ* orbital involved in the P–R, bonding of the phosphine[1,3,9] thereby not leaving too much electron density on the metal which may destabilise the complex. In all these cases, the valency and the coordination number of phosphorus are 3 before coordination and become 4 after coordination.

In metal complexes, the central metal as well as the type of ligand determine the reactivity of the complexes *i.e.* the ability to react with substrate molecules and eventually the capability to catalyse chemical transformations.

While there are many species that serve as useful homogeneous catalysts (*e.g.* H^+, OH^-, Al^{3+} etc), complexes of transition metals are the most suited due to the following reasons.[1] Firstly, various ligands will bind to transition metals; almost any molecule with a lone pair of electrons can coordinate to a specific centre as ligands; upon coordination the reactivity of the functional groups may change dramatically. Ligands may either be directly involved in the catalytic process or indirectly affect catalysis by exerting steric and / or electronic effects on the complex.[1] Secondly, transition metals have the ability to bind ligands in a number of ways. The availability of *d*- as well as *s*- and *p*-orbitals on the metal allows for the formation of σ and π bonds from metal to ligands.[1] Carbonyl ligands attach to a metal in a terminal or bridging bonding mode. Groups such as methyl or hydride may be considered to be anionic, neutral (radical), or cationic depending on the electron density of the metal. The strength of metal–ligand bonds is moderate (126–335 kJ/mole), allowing bonds to form or break relatively easily. This is a requirement for the catalytic cycle to proceed.[1] Thirdly, transition metals have a variety of oxidation states. When ligands are added to or removed from the metal by oxidative addition and reductive elimination processes, the oxidation state of the metal changes. The *d*-valence electrons of these metals usually have a rather large number of oxidation states available as compared to main group metals.[1] The elements in Groups 9 and 10 especially possess a tendency to form rapid, reversible two-electron change (such as from 18 electron to 16 electron and vice versa), hence are often involved in homogeneous catalysis.[1] Other important characteristics of transition metal complexes include the exhibition of several different geometries, depending on the coordination number. Geometries such as square-planar, octahedral, tetrahedral, square pyramidal and trigonal bipyramidal are common in

transition metal complexes. Knowledge of the behaviour of ligands attached to metals in these geometries is very useful. For example in square planar complexes, a ligand *trans* to another may cause the latter ligand to be quite labile and thus easily dissociates from the metal. If loss of the latter ligand is a requirement for effective catalysis, it is desirable to design the catalytic cycle in such a way that a square-planar complex is one of the intermediates along the path to the product and to have the directing group with high *trans* effect positioned *trans* to the leaving group.[1] Another example might involve a process where a key step is the reductive elimination of two ligands. Reductive elimination requires the two leaving groups to be *cis* with respect to each other before reaction may occur. The catalysis will be successful in this case if an intermediate forms such that the two leaving groups are *cis*. Transition metal complexes are also unique because, with their well-defined geometries, they serve as "templates" for the occurrence of reliable stereospecific or stereoselective ligand interaction.[1] It is known that alkyl migration to a carbonyl group occurs with retention of configuration and that reductive elimination involves retention of configuration in the two leaving groups.Thus transition metal complexes mimic the stereospecific reactions often catalysed by enzymes. Finally, transition metal complexes possess the "correct" stability.[1] By varying metal and ligands, transition metal complexes are readily available to serve as intermediates that are not too unreactive. In order for a catalytic turn over to occur, each intermediate in the cycle must be reactive enough to proceed to the next stage, yet not so reactive that other pathways *e.g.* decomposition or a different bonding mode, become feasible. Thus transition metal complexes are versatile as catalysts.[1,40]

Phosphines are among the most common ancillary ligands used in organometallic chemistry, owing to their ability to stabilise low valent metal oxidation states as well as their capacity to influence both steric and electronic properties of catalytic species. One major advantage of using phosphines as ligands is that they can be easily modified by changing the organic substituents, thus allowing the fine-tuning of the electronic and steric properties of the metal complexes.[34] This is very important in homogeneous catalysis in order to change the activity or selectivity of the catalyst. In addition to these advantages, in homogeneous catalysis where product separation is a problem, solubility in water can be added by modifying the phosphine structure when polar substituents such as hydroxyl or amino functionalities or ionic groups such as sulfonate, carboxylate,

ammonium, etc. are introduced. Such water-soluble phosphines are useful in homogeneous aqueous biphasic catalysis.

The bonding of phosphine ligands, like that of carbonyls comprises of two important components. The primary component is σ-donation of the phosphine lone pair to an empty orbital on the metal. The second component is back donation from a filled metal orbital to an empty orbital on the phosphine ligand (Figure 1.4). There are alternative views regarding the nature of the back-bonding interaction in metal phosphine complexes. The classical back-bonding model is that the empty phosphorus *d*-orbitals are available for overlap with suitable filled metal orbitals (Figure 1.4a). This is to complement the σ-bond resulting from the donation of an electron pair from phosphorus to the metal. A more recent model invokes back-bonding from the metal *d* orbitals into the P–R σ* orbitals (the antibonding orbitals associated with the P–R σ-bonds) as shown in Figure 1.4b. The recent model is preferred because the energy of a σ*-orbital is lower than that of a phosphorus *d*-orbital.[1,3,9]

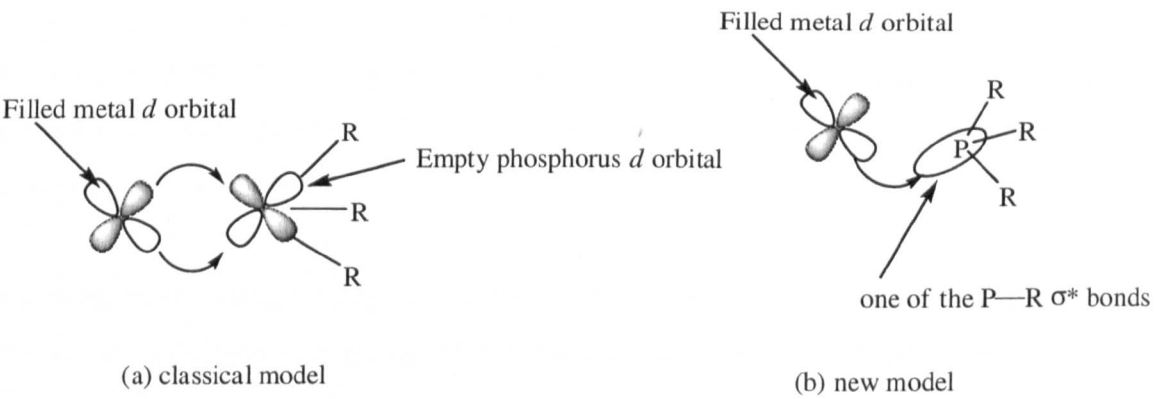

Figure 1.4 Types of back-bonding in metal phosphine complexes.

As electron-withdrawing (electronegative) groups are placed on the phosphorus atom, the σ-donating capacity of the phosphine ligand tends to decrease. At the same time, the energy of the π-acceptor on phosphorus is lowered, providing an increase in back bonding ability. Therefore phosphines can exhibit a wide range of σ-donor and π-acceptor capabilities, and the electronic properties of a metal centre can be tuned by the substitution of electronically different but isosteric phosphines. A rough ordering of the σ-donating and π-accepting capabilities of phosphines can be accomplished by synthesising a series of complexes in which the only difference is the nature of the phosphine ligand. If these complexes contain a carbonyl (CO) ligand *trans* to the

phosphines, then the carbonyl (CO) stretching frequency can be used as an indicator of electron density at the metal because the M→CO back donation is affected (the lower the value of the CO stretching frequency, the greater the σ-bonding to the metal and thus the higher the electron density at the metal). Experiments such as this give the following empirical ordering:[3]

$$PMe_3 \approx P(NR_2)_3 < PPh_3 < P(OMe_3) < P(OPh_3) < PCl_3 < CO \approx PF_3$$

Greater π-acidity →

← Greater σ-donation

An additional factor that is very important in phosphine chemistry is the amount of space occupied by the R group when bonded to a metal. This factor is important in a variety of contexts; for example, the rate at which phosphine dissociates from a metal is related to the amount of space occupied by the phosphine and the resultant crowding around the metal. To describe the steric effects of phosphines and other ligands, Tolman has defind the *cone angle* as the apex angle, θ of a cone that encompasses the van der Waals radii of the outermost atoms of a ligand when bonded to a metal.[43] As might be expected, the presence of bulky ligands can lead to more rapid ligand dissociation as a consequence of crowding around the metal.

As mentioned earlier, an important aspect of organometallic chemistry involves varying the steric and electronic nature of the ligand environment of a complex to promote whatever properties are desired: activity or selectivity in homogeneous catalysis, reversible binding of a ligand, facile decomposition or high stability. A key feature of the PR_3 series of ligands is that electronic effects can be changed without changing steric effects *e.g.* by moving from P^tBu_3 to $P(O^iPr)_3$ or change steric effects without changing electronic effects *e.g.* by moving from PMe_3 to P(*o*-tolyl)$_3$. One result of increasing the ligand electron donor strength for example might be to perturb an oxidative addition/reductive elimination in favour of the oxidative addition product,[44] likewise increasing the steric bulk is expected to favour low coordination number species.[45] The chemistry of a phosphine-containing complex is therefore expected to change with the position of the phosphine in the Tolman map.[43] Other types of ligand have similar possibilities but the situation is best defined for PR_3.

Phosphines are widely used as ligands for transition metals. They promote the solubility of metal complexes in a wide range of organic media. The majority of phosphines are insoluble in water; though water-soluble phosphines such as the sulfonated phenylphosphines and pyridylphosphines are known.[46–48] The property of phosphines to stabilise low oxidation states of metal atoms provides compounds that are useful in homogenous catalysis. Asymmetric or chiral phosphines are designed for stereoselective catalytic reactions.[3,40–42] The Heck reaction, Suzuki, Stille, and Sonogashira are examples of coupling reactions that use phosphine metal complexes as catalysts.[3] Phosphine metal complexes are also useful as catalysts in hydroformylation,[47–49] hydrogenation and hydrocyanation[50] reactions.

Apart from catalysis, metal complexes have also been evaluated extensively for their medicinal properties.[51] Although most new drugs are carbon-based compounds, there is an increasing realisation and understanding of how metal ions are involved in many natural biological processes and some diseases indicate that metal ions have new roles in therapeutic strategies.[2,52] Metal complexes have a wide range of coordination numbers, coordination geometries, thermodynamic and kinetic preferences for ligand atoms and redox activity in some cases. These offer novel mechanisms that are not available to organic compounds. Generally, the nature of the metal ion, its oxidation state and the number and type of bound ligands can all exert a critical influence on the biological activity of a metal complex. An understanding of how these factors affect biological activity is important in the design of metal complexes with specific medicinal properties. For instance the *cis* and *trans* isomers of the diaminedichloroplatinum(II) complex, $PtCl_2(NH_3)_2$ has contrasting biological activities; the *cis* isomer (cisplatin) is an anticancer drug, while the *trans* isomer (transplatin) is inactive against cancer.

Whilst phosphine ligands and their complexes have been studied for many years, there is now an increase in activity to find improvements in ligand design not only for homogeneous catalysis but for site-specific drug delivery. Presently, complexes bearing phosphine ligands are not only candidates for pharmaceutical application, but water-soluble phosphines with potential for stabilising pharmaceutical and radiopharmaceutical complexes *in vivo* with links to targeting biomolecules as diagnostic agents are also under intense study. For example there is considerable interest in the caged, aliphatic tertiary phosphine, 1,3,5-triaza-7-phosphaadamantane (PTA) which has many desirable qualities

including water solubility,[53] in the preparation of metallopharmaceuticals. Ruthenium(II) arene compounds with PTA ligands (RAPTA) have been shown to exhibit a pH-dependent activity, which is conducive to providing excellent pharmacological properties[51] and have been found to exhibit superior anticancer properties compared to the ubiquitous anticancer platinum drugs.[54] In the area of radiopharmaceuticals, bidentate water-soluble phosphines form stable ^{99m}Tc complexes in both biological liquids and targeted tissues. Examples of such radiopharmaceuticals include the commercial drugs ^{99m}Tc-fosfim® and ^{99m}Tc-furifosfim® used for myocardial perfusions.[34]

1.2.2 PHOSPHORINANES

The usefulness of organophosphorus compounds has led to the synthesis of many ring compounds containing phosphorus and carbon.[6] These simulate the well established ring systems, both homocyclic and heterocyclic which are based on carbon, the P–C bond strength confers on them a comparable level of stability.[6] The known ring systems based on saturated carbon and a single phosphorus atom includes the 3-, 4-, 5-, 6-, 7-, 8-membered ring compounds named phosphirane, phosphetane, phospholane, phosphorinane, phosphepane, and phosphocaine respectively (Figure 1.5).[6] Not all phosphorus containing analogues have yet been synthesised, and in many instances only derivatives rather than the parent compounds are known.[6]

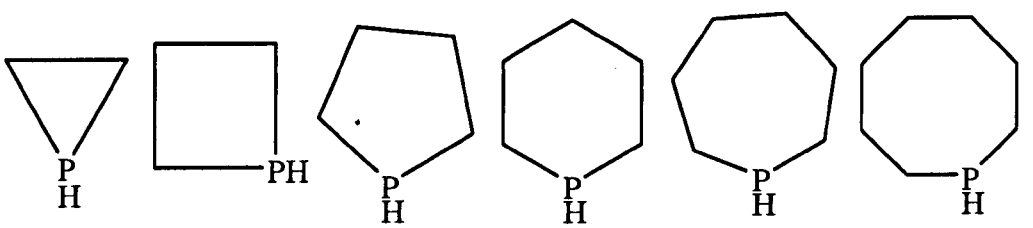

Figure 1.5 Ring compounds with phosphorus and saturated carbon.

Phosphorinanes are known to exist in the chair form.[6] Thus axial or equatorial isomers are possible. Crystallography has confirmed that in several derivatives, the rings are chair-shaped with the exocyclic group attached to phosphorus in the axial position (Figure 1.6).[6]

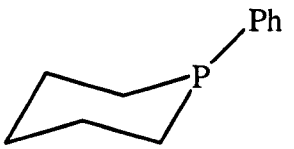

Figure 1.6 Phenylphosphorinane, **16**

These compounds are cyclic tertiary phosphines and several methods of preparation leading to important derivatised phosphorinanes are known.[6] For example, phenylphosphorinane can be made by direct reaction of phenyldilithiophosphine with 1,5-dibromopentane in tetrahydrofuran (THF) or by the action of ultra-violet (uv) radiation on 4-pentenylphenylphosphine (Scheme 1.3). Further derivatisation is achieved when **16** reacts with sulfur in boiling benzene to give the sulfide (**17**) and with methyl iodide to give the phosphonium salt (**18**) as shown in Scheme 1.3.

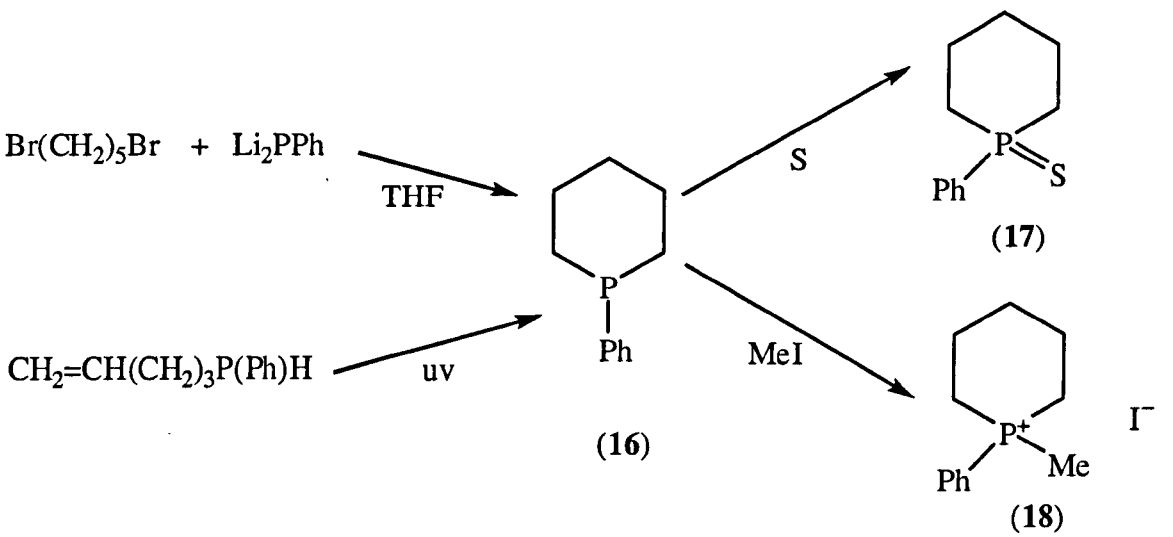

Scheme 1.3

The development of phosphorinanes as ligands and reagents started recently[55] with the synthesis of some phosphorinane-borane complexes by McNulty *et al.*[56] In the derivatised phosphorinanes where the exocyclic group as in compound **16** is an aryl, a trialkylphosphine ligand is formed. Brenstrum *et al.*[55] have demonstrated that such phosphorinanes as a family of trialkylphosphines are suitable ligands for organopalladium chemistry and are comparable in efficacy to other popular ligands such as P^{t}Bu$_3$. They highlighted the ease of generation, economic considerations in the synthesis, and structural modification possibilities all favour the phosphorinanes being regarded as suitable organopalladium cross-coupling ligands. Furthermore, the preparative route where the intermediate phosphorinones allow entry to P-protected 4-

hydroxyphosphorinanes,[56] through hydride reduction, provides structural features that could be used in the immobilisation onto a solid support.[57,58]

1.2.3 AMINOPHOSPHINES

Aminophosphines are tertiary phosphines with phosphorus and amino donor sites they are potential ligands for the formation of polynuclear or heterobimetallic metal clusters or organised assemblies because of the multiple P and N donor sites. They form triangular complexes which are of current interest[59] both for their potential in new stoichiometric and catalytic transformations, due to the ability of adjacent metals to cooperatively[60] activate substrates[61] and their physical properties such as luminescence,[62] magnetic spin-frustration[63–67] and spin-mediated superconductivity.[68] Such cluster compounds are of immense importance in biological systems where clusters of metals can assist in the transfer of electrons[69] to activate relatively inert substrates.[70]

Unfortunately, the design of ligands that can support clusters or assemblies of metals with a variety of transition metals is rarely straightforward. Be this as it may, various workers,[59, 71–73] have synthesised aminophosphines of the type $P(CH_2NHAr^R)_3$, where Ar^R is an aryl substituent.[59] These ligands can simultaneously bind to two metal centres on losing the amino H atoms forming an amido complex. The binding mode of $P(CH_2NAr^R)_3$ to two metal centres (M and M') is illustrated in Figure 1.7.

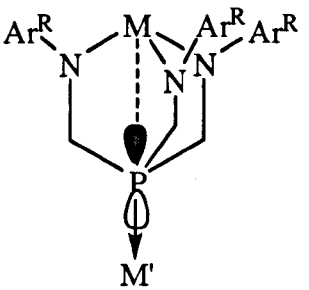

Figure 1.7 Potential bonding mode of $P(CH_2NAr^R)_3$ to two metal centres.

Keen *et al.*[72] synthesised one such ligand by using compounds hitherto tested as flame retardants[10] as ligand precursors. Tris(hydroxymethyl)phosphine, $P(CH_2OH)_3$ was reacted with an excess of 3,5-bis(trifluoromethyl)aniline in toluene forming $P(CH_2NHAr^R)_3$ where R is CF_3, in excellent yield. These ligands on losing the amino H atoms can adopt a conformation where the phosphine and amido lone pairs are arranged approximately parallel and are incapable of all coordinating to the same metal; such a

bonding mode was observed in a nonanuclear Cu(I) amido complex.[72] With a high-oxidation-state transition metal, all the amido donors coordinate to the metal.[74–76] In such a bonding mode, the phosphine ligand cannot bind its lone pair to the metal, coordinated to the amido donors, but is available to coordinate to a second metal. These ligands are thus well suited for the facile synthesis of transition metal heterobimetallic complexes, providing that there is interaction between the two metal centres. Hatnean *et al.*[71] have also shown that triamidophosphine ligands readily assemble trinuclear clusters with divalent Mn and Mg. However, when used with trivalent or higher oxidation state metal centres with three labile ligand sites; these ligands have a tendency to coordinate all three amido donors to a single metal[73] which does not allow for the assembly of complexes with multiple adjacent metal centres. This is shown as complex A in Figure 1.8, while the use of diamidoselenophosphinito ancillary ligand favours the formation of triangular complexes with aluminium as shown in complex B in Figure 1.8 and Scheme 1.4.[59]

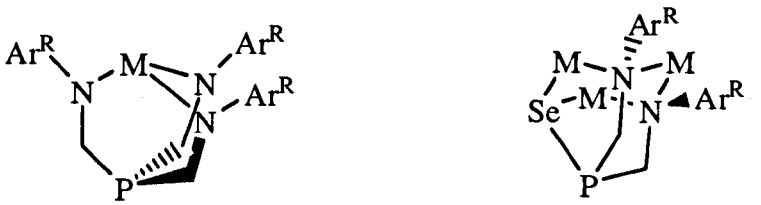

(A) (B)

Figure 1.8 Potential bonding modes of the formally trianionic ligands $P(CH_2NAr^R)_3$ and $Se{=}P(CH_2NAr^R)_2$ to form metal complexes.[59]

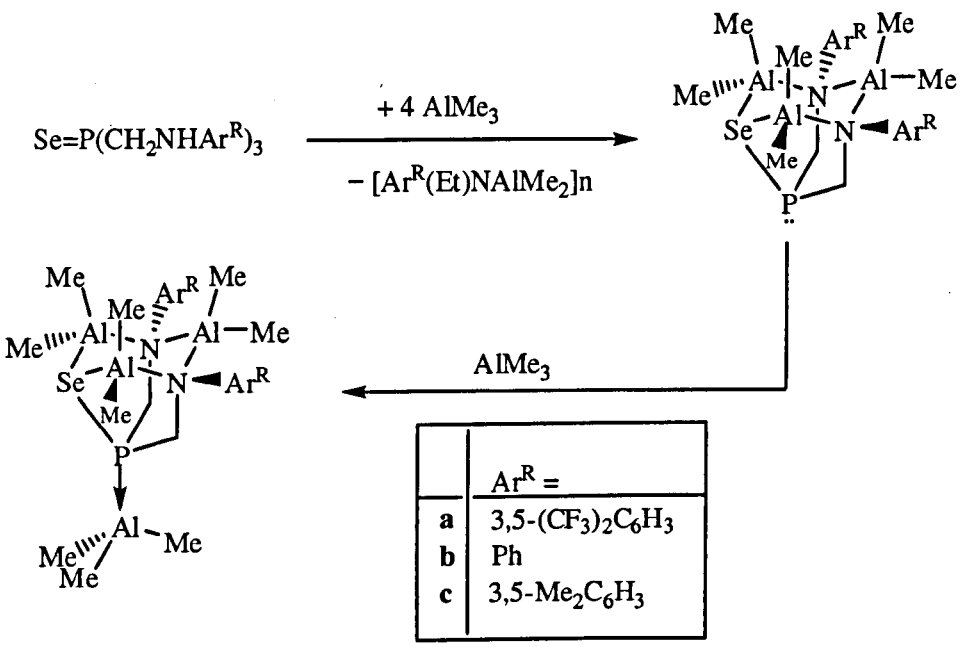

	Ar^R =
a	3,5-$(CF_3)_2C_6H_3$
b	Ph
c	3,5-$Me_2C_6H_3$

Scheme 1.4

To circumvent the above drawback, Han *et al.*[59] investigated selenium donors in polydentate ligand design, because of both the increased polarisability of the heavier chalcogenides, which encourage electronic communication between metal centres, and their propensity to bridge metal centres. Thus these selenium ligands were found to be an improvement on the $P(CH_2NHAr^R)_3$ ligands for the formation of polynuclear clusters of paramagnetic metals, where strong magnetic coupling between metal centres is desired due to increased polarisability of the selenophosphinito donor relative to amido donors.

1.2.4 WATER-SOLUBLE PHOSPHINES

There is an increased interest in the use of water as a solvent in chemical transformations mainly driven by environmental and economic concerns. The utility of water as a solvent, however requires the development of new catalysts or reagents that are stable and soluble in water.[77,78]

Grafting of highly polar functional groups such as $-SO_3^-$, $-CO_2^-$, $-NR_3^+$, $-PR_3^+$, -OH, etc. into phosphines brings about the desired solubility.[79,80] Water-soluble phosphines are used in biphasic catalysis. The most frequently used water-soluble phosphines for catalytic applications are the mono- and trisulfonated triphenylphosphines, TPPMS, TPPTS and the mono and tricarboxylated triphenylphosphines. These ligands have been developed by various workers and put to effective industrial use. For example Kuntz's work on trisulfonated triphenylphosphine (TPPTS),[81] eventually led to the famous Ruhrchemie's commercially successful oxo process.

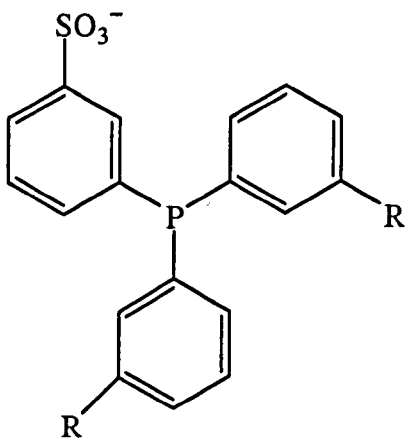

Figure 1.9 Mono- and trisulfonated triphenylphosphines
(R = H, TPPMS; R = SO_3^-, TPPTS).

The structures of TPPMS and TPPTS are shown in Figure 1.9. Certain features make these ligands attractive for synthesising water-soluble metal catalysts for use in homogeneous catalysis. These include their relatively high solubilities in water as well as amphiphilicity among others. For example TPPTS has a very high solubility in water; 1100 g/L compared to its monosulfonated equivalent, TPPMS which has a solubility of 80 g/L in water,[81] and thus gives highly concentrated aqueous solutions. This leads to efficient biphasic catalysis with better phase separation. Secondly the metal complexes of TPPMS, TPPTS and the mono- and tricarboxylated triphenylphoshines are amphiphilic in character due to the presence of hydrophilic sulfonate, carboxylate groups and hydrophobic phenyl groups. This feature allows the complex to transfer readily between the aqueous and organic phases in a biphasic system.

The most important use of water-soluble phosphines is in the area of homogeneous catalysis. Numerous complexes with the metal in low oxidation state widely used in homogeneous catalysis are stabilised by phosphine ligands. The advantages of homogeneous catalysts with respect to reactivity and selectivity are well documented.[40] However; the problems associated with the separation of the products from the catalyst have frequently presented a major economic barrier to commercial applications. Several methods have been used to overcome this problem, usually by thermal operations[82] such as distillation, decomposition, etc, which normally lead to thermal stresses on the catalyst. Similarly use of polymer bound catalysts[83] is prone to polymer degradation and metal leaching.

A good approach to solving this problem is to use water-soluble phosphine ligands that are poorly soluble in the organic media allowing the catalysis to be carried out in a liquid-liquid biphasic system. Catalyst recovery is thus easily achieved by decantation and separation of the two phases. Apart from the simple and complete separation of the product from the catalyst, other advantages of aqueous catalysis among others include the economy and the safety of using the environmentally friendly solvent, water. However, comparing biphasic reaction with their monophasic equivalents, reaction rates are lower in the biphasic systems. This is mainly due to the fact that when the catalyst and substrates are in different phases, interaction between the catalyst and the substrates is lower than in a monophasic system, thus reducing the rate of reactions. The use of thermoregulated phase transfer catalysts have been mentioned.[84] These have an inverse

temperature-dependent solubility in water. For example poly(ethylene oxide) substituted triphenylphosphines (PEOTPPs) combined with the rhodium precursor $Rh(acac)(CO)_2$ have been tested for the two-phase (water/heptane) hydroformylation of higher olefins such as 1-hexene, 1-octene, 1-decene or 1-dodecene for the thermoregulated phase transfer hydroformylation.[84] At room temperature, almost all the Rh-PEOTPP catalyst remains in the aqueous phase. On heating to a temperature higher than the cloud point (C_{pt}), the catalyst precipitates from water and transfers into heptane where it transforms olefins into aldehydes. After hydroformylation is complete and the system is cooled, the catalyst returns to water. Thus, a simple phase separation enables the continuous re-use of the catalyst.

The process of temperature regulated phase transfer catalysis (TRPTC) combines the advantages of both bi- and monophasic catalyses. Furthermore, TRPTC is more 'homogeneous' than aqueous/organic two-phase catalysis, because the substrates and catalyst remain in the same organic phase at the reaction temperature and thus, can provide higher yields than the classical biphasic catalytic reactions.

Apart from the area of catalysis, the hydroxyalkyl containing water-soluble phosphines such as tris(hydroxymethyl)phosphine, THP and related compounds including tetrakis(hydroxymethyl)phosphonium chloride, THPC have attracted much interest in recent times as bleaching agents for pulps[33,85,86] in the paper industry. They are a new class of bleaching and brightness stabilising agents discovered for mechanical and chemical pulps.[33] Studies have shown that the related 1,2-bis[bis(hydroxymethyl)phosphino] ethane {BBHPE; $[(HOCH_2)_2PCH_2]_2$} has a higher bleaching activity than, THP.[87]

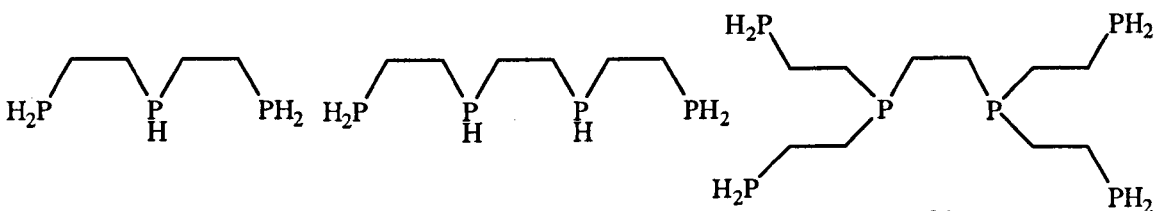

19 **20** **21**

Methods of preparing hydroxymethylphosphorus compounds abound in the literature,[33] for example another method by which THP can be made is by the reaction of phosphine (PH_3) with formaldehyde in the presence of $K_2[PtCl_4]$ as catalyst.[35] New phosphines

$(H_2PCH_2CH_2)_2PH$, $[H_2PCH_2CH_2P(H)CH_2]_2$, and $[(H_2PCH_2CH_2)_2PCH_2]_2$ (**19**, **20** and **21** respectively) have been synthesised by hydrophosphination of diethyl vinylphosphonate with $H_2P(CH_2)_2PH_2$ and converted into the related corresponding water-soluble, tri-, tetra- and hexaphosphonium chlorides by incorporation of hydroxymethyl groups at the P atoms.[33] These are potential bleaching agents like the well known THPC.

Moiseev *et al.*[86] have recently investigated the mechanism of the bleaching action of the (hydroxyalkyl)phosphorus compounds, by reacting tris(3-hydroxypropyl)phosphine, $[(CH_2)_3OH]_3P$ (THPP), with conjugated carbonyl components of lignin likely involved in the bleaching process using various model aromatic aldehydes, and discovered that THPP reduces aromatic aldehydes (ArCHO) to the corresponding alcohols. THPP is also a bleaching agent for pulps and gives cleaner reactions than THP, which is prone to loss of formaldehyde.[85]

The coordination chemistry of THP, though water-soluble and moderately air stable, has not received much attention.[35] The coordination chemistry of THP with Pt, Pd, Ni, Ru, Re and Au have been studied extensively but the first complex with Cu was synthesised not too long ago. A copper(I) complex was obtained from the reaction of THP with $[Cu(CH_3CN)_4]ClO_4$ in acetonitrile.[88] Its complexes with Pt(II) and Pd(II) are water-soluble but similar to analogous PMe_3 or PEt_3 in most respects, whereas its complexes with Ni(0), Pd(0) and Pt(0) have exceptional properties in terms of stability and reactivity.[35] The use of THP for the removal of trace Ru from polymers synthesised by Grubbs-type carbene catalysts has been mentioned,[33] and with related compounds are potential powerful metal sequestering agents and will certainly have a rich coordination chemistry.

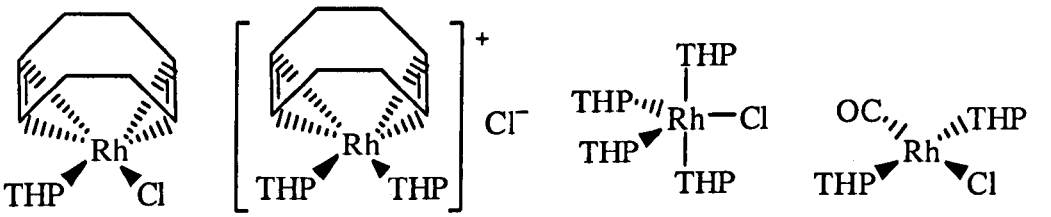

22 **23** **24** **25**

Figure 1.10 Water-soluble THP complexes of rhodium(I).[89]

Four water-soluble Rh^{I}–THP complexes (Figure 1.10) RhCl(1,5-COD)(THP) (**22**), [Rh(1,5-COD)(THP)$_2$]Cl (**23**), RhCl(THP)$_4$ (**24**) and *trans*-RhCl(CO)(THP)$_2$ (**25**) have been synthesised and characterised, the first three are potentially useful entries into Rh(I)THP chemistry while the first and last are the first structurally characterised Rh(I)THP complexes.[89]

Water-soluble phosphines, apart from forming water-soluble transition metal complexes used as catalysts, also form important complexes useful in medicinal chemistry. The clinical usefulness of transition metal complexes binding to DNA as antitumoral drugs has in fact led to a renewed interest in the synthesis of metal complexes that exhibit water solubility and the capacity to link to DNA and other biomolecules due to their potential as anticancer and antimetastasis agents.[90] For example the water-soluble ruthenium(II) arene PTA complexes are now being considered as an alternative to platinum anticancer drugs due to their high hydrosolubility coupled with reduced toxicity. The low toxicity is due to the ability of ruthenium to mimic iron in binding to DNA, exploiting the mechanisms the body has evolved for the non-toxic transport of iron.[90]

1.3 1,3,5-TRIAZA-7-PHOSPHAADAMANTANE (PTA) AND RELATED COMPOUNDS

Apart from the popular water-soluble sulfonated analogues of triphenylphosphine (PPh_3), TPPMS and TPPTS (mentioned in Section 1.2.4), the sulfonated derivatives of bidentate diphosphines and tridentate tripodal as well as cage-like water-soluble phosphines are known.[34] Examples of cage-like water-soluble phosphines include the Verkade-type bases (Figure 1.11) used in a number of organic reactions.[91]

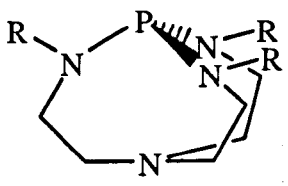

Figure 1.11 Verkade-type base, R = H, alkyl, etc.

In 1974, Daigle *et al.*[53] synthesised another cage adamantane-like water-soluble phosphine, 1,3,5-triaza-7-phosphaadamantane (PTA), Figure 1.12, for the purpose of

creating flame-proof polymers.[34] However, with the recent interest in biphasic homogeneous catalysis, PTA and its derivatives have received renewed interest.[34] In addition to homogeneous catalysis, PTA and its related compounds are also important as co-ligands in biologically active transition metal compounds such as the ruthenium(II) arene complexes due to their cytotoxicity and are excellent ligands for preparing luminescent gold complexes.[34]

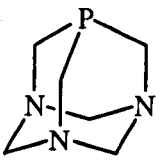

26

Figure 1.12 1,3,5-triaza-7-phosphaadamantane (PTA).

The synthesis of PTA involves the condensation of the highly hygroscopic THP as the source of phosphorus with formaldehyde and hexamethylenetetramine, (HMT) or ammonia,[34] as the source of nitrogen, the final yield being *ca.* 40%.

$$[P(CH_2OH)_4]Cl + NaOH \rightarrow P(CH_2OH)_3 + H_2O + HCHO + NaCl$$

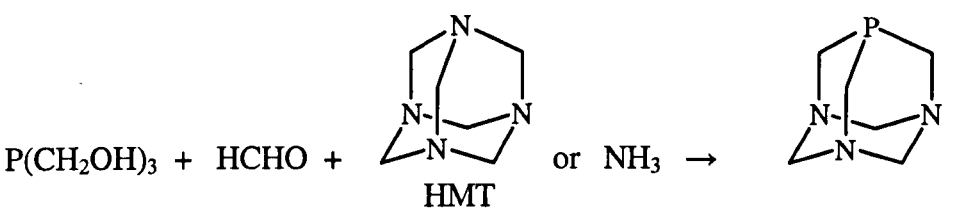

Scheme 1.5

Later research has shown that higher yields are obtained when the THP is generated *in situ* from the reaction of the commercially available and less expensive THPC with NaOH (Scheme 1.5).[32]

PTA is neither air nor moisture sensitive, hence does not require an inert atmosphere for its synthesis. It is thermally stable, with decomposition temperatures higher than 260 °C. PTA is soluble in water (S = 1.5 M, *ca.* 235 g/L), MeOH and EtOH but less soluble in higher alcohols like 2-propanol and 1-butanol and THF at room temperature.[34] The solubility of PTA is enhanced in acidic media due to the formation of its protonated species. For example in 0.1 M HCl its solubility is approximately 350 g/L (S = 2.2 M).[34]

It is also soluble in DMSO, acetone, chloroform, dichloromethane, but not soluble in hydrocarbons like heptane, toluene or benzene.[34]

The high solubility of PTA is due to the extensive participation of its three nitrogen atoms in hydrogen bonding interactions with water molecules.[53,92] The nitrogen atoms with their lone pair of electrons and relatively high electronegativity values (3.0 on the Pauling scale) strategetically placed in the structure interact with the water molecules through intermolecular N···H–O hydrogen bonds. This among other properties has made it a water-soluble ligand amenable for aqueous biphasic catalysis and metal carrier in biological systems. Indeed with respect to other water-soluble phosphines, it has the advantage of air stability and a low steric demand. Furthermore, it binds more strongly to the metal centres than the triphenylsulfonated phosphines mentioned in Section 1.2.4. PTA is a neutral and air-stable molecule which is both sterically (with cone angle = 103°) and electronically comparable with the extremely air sensitive trimethylphosphine.[34]

In terms of reactivity PTA is comparable to other alkylphosphines, with the notable exception that PTA is stable in air, in contrast to PMe_3 and PEt_3 which are both known to ignite violently in air. Furthermore, PTA appears to have higher resistance to oxidation than other water-soluble phosphines such as TPPMS and TPPTS. It is also a known fact that it preferentially coordinates metals through the soft phosphorus centre; the harder amine functionalities are the preferred sites of alkylation and protonation,[34] this can be rationalised using the hard soft acid base (HSAB) theory.[93]

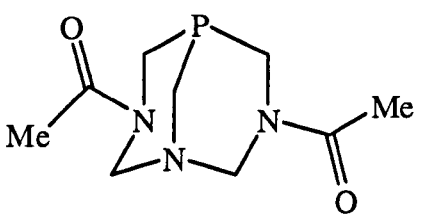

(a) **27**
(DAPTA)

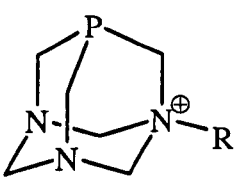

(b) R = Me, **28**; R = Et, **29**;
R = CH_2Ph, **30**; R = $(CH_2)_4I$, **31**

Figure 1.13 DAPTA and other derivatives of PTA.

In order to enhance water solubility and other desirable properties for catalytic and other uses, PTA has been derivatised by the incorporation of certain functionalities resulting in

the formation of new related compounds. The reaction of PTA with acetic anhydride,[94] forms 3,7-diacetyl-1,3,7-triaza-5-phosphabicyclo[3.3.1]nonane (DAPTA) shown in Figure 1.13a. The *N*-alkylation of PTA using MeI, EtI, $PhCH_2Cl$ or $I(CH_2)_4I$ in acetone or methanol under reflux gives the alkyl salts PTA(R), Figure 1.13b. These are air-stable and water-soluble but less soluble in organic solvents than PTA due to their ionic character.[34]

Krogstad *et al.*[95] have synthesised 1-pyridylmethyl-3,5-diaza-1-azonia-7-phosphatricyclo[3.3.1.1]decane bromide [PymePTA]Br and the di-N-formylated analogue of DAPTA, 3,7-diformyl-1,3,7-triaza-5-phosphabicyclo[3.3.1]nonane (DFPTA) by reacting PTA with bromomethylpyridine and formic anhydride respectively. DFPTA is the second acyl derivative of PTA to be synthesised, while [PymePTA]Br is the second derivative of PTA reported that contains an aromatic appendage. These have been fully characterised and their water solubilities explored.[95]

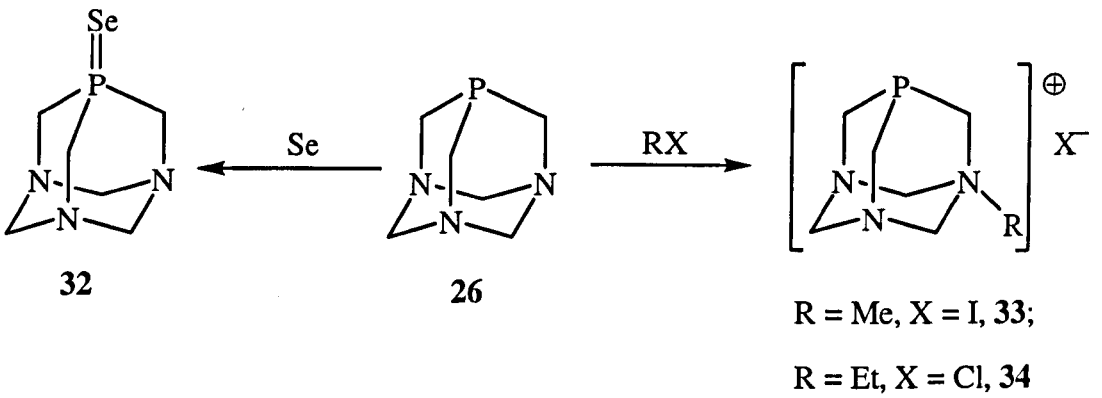

32 **26**

R = Me, X = I, **33**;

R = Et, X = Cl, **34**

Figure 1.14 Some PTA derivation reactions.

Note that such PTA transformations lead to P(III) or P(V) derivatives which maintain the original phosphaadamantane skeleton as shown in Figure 1.14.[34]

Structural modifications of PTA have so far been focussed on either alkylation at P or N atoms,[96–98] or opening of the cage to yield potentially bidentate P,N[99,100] or tridentate P,N,N[101] derivatives of PTA. For example in the comparative structural and reactivity investigation of PTA and its derivative, 2-thia-1,3,5-triaza-7-phosphaadamantane 2,2-dioxide ($PASO_2$), apart from water-insolubility in the case of $PASO_2$, the most striking differences were the products observed for the alkylation reactions with methyl iodide. While it was generally accepted that PTA is only alkylated at one of its three nitrogen

atoms, $PASO_2$ was observed to produce predominantly a phosphonium salt upon alkylation.[98] Most of these changes especially on the "lower rim" (the triazacyclohexane ring) are relatively far from the coordinating P atom and thus unlikely to impart significant stereoelectronic effects on any coordinated metal centre.[102] The stereoelectronic effects are often required for chemo- or enantioselective catalytic applications and for fine-tuning of biological effects in the design of water-soluble metal-based drugs.[102] Therefore, there is an interest in the development of chiral PTA derivatives that are substituted at the methylene groups bridging P and N atoms at the "upper rim" such as **35**.

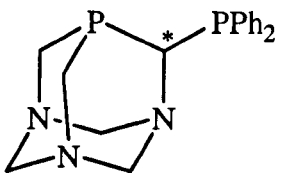

Figure 1.15 Structure of **35**.

Wong *et al.*[103] have synthesised the bidentate phosphine, PTA-PPh_2, **35** with a binding arm and a chiral centre on the α-carbon to phosphorus (Figure 1.15) by reacting PTA with *n*-BuLi and $ClPPh_2$. Although **35**, was not soluble in water and its racemic mixture was not resolved, the protocol has opened a method for the synthesis of a new class of chiral PTA-based ligands. Exploiting the protocol, the synthesis of a novel water-soluble ligand with two chiral centres, *i.e.* phenyl(1,3,5-triaza-7-phosphtricyclo[3.3.1.$1^{3,7}$]dec-6-yl)methanol PZA, **36** together with the corresponding sulfide [PZA(S)], **37** and oxide [PZA(O)], **38** from PTA lithium salt and benzaldehyde has been reported.[102] In a related development, the synthesis and characterisation of a series of novel water-soluble chiral upper-rim PTA derivatives by the addition of PTA-Li to CO_2, ketones and aldehydes has also been reported.[104]

Since its synthesis and characterisation, PTA has been used in a variety of studies, including catalytic biphasic hydrogenation reactions,[105,106] ligand substitution reactions in metal clusters,[107] and enzyme mediated oxygen transfer processes.[108] Among the different PTA transition metal complexes, those of Ru and Rh have attracted a lot of interest as potential catalysts for a variety of processes in aqueous biphasic conditions and have been adjudged superior to other water-soluble transition metal complexes.[19] Similarly,

the well characterised ruthenium(II) arene PTA complexes (RAPTA) have attracted considerable attention, because of their relatively low toxicity,[109] and the DNA damaging properties of (η^6-*p*-cymene)$RuCl_2$(PTA), RAPTA-C, and related analogues have been reported.[110] RAPTA complexes have been evaluated *in vitro* and *in vivo* and have been found to be highly selective towards metastasis.[111] Dorcier and co-workers[51] have reported the *in vitro* evaluation of the rhodium and osmium RAPTA analogues and showed that they are worth considering within the context of organometallic anticancer drugs.[51] Recently, studies on the reactivity of RAPTA-type complexes of ruthenium, rhodium and osmium towards model DNA bases with a view towards determining their relative and preferential binding modes have also been reported.[112]

1.3.1 COORDINATION CHEMISTRY OF PTA

PTA transition metal complexes are relatively uncommon, when compared to other tertiary phosphines in spite of its synthesis and characterisation being reported more than three decades ago. The coordination chemistry of PTA has undergone a remarkable increase in interest in the past decade.[34] The renewed interest has been mainly due not only to the successful utilisation of PTA-organometallic compounds as water-soluble catalysts,[113–115] but also to their use as luminescent complexes[116–118] and promising anticancer agents.[110,119,120] Historically, the first PTA metal complex was $Mo(CO)_5$(PTA). It has formed a good number of transition metal complexes across the periodic table and in all PTA complexes, the adamantane skeleton is maintained. Metals that form PTA complexes include Au, Ru, Pt, Pd, Rh, Ir, etc.[34]

Most of the distinctive features of PTA, including its high hydrosolubility and ability to form water-soluble transition metal complexes, derive from its intrinsic tendency to establish hydrogen bonds *via* the three *N*-donor atoms residing in the lower rim of the adamantane skeleton.[121]

In almost all the PTA metal complexes, the phosphine acts as a *P*-donor ligand[122] (Figure 1.16a). However, the first examples of *N*-coordinated PTA have been observed in manganese complexes $MnX_2(PTA)_2(H_2O)_2$ (X = Cl, Br)[93] (Figure 1.16b). Lidrissi *et al.*[122] have also reported the organometallic Ru/Ag coordination polymers $[CpRu(L)(\mu\text{-P,N-PTA})_2AgCl_2]_n$ (L = DMSO, H_2O), these constitute the very first and so far only examples of a PTA complexing with a bridging *N,P*-coordination mode. In these complexes, the

nitrogen coordination occurs after the metal coordination of the phosphorus (Figure 1.16c).[122] The first example of a complex that contains PTA in a triply bridging *P,N,N'*-coordinate mode by the reaction between PTA and $AgNO_3$ in water has also been reported (Figure 1.16d).[123]

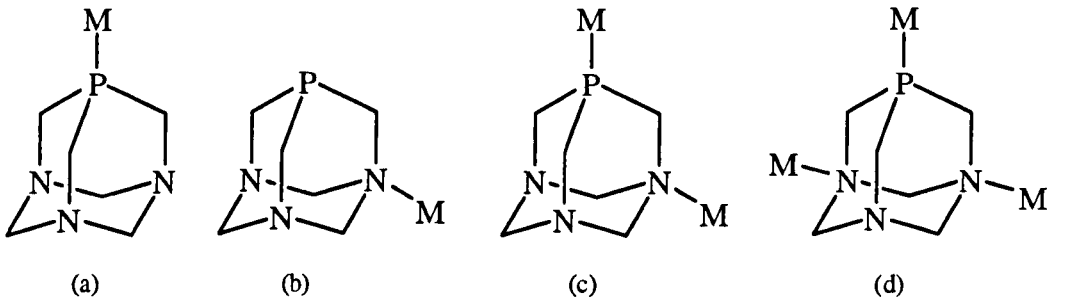

Figure 1.16 Some PTA bonding modes to metal centres, M.

Such *N*-bound PTA complexes previously thought to be abnormal could be rationalised in line with the HSAB theory. This theory helps to predict which bonding site on PTA a Lewis acid will preferentially coordinate. For example the very hard manganese(II) centre binds to the hard nitrogen atom in preference to the phosphorus atom.[93]

1.3.2 PTA-RUTHENIUM COMPLEXES

Ruthenium complexes generally are important due to their catalytic and medicinal potential. They are of particular interest for clinical applications as they have similar ligand exchange kinetics as the successful and widely used platinum anticancer drugs. In addition they have low general toxicity, possibly through mimicking iron binding to biological molecules for transport and storage.[124] While ruthenium(III) compounds have been most widely studied to date, they are believed to be activated by reduction to ruthenium(II) in cancer cells prior to binding DNA.[125] Apart from applications as anticancer drugs, other medical applications of ruthenium compounds have been explored, including their use as immunosupressants, nitric oxide scavengers and antimicrobial agents.[125] It has been shown that ruthenium complexes of organic drugs can overcome resistance developed by the microbe to the organic compound alone. For example a ruthenium(II)–chloroquine complex is two to fivefold more active than chloroquine against drug resistant *Plasmodium* parasites that cause malaria.[126]

The appearance of ruthenium complexes of PTA in the literature is quite recent. The catalytic ability and potential medicinal properties of ruthenium complexes of PTA and

its derivatives have been a key point in the development of PTA coordination chemistry.[34] The initial work was concentrated on the halogenated complexes; *cis*-$RuCl_2(PTA)_4$, **39** and *fac*-$RuCl_2(CO)(PTA)_3$, **40**. Complex **39** was synthesised by either reacting excess PTA with $RuCl_3$ in refluxing ethanol,[105] or reacting aqueous solutions of PTA with toluene solution of $RuCl_2(PPh_3)_3$.[127] Complex **39** is insoluble in non-polar organic solvents but soluble in alkaline or neutral aqueous solution. The ligand displacement reaction of *cis*-$RuCl_2(PTA)_4$ with CO forms $RuCl_2(CO)(PTA)_3$, **40** as identified by IR spectroscopy [υ(CO) = 1987 cm^{-1}].[105] The protonated analogue $[RuCl_2(PTA)_2\{PTA(H)\}_2]Cl$, **41** has also been obtained with a small amount of Ru(III) complex $[RuCl_4\{PTA(H)\}_2]Cl$, **42** by the reaction of *cis*-$RuCl_2(PTA)_4$ with aqueous HCl solution. The iodo-methylated complexes *trans*-$RuI_4\{PTA(Me)\}_2\cdot 2H_2O$, **43** and *mer*-$RuI_2(H_2O)\{PTA(Me)\}_3]I_3$, **44** have also been synthesised by reacting a combination of $RuCl_3$ and KI with an appropriate amount of PTA in water at 40 or 80 °C and characterised by $^{31}P\{^1H\}$ NMR and single crystal X-ray crystallography.[96] The complexes **43** and **44** are soluble in polar solvents (DMSO, MeCN, DMF) including alcohols and water. The catalytic performance of both **43** and **44** in the hydroformylation of 1-hexene and in the hydrogenation of cinnamaldehyde have been evaluated.[96]

Another class of catalytically active compounds include $RuCl_2$(*p*-cymene)(PTA), **45** and $[RuCl(p\text{-cymene})(PTA)_2]BF_4$, **46**. Dyson *et al.*[128] have accomplished the hydrogenation of substituted arenes into completely saturated cyclohexanes using **45** and **46** under biphasic conditions. Complex **45** was synthesised by reacting PTA with the dimer $[Ru(p\text{-cymene})Cl_2]_2$ in refluxing methanol, whereas **46** was synthesised by adding one equivalent of PTA to **45** in dichloromethane followed by the addition of $AgBF_4$.[128]

The two complexes **45** and **46** gave rise to the new class of compounds known as RAPTA (ruthenium/arene/PTA), being tested for potential use in cancer therapy.[34]

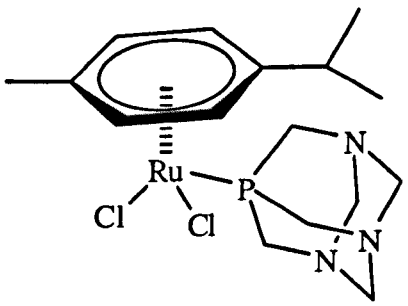

Figure 1.17 Structure of **45**.

Complex **45** is soluble in polar organic solvents such as dichloromethane, chloroform and acetone and the X-ray structure has been reported, exhibiting a typical three-legged piano-stool geometry (Figure 1.17).

The cyclopentadienyl and pentamethylcyclopentadienyl Ru-PTA complexes $CpRuCl(PTA)_2$, **47** and $Cp^*RuCl(PTA)_2$, **48** have also been synthesised and characterised.[113] The catalytic hydrogenation of benzylidene acetone to 4-phenylbutan-2-one by **47** and **48** under biphasic conditions as well as the antimetastatic activity of these complexes have been demonstrated.[113] $CpRuCl(PTA)_2$ was prepared by phosphine exchange of $CpRuCl(PPh_3)_2$ with PTA in refluxing toluene, while $Cp^*RuCl(PTA)_2$ can be prepared in a similar method or by reacting the chlorobridged dimer, $[Cp^*RuCl(\mu\text{-}Cl)]_2$ with PTA in the presence of Zn as reducing agent. The complexes are soluble in water and in chlorinated organic solvents. The single X-ray crystal structure of **48** has been reported, similar to **45**, also exhibiting typical three-legged piano stool geometry, with comparable Ru–P and Ru–Cl distances.[34]

Recently, Dyson and co-workers[54] have prepared two new cyclopentadienyl Ru-PTA complexes, $(Cp'OR)RuCl(PTA)_2$ ($Cp'OR$ = η^5-1-alkoxy-2,4-di-tert-butyl-3-neopentylcyclopentadienyl; R = Me, **49** and R = Et, **50**) from the chlorobridged complexes $[(Cp'OR)RuCl(\mu\text{-}Cl)]_2$ (R = Me, Et) and PTA. The new complexes were characterised spectroscopically and in the case of complex **49**, also by X-crystallography. Complex **49** displays the expected three-legged piano-stool geometry with two PTA and one chloro ligand co-ordinated opposite to the $Cp'OR$ ligand. The *in vitro* anticancer activities of **49** and **50** were evaluated and found to be considerably more cytotoxic (*ca.* 2 orders of magnitude) than the analogous cyclopentadienyl complex $CpRuCl(PTA)_2$.

Water soluble ruthenium PTA cluster complexes have also been reported. The cluster complex $Ru_3(CO)_9(PTA)_3$, **51** has been synthesised by adding PTA in CH_2Cl_2 to solution of $Ru_3(CO)_{12}/CH_2Cl_2$ and refluxing for one hour.[34] Ruthenium hydride complexes of PTA important for catalytic hydrogenation mechanisms such as $RuHCl(PTA)_4$ **52**, and $RuH_2(PTA)_4$ **53** have been synthesised and characterised.[129] The synthesis of the cyclopentadienyl variants of the monohydride complexes, $CpRuHCl(PTA)_2$ **54** and $Cp^*RuHCl(PTA)_2$ **55** have also been accomplished using sodium formate as the hydride source.[34]

1.3.3 PTA-RHODIUM COMPLEXES

Rhodium-PTA complexes have received great attention because of their catalytic[34] and recently medicinal potential.[51,112] Rhodium, apart from being a catalytically active metal is also known to be a potential metal for the design of anticancer drugs.[112, 130] Recently, complexes with a Cp* ligand in place of an arene ligand, have been synthesised and shown to exhibit similar *in vitro* activities to the ruthenium analogues.[51,112]

The water-soluble trisubstituted rhodium(I) PTA complex, $RhCl(PTA)_3$ **56** has been synthesised by reacting $RhCl_3$ with an excess of PTA in refluxing ethanol.[105] Complex **56** has been shown to be a hydrogenation catalyst.[131] The bis-substituted complex $[RhCl(PTA)_2]\cdot 2HCl$, **57** was obtained when **56** was reacted with dilute HCl, and the rhodium(III) iodo species $[RhI_4\{PTA(Me)\}_2]I$, **58** has been synthesised by mixing $RhCl_3$ with KI in water followed by the addition of [PTA(Me)]I.[34]

The Rh-PTA carbonyl complexes $[RhI(CO)\{PTA(Me)\}_2]I_2$, **59** and $[RhI(CO)\{PTA(Me)\}_3]I_3$ **60** have also been synthesised by reacting the dimer $[Rh_2Cl_2(CO)_4)]$ with [PTA(Me)]I in the presence of NaI under an inert atmosphere.[132] Both complexes are very sensitive to oxidation in solution but are stable in the solid state. They are highly soluble in water but only sparingly soluble in methanol.

A new carbonyl Rh(I) complex bearing PTA and tris(1-pyrazoly)methanesulfonate (Tpms) ligands, Rh(Tpms)(CO)(PTA) **61** has been recently synthesised in high yield by a simple one-pot reaction of $[Rh_2Cl_2(CO)_4]$ with PTA and Tpms lithium salt, (LiTpms) in a CH_2Cl_2/MeOH solution at room temperature.[133] Complex **61** is water soluble and is the first transition metal complex that bears the PTA and Tpms ligands. This synthetic strategy can be applied to the preparation of other Rh-PTA carbonyl complexes of the type, Rh(Tpms)(CO)(L) (L = phosphine) and constitutes an improvement over the previously described procedures,[134] since it does not require the isolation of any intermediate nor the use of CO and the synthesis of the thallium salt TlTpms.[134] Unlike the Rh(Tpms)(CO)(L) ($L = PMe_3$, PPh_3, PCy_3) analogues,[134] complex **61** is quite stable in water under inert atmosphere and thus constitutes a promising catalyst precursor for catalytic reactions in liquid biphasic systems.

Another family of water-soluble carbonyl Rh-PTA complexes have been synthesised by reacting $[Rh_2Cl_2(CO)_4]$ with the *N*-alkylated derivatives of PTA, called *tpa* by the authors,[132,135] namely 1-alkyl-1-azonia-3,5-diaza-7-phosphaadamantane iodides ($Rtpa^+I^-$) with alkyl (R) = methyl ($mtpa^+I^-$), ethyl ($etpa^+I^-$) and *n*-propyl ($ptpa^+I^-$) and ($mtpa^+Cl^-$) to give the rhodium(I) complexes $RhCl(CO)(tpa)_2$, $RhI(CO)(Rtpa^+I^-)_2$, $RhCl(CO)(mtpa^+Cl^-)_3$ and $RhI(CO)(Rtpa^+I^-)_3$. The properties and reactivities have been investigated using ^1H and $^{31}P\{^1H\}$ NMR and IR spectroscopies. The complexes have been evaluated as catalysts for the water-gas shift reaction, the hydrogenation of C=C and C=O bonds, the hydroformylation of alkenes and the isomerisation of unsaturated compounds.[135] Rh(I) acetylacetonato complex featuring PTA has also been reported. Rh(acac)(CO)(PTA), **62**, was synthesised by reacting $Rh(acac)(CO)_2$ with one equivalent of PTA in ethanol, refluxing for 3 h.[136]

Mixed rhodium complexes featuring both PTA and $PTA(H)^+$ have also been synthesised. For example the complex $[RhCl\{PTA(H)\}(PTA)_2]Cl$ **63** was prepared by refluxing for 2 h in ethanol solution of $RhCl_3$ and six equivalents of PTA, whereas $[RhCl\{(PTA(H)\}_3(PTA)]Cl_3$ **64** was prepared by reacting $RhCl(PTA)_3$ with two equivalents of PTA in water.[106] Complex **63** is an active hydroformylation catalyst, whereas **64** is inactive. Rhodium hydride complexes having alkylated PTA have also been reported. The complexes $[RhH\{(PTA(Me)\}_4]I_4$ and $[RhH\{(PTA(Et)\}_4]I_4$ have been prepared by addition of one equivalent of [PTA(R)]I to $[Rh(CO)\{PTA(R)\}_3]I_3$ (R = Me or Et), followed by treatment with $NaBH_4$.[137]

Recently, Bolaño *et al.*[138] have described the synthesis and characterisation of a new family of rhodium complexes containing the *N*-boranyl $PTA(BH_3)$ cage-like phosphines as a monodentate *P*-coordinated ligand. The reaction between 1-boranyl-1,3,5-triaza-7-phosphaadamantane ligand, *N*-B-$PTA(BH_3)$ and $[Cp^*RhCl(\mu\text{-}Cl)]_2$ gave $Cp^*Rh\{N\text{-}B\text{-}PTA(BH_3)\}Cl_2$ **65** or $[Cp^*Rh\{N\text{-}B\text{-}PTA(BH_3)\}_2Cl]Cl$ **66** containing one or two P-bonded boranated PTA ligands. The hydride $Cp^*Rh\{N\text{-}B\text{-}PTA(BH_3)\}H_2$ was also obtained when **65** was reacted with $NaBH_4$ and alternatively by direct boronation of $Cp^*Rh(PTA)Cl_2$ with excess $NaBH_4$.

1.3.4 PTA-IRIDIUM COMPLEXES

Iridium complexes of PTA are few compared to their rhodium analogues. This might be due to the generally assumed poor catalytic activity of iridium derivatives in comparison to rhodium species and the minor interest in studying the coordination chemistry of this metal.[34] The first PTA ligated iridium complexes, $IrCl(CO)(PTA)_2$, $IrCl(CO)(PTA)_3$ and others were synthesised by Krogstad *et al.*[139] The water-soluble version of Vaska's complex *trans*-$IrCl(CO)(PTA)_2$ **67** was prepared by stirring a hexane/CH_2Cl_2 solution of PTA and $[Ir(COD)Cl]_2$ under an atmosphere of CO.[139] The related complexes *trans*-$IrCl(CO)(PTA)_3$, **68** and *trans*-$[Ir(CO)(PTA)_4]Cl$, **69** were prepared *via* ligand substitution reactions of PTA with Vaska's compound, *trans*-$IrCl(CO)(PPh_3)_2$, in absolute and 95% ethanol respectively.[139] In contrast to **68**, complex **69** is highly soluble in water but not in organic solvents. The single crystal X-ray structure of *trans*-$[Ir(CO)(PTA)_4]Cl$, **69** has been determined and shows a trigonal bipyramidal structure in which the CO occupies an axial position. This is the first crystallographically characterised $[IrP_4(CO)]^+$ complex in which the CO is axially ligated.[139] The formation of the higher substituted PTA complexes **68** and **69** is favoured over the bis-PTA complex **67**, probably because of the smaller cone angle of PTA in comparison to most tertiary phosphines.[139]

Mixed iridium-PTA complexes and hydrides have also been obtained. Complex **68** can be converted into **69** by ligand substitution with one equivalent of PTA in water, but interestingly, addition of excess NaCl to **69** in MeOH under aerobic conditions does not restore **68**, but instead forms the decarbonylated iridium(III) octahedral dichlororide $[IrCl_2\{PTA(H)\}_2(PTA)_2]Cl_3$, **70** with two *N*-protonated PTA ligands.[139] All three complexes **67–69** can be protonated in aqueous solution. For example, dissolution of **68** or **69** in dilute HCl produces **70** and a dihydrido species $[IrH_2\{PTA(H)\}_4]Cl_5$, **71** which were easily crystallised and separated by inspection due to their different crystal habits.[139] Complex **71** was authenticated by X-ray diffraction analysis and exhibits an octahedral geometry with two hydride ligands in a *cis*- configuration.[139]

The preparation of the water-soluble complex $[IrCl(COD)(PTA)_3]Cl$, **72** by reacting $[IrCl(COD)]_2$ with six equivalents of PTA under nitrogen atmosphere has also been reported.[140] Complexes *trans*-$IrCl(CO)(PTA)_3$, **68** *trans*-$[Ir(CO)(PTA)_4]Cl$, **69** and $[IrCl(COD)(PTA)_3]Cl$, **72** have been used as catalysts for the intramolecular

hydroamination of 4-pentyne-1-amine in water, the first reported study of the Ir(I) mediated transformation in aqueous media.[140]

The water-soluble iridium carbonyl cluster $Ir_4(CO)_7(PTA)_5$ **73** was synthesised by refluxing $Ir_4(CO)_{12}$ with an excess of PTA in toluene.[141] The isolated red-orange solid, which was characterised by X-ray crystallography, is soluble in water at pH 7 or below and in a variety of solvents including CH_2Cl_2.

Recently, the synthesis of enantiomerically pure water-soluble iridium PTA complexes was reported.[102] A diastereomerically enriched analogue of PTA was obtained by reaction of the PTA lithium salt with benzaldehyde to give the water-soluble derivative phenyl(1,3,5-triaza-7-phosphtricyclo[3.3.1.1^{3,7}]dec-6-yl)methanol (PZA) as a mixture of two diastereoisomers and used as a *P*-monodentate ligand towards iridium(III). The resulting piano-stool complex $Cp^*IrCl_2(PZA)$ **74** was obtained as a mixture of diastereoisomers both in solution and in the solid state.[102] The resolution of such water-soluble PTA derivatives and their potential use in enantioselective catalysis and biological applications will be promising areas for exploration.[102]

1.3.5 PTA-PALLADIUM COMPLEXES

The interest in palladium-PTA complexes, like those of other catalytically active metals such as ruthenium and rhodium is due to their potential as water-soluble catalysts.[34] Organopalladium compounds containing PTA are quite few, the first ever reported was probably Pd-(salicylaldiminato)(Me)(PTA).[142] A monomeric complex Pd(dmba)Cl(PTA) [dmba = N,C-chelating 2-(dimethylaminomethyl)phenyl], **75** has been obtained by reacting the dimer $[Pd(dmba)(\mu\text{-}Cl)]_2$ with two equivalents of PTA in CH_2Cl_2 at room temperature (Equation 1.19) and its crystal structure established by X-ray diffraction.[143] Complex **75** was shown to catalyse the Sonogashira reaction of aryl bromides and chlorides with excellent results in the absence of amine and CuI.[143] Its efficiency was similar to that found for $Pd(PA\text{-}Ph)_2{\cdot}dba$ (PA-Ph = 1,3,5,7-tetramethyl-2,4,8-trioxa-6-phenyl-6-phosphadamantane)[144] the unique adamantane-type phosphine that has been used until now in coupling reactions.

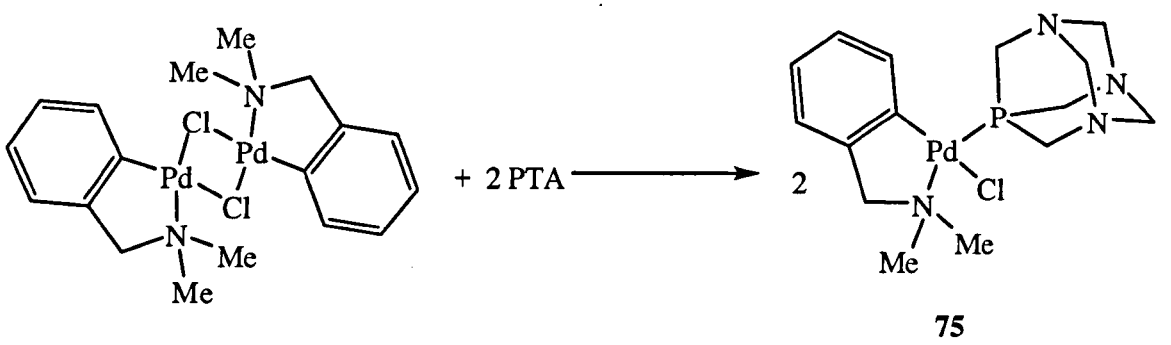

75

Equation 1.19

Some bis-, tris- and terakis-substituted complexes of PTA have also been synthesised and characterised. The synthesis of *cis*-$PdCl_2(PTA)_2$, **76** is accomplished by reacting $PdCl_2$ with excess PTA in H_2O. Complex **76** can also be synthesised by ligand exchange of MeCN or PhCN with PTA from both $PdCl_2(MeCN)_2$ or $PdCl_2(PhCN)_2$ respectively,[145] or metathesis reaction of $(NH_4)_2PdCl_4$ with double the amount of PTA in refluxing ethanol.[43] The X-ray structure of **76** reveals a *cis*-arrangement of the two PTA ligands in a square planar geometry.

Another bis-PTA derivative, *cis*-$PdBr_2(PTA)_2$ **77** which is the bromide analogue of **76** was obtained by reaction of LiBr with the tris-PTA derivative $[PdCl(PTA)_3]Cl$, **78** in water.[34] The X-ray structure determination confirmed the square planar geometry but unlike **76**, the two PTA ligands are in a *trans* arrangement. The complex **78** was itself prepared by the addition of $(NH_4)_2PdCl_4$ to five equivalents of PTA in ethanol and refluxing for 3 h.[146] However the reaction also contains some $PdCl_2(PTA)_2$ and free PTA.

The tetrakis-substituted complex $Pd(PTA)_4$, **79** can be obtained by reacting $PdCl_2$ with five equivalents of PTA in H_2O.[147] Alternatively, complex **79**, can be prepared by reacting $PdCl_2$ with four equivalents of PTA in refluxing DMSO followed by reduction with hydrazine monohydrate.[146] A further alternative synthesis involves the addition of $Pd_2(dba)_3$ (dba = dibenzylideneacetone) to a solution of PTA in methanol.[34] The solubility of complex **79** in water is exceptionally high (240 g/L) and it has been tested for the catalytic oligomerisation of but-1,3-diene into various dienes under biphasic water/substrate conditions.[34]

A series of phenylselenolato palladium(II) complexes with a variety of different phosphine ligands has been reported.[148] For example, complex $Pd(SePh)_2(PTA)_2$, **80** was obtained by reacting $PdCl_2(PTA)_2$ with NaSePh in CH_2Cl_2/MeOH solution. A series of palladium salicyladiminato-PTA complexes were prepared by Darensbourg and co-workers by reacting PTA and the appropriate salicylaldimine ligand with $(TMEDA)Pd(CH_3)_2$ (TMEDA = tetramethylethylenediamine) in MeOH at –30 °C.[142]

A unique PTA complex worth mentioning here is the molybdenum-palladium PTA cation $[Mo_3Pd(PTA)_4(H_2O)_9]^{4+}$ **81**, reported by Sykes and co-workers.[149] The molybdenum-palladium cluster was prepared through Pd-S cleavage of a dimeric cuboidal Mo_3PdS_4 cluster, the PTA having the ability to dissociate dimers $[\{Mo_3PdS_4(H_2O)_9\}_2]^{8+}$ by coordinating to the Pd centres.[149] PTA was found to be particularly suitable for this reaction because of its water-soluble properties, the rate of dissociation/coordination was faster than that of trisodium triphenyl phosphine trisulfonate, TPPTS (2.78×10^6 M^{-1} s^{-1} versus 9.6×10^5 M^{-1} s^{-1}) which provide a similar reaction with the Mo_3PdS_4.[34]

1.3.6 PTA-PLATINUM COMPLEXES

In contrast to its congeners nickel and palladium, platinum PTA complexes have been much more widely studied, especially the tetrakis derivative $Pt(PTA)_4$, **82**. The preparation involves reacting $Pt(PPh_3)_4$ with excess PTA in a ligand exchange reaction. If excess PTA is not used, mixed PPh_3/PTA species $Pt(PPh_3)_{4-n}(PTA)_n$ (n = 1–3) can be formed. Such mixed complexes are all insoluble in water, whereas complex **82** is soluble in water (295 g/L) as well as in 0.1 M HCl (290 g/L).[146] Alternatively, complex **82** can be prepared by the addition of $PtCl_2$ to PTA in H_2O.[147] After stirring for 2 days, the product was obtained as off-white micro-crystals accompanied by the formation of a second Pt(0) complex identified as the fully protonated species $[Pt\{PTA(H)\}_4]Cl_4$, **83**. The synthesis of complex **83** can however be straightforwardly accomplished by repeating the addition of $PtCl_2$ to PTA in 0.1 M HCl or simply dissolving a sample of $Pt(PTA)_4$ in acidic media (HCl 0.1 M). The crystal structure of $[Pt\{PTA(H)\}_4]Cl_4$ has been determined, showing a slightly distorted tetrahedron which does not significantly differ from that of the analogous Ni and Pd complexes.[146]

The behaviour of $Pt(PTA)_4$ in acidic media of different acid strength has been evaluated.[147] Strong acids such as 0.1 M HCl or H_3PO_4 yield regioselective protonation at

the nitrogen centres forming the tetrachloride salt **83**, mentioned above. In contrast, if weak acids such as carbonic acid are used, protonation occurs selectively at the platinum centre forming $[PtH(PTA)_4]Y$, **84** (Y = singly charged anion). These water-soluble platinum hydride species have been characterised by ^1H, $^{31}P\{^1H\}$ and $^{195}Pt\{^1H\}$ NMR spectroscopies.[147]

The bis-substituted PTA derivative *cis*-$PtCl_2(PTA)_2$, **85** can be prepared by reacting either K_2PtCl_4 or $PtCl_2(SMe_2)_2$ with two equivalents of PTA in hot aqueous solution or, in the case of K_2PtCl_4, hot 95% EtOH.[43] Complex **85** has also been obtained using Zeise's salt, $[PtCl_3(C_2H_4)]Cl$ which is known to force *trans*-disposition in Pt(II)-diphosphine complexes, but failed to produce the *trans*-isomer, yielding only the *cis*-isomer of complex **85**. Alternatively, **85** can be formed through ligand exchange of PhCN with PTA from $PtCl_2(PhCN)_2$ in MeOH.[145] The asymmetric unit in the crystal structure of **85** obtained is composed of two independent molecules held together by a bridging H_2O molecule, forming a dimeric unit $[\{PtCl_2(PTA)_2(\mu\text{-}H_2O)\}_2]$, with strong intermolecular hydrogen bonds [$d(N\cdots H\text{–}O)_{ave}$ = 2.914 Å].[150] In each dimeric unit, two platinum atoms are surrounded by two PTA ligands and by two chlorides both in a *cis*-arrangement and attain a regular square planar geometry.

A double protonated PTA platinum complex has been reported. Complex $[PtCl_2\{PTA(H)\}_2]Cl_2$, **86** was obtained by crystallisation of **85** in 0.1 M HCl solution. The crystal structure of **86** was obtained and displayed a distorted square planar geometry with two *cis* protonated PTA ligands and two *cis* chlorides, with an extensive pattern of hydrogen bonding involving Cl^- and $PTA(H)^+$ ligands as well as solvated water molecules.[146]

Tris- substituted PTA complex $[PtCl(PTA)_3]Cl$, **87** was prepared by either refluxing an aqueous solution of $PtCl_2$ and PTA or ligand exchange of PhCN with PTA from $Pt(PhCN)_2Cl_2$.[34] The tetraphenylborate salt, $[PtCl(PTA)_3]BPh_4$, was isolated upon addition of $Na[BPh_4]$ to a dichloromethane solution of $Pt(PhCN)_2Cl_2$ in the presence of PTA in MeOH.[34] X-ray diffraction analysis of $[PtCl(PTA)_3]Cl$ shows that the structure is isomorphous with the palladium analogue $[PdCl(PTA)_3]Cl$, **78** and confirms the expected square planar geometry.[34]

The pentacoordinate iodide complex $PtI_2(PTA)_3$, **88** was obtained by reacting $[PtCl(PTA)_3]Cl$, **87** with sodium iodide in aqueous methanol.[151] The crystal and molecular structure of **88** were determined by X-ray crystallography and was found to be pentacoordinate in the solid state. Pentacoordinate complexes of Pt(II) are rare, and the geometry is best described as a severely distorted square pyramid with one iodo and three PTA ligands occupying the equatorial plane, with the second iodo ligand in the apical position.[151] The complex *trans*-$PtI_2(PTA)_2$, **89** was however obtained by halogen exchange of Cl with I of *trans*-$PtCl_2(PTA)_2$ using excess NaI in water.[152] A similar square planar geometry, with *trans*-disposition of the two PTA ligands, was ascertained by X-ray diffraction for the dicyano derivative *trans*-$Pt(CN)_2(PTA)_2$ obtained by the reaction of $K_2Pt(CN)_4$ with the gold complex $AuCl(PTA)_3$ has been reported.[153]

The platinum(II)PTA complex, Pt(ts)PTA, **90** (ts = thiosalicylate, $SC_6H_4COO^-$), was synthesised by ligand displacement from Pt(ts)(COD) with PTA in methanol.[154] Complex **90** is highly water soluble, its stability has been shown to be very high in a study involving other platinum(II) thiosalicylate-phosphine complexes using electrospray mass spectrometry (ESMS). For example in this study, there was no fragmentation of complex **90** even at 200 V, in contrast to the PPh_3 derivative which fragments at 80 V.[34]

Traditionally, it was believed that only complexes of platinum(II) containing two inert and two semilabile and mutually *cis* ligands display antitumor activity until Farrel and co-workers[155] showed that complexes with *trans* geometry are also cytotoxic. Examples of such bioactive Pt(II) complexes include *trans*-$PtCl_2\{NH_2CH(CH_3)_2\}\{NH(CH_3)_2\}$[156] and *trans*-$PtCl_2(iminoether)_2$.[157] Generally, the low water solubilities of *trans*-diaminechloroplatinum(II) and analogous complexes have limited their usefulness, and efforts have therefore focused on modifying the nature of the anionic and neutral ligands.[158,159] Only relatively recently have the biological activities of platinum complexes with other neutral ligands such as phosphines and thiolates been investigated.[159] Platinum(II) derivatives with various ligands including aminodiphosphines,[160–162] lipophilic PPh_3 and/or hydrophilic PTA and thiotheophyllines as anionic ligands[163,164] as well as $Pt(ts)(P)_2$ (P = PPh_3, dppe) have been reported to show significant biological activity.[165]

Recently, a range of platinum(II) complexes of the type *trans*-$[Pt(SR)_2(P)_2]$, [SR = 2-pyridinethione (Spy), 2-thiopyrimidine (SPyrim); P = 1,3,5-triaza-7-phosphaadamantane (PTA), 3,7-diacetyl-1,3,7-triaza-5-phosphabicyclo[3.3.1]-nonane (DAPTA)] have been prepared and characterised, and their *in vitro* cytotoxicities against some human cancer cells evaluated.[159] The complexes $Pt(SPyrim)_2(PTA)_2$, **91**; $Pt(Spy)_2(PTA)_2$, **92**; $Pt(SPyrim)_2(DAPTA)_2$, **93** and $Pt(Spy)_2(DAPTA)_2$, **94** all demonstrated potent cytoxicity for ovarian, colon, renal and melanoma cancer cell lines on the basis of a comparison with ID_{50} values for some known cancer drugs.[159] Single crystals of **91**, **92** and **94** were obtained and X-ray diffraction analysis revealed the *trans* configuration in the solid state. These are the first *trans*-platinum(II) complexes with S- and P-donor ligands that demonstrate considerable biological activity. The complexes are highly water-soluble and are suitable candidates for use as anticancer drugs and the *in vitro* activities of these complexes against the ovarian cancer and colon cancer cell lines were found to be promising.[159]

1.3.7 PTA-GOLD COMPLEXES

The importance of PTA as a ligand in gold chemistry is mainly as a result of preparing water-soluble phosphine-gold complexes which shows unusual reactivity patterns and self-aggregating properties, where short intermolecular Au···Au contacts, representing weak second order metal-metal bonding results in dimers, tetramers or even polymers.[34,166] The important prerequisite for this novel type of aggregation "aurophilicity" is the presence of structurally non-demanding ligands. Any overcrowding of the molecules can prevent the Au···Au contacts with their rather small bond energies;[166] hence with the advent of water-soluble ligands, PTA is a suitable ligand in the study of these gold complexes as low energy luminescent materials. The water-soluble gold-PTA complexes apart from their use in photoluminescent devices are also important for the preparation of "liquid metals" for metallic deposition[167] *e.g.* deposition on tiles for decorative purposes. The water solubility avoids the use of toxic organic solvents for this purpose.

PTA-gold complexes are also important for medicinal applications. Metallic gold and gold compounds, in particular, have had a long history of use in medicine, and several gold compounds are in use as antiarthritic drugs *e.g.* Solganol, Myocrisin and Auranofin.[159] Recently, some water-soluble Au(I) thionate complexes containing PTA or

DAPTA ligands have been synthesised, characterised and evaluated as anticancer drugs and found to have some cytotoxicity.[159]

A detailed investigation of the coordination chemistry of gold(I) with PTA aimed at evaluating the hydrophilicity and the photoluminescence properties of PTA-gold complexes have been carried out.[168] The dicoordinate, mono-substituted PTA-gold complex AuCl(PTA), **95** was synthesised by reacting the dimethylsulfide complex $AuCl(SMe_2)$ with PTA in chloroform.[168] Halide exchange reactions, upon mixing **95** with HBr in H_2O/acetone or KBr in dichloromethane/acetonitrile gave the bromide analogue, AuBr(PTA), **96** whereas a similar reaction using KI in refluxing acetone gave the analogous iodide complex, AuI(PTA), **97**.[168] The methyl gold complex, Au(Me)(PTA) has also been synthesised by reacting AuCl(PTA), **95** with MeLi at 0 °C in diethyl ether.[168] The solid state thermal stability of the methyl gold complex, Au(Me)(PTA) was found to be significantly lower than the related halide complexes AuX(PTA) (X = Cl, Br, I) probably due to the lack of hydrogen bonding in the methylated complex. Reaction of AuCl(PTA), **95** with MeOTf in CH_2Cl_2 at −35 °C results in the isolation of PTA(Me) containing the complex [AuCl{PTA(Me)}]OTf, **98** in high yield confirmed from FAB-MS data.

The molecular structures of the complexes **95** and **96** containing MeCN solvate molecules, have been determined by X-ray methods which showed the existence of dimeric aggregates in the solid state through weak Au···Au (aurophilic) interactions. Complex **95** displayed a gold-gold separation of 3.092 Å, while the separation in **96** was 3.104 Å. These distances are among the shortest distances found in the wide family of tertiary phosphine gold(I) halide complexes and have been ascribed by the very small cone angle exhibited by PTA.[117,168] Unsolvated crystals of **95** have been obtained by crystallisation from 1,2-dichloroethane/*n*-hexane solution, and X-ray diffraction analysis has revealed, a polymeric helical chain of gold atoms featuring a longer Au···Au separation [3.394 Å] instead of the dimeric aggregation in the solvated form.[169]

Protonation of AuCl(PTA) has been accomplished by using 0.1 M HCl giving the complex [AuCl{PTA(H)}]Cl, **99**. The bromide analogue, [AuBr{PTA(H)}]Br, **100** is obtained in a similar way using HBr. In contrast, when the same protocol is applied to the iodide derivative AuI(PTA), the diiodoauride complex, $[AuI\{PTA(H)\}][AuI_2]$, **101** was

obtained. The structures of the protonated chloro- and iodo-derivatives have been obtained by X-ray crystallography. The main structural pattern of the protonated chloro complex **99** was similar to that of **95** except that there was significant lengthening of the aurophilic interaction to 3.322 Å.[117] In contrast, the structure of **101** does not exhibit any dimeric pairing of the $[AuI\{PTA(H)\}]^+$ cation; instead, it shows an Au···Au contact of 2.920 Å between the gold atom of the $[AuI\{PTA(H)\}]^+$ cation and the gold atom of the $[AuI_2]^-$ anion.[34] It is interesting to note that the Au···Au distance in **101** changes with the temperature, slightly decreasing with the lowering of the temperature.[117]

Gold(I) complexes with two or more PTA ligands have also been synthesised by Fackler and co-workers. The bis-substituted, three-coordinate gold(I) complex, $[Au(PTA)_2]Cl$ **102** was prepared by reacting AuCl(THT) with two equivalents of PTA in MeCN.[170] The crystal structure of **102** has been determined and shows a linear two-fold coordination about the gold.[171] Another bis-substituted PTA complex $[Au(PTA)_2][Au(CN)_2]$, **103** was synthesised by reacting $[Au(PTA)_2]Cl$ with one equivalent of $K[Au(CN)_2]$ in water.[170] The structure of **103** was determined by X-ray crystallography and showed linearly dicoordinated $[Au(PTA)_2]^+$ cations and $[Au(CN)_2]^-$ anions in a 1:1 ratio forming an alternating linear chain with a uniform Au···Au aurophilic interaction of 3.457 Å.[169]

The four-coordinate Au(I) complex $AuCl(PTA)_3$ **104** was synthesised by stirring together AuCl(THT) with three equivalents of PTA in a 1:2 MeCN/MeOH mixture.[159] This complex is fluxional at room temperature, indicating a dynamic behaviour as confirmed by two broad resonances in the $^{31}P\{^1H\}$ NMR spectrum instead of the expected single resonance.[169]

Gold(I) complexes with more than one alkylated PTA ligand have been synthesised. The complex $[AuI\{PTA(Et)\}_3]I_3$ **105** was prepared by reacting three equivalents of [PTA(Et)]I with $AuCl(SMe_2)$ in an aqueous CH_2Cl_2 biphasic mixture.[172] The crystal structure has been determined by X-ray diffraction and showed that the gold(I) centre is coordinated to three PTA(Et) ligands in a distorted trigonal planar environment. The gold(I) centre is located on a three-fold axis lying slightly above the trigonal plane weakly interacting with the coordinated iodide [d(Au···I) = 2.9129 Å].

Fully substituted Au(I) complexes with either PTA or $[PTA(Me)]^+$ have also been reported.[173] The tetrakis-PTA complex $[Au(PTA)_4]Cl$, **106** was prepared by addition of four equivalents of PTA to $AuCl(SMe_2)$ in an alkaline H_2O/CH_2Cl_2 solution and another complex, $[Au\{PTA(Me)\}_4](PF_6)_5$ **107** was similarly prepared by reacting five equivalents of $[PTA(Me)]PF_6$ with $AuCl(SMe_2)$ in H_2O/CH_2Cl_2 solution.

A four-coordinate Au(I) salt containing mixed PTA/PTA(H) ligands has also been described. The tris-protonated complex $[Au\{PTA(H)\}_3(PTA)](PF_6)_4$ **108** was obtained when four equivalents of [PTA(H)]Cl were added to Au(THT)Cl in MeCN/MeOH solution.[173] Furthermore, the hexafluorophosphate salt, $[Au(PTA)_4]PF_6$ **109** can be prepared by reacting $Na[PF_6]$ with $[Au\{PTA(H)\}_3(PTA)](PF_6)_4$ in a 1:1 molar ratio.[173] It is interesting to note that one proton is lost from one of the four protonated PTA ligands and attempts to obtain fully protonated tetrakis-PTA(H) derivatives have so far failed. In this mixed PTA/PTA(H) derivative, a complete exchange of proton takes place between the four coordinated phosphines hence is not fluxional, this is confirmed by a single broad resonance in the $^{31}P\{^1H\}$ NMR spectrum. The X-ray crystal structures of the four-coordinate complexes **106–109** have been determined with the complex cation sharing a similar tetrahedral arrangement of PTA (**106** and **109**), PTA(H) (**108**) and PTA(Me) (**107**) ligands around the Au(I) centre. Extensive three-dimensional $N–H^+\cdots N$ hydrogen-bonding networks, sometimes supported by intermolecular hydrogen-bonding interactions with water solvate molecules has been observed. This provides a robust scaffold for building up supramolecular assemblies of AuL_4 tetrahedra.[173]

Four-coordinate Au(I) methylated iodo- as well as phenylated PTA derivatives have been reported.[34] The complex, $[AuI\{PTA(Me)\}_3]I_3$ **110** was prepared by treatment of $AuCl(SMe_2)$ with [PTA(Me)]I in CH_2Cl_2/H_2O followed by addition of KI. Metathesis of the three iodide counteranions of complex **110** with $Na[PF_6]$ formed the salt $[AuI\{PTA(Me)\}_3](PF_6)_3$ **111**, retaining the coordinated iodide to the Au(I) centre, but the reaction with $Na[BPh_4]$ resulted in transfer of a phenyl group to gold, yielding an unexpected dicoordinate gold-phenyl salt $[AuPh\{PTA(Me)\}]BPh_4$ **112**.[174] Similarly, the complex AuPh(PTA) **113**, was obtained by a phenyl transfer reaction involving $AuCl(PTA)_3$ and $Na[BPh_4]$. X-ray quality crystals of **110**, **112** and **113** have been obtained by slow evaporation of aqueous solution and the structures determined by diffraction methods. The structure of **110** is similar to that of **105** with the coordinated

iodide ion lying at 2.936(1) Å from the Au centre, while the two phenylated derivatives **112** and **113** show approximately linear coordinations about the gold atom.[174]

Mononuclear gold(I) complexes have been shown to exhibit interesting luminescence. The AuX(PTA) (X = Cl, Br, I) complexes all show short gold–gold contacts between neighbouring molecules in the solid state, and they also luminescence at 77 K.[168,169] In solution, where it is assumed that these weak intermolecular interactions no longer exist, no luminescence is observed. In addition it was found that the strength of the gold-gold interaction increases with an increase in the softness of the ligand X.[175] In order to investigate whether a correlation between the emission energy and the Au···Au distance is a general phenomenon, Fackler Jr. and co-workers[175] synthesised and studied a series of gold(I) monomeric arylthiolate PTA-Au complexes of formula Au(SAr)PTA **114**, (Ar = Ph, *o*-C_6H_4OMe, *m*- C_6H_4OMe, *o*- C_6H_4Cl, *m*- C_6H_4Cl, 3,5- $C_6H_4Cl_2$). These complexes were prepared by firstly deprotonating ArSH with KOH in MeOH followed by reaction with AuCl(PTA) in MeCN. These complexes are of interest due to their photochemistry as well as the presence of the L-Au-SAr linkage in many antiarthritic and cancerostatic drugs.[175] They demonstrated that the complexes exhibited luminescence at low temperatures, and the energy of the emission can be varied either by changing the substituents on the ligand or by the presence of gold-gold interactions in the solid state. However, no direct correlation was found in the study between the separation of the neighbouring gold atoms and the emission energy as was found for AuCl{PTA(H)} and AuCl(PTA).[175] There was also no effect of the nature of the thiolate groups on the phosphorus chemical shift in the $^{31}P\{^1H\}$ NMR spectra of the complexes; only the luminescence properties of the complexes were affected.

The syntheses of other gold(I) thiolato complexes containing PTA or DAPTA, suitable for preparing "liquid metals" for metallic deposition has also been reported.[167] The thiolato gold(I) complexes Au(SR)(PR′$_3$) (SR = various thiolato derivatives as shown in Scheme 1.6; PR′$_3$ = PTA, DAPTA) were easily prepared in good yields by treating the complexes AuCl(PR′$_3$) with the thiol derivatives in the presence of base (Scheme 1.5). The complexes AuCl(PTA) and AuCl(DAPTA) were prepared by replacement of THT from AuCl(THT) with the appropriate phosphine.[167] The resulting complexes were characterised by spectroscopic techniques and in the case of Au**L7**(PTA), Au(S_2CNEt_2)(PTA), by X-ray diffraction showing a pseudolinear gold(I) coordination.

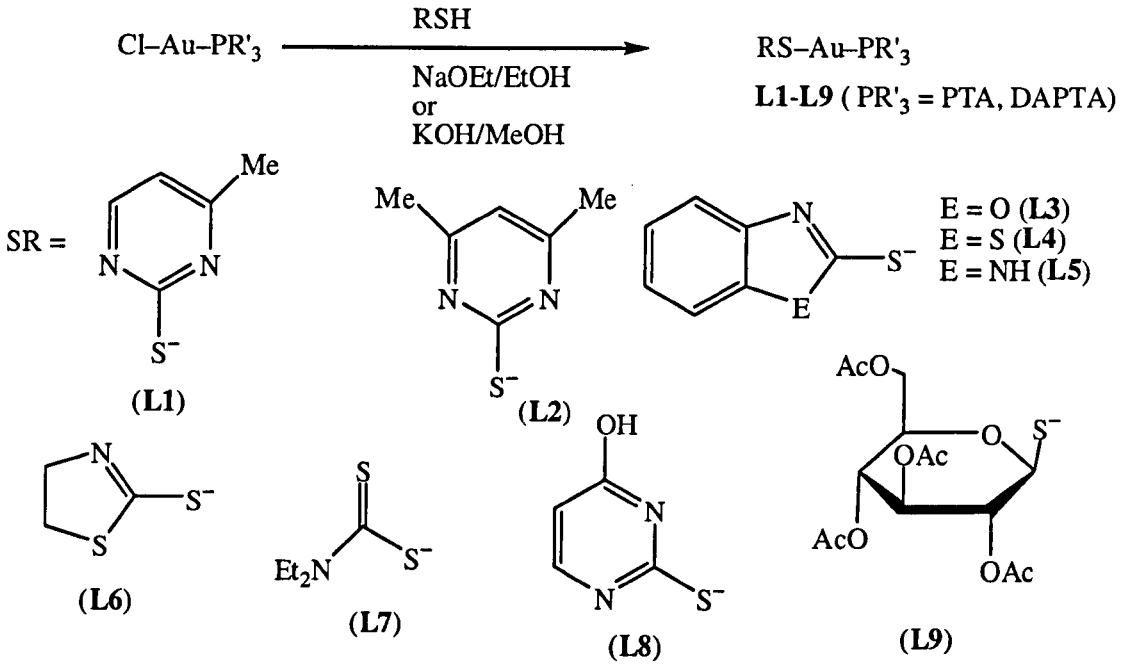

Scheme 1.6

Recently, a range of gold(I) thionate complexes containing water-soluble PTA and DAPTA ligands of the type Au(SR)(P), [SR = 2-pyridinethione (Spy), 2-thiopyrimidine (SPyrim); P = PTA, DAPTA] have been prepared and characterised, and their *in vitro* cytotoxicities against some human cancer cells evaluated.[159] The highly water-soluble complexes Au(Spy)(PTA), **115**; Au(SPyrim)(PTA), **116**; Au(Spy)(DAPTA), **117**; Au(SPyrim)(DAPTA), **118** demonstrated some cytoxicity for ovarian, colon, renal and melanoma cancer cell lines on the basis of a comparison with ID_{50} values for some known cancer drugs.[159] Single crystals of **116** were obtained and X-ray diffraction analysis displays a typical linear geometry about the gold centre.[159]

Alkynyl complexes of gold(I) containing phosphine ligands have been known for many years and studied in great detail because of their luminescence,[176,177] nonlinear optical properties[178] and the supramolecular chemistry of gold(I) acetylide complexes.[179–181] The majority of the known alkynylgold(I) phosphine complexes are insoluble in water, containing either an arylalkylphosphine such as PPh_3, $P(4\text{-}MeOC_6H_4)_3$, PPh_2Me, $PPhMe_2$ or less frequently PMe_3 or PCy_3 (Cy = cyclohexyl). Laguna and co-workers[182] have synthesised and characterised some gold(I) and gold(III) alkynyl complexes that are both soluble and stable in water, by utilising a combination of organometallic ligands with solubilising groups in combination with the highly water-soluble PTA ligand. The

reaction of AuCl(PTA) with propargyl alcohols in the presence of base affords the alkynylgold(I) complexes **119–122** as shown in Scheme 1.7.[182]

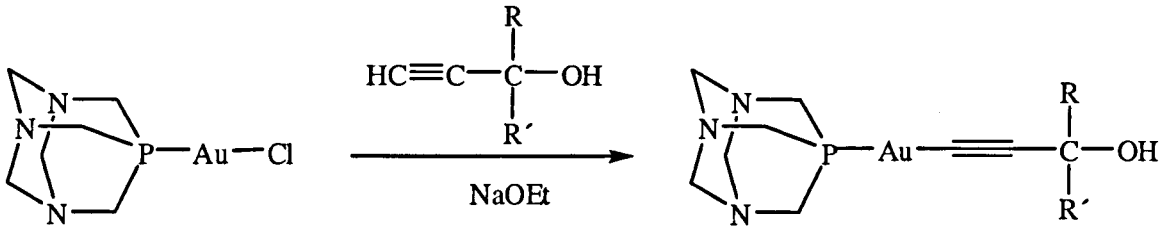

R = R′ = H (**119**)
R = R′ = Me (**120**)
R = R′ = Ph (**121**)
R = Me, R′ = Et (**122**)

Scheme 1.7

The neutral gold(I) complex $Au(C_6F_5)(PTA)$ **123** and the cationic and neutral gold(III) complexes *trans*-$[Au(C_6F_5)_2(PTA)_2]OTf$ **124** and $Au(C_6F_5)_3(PTA)$ **125** were prepared by displacement of the labile THT ligand from $Au(C_6F_5)(THT)$, *trans*-$[Au(C_6F_5)_2(THT)_2]OTf$ and $Au(C_6F_5)_3(THT)$, respectively.[182] Complexes **124** and **125** are the first gold(III) complexes containing PTA and are examples of gold compounds that are soluble and stable in water.

The number of gold(II) complexes is very scarce when compared with the more common gold(I) and gold(III) derivatives. The gold(II) oxidation state is relatively less stable. There is a strong tendency for disproportionation from Au^{2+} to give Au^{+} and Au^{3+} because the odd electron in d^9 metal complexes is in the $d_{x^2-y^2}$ orbital (octahedral tetragonally distorted or square planar arrangement). The formation of a gold-gold bond gives more stable compounds and the Au_2^{4+} core derivatives are the more stable and abundant types of gold(II) complexes.[183] The synthesis of the dicationic digold(II) complexes $[Au_2\{\mu\text{-}(CH_2)_2PPh_2\}_2(PTA)_2](OTf)_2$, **126** and $[Au_2\{\mu\text{-}(CH_2)_2PPh_2\}_2(DAPTA)_2](OTf)_2$, **127** by metathesis reaction from $Au_2Cl_2\{\mu\text{-}(CH_2)_2PPh_2\}_2$ with the respective silver(I) salts Ag(OTf)(PTA) and Ag(OTf)(DAPTA) has been reported (Scheme 1.8).[184] The complexes were fully characterised by spectroscopic techniques and, in the case of **126**, by X-ray diffraction. Analogous dicationic digold(II) complexes were also synthesised and characterised using other water-solube phosphines: mono-, di-, and trisulfonated triphenylphosphines (TPPMS, TPPDS, TPPTS) in place of PTA and DAPTA.[184]

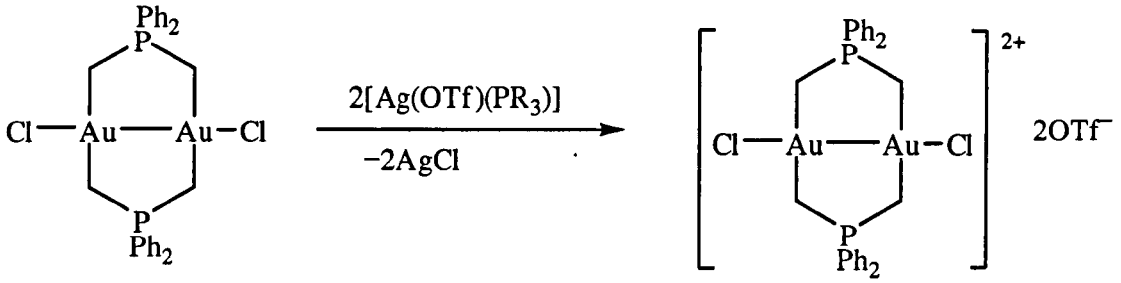

PR_3 = PTA, DAPTA, TPPMS, TPPDS, TPPTS

Scheme 1.8

This suggests that by judicious choice of ligands, even normally unstable organometallic species in labile oxidation states can be solubilised and stabilised in water. Generally, this implies that it can be possible to do chemistry with metal complexes in any attainable oxidation state in water just as easily as in nonaqueous solvents.[184]

1.4 AIMS OF THE RESEARCH

The aims of the research include the preparation of new phosponium salts and phosphorus(III) ligands from cheap, readily available THPC, under aerobic conditions. The primary focus being the preparation and characterisation of new ruthenium, rhodium, iridium, palladium, platinum and gold complexes with these ligands, and in selected cases, as potential catalysts for some organic transformations such as the Heck reaction.

Secondly, to compare these ligands with the well-known cage adamantane-like phosphorus(III) ligand, PTA. A comparison of the complexes with some biologically active compounds in the literature will also be described in this thesis.

CHAPTER TWO

NEW NEUTRAL CYCLIC PHOSPHORUS(III) LIGANDS AND THEIR COORDINATION CHEMISTRY

2.0 INTRODUCTION

Phosphines are phosphorus(III) ligands and their chemistry is centred on the lone pair of electrons and its availability for forming new bonds to phosphorus. Reduction of phosphonium salts is one of the main methods used in the preparation of phosphines. THPC has previously been shown to react with aromatic amines, through a series of condensation and elimination steps to give aniline based tertiary phosphines.[10,71–73] Frank *et al.*[10] have synthesised phosphorus(III) ligands from THPC involving reduction of the phosphonium salt condensation product from its reaction with aniline using Et_3N or NH_3 (Scheme 1.1). The chapter begins with the synthesis and characterisation of two new classes of phosphonium salts by reacting THPC with aniline or phenylenediamine precursors in EtOH as aniline and phenylenediamine derivatives of THPC respectively. The aniline derivatives of THPC are represented as $[P(CH_2NHR)_4]Cl$, where R is phenyl or a substituted phenyl group. While the phenylenediamine derivatives of THPC are represented as $[P\{(CH_2NH)_2R\}_2]Cl$ where R is C_6H_4, C_6H_3Me, C_6H_3COPh or $C_6H_2C_4H_4$.

The coordination potential of the new neutral cyclic phosphorus(III) ligands towards late transition metals including ruthenium(II), rhodium(III), iridium(III), palladium(II) and platinum(II) is also described. The aniline and phenylenediamine derivatives of THPC, neutral cyclic tertiary phosphorus(III) ligands and complexes were characterised by a combination of NMR [$^{31}P\{^1H\}$, ^1H], MS, FT–IR spectroscopy, microanalysis and in several cases by single crystal X-ray crystallography.

2.1 SYNTHESIS OF ANILINE DERIVATIVES (128–146) OF THPC

A range of new aniline derivatives of THPC were synthesised by reacting THPC and some aniline precursors using the procedure first published by Frank *et al.*[10] This procedure was initially used for the development of flame-retardant finishes for cotton based on the reaction of THPC and polyfunctional amines.

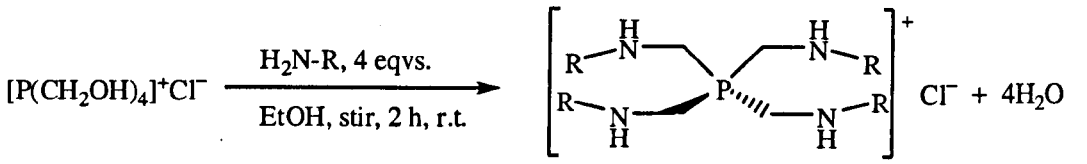

Where R = 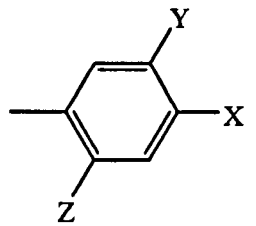 and X = Y = Z = H, **128**; X = F, Y = Z = H, **129**;

X = Cl, Y = Z = H, **130**; X = Br, Y = Z = H, **131**;

X = Y =H, Z = F, **132**; X = I, Y = Z =H, **133**;

X = Me, Y = Z = H, **134**; X = CO_2H, Y = Z = H, **135**;

X = MeO, Y = Z = H, **136**; X = OH, Y = Z = H, **137**;

X = CF_3, Y = Z = H, **138**; X = NO_2, Y = Z = H, **139**;

X = Y = H, Z = CN, **140**; X = Y = H, Z = CO_2H, **141**;

X = H, Y = CO_2H, Z = H, **142**; X = CMe_3, Y = Z = H, **143**;

X = Et, Y = Z = H, **144**; X = ^{n}Pr, Y = Z = H, **145**

or R = $-C(N)SC_6H_4$, **146**

Equation 2.1.

Four equivalents of the aniline precursors reacted readily with THPC in ethanol at room temperature under aerobic conditions by a series of condensation and elimination reactions (Equation 2.1). These reactions afforded the desired products in good to excellent yields (Table 2.1). Some of the aniline precursors are solids while others are liquids. The products of these reactions were usually crystalline solids; colourless in most cases though a few were coloured, for instance the reaction between 4-nitroaniline and THPC gave an orange coloured solid. The reaction between aniline and THPC gave a colourless solid which gradually turned yellow on exposure to light, thus all the products were kept in the dark as a precautionary measure.

2.1.1 CHARACTERISATION OF COMPOUNDS 128–146

Characterisation was achieved by MS, microanalysis, FT-IR, NMR and single crystal X-ray crystallography in one case. The results are shown in Tables 2.1–2.4. Mass

Spectrometry (MS) is useful in elucidating the molecular weight of a compound, and coupled with the resulting fragmentation pattern gives a clue about the structure of a compound.

Table 2.1 Percentage yield (isolated), FAB-MS and selected FT-IR data[a] (in cm^{-1}) for compounds **128–146**.

	% yield	*m/z* $[M-Cl]^+$	ν (NH)	ν(C=O)	ν(OH)	ν(CN)
128	90	455	3237 (vs)			
129	83	527	3250 (vs)			
130	90	592	3242 (vs)			
131	83	770	3253 (vs)			
132	97	527	3265 (vs)			
133	97	959	3246 (s)			
134	95	510	3220 (s)			
135	86	635	3203 (vs)	1675 (vs)	2995 (vs)	
136	97	574	3251 (vs)			
137	71	n.o.	3287 (vs)			
138	83	727	3224 (vs)			
139	76	n.o.	3232 (s)			
140	94	555	3201 (s)			2217 (vs)
141	84	631	3299 (s)	1674 (vs)	2973 (s)	
142	86	n.o.	3237 (vs)	1687 (vs)	2940 (vs)	
143	90	n.o.	3254 (vs)			
144	93	567	3217 (vs)			
145	85	623	3237 (vs)			
146	69	683	3173 (vs)			

[a] Recorded as a pressed KBr disk; n.o. = not observed.

Thus it complements microanalysis in supporting the proposed molecular formula of a compound. It was not easy to verify the amount of cosolvent present in these samples using ^1H NMR spectroscopy since nondried NMR solvents were used. The FAB-MS data for most of the compounds resulting from loss of the chloride ion (*m/z* $[M-Cl]^+$) are

given in Table 2.1. In almost all the compounds, the fragmentation pattern gives the $[XC_6H_4NHCH_2]^+$ fragment, where X is a substituent on phenyl group as the base peak, (with relative intensity of 100%), characteristic of methyleneaniline derivatives.[10] In compounds **130** and **131**, there was evidence of the *m/z* $[M-Cl]^+$ peak appearing as a multiplet, separated by two mass units because of the presence of four chlorine and bromine atoms respectively, exhibiting the phenomenon of isotopic abundance.

In the same vein, there were two peaks due to the $[XC_6H_4NHCH_2]^+$ fragments in **130** and **131**, where X is Cl or Br respectively. In **130**, the two peaks separated by two mass units (*m/z*, 140 and 142) in approximately 3:1 ratio corresponds to the fragment, $[ClC_6H_4NHCH_2]^+$ indicative of the presence of chlorine (^{35}Cl and ^{37}Cl), similarly in **131**, the two peaks (*m/z* 184 and 186) in approximately 1:1 ratio corresponds to the fragment $[BrC_6H_4NHCH_2]^+$ indicative of the presence of bromine (^{79}Br and ^{81}Br). In compounds **137** and **143** the *m/z* $[M-Cl]^+$ peak was not seen but the characteristic $[XC_6H_4NHCH_2]^+$ fragments were evident with *m/z* values of 122 and 162 for compounds **137** and **143** respectively, while in compounds **139** and **142** neither the expected *m/z* $[M-Cl]^+$ peak nor the characteristic $[XC_6H_4NHCH_2]^+$ fragment was observed probably due to decomposition.

A good idea about the functional groups present in a compound can be established by infrared spectroscopy. Infrared spectroscopy was used to identify various functional groups present in these compounds. All the compounds have an NH group. Compounds **135**, **141** and **142**, in addition to the NH group also have the functional C=O and OH groups while compound **140** has a CN group. Upon condensation, the vibrations from the OH groups in THPC were replaced by similar vibrations corresponding to the NH groups in these compounds. Selected IR data for compounds **128–146** are given in Table 2.1.

The infrared spectra of all the compounds were run as pressed KBr disks and showed the characteristic ν(NH) stretch at about 3200 cm^{-1}. In the infrared spectrum of THPC, also run as KBr disk, the ν(OH) stretches were very strong and broad, observed at *ca.* 3467 cm^{-1} and absent in compounds **128–146**. The OH groups in THPC after the condensation reaction with the aniline precursors gave rise to the NH groups in these compounds, observed at a similar range (3173–3299 cm^{-1}) but were sharper. In addition, compounds **135**, **141** and **142** which are derivatives of carboxylic acids showed the carbonyl

stretches, ν(C=O) at 1675, 1674 and 1687 cm^{-1} respectively. The corresponding hydroxyl stretches, ν(OH) were observed at 2995, 2973 and 2940 cm^{-1}. Compound **140**, whose precursor has the CN functional group, showed the characteristic nitrile stretch ν(CN) at 2217 cm^{-1}. There was no evidence of hydroxyl group, stretches in the IR spectra of the products of these reactions apart from **135**, **141** and **142** mentioned above which are from the carboxyl group (–COOH). This confirms that, during the condensation reactions all four hydroxyl groups of THPC were replaced by NH groups.

Table 2.2 Microanalysis (%) and molecular formulae for compounds **128–146**.[a]

	C	H	N	Molecular formula
128	68.07 (68.49)	6.60 (6.57)	11.31 (11.41)	$C_{28}H_{32}N_4PCl$
129	59.55 (59.74)	5.03 (5.01)	9.93 (9.95)	$C_{28}H_{28}N_4F_4PCl$
130	53.37 (53.48)	4.45 (4.49)	8.89 (8.91)	$C_{28}H_{28}N_4PCl_5$
131	41.42 (41.69)	3.44 (3.50)	6.96 (6.95)	$C_{28}H_{28}N_4Br_4PCl$
132	58.66 (58.80)	5.14 (5.11)	9.39 (9.80)	$C_{28}H_{28}N_4F_4PCl{\cdot}0.5H_2O$
133	33.74 (33.81)	2.77 (2.84)	5.76 (5.63)	$C_{28}H_{28}N_4I_4PCl$
134	70.20 (70.25)	7.02 (7.37)	10.11 (10.24)	$C_{32}H_{40}N_4PCl$
135	56.06 (56.10)	5.01 (5.00)	8.13 (8.18)	$C_{32}H_{32}N_4O_8PCl{\cdot}H_2O$
136	62.78 (62.89)	6.63 (6.60)	9.22 (9.17)	$C_{32}H_{40}N_4O_4PCl$
137	59.69 (59.63)	5.77 (5.90)	9.85 (9.93)	$C_{28}H_{32}N_4O_4PCl{\cdot}0.5H_2O$
138	50.31 (50.37)	3.65 (3.70)	7.35 (7.34)	$C_{32}H_{28}N_4F_{12}PCl$
139	49.17 (49.45)	4.34 (4.30)	16.03 (16.48)	$C_{28}H_{28}N_8O_8PCl{\cdot}0.5H_2O$
140	64.49 (64.54)	4.94 (4.82)	19.07 (18.82)	$C_{32}H_{28}N_8PCl{\cdot}0.25H_2O$
141	53.61 (53.30)	5.04 (5.31)	7.42 (7.77)	$C_{32}H_{32}N_4O_8PCl{\cdot}3H_2O$
142	55.09 (54.67)	4.97 (5.16)	7.94 (7.97)	$C_{32}H_{32}N_4O_8PCl{\cdot}2H_2O$
143	73.26 (73.41)	9.06 (9.03)	7.85 (7.78)	$C_{44}H_{64}N_4PCl{\cdot}0.25H_2O$
144	70.32 (70.11)	8.04 (8.09)	9.01 (9.08)	$C_{36}H_{48}N_4O_8PCl{\cdot}0.75H_2O$
145	72.82 (72.87)	8.50 (8.56)	8.45 (8.50)	$C_{40}H_{56}N_4PCl$
146	52.16 (52.44)	3.94 (3.85)	15.12 (15.43)	$C_{33}H_{28}N_8S_4PCl{\cdot}0.75H_2O$

[a] Calculated values in parentheses.

Microanalysis gives the percentage composition of the elements present in the compound. Agreement between observed and calculated values (*ca.*± 0.50%) often supports a given molecular formula for a compound under consideration. The microanalytical data of the compounds are shown in Table 2.2. The agreement between the observed and calculated CHN values is consistent with the formulae of the compounds, **128–146.**

Table 2.3 Selected $^{31}P\{^{1}H\}$ NMR data (in ppm) for compounds **128–146.**[a]

Compound	δ(P)	Other δ(P)
128	9.13	30.62, –50.13
129	8.51	30.62, –51.65
130	11.05	30.58, –52.13
131	11.37	26.93, –51.91
132	30.36	44.00, 8.21
133	11.84	30.26, –51.50
134	7.95	–30.97, –50.79
135	31.50	29.81, 15.03
136	6.70	–35.83, –50.63
137	5.71	–36.26, –51.04
138	30.41	17.72, –37.76
139	28.59	–32.96, –43.85
140	30.33	28.83, –34.84
141	31.61	–33.69
142	11.06	30.48, –53.98
143	8.29	–48.40
144	8.19	–49.78
145	8.22	–49.41
146	29.97	

[a] All NMR recorded in d^6-DMSO.

The solution $^{31}P\{^{1}H\}$ and ^{1}H NMR spectra of compounds **128–146** were recorded in d^6-DMSO. While the $^{31}P\{^{1}H\}$ NMR spectrum of THPC in d^6-DMSO showed a single resonance around 26.5 ppm, indicative of the presence of a P(V) compound, the $^{31}P\{^{1}H\}$

NMR spectra of salts **128–146** in nondried d^6- DMSO showed more than one ^{31}P resonance indicating the presence of P(V) and/or P(III) compounds except **146** where a single resonance was observed at 29.97 ppm (Table 2.3). The multiple resonances could be due to possible decomposition in the NMR solvent, a similar observation was made by Frank *et al.*[10]

Although the complex $^{31}P\{^1H\}$ NMR spectra of these compounds suggested a mixture of phosphorus containing products resulting from the possible decomposition of either P^{III} or P^V compounds such as tertiary phosphines (*ca.* –50.00 ppm) and phosphine oxide (*ca.* 30.00 ppm) respectively in the NMR solvent, the reaction of some of these salts with Et_3N gives clean products as discussed in Section 2.3. With the mixture of phosphorus containing compounds formed in the NMR solvent mentioned above, the ^1H NMR spectra appear complex hence were not analysed at all. However, in **146** where a single phosphorus resonance (100%) was observed, the various proton resonances were assigned as follows: 7.01–7.83 (m, arom. H), 4.75–5.08 ppm (m, CH_2), 8.89 ppm (s, NH) consistent with the expected product.

In the case of compound **129**, X-ray quality crystals were obtained when the EtOH filtrate was allowed to stand for more than 24 h, information about molecular geometry, bond lengths and angles was obtained from single crystal X-ray diffraction analysis of **129** (Figure 2.1 and Table 2.4).

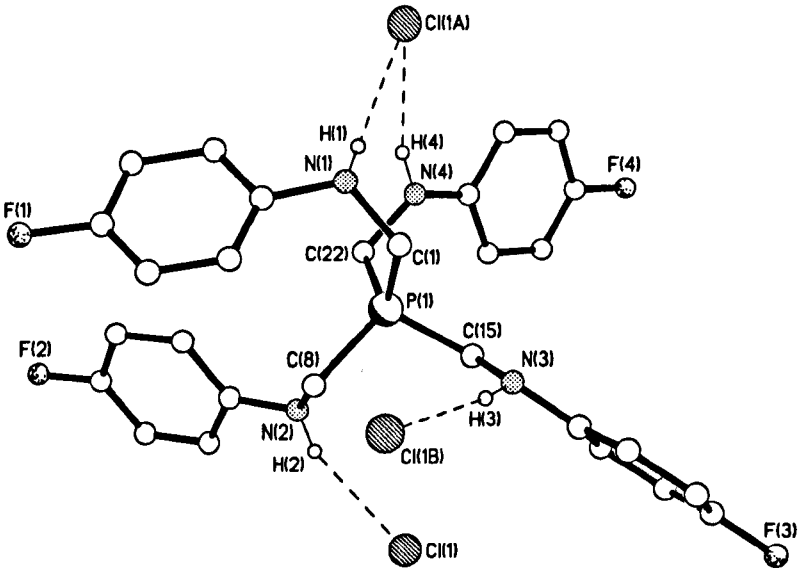

Figure 2.1 Molecular structure of $[P(CH_2NH\text{-}4\text{-}FC_6H_4)_4]Cl$, **129**, showing H-bond interactions. One chloride is unique.

Selected bond lengths, angles as well as hydrogen bond parameters for **129** are given in Table 2.4.

The P(1) atom exhibits a tetrahedral environment with C–P–C bond angles in the range of between 105.81(16) and 114.91(15)°; and the average P–C bond lengths of 1.835(3) Å falls within the range reported for other organophosphorus compounds: $[(HOCH_2)_3PCH_2]_2Cl_2$,[33] $(HOCH_2)_2PCH_2CH_2P(CH_2OH)_2$,[185] $R_2PCH_2CH_2PR_2$ (R = Me, Et, or ^iPr)[186] and $[P(CH_2Fc)(CH_2OH)_3]Cl$, {Fc = $Fe(\eta^5\text{-}C_5H_4)(\eta^5\text{-}C_5H_5)$}.[187]

Table 2.4 Selected bond lengths and angles for **129**.[a]

Bond lengths (Å)		Bond lengths (Å)		Bond angles (°)	
P(1)–C(1)	1.855(3)	C(1)–N(1)	1.433(5)	C(1)–P(1)–C(22)	108.69(17)
P(1)–C(8)	1.840(3)	C(8)–N(2)	1.448(4)	C(1)–P(1)–C(8)	114.91(15)
P(1)–C(15)	1.812(3)	C(15)–N(3)	1.449(4)	C(8)–P(1)–C(15)	105.81(16)
P(1)–C(22)	1.831(4)	C(22)–N(4)	1.445(5)	C(15)–P(1)–C(22)	108.27(16)

Selected hydrogen bonding contacts

D–H···A	d(D–H) (Å)	d(H···A) (Å)	d(D···A) (Å)	<(DHA) (°)
N(1)–H(1)···Cl(1A)	0.88(2)	2.57(3)	3.416(4)	163(5)
N(2)–H(2)···Cl(1)	0.822(19)	2.49(3)	3.251(3)	154(4)
N(3)–H(3)···Cl(1B)	0.836(19)	2.66(2)	3.487(3)	172(4)
N(4)–H(4)···Cl(1A)	0.851(19)	2.50(2)	3.312(3)	161(4)

[a] Estimated standard deviations in parentheses.

The chloride ion is hydrogen bonded to the secondary amine hydrogens; the linearity of the H-bonds (DHA bond angles) as given in Table 2.4 is indicative of strong and directional H-bond interactions. In the N–H···Cl intermolecular bonds, the average N–H bond length of 0.85(2) Å and H···Cl of 2.56(3) Å are comparable to O–H···Cl bonds with the O–H distances between 0.82(3) and 0.91(3) and the H···Cl distances between 2.17(3) and 2.23(3) Å found in $[(OHCH_2)_3PCH_2)_3PCH_2]_2Cl_2$, also suggestive of relatively strong hydrogen bonding.[33,88,188,189] The crystal data and structure refinement details for **129** are shown in Appendix 8.1.

2.2 SYNTHESIS OF PHENYLENEDIAMINE DERIVATIVES (147–150) OF THPC

A range of new phosphonium salts were synthesised by reacting THPC with different phenylenediamine precursors in ethanol using a similar procedure first published by Frank *et al.*[10]

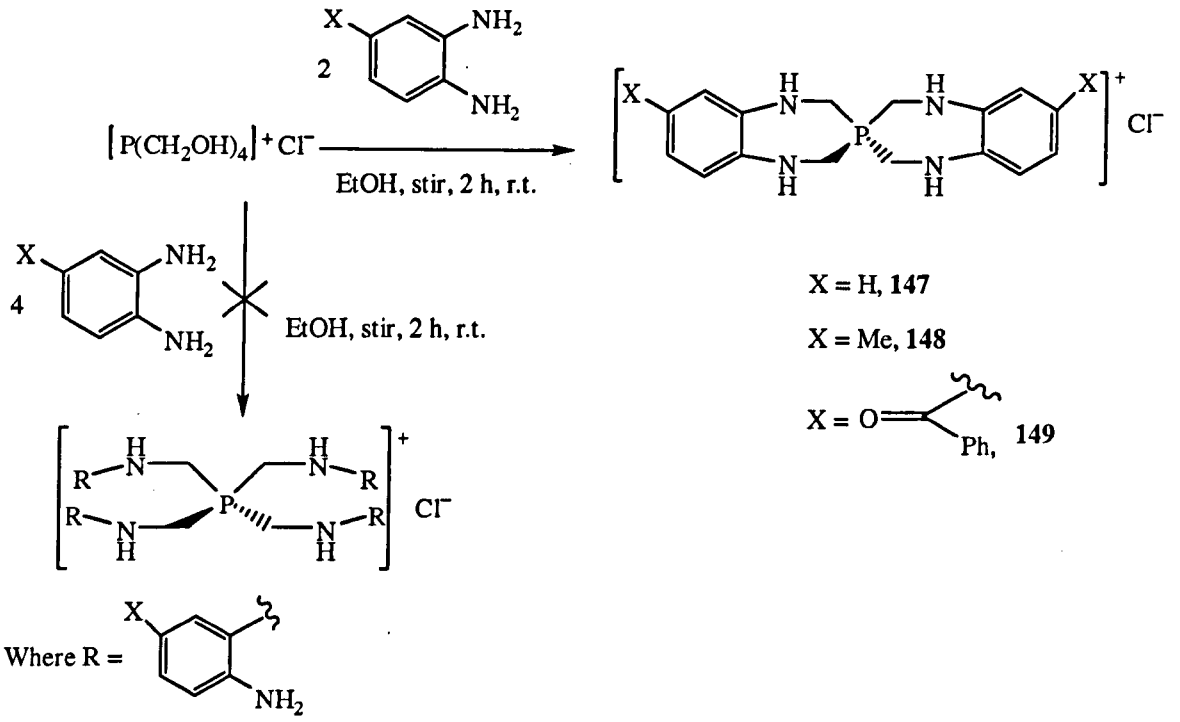

Equation 2.2a

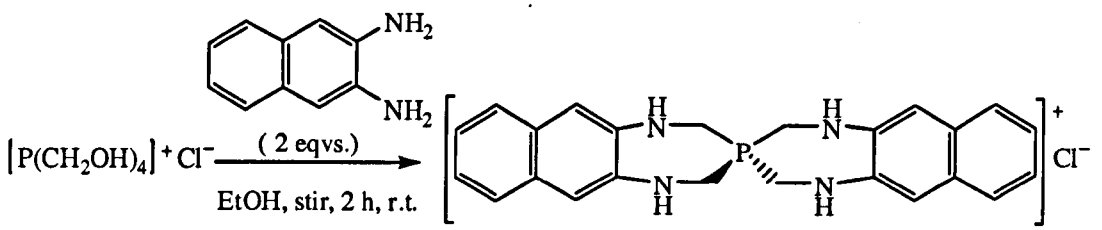

150

Equation 2.2b

Four equivalents of phenylenediamine derivatives was initially chosen, in the anticipation of forming $[P(CH_2NHR)_4]Cl$ type of compounds as was in the case with the aniline precursors. However, analysis of the products obtained agrees with the formation of a spirocylic compound which requires two equivalents of the phenylenediamine derivatives as shown in Equations 2.2a and 2.2b. The phosphonium chlorides were obtained in good to excellent yields as given in Table 2.5. The phosphonium ions in these salts form a

spirocycle in which the central atom is phosphorus. The products are crystalline and coloured solids.

2.2.1 CHARACTERISATION OF COMPOUNDS 147–150

Characterisation was achieved by MS, microanalysis, FT–IR, NMR and single crystal X-ray crystallography as in the case of Section 2.1.1. The results are given in Tables 2.5–2.8. The FAB-MS, data for the compounds resulting from the loss of the chloride ions $[M-Cl]^+$ are given in Table 2.5 and are consistent with the molecular formulae of the phosphonium ions of these salts.

Table 2.5 Percentage yield (isolated), FAB-MS and selected FT-IR data[a] (in cm^{-1}) for compounds **147–150**.

Compound	% yield	*m/z* $[M-Cl]^+$	ν(NH)	ν(C=O)	ν(CH)
147	91	299	3263 (vs)		
148	83	327	3273 (vs)		3527 (s)
149	87	507	3336 (vs)	1637 (vs)	
150	74	399	3255 (vs)		

[a] Recorded as a pressed KBr disk.

The FT–IR spectra of compounds **147–150** were run as pressed KBr disks and the ν(NH) stretches observed at about 3200–3300 cm^{-1} (Table 2.5) were not significantly different from those of the aniline derivatives of THPC (Table 2.1). Thus the observed ν(NH) stretches in both types of phosphonium salts synthesised were higher than the expected value of 2250–2700 cm^{-1} probably due to hydrogen bonding.[190] In compounds **148** and **149**, in addition to the ν(NH) stretches, the infrared vibrations at 3527 and 1637 cm^{-1} are assigned to the ν(CH) and ν(CO) stretches respectively.

The microanalytical data (Table 2.6), were within acceptable limits hence are consistent with the formulae of compounds **147–150**. Coprecipitation of solvent molecules was evident in all the compounds except **147** as observed in the microanalytical data.

Table 2.6 Microanalysis (%) and molecular formulae for compounds **147–150**.[a]

Compound	C	H	N	Molecular formula
147	57.28 (57.40)	5.94 (6.02)	16.85 (16.74)	$C_{16}H_{20}N_4PCl$
148	56.35 (56.76)	6.46 (6.88)	14.61 (14.71)	$C_{18}H_{24}N_4PCl{\cdot}H_2O$
149	64.77 (64.75)	5.14 (5.34)	10.50 (10.07)	$C_{30}H_{28}N_4O_2PCl{\cdot}0.75H_2O$
150	62.41 (62.41)	5.54 (5.89)	11.79 (12.13)	$C_{24}H_{24}N_4PCl{\cdot}1.5H_2O$

[a] Calculated values in parentheses.

The $^{31}P\{^1H\}$ NMR spectra of these salts, recorded in d^6-DMSO, gave phosphorus resonances in the range δ(P) 24.52–28.56 ppm as given in Table 2.7. Compounds **147–149** gave single resonances suggestive of the absence of any phosphorus containing decomposition products.

Table 2.7 Selected NMR data (in ppm or Hz) for compounds **147–150**.[a]

	δ(P)	Other δ(P)	δ(H)/arom.	δ(H)/CH_2	δ(H)/NH	$^3J_{PH}$
147	24.71		6.37–6.83	4.01–4.18	5.81–5.87	18.0
148	25.05		6.44–6.90	4.04–4.19	5.69–5.81	n.r.
149	24.52		6.45–6.78	4.45–4.11		n.r.
150	28.56	–41.64	7.06–7.58	3.38–3.51		n.r.

[a] All NMR recorded in d^6-DMSO, n.r. = not resolved.

On the other hand, compound **150** gave a minor resonance (< 3%) at –41.64 ppm significantly downfield of the major phosphorus signal at 28.56 ppm, indicating the presence of a small proportion of phosphorus containing decomposition products in the NMR solvent. Unlike the $^{31}P\{^1H\}$ NMR spectra of the aniline-based phosphonium salts with multiple resonances, the $^{31}P\{^1H\}$ NMR spectra of the phenylenediamine-based phosphonium salts exhibited relatively fewer resonances. In both **148** and **149**, with Me and COPh substituents respectively, single phosphorus resonances at 25.05 and 24.52 ppm were observed. This suggested the existence of only one isomer or two possible isomers with equivalent ^{31}P resonanaces (Figure 2.2).

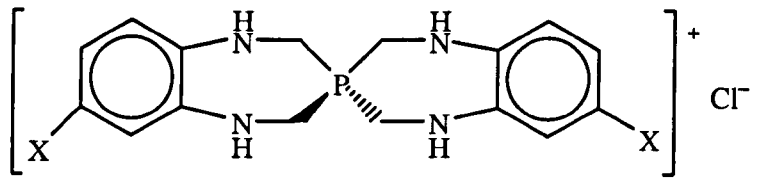

cis-arrangement

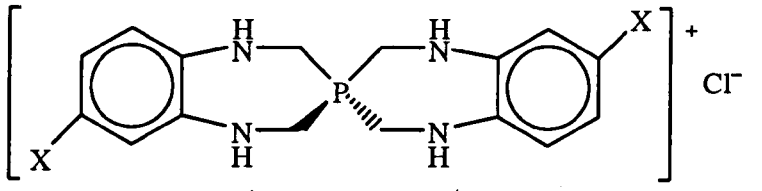

trans-arrangement

Where X = Me or COPh

Figure 2.2 Possible isomers of **148** or **149**.

Selected ^1H NMR data are given in Table 2.7. The aromatic resonances for these compounds are multiplets in the range 6.37–7.58 ppm, while the CH_2 resonances were in the range 3.38–4.19 ppm. In compounds **147** and **148**, the NH protons were also observed as multiplets in the range 5.69–5.87 ppm, they were however not observed in **149** and **150** probably being overlapped by the aromatic protons. In compound **148**, there were multiplets observed in the region 1.04–1.11 ppm, these could be assigned to the CH_3 protons.

A few X-ray quality crystals of compound **147** were obtained from the EtOH filtrate of the reaction of four equivalents of 1,2-phenylenediamine with THPC when allowed to stand for more than 24 h. Single-crystal X-ray structure determination of **147** was done which gave a phosphorus based spirocycle which co-crystallised with one mole of the phenylenediamine precursor (1,2-phenylenediamine), as shown in Figure 2.3. This represents the first crystallographic example of a spirocyclic compound in which the central atom is phosphorus. This is supported by the absence of any hits from a CSD Search.[191,192]

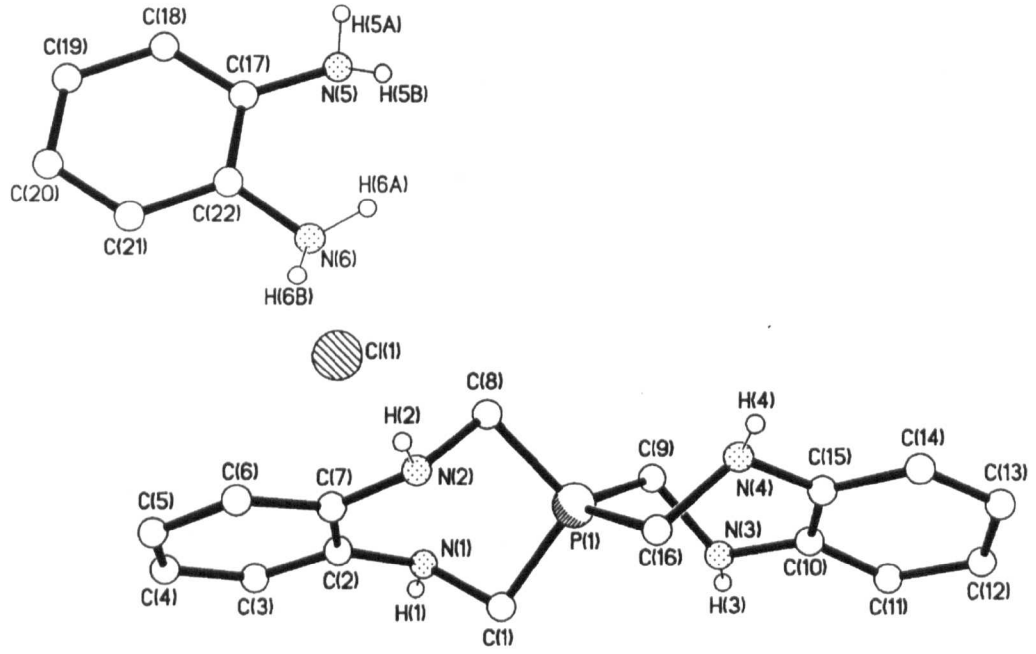

Figure 2.3 Molecular structure of $[P\{(CH_2NH)_2C_6H_4\}_2]Cl$, **147** with one mole of the precursor $1,2\text{-}C_6H_4(NH_2)_2$.

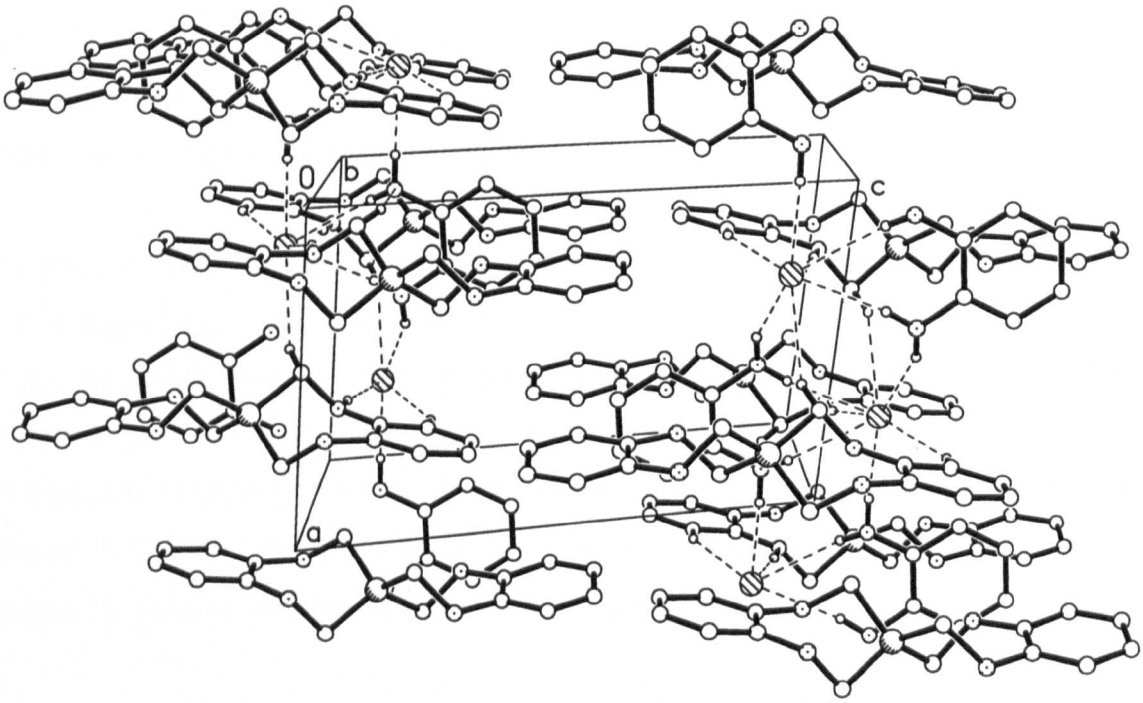

Figure 2.4 Packing plot for compound **147**·$1,2\text{-}C_6H_4(NH_2)_2$.

Table 2.8 Selected bond lengths and angles for **147**.[a]

Bond lengths (Å)		Bond lengths (Å)		Bond angles (°)	
P(1)–C(1)	1.8161(17)	C(1)–N(1)	1.464(2)	C(1)–P(1)–C(16)	115.56(8)
P(1)–C(8)	1.8124(17)	C(8)–N(2)	1.469(2)	C(8)–P(1)–C(1)	103.98(8)
P(1)–C(9)	1.8163(17)	C(9)–N(3)	1.462(2)	C(8)–P(1)–C(9)	119.66(8)
P(1)–C(16)	1.8163(17)	C(16)–N(4)	1.460(2)	C(9)–P(1)–C(16)	103.55(8)

Selected hydrogen bonding contacts

D–H···A	d(D–H) (Å)	d(H···A) (Å)	d(D···A) (Å)	<(DHA) (°)
N(1)–H(1)···Cl(1A)	0.82(2)	2.80(2)	3.5875(15)	162(2)
N(2)–H(2)···Cl(1)	0.81(2)	2.58(2)	3.3911(15)	175(2)
N(5)–H(5B)···Cl(1B)	0.84(3)	2.59(3)	3.3763(18)	155(2)
N(5)–H(5A)···Cl(1C)	0.90(3)	2.45(3)	3.3265(18)	165(2)
N(6)–H(6A)···Cl(1B)	0.87(3)	2.52(3)	3.3732(18)	168(2)

[a] Estimated standard deviations in parentheses.

The molecular geometry, bond lengths and angles were obtained from the single-crystal X-ray diffraction analysis. Selected bond lengths, angles as well as hydrogen bond lengths and angles for **147** are shown in Table 2.8.

The phosphorus atom, as in the case of **129**, exhibits a tetrahedral geometry with a C–P–C bond angle range of between 103.55(8) and 119.66(8)°. As is expected, because of the spirocycle, two of the tetrahedral angles engaged in the rings are contracted [103.98(8)° and 103.55(8)°, less than the normal tetrahedral angle of 109°] while the rest are expanded [115.56(8)° and 119.66(8)°, greater than the normal tetrahedral angle]. The average P–C and C–N bond lengths of 1.815(17) Å and 1.464(2) Å respectively are comparable to those found in **129** and other reported structures.[33,185,186]

The packing plot exhibits a pattern where two or more spirocycles and the co-crystallised precursors (1,2-phenylenediamine) are linked together *via* the chloride counterions involving N–H···Cl intermolecular H-bonding as shown in Figure 2.4. The chloride ions are again hydrogen bonded to the secondary amine hydrogens with the hydrogen bonding

data similar to those of **129** and indicative of strong hydrogen bonding. The crystal data and structure refinement details for **147** are shown in Appendix 8.2.

Reaction of the phenylenediamine derivatives of THPC with Et_3N to obtain the corresponding P(III) compounds was attempted. Unlike the case of the aniline based phosphonium salts which were soluble in acetone and reacted with Et_3N to form clean P(III) compounds in high yields, the reaction of **147** with Et_3N in acetone following a similar procedure first published by Frank *et al.*[10] could not be performed due to extreme insolubility of **147** in acetone.

2.2.2 SYNTHESIS OF COMPOUND $[P\{(CH_2NH)_2C_6H_4\}_2]BPh_4$ 151

Anion metathesis of the phenylenediamine derivatives of THPC was demonstrated when compound **147** was reacted with 1.5 equivalents of $Na[BPh_4]$ in HPLC grade MeOH. This was followed by concentration of the resulting solution under reduced pressure and addition of distilled water afforded the desired compound $[P\{(CH_2NH)_2C_6H_4\}_2]BPh_4$, **151** in high yield. Compound **151** was similarly characterised as in the case of **147**. The change in the counterion does not significantly affect the spectroscopic properties, for example the $^{31}P\{^1H\}$ NMR spectrum of **151** recorded in d^6-DMSO was similar to that of **147** with a single phosphorus resonance at δ(P) 24.53 ppm (See Experimental Section).

2.3 SYNTHESIS OF DIAZAPHOSPHORINANE LIGANDS 152–161

A range of new diazaphosphorinane ligands were synthesised by reacting some of the aniline derivatives of THPC synthesised in Section 2.1 with triethylamine using the procedure first published by Frank *et al.*[10] involving intramolecular mechanism (Scheme 1.2). The aniline derivatives of THPC react readily with triethylamine in acetone at room temperature under aerobic conditions giving a precipitate of triethylamine hydrochloride and a pale yellow oil which, after separation, followed by concentration and stirring vigorously with ethanol (Equation 2.3) gives compounds **152–161**. All the products were colourless solids and the reactions afforded the desired products in good to excellent yield as given in Table 2.9.

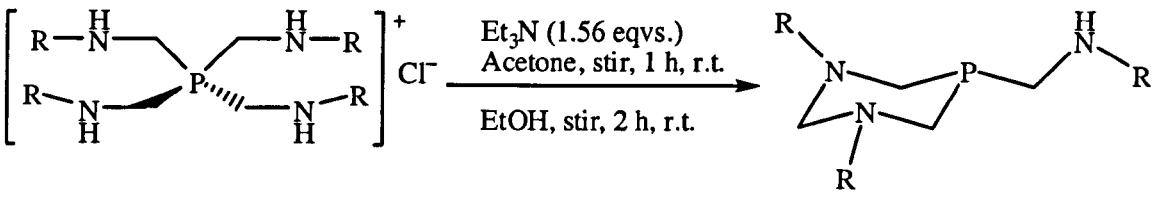

Where R = 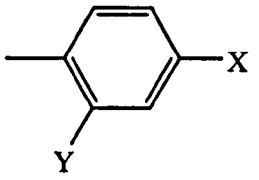

and X = Y = H, **152**; X = F, Y = H, **153**;

X = Cl, Y = H, **154**; X = Br, Y = H, **155**;

X = H, Y = F, **156**; X = I, Y = H, **157**;

X = Me, Y = H, **158**; X = Et, Y = H, **159**;

X = ^{n}Pr, Y = H, **160**; X = CMe_3, Y = H, **161**

Equation 2.3.

2.3.1 CHARACTERISATION OF COMPOUNDS 152–161

As in the previous cases, characterisation was achieved by MS, microanalysis, FT–IR, NMR and single crystal X-ray crystallography. The FAB-MS data for most of the compounds are given in Table 2.9. In all the compounds, the fragmentation pattern as in the case of the precursor aniline-based phosphonium salts (Section 2.1), give the $[XC_6H_4NHCH_2]^+$ fragment, where X is a substituent on phenyl group as the base peak, (with relative intensity of 100%), characteristic of methyleneaniline derivatives.[10] As in the case of the precursor phosphonium salts, there were two peaks due to the $[XC_6H_4NHCH_2]^+$ fragments in **154** and **155**, where X is Cl or Br respectively. In **154**, the two peaks separated by two mass units (*m/z*, 140 and 142) in approximately 3:1 ratio corresponds to the fragment, $[ClC_6H_4NHCH_2]^+$ indicative of the presence of chlorine (^{35}Cl and ^{37}Cl), similarly in **155**, the two peaks (*m/z* 184 and 186) in approximately 1:1 ratio corresponds to the fragment $[BrC_6H_4NHCH_2]^+$ indicative of the presence of bromine (^{79}Br and ^{81}Br).

The infrared spectra of all the compounds were run as pressed KBr disks and displayed the characteristic ν(NH) stretches in the range 3299–3351 cm^{-1} (Table 2.9) which is within the expected range, but higher than values for the precursor salts (Table 2.1).

Table 2.9 Percentage yield (isolated), FAB-MS and selected FT-IR data[a] (in cm^{-1}) for compounds **152–161**.

Compound	% yield	*m/z* $[M]^+$	ν(NH)
152	78	361	3301 (vs)
153	68	415	3351 (s)
154	61	464	3299 (s)
155	62	598	3299 (vs)
156	78	415	3302 (vs)
157	81	n.o.	3301 (m)
158	92	403	3301 (s)
159	75	445	3307 (s)
160	88	n.o.	3300 (s)
161	83	529	3321 (s)

[a] Recorded as a pressed KBr disk; n.o. = not observed.

Table 2.10 Microanalysis (%) and molecular formulae for compounds **152–161**.[a]

Compound	C	H	N	Molecular formula
152	72.90 (73.10)	6.61 (6.69)	11.52 (11.63)	$C_{22}H_{24}N_3P$
153	63.62 (63.61)	5.01 (5.10)	10.04 (10.12)	$C_{22}H_{21}N_3F_3P$
154	56.80 (56.83)	4.43 (4.55)	8.95 (9.04)	$C_{22}H_{21}N_3Cl_3P$
155	44.02 (44.18)	3.41 (3.54)	6.86 (7.03)	$C_{22}H_{21}N_3Br_3P$
156	63.47 (63.61)	4.97 (5.10)	10.05 (10.12)	$C_{22}H_{21}N_3F_3P$
157	36.07 (35.75)	2.75 (2.86)	5.48 (5.69)	$C_{22}H_{21}N_3I_3P$
158	74.12 (74.42)	7.36 (7.49)	10.61 (10.41)	$C_{25}H_{30}N_3P$
159	73.22 (73.26)	8.08 (8.23)	8.89 (9.15)	$C_{28}H_{36}N_3P{\cdot}0.75H_2O$
160	74.52 (74.29)	8.60 (8.75)	8.56(8.38)	$C_{31}H_{42}N_3P{\cdot}0.75H_2O$
161	76.14 (76.44)	8.96 (9.15)	7.87 (7.88)	$C_{34}H_{48}N_3P{\cdot}0.25H_2O$

[a] Calculated values in parentheses.

In the microanalytical data, observed and calculated CHN values agree within ±0.50%, hence are consistent with the compounds **152–161** (Table 2.10).

The $^{31}P\{^{1}H\}$ NMR spectra in d^{6}-DMSO were relatively clean with one or two ^{31}P signals; the major ^{31}P signal at between –48.28 and –52.87 ppm (Table 2.11). All the compounds had single phosphorus ^{31}P signals except **155**, **157**, **158** and **160** which display two ^{31}P signals, probably due to possible decomposition in the NMR solvent; the minor signal (< 10 %) being at between –54.07 and –56.82 ppm. The $^{31}P\{^{1}H\}$ NMR spectra of compounds **152–161** showed a significant upfield shift from about 10.00 ppm in the precursor phosphonium salts (phosphorus(V) compound) to about –50.00 ppm, thus confirming the formation of a new compound (phosphorus(III) compound). The single ^{31}P signal in **153** and **156**, the 4- and 2-fluoro analogues respectively suggests that there are no J_{PF} couplings in these compounds, probably due to the distance between these NMR active nuclei. In **153**, the P and F atoms are seven bonds apart, while in **156**, they are five bonds apart hence $^{7}J_{PF}$ or $^{5}J_{PF}$ couplings respectively were not observed. The spin quantum number, I of both ^{31}P and ^{19}F nuclei is greater than zero (I = ½), thus if the atoms are close to each other, coupling would have been observed in the $^{31}P\{^{1}H\}$ NMR spectra of compounds **153** and **156**.

Table 2.11 Selected NMR data (in ppm or Hz) for compounds **152–161**.[a]

	δ(P)	Other δ(P)	δ(H)/arom.[b]	δ(H)/NH[c]	δ(H)/CH_2[d]	δ(H)/CH_2[e]	δ(H)/CH_2[f]	δ(H)/CH_2[g]
152	–49.77		6.48–7.27	5.74	5.02 (13.6)	4.70 (13.6)	3.63–3.95	3.45
153	–51.06		6.30–7.38	5.72	4.87 (13.2)	4.61 (13.2)	3.53–4.04	3.36
154	–51.67		6.50–7.26	6.02	4.98 (13.6)	4.77 (13.6)	3.77–3.93	3.34
155	–51.61	–56.82	6.35–7.37	6.09	4.97 (13.6)	4.78 (13.6)	3.45–3.92	3.37
156	–52.87		6.69–7.38	5.55	4.59 (12.8)	4.50 (12.8)	3.38–3.79	3.33
157	–50.95	–56.29	6.38–7.60	6.04	4.96 (13.6)	4.77 (13.6)	3.42–3.91	3.32
158	–50.43	–54.41	6.43–7.36	5.48	4.88 (13.2)	4.58 (13.2)	3.54–3.91	3.34
159	–49.65		6.43–7.08	5.53	4.90 (13.6)	4.57 (13.6)	3.68–3.90	3.38
160	–49.36	–54.07	6.42–7.05	5.49	4.92 (12.8)	4.53 (12.8)	3.51–3.87	3.40
161	–48.28		6.37–7.26	5.48	5.12 (13.6)	4.97 (13.6)	3.55–3.89	3.42

[a] All NMR recorded in d^6-DMSO; [b]Aromatic H, m, (15 H, C_6H_5 for **152** or 12 H, C_6H_4 for **153–161**)

[c] NH proton signals, s, 1H; [d] NCH_2N protons, d, 1 H, $^2J_{HH}$ coupling in brackets

[e] NCH_2N protons, d, 1 H, $^2J_{HH}$ coupling in brackets; [f] $P(CH_2)_2N$ protons, m, 4 H

[g] PCH_2N protons, 2 H, multiplicity obscured by solvent signal

Selected ^{1}H NMR data are given in Table 2.11. The aromatic proton signals for these compounds were multiplets observed in the range 6.30–7.60 ppm. The NH proton signals were observed as singlets in all the compounds at between 5.48 and 6.09 ppm, while some of the CH_2 protons were doublets with $^{2}J_{HH}$ couplings of about 13 Hz.

Crystals of **156** were obtained from the EtOH filtrate of the reaction between $[P(CH_2NH\text{-}2\text{-}FC_6H_4)_4]Cl$ and Et_3N (Equation 2.3) when allowed to stand for more than 24 h, and the X-ray structure has been determined. The X-ray structure of **156** reveals a six-membered P–C–N–C–N–C ring, pyramidal around the phosphorus atom which is at the apical position (Figure 2.5). The structure reveals that the P atom is separated from each of the three F atoms by five bonds. This explains the absence of J_{PF} coupling in the $^{31}P\{^{1}H\}$ NMR spectrum of **156**.

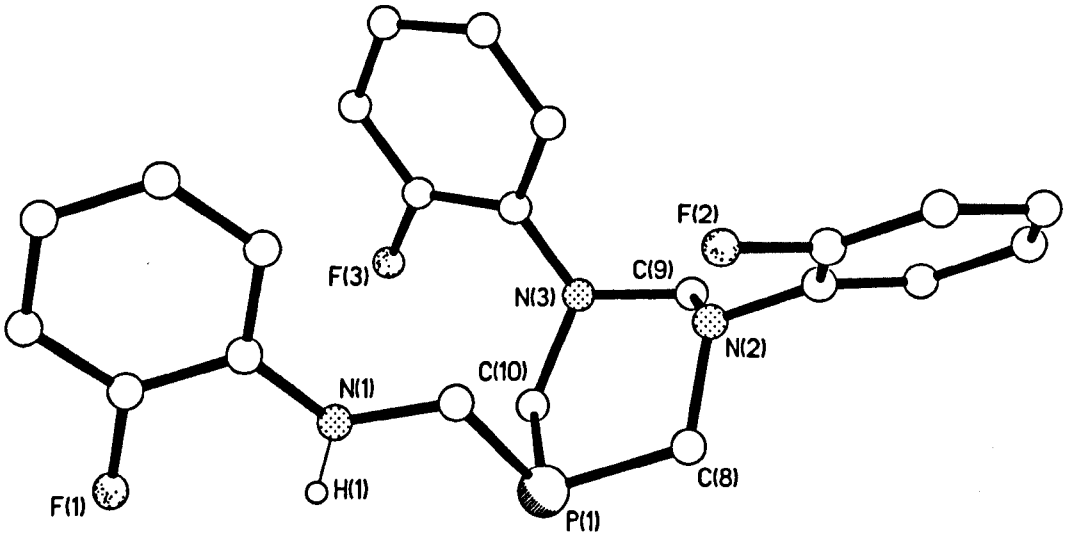

Figure 2.5 Molecular structure of **156**.

The lone pair of electrons on the phosphorus(III) centre make it a potential ligand. Unlike in the case of **129**, where there was evidence of strong hydrogen bonding obtained from the X-ray diffraction analysis, there was no evidence for hydrogen bonding in **156**. The formation of N–H···F intramolecular H-bonding, involving N(1), H(1) and F(1) is possible, but such H-bonds are rarely formed, consistent with the observation by Dunitz *et al.*[193] that covalently bound fluorine (in contrast to anionic fluoride) hardly ever acts as a hydrogen-bond acceptor.

Table 2.12 Selected bond lengths and angles for **156**.[a]

Bond lengths (Å)		Bond lengths (Å)		Bond angles (°)	
P(1)–C(1)	1.853(2)	C(1)–N(1)	1.452(3)	C(1)–P(1)–C(10)	100.93(10)
P(1)–C(8)	1.847(2)	C(8)–N(2)	1.478(3)	C(8)–P(1)–C(10)	99.26(10)
P(1)–C(10)	1.858(2)	C(10)–N(3)	1.474(3)	C(8)–P(1)–C(10)	98.87(10)

[a] Estimated standard deviations in parentheses.

Selected bond lengths and angles for **156** are given in Table 2.12; the average P–C bond length about the apical phosphorus atom is 1.853(2) Å. The P–C bond lengths are in the range 1.847(2) and 1.858(2) Å and are similar to those observed in **129** as well as in other previously reported compounds.[33,185,186] The crystal data and structure refinement details for **156** are shown in Appendix 8.3. The average C–N bond length of 1.468(3) Å is also comparable with the average C–N bond length reported for **129** and other previously reported compounds.[194] The usual pyramidal configuration is retained with C–P–C angles of 100.93(10), 99.26(10) and 98.87(10)°. These values are similar to those in the well known pyramidal compound, triphenylphosphine.[195]

2.3.2 SYNTHESIS OF COMPOUND $P(CH_2NHC_6H_5)_3$ 162

In addition to the diazaphosphorinane ligands mentioned above, the preparation of a range of new tertiary phosphines by bubbling ammonia into solutions of selected aniline derivatives of THPC earlier prepared was attempted, using the procedure first published by Frank *et al.*[10] Ammonia was bubbled into a slurry of compounds **128–134**, in acetone at room temperature and ammonium chloride precipitate was separated from the resulting yellow oil by filtration. The solvent was removed under reduced pressure and the yellow oil became viscous, the $^{31}P\{^1H\}$ NMR spectra of the corresponding oils were taken in $CDCl_3$ giving a major ^{31}P signal at –32.05 ppm with a minor ^{31}P signal similar to that of the corresponding diazaphosphorinane ligands. The work-up procedure using benzene to precipitate the desired product gave about 60% yield of compound $P(CH_2NHC_6H_5)_3$ **162** in the case of **128**, but was not successful in the other cases. The microanalytical data for compound **162** was consistent with coprecipitation of 0.25 mol of acetone (See Experimental Section). This is consistent with the molecular formula of **162**, and the IR ν(NH) stretch of **162** was at 3024 cm^{-1}, lower

than the ν(NH) stretch of 3237 cm^{-1} for the precursor compound **128**. Compound **162** was recrystallised from benzene and the $^{31}P\{^{1}H\}$ NMR spectrum in d^6-DMSO gave a 100% pure product at δ(P) –38.00 ppm which is significantly different from the major δ(P) signal of the $^{31}P\{^{1}H\}$ NMR spectrum of the precursor compound **128** which was at δ(P) 9.13 ppm.

2.4 COORDINATION STUDIES

All the diazaphosphorinane ligands with the lone pair of electrons on P are potential ligands hence were reacted with relevant Ru(II), Rh(III), Ir(III), Pd(II) and Pt(II) precursors to form the expected complexes in good to excellent yields.

2.4.1. SYNTHESIS OF RUTHENIUM(II) DIAZAPHOSPHORINANE COMPLEXES 163 AND 164

Two organometallic ruthenium(II) complexes were synthesised by reacting **152** or **153** respectively with $\{RuCl_2(\eta^6\text{-}p\text{-cymene})\}_2$ in CH_2Cl_2 at room temperature.

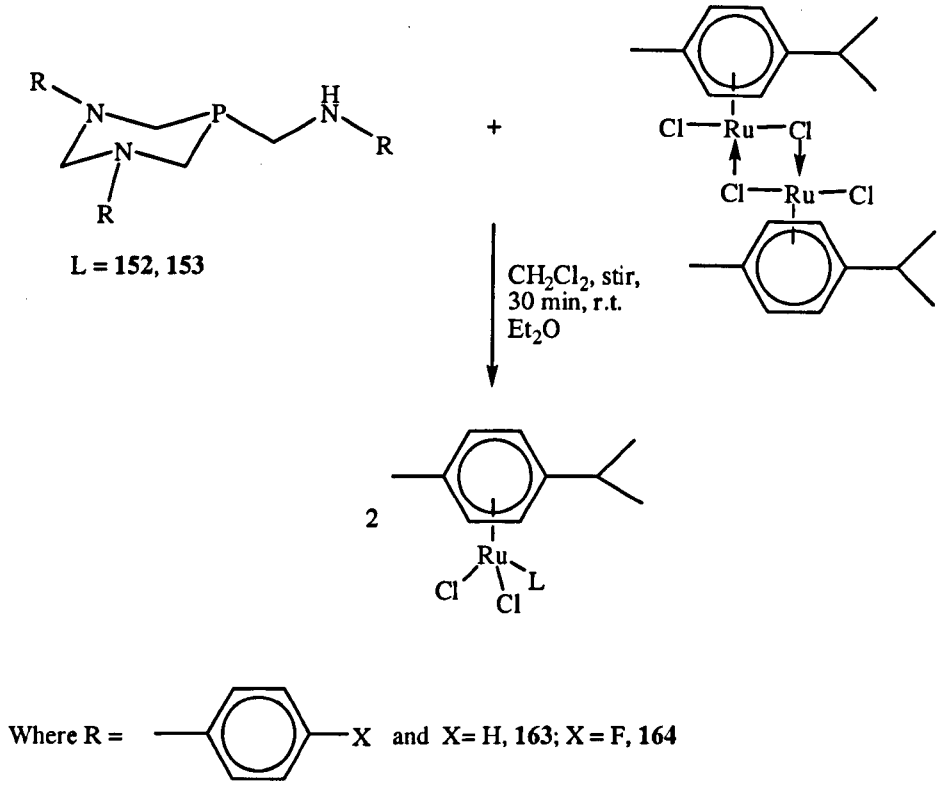

Equation 2.4.

Isolation of the products was achieved by precipitation with Et_2O after concentration of the solution; all the complexes were orange solids. In both cases the ligand readily

reacts to form the desired ruthenium(II) complexes **163** and **164** in excellent yield (Table 2.13). Two equivalents of the ligand react by standard bridge cleavage of the ruthenium dimer to form two moles of the "piano-stool" ruthenium(II) complex according to Equation 2.4.[196]

2.4.1.1 CHARACTERISATION OF COMPOUNDS 163 AND 164

Characterisation of the complexes was achieved by MS, microanalysis, FT-IR and NMR spectroscopy. The data obtained from the MS, microanalysis, FT–IR and NMR techniques are given in Tables 2.13–2.15.

The FAB-MS data for compounds **163** and **164** are given in Table 2.13, and show the molecular ion $[M]^+$. The fragmentation pattern as in the case of the precursor diazaphospharinane compounds (Section 2.3), give the $[XC_6H_4NHCH_2]^+$ fragment, where X is a substituent on phenyl group as the base peak, (with relative intensity of 100%), characteristic of methyleneaniline derivatives.[10] In compound **163**, where X = H, the base peak at *m/z* (106), corresponds to the fragment $[C_7H_8N]^+$, while in **164**, where X = F, the base peak at *m/z* (124), corresponds to the fragment $[C_7H_7FN]^+$.

Table 2.13 Percentage yield (isolated), FAB-MS and selected FT-IR data[a] (in cm^{-1}) for compounds **163** and **164**.

	% yield	*m/z* $[M]^+$	ν(NH)	ν(RuCl)
163	92	668	3352 (w)	295 (w)
164	86	722	3348 (w)	295 (m)

[a] Recorded as a pressed KBr disk.

Selected diagnostic IR spectral data are given in Table 2.13. The terminal stretching vibration of the ν(Ru-Cl) bands for both complexes observed at 295 cm^{-1} was comparable to those of other previously reported similar ruthenium(II) phosphine complexes.[197]

The microanalytical data are given in Table 2.14; values agree within acceptable limits and are consistent with the formulae of the ruthenium(II) complexes **163** and **164**.

Coprecipitation of solvent molecules was evident in the case of complex **163** as obseved in the microanalytical data in Table 2.14.

Table 2.14 Microanalysis (%) and molecular formulae for compounds **163** and **164**.[a]

Compound	C	H	N	Molecular formula
163	53.10 (52.67)	5.27 (5.36)	5.49 (5.58)	$C_{32}H_{38}N_3PRuCl_2 \cdot CH_2Cl_2$
164	53.05 (53.26)	4.89 (4.82)	5.90 (5.82)	$C_{32}H_{35}N_3PF_3RuCl_2$

[a] Calculated values in parentheses.

The $^{31}P\{^1H\}$ NMR spectra of these complexes recorded in d^6-DMSO showed single phosphorus resonances (Table 2.15), suggestive of the absence of any phosphorus containing decomposition products. These phosphorus signals are significantly downfield of the δ(P) values for the corresponding precursor diazaphosphorinane ligands, as given in Table 2.11 and are in good agreement with *P*-monodentate coordination.

Table 2.15 Selected NMR data (in ppm or Hz)[a] for compounds **163** and **164**.

	δ(P)	δ(H)/arom	δ(H)/NH[b]	δ(H)/CH_2	δ(H)/4-$CH_3C_6H_4CH(CH_3)_2$[d]
163	14.62	6.30–7.25	5.33 (13.6)	3.27–4.49	1.92, (5.79–5.90), 2.63, 1.14 (6.8)[c]
164	14.27	6.98–7.57	5.12 (12.8)	3.71–4.39	1.92, (5.87–5.90), 2.61, 1.16 (6.8)[c]

[a] All NMR spectra were recorded in d^6-DMSO;

[b] Doublets, $^3J_{PH}$ coupling in brackets; [c] Doublets, $^3J_{HH}$ coupling in brackets

[d] *p*-Cymene resonances: CH_3, C_6H_4, CH and $(CH_3)_2$ protons respectively.

Selected ^1H NMR spectral data are given in Table 2.15. The $-C\underline{H}(CH_3)_2$ protons in the *p*-cymene (Figure 2.6) displayed a characteristic septet at *ca.* 2.60 ppm indicating that it is adjacent to six hydrogens $[-(CH_3)_2]$, while the CH_3 protons were at about δ(H) 1.90 ppm not significantly different from those of other related ruthenium(II) complexes.[198]

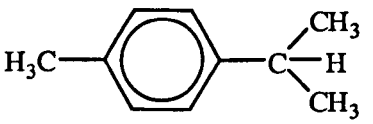

Figure 2.6 Structure of *p*-cymene.

2.4.2. SYNTHESIS OF RHODIUM(III) AND IRIDIUM(III) DIAZAPHOSPHORINANE COMPLEXES 165–168

The dimeric chloro bridged complexes $[MCl_2(\eta^5\text{-}Cp^*)]_2$, M = Rh or Ir are known to undergo chloro bridge cleavage reactions leading to the formation of mononuclear complexes.[196] In these reactions, the metal complexes have a classic "piano stool" geometry as shown in Equation 2.5.

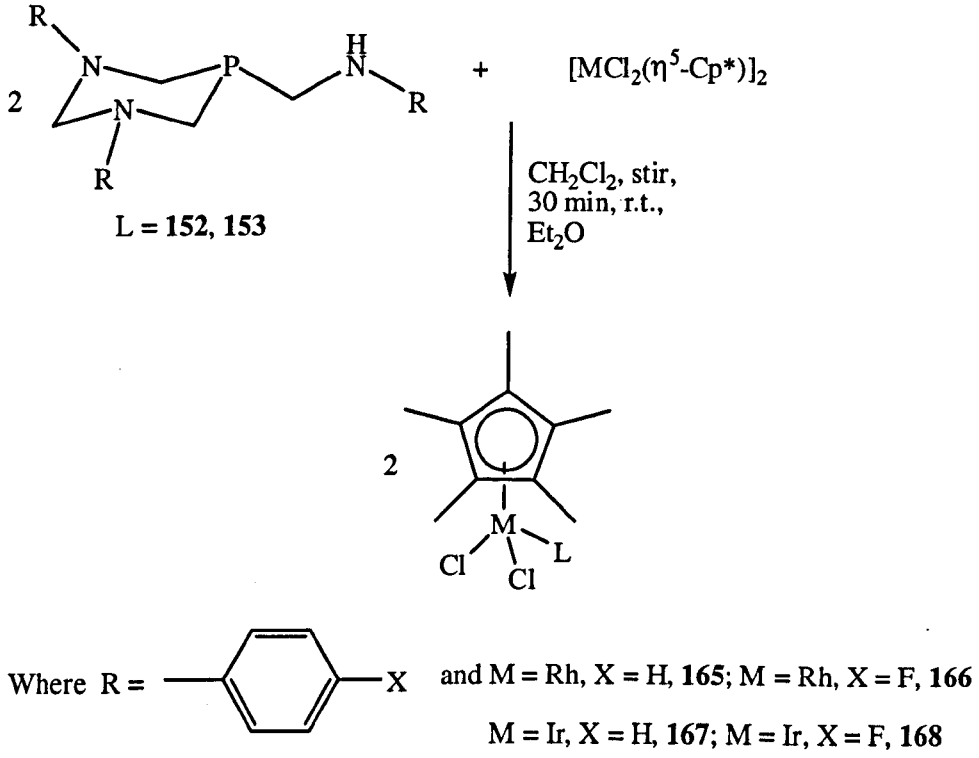

Equation 2.5

Two complexes each of rhodium(III) and iridium(III) were synthesised by reacting compound **152** or **153** with $[MCl_2(\eta^5\text{-}Cp^*)]_2$, M = Rh or Ir in 2:1 molar ratio in CH_2Cl_2 at room temperature under aerobic conditions. This was followed by precipitation with Et_2O, upon concentration of the solution under reduced pressure (Equation 2.5). In all the cases, the desired orange coloured solid M(III) complexes were obtained in good to excellent yields (> 80%) as given in Table 2.16.

2.4.2.1 CHARACTERISATION OF COMPOUNDS 165–168

The complexes were characterised as in the previous cases by both analytical and spectroscopic (IR, NMR) methods and the results given in Tables 2.16–2.18. Single

crystal X-ray crystallography was also used for **166** and **168** where suitable crystals were obtained.

Table 2.16 Percentage yield (isolated), FAB-MS and selected FT-IR data[a] (in cm^{-1}) for compounds **165–168**.

	% yield	*m/z* $[M]^+$	ν(NH)	ν(MCl)
165	92	670	3316 (w)	283 (w)
166	85	723	3306 (m)	279 (w)
167	74	759	3314 (w)	279 (w)
168	84	814	3329 (m)	289 (w)

[a] Recorded as a pressed KBr disk; MCl = RhCl or IrCl.

The FAB–MS data for compounds **165–168** are given in Table 2.16 and shows the molecular ion, $[M]^+$ and the fragmentation pattern was similar to those previously observed in the case of the ruthenium(II) complexes **163** and **164**..

The FT–IR spectra for compounds **165–168** were recorded in the solid state as pressed KBr disks (Table 2.16). The ν(NH) stretches were similar to those of the free ligands (**152, 153**) and were observed at *ca.* 3300 cm^{-1}. The M–Cl stretches were very weak and similar to those of the ruthenium(II) complexes synthesised in Section 2.4.1.

Table 2.17 Microanalysis (%) and molecular formulae for compounds **165–168**.[a]

	C	H	N	Molecular formula
165	48.03 (47.75)	4.69 (5.09)	5.11 (4.88)	$C_{32}H_{39}N_3PRhCl_2 \cdot 2.25CH_2Cl_2$
166	60.70 (60.92)	5.95 (5.87)	3.32 (3.49)	$C_{32}H_{36}N_3F_3PRhCl_2 \cdot 0.25CH_2Cl_2$
167	47.66 (47.77)	4.93 (4.96)	5.18 (5.10)	$C_{32}H_{39}N_3PIrCl_2 \cdot 0.75CH_2Cl_2$
168	44.21 (44.11)	4.37 (4.26)	4.79 (4.68)	$C_{32}H_{36}N_3F_3PIrCl_2 \cdot CH_2Cl_2$

[a] Calculated values in parentheses.

All the complexes precipitated with some amount of solvent as shown by the microanalytical data (Table 2.17), and the values agree within acceptable limits and are

consistent with the formulae of the rhodium(III), [**165**, **166**] and iridium(III) [**167**, **168**] complexes respectively.

The NMR spectral data recorded in d^6-DMSO are given in Table 2.18. The $^{31}P\{^1H\}$ NMR spectra showed the expected doublets in **165** and **166**, with an average $^1J_{PRh}$ coupling constant of 142 Hz comparable with other compounds reported previously.[199] On the other hand, the $^{31}P\{^1H\}$ NMR spectra of **167** and **168** showed single phosphorus resonances and are significantly downfield in comparison to the corresponding precursor ligands. For example the δ(P) value for **167** is −12.74 ppm, but the value for the corresponding precursor ligand, **152** was –49.77 ppm (Table 2.11).

Table 2.18 Selected NMR data (in ppm or Hz) for **165–168**.[a]

	δ(P)	δH/(arom.)	δH/NH[c]	δH/(η^5-Cp*)	δH/(CH_2)	$^4J_{PH}$
165	16.38(143)[b]	6.06–7.06	5.22 (14.0)	1.47	3.38–4.32	n.r.
166	15.13(141)[b]	6.24–7.23	5.17 (15.2)	1.64	3.60–4.40	3.6
167	−12.74	6.20–7.23	5.51(14.0)	1.68	3.62–4.50	n.r.
168	−15.20	6.10–7.04	5.18(14.8)	1.67	3.51–4.48	n.r.

[a]All NMR spectra were recorded in d^6-DMSO; [b]Doublets $^1J_{PRh}$ coupling in brackets; [c]Doublets $^3J_{PH}$ coupling in brackets, n.r. = not resolved.

In the ^1H NMR spectra, there was either no long range coupling between phosphorus and the ring methyl protons of the pentamethylcyclopentadienyl moiety (C_5Me_5), $^4J_{PH}$, or this was not resolved, hence showed as a singlet in the case of **165**, **167** and **168**, while such couplings were evident in the case of **166** and showed as a doublet at 1.64 ppm, consistent with the range 1.47–1.68 ppm displayed by the C_5Me_5 protons in similar rhodium(III) and iridium(III) complexes.[196]

A few X-ray quality crystals of compounds **166** and **168** were obtained by layering petroleum ether (b.p. 40–60 °C) on a CH_2Cl_2 solution and slow vapour diffusion of diethyl ether into CH_2Cl_2 solution kept for several days respectively. The X-ray structures have been determined and confirm a classic "piano-stool" geometry formed by the pentamethylcyclopentadienyl ligand being the seat and the three "legs", being

the phosphorus donor of the *P*-monodentate diazaphosphorinane ligand and the two chlorides in each case and also showed that **166** and **168** were isostructural (Figures 2.7 and 2.8). All the hydrogen atoms except those on N(1) and N(4) in the two independent molecules shown in Figures 2.7 and 2.8 have been omitted for clarity. The η^5-coordination is illustrated by thick dashed lines between the Rh or Ir atoms and the centroid of the pentamethylcyclopentadienyl ring (Figures 2.7 and 2.8).

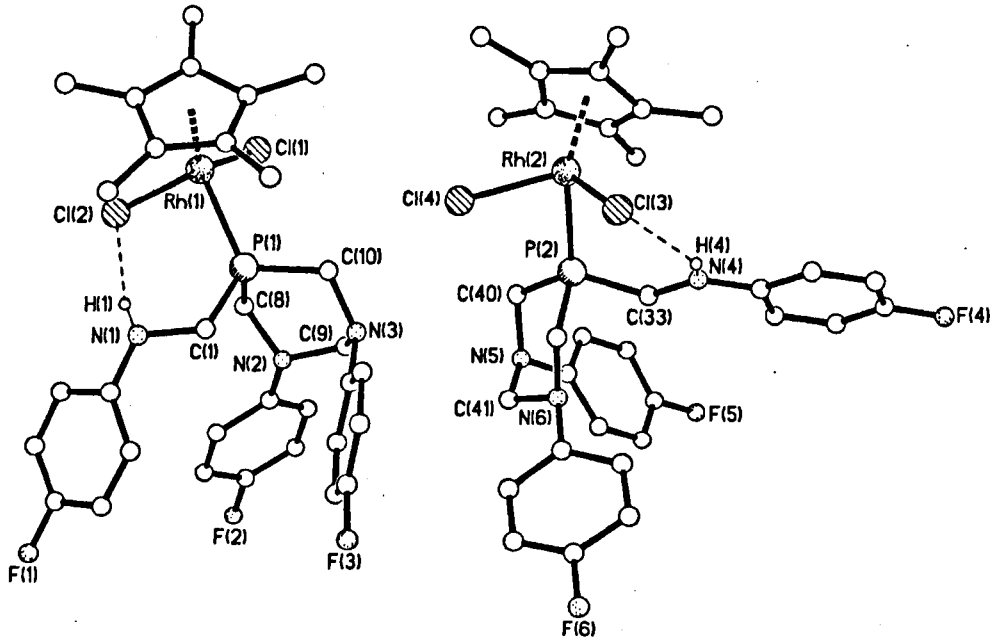

Figure 2.7 Molecular structures of two independent molecules of **166**. $0.5CH_2Cl_2$ solvent molecule of crystallisation has been omitted for clarity.

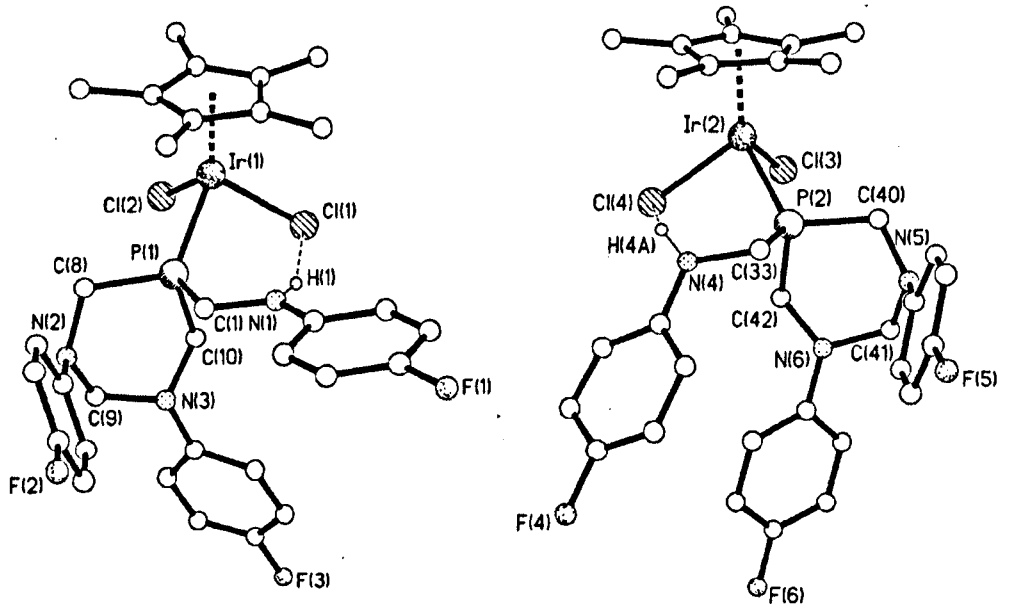

Figure 2.8 Molecular structures of two independent molecules of **168**. $0.5CH_2Cl_2$ solvent molecule of crystallisation has been omitted for clarity.

Selected bond lengths and angles for compounds **166** and **168** are given in Tables 2.19 and 2.20. Two independent molecules of **166** and **168** are shown in Figures 2.7 and 2.8 respectively. In each case, the bond lengths and angles of the independent molecules were not significantly different (Tables 2.19 and 2.20).

Table 2.19 Selected bond lengths and angles for **166**.[a]

Bond lengths (Å)		Bond lengths (Å)		Bond angles (°)	
Rh(1)–P(1)	2.283(14)	C(1)–N(1)	1.450(7)	P(1)–Rh(1)–Cl(1)	88.34(5)
Rh(1)–Cl(1)	2.404(15)	C(8)–N(2)	1.466(7)	P(1)–Rh(1)–Cl(2)	87.77(5)
Rh(1)–Cl(2)	2.420(14)	C(10)–N(3)	1.475(7)	Cl(1)–Rh(1)–Cl(2)	90.75(6)
Rh(1)–$C_{av.}$	2.186(5)	C(2)–N(1)	1.380(8)	C(1)–P(1)–C(10)	105.6(2)
P(1)–C(1)	1.837(5)	C(11)–N(2)	1.425(7)	C(1)–P(1)–C(8)	101.8(3)
P(1)–C(8)	1.834(5)	C(17)–N(3)	1.427(7)	C(8)–P(1)–C(10)	99.7(3)
P(1)–C(10)	1.838(5)	C(33)–N(4)	1.429(7)	P(2)–Rh(2)–Cl(3)	88.13(5)
Rh(2)–P(2)	2.2795(13)	C(40)–N(5)	1.458(7)	P(2)–Rh(2)–Cl(4)	85.92(5)
Rh(2)–Cl(3)	2.4182(14)	C(42)–N(6)	1.477(6)	Cl(3)–Rh(2)–Cl(4)	93.36(5)
Rh(2)–Cl(4)	2.4042(14)	C(34)–N(4)	1.384(8)	C(33)–P(2)–C(40)	105.7(3)
Rh(2)–$C_{av.}$	2.187(5)	C(43)–N(5)	1.425(7)	C(33)–P(2)–C(42)	100.3(2)
P(2)–C(33)	1.835(5)	C(49)–N(6)	1.436(7)	C(40)–P(2)–C(42)	98.9(3)
P(2)–C(40)	1.849(5)	P(2)–C(42)	1.829(5)		

Selected hydrogen bonding contacts

D–H···A	d(H···A) (Å)	d(D···A) (Å)	<(DHA) (°)
N(1)–H(1)···Cl(2)	2.52(7)	3.301(5)	163(6)
N(4)–H(4)···Cl(3)	2.78(7)	3.441(6)	149(7)

[a] Estimated standard deviations in parentheses.

The M–P and M–Cl bond lengths for **166** and **168** were similar and are comparable to other previously reported compounds.[138] The similarity between the Rh–P and Ir–P bond lengths demonstrates the similarity in atomic radii between second and third row transition metals [Rh and Ir], as a consequence of the lanthanide contraction.

Table 2.20 Selected bond lengths and angles for **168**.[a]

Bond lengths (Å)		Bond lengths (Å)		Bond angles (°)	
Ir(1)–P(1)	2.2691(19)	C(1)–N(1)	1.437(5)	P(1)–Ir(1)–Cl(1)	88.46(3)
Ir(1)–Cl(1)	2.4182(9)	C(8)–N(2)	1.450(5)	P(1)–Ir(1)–Cl(2)	86.51(3)
Ir(1)–Cl(2)	2.4074(9)	C(10)–N(3)	1.480(5)	Cl(1)–Ir(1)–Cl(2)	90.25(4)
Ir(1)–C_{av}	2.193(4)	C(2)–N(1)	1.386(5)	C(1)–P(1)–C(10)	100.58(18)
P(1)–C(1)	1.831(4)	C(11)–N(2)	1.414(5)	C(1)–P(1)–C(8)	104.91(18)
P(1)–C(8)	1.852(4)	C(17)–N(3)	1.424(5)	C(8)–P(1)–C(10)	98.87(19)
P(1)–C(10)	1.826(4)	C(33)–N(4)	1.464(5)	P(2)–Ir(2)–Cl(3)	88.55(4)
Ir(2)–P(2)	2.2780(10)	C(40)–N(5)	1.469(5)	P(2)–Ir(2)–Cl(4)	88.28(3)
Ir(2)–Cl(3)	2.4094(10)	C(42)–N(6)	1.466(5)	Cl(3)–Ir(2)–Cl(4)	87.92(4)
Ir(2)–Cl(4)	2.4225(10)	C(34)–N(4)	1.386(6)	C(33)–P(2)–C(40)	105.54(18)
Ir(2)–C_{av}	2.195(4)	C(43)–N(5)	1.427(5)	C(33)–P(2)–C(42)	102.30(19)
P(2)–C(33)	1.839(4)	C(49)–N(6)	1.422(5)	C(40)–P(2)–C(42)	99.58(18)
P(2)–C(40)	1.846(4)				
P(2)–C(42)	1.835(4)				

Selected hydrogen bonding contacts

D–H···A	d(H···A) (Å)	d(D···A) (Å)	<(DHA) (°)
N(1)–H(1)···Cl(1)	2.69	3.508(4)	156.0
N(4)–H(4A)···Cl(4)	2.79	3.343(4)	122.1

[a] Estimated standard deviations in parentheses.

There is evidence of intramolecular hydrogen bonding in the complexes as shown in Figures 2.7 and 2.8 and Tables 2.19 and 2.20. The crystal data and structure refinement details for compounds **166** and **168** are shown in Appendices 8.4 and 8.5 respectively.

2.4.3 SYNTHESIS OF PALLADIUM(II) DIAZAPHOSPHORINANE COMPLEXES 169–177

A range of palladium(II) complexes were synthesised by reacting some of the diazaphosphorinane ligands, synthesised in Section 2.3, with $PdCl_2(COD)$ in CH_2Cl_2 at room temperature under aerobic conditions followed by precipitation with diethyl ether

upon concentration of the solution under reduced pressure. In all cases the ligands readily react to form the desired palladium complex in good yield (Table 2.21). Two equivalents of the ligand react with $PdCl_2(COD)$ to form either the *cis* or *trans* isomers according to Equation 2.6. All the products were yellow solids.

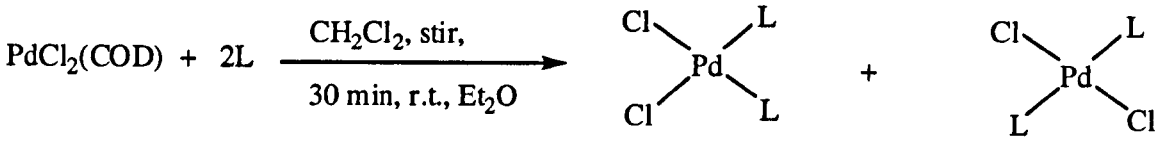

Where L =

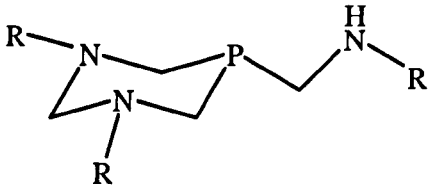

R =

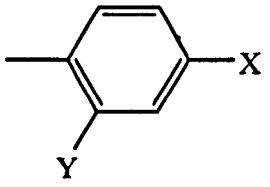

and X = Y = H, **169**; X = F, Y = H, **170**;

X = Cl, Y = H, **171**; X = Br, Y = H, **172**;

X = H, Y = F, **173**; X = Me, Y = H, **174**;

X = Et, Y = H, **175**; X = ^{n}Pr, Y = H, **176**;

X = CMe_3, Y = H, **177**

Equation 2.6.

2.4.3.1 CHARACTERISATION OF COMPOUNDS 169–177

As in the previous cases characterisation was achieved by MS, microanalysis, FT-IR, NMR spectroscopy and single crystal X-ray crystallography. The results are given in Tables 2.21–2.23. In the FAB–MS data (Table 2.21); the fragmentation pattern involves at least the loss of one chloride ligand coordinated to the Pd(II) centre, consistent with the molecular formulae of the complexes.

The ν(NH) stretches of the ligands slightly increased on coordination to the metal centre, for example the ν(NH) stretch in the precursor **159** was 3307 cm^{-1} but on coordination in

175, it became 3337 cm^{-1}. The infrared spectra of the metal complexes showed two M–Cl stretches (Table 2.21), indicating the formation of a *cis* isomer in all cases.

Table 2.21 Percentage yield (isolated), FAB-MS and selected FT-IR data[a] (in cm^{-1}) for **169–177.**

	% yield	*m/z* $[M-Cl]^+$	ν(NH)	ν(PdCl)
169	93	864	3339 (m)	263, 295
170	75	972	3335 (w)	278, 303
171	89	1069	3319 (w)	279, 303
172	79	1337	3415 (w)	276, 307
173	82	972	3426 (w)	287, 311
174	77	-	3426 (m)	287, 311
175	77	-	3337 (s)	278, 303
176	85	1115	3333 (m)	283, 304
177	75	1200	3348 (m)	289, 316

[a] Recorded as a KBr disk.

Table 2.22 Microanalysis (%) and molecular formulae for compounds **169–177.**[a]

	C	H	N	Molecular formula
169	57.76 (57.68)	5.49 (5.31)	9.13 (9.12)	$C_{44}H_{48}N_6P_2PdCl_2 \cdot 0.25CH_2Cl_2$
170	52.42 (52.42)	4.33 (4.20)	8.37 (8.34)	$C_{44}H_{42}N_6P_2F_6PdCl_2$
171	44.77 (45.35)	3.68 (3.72)	7.03 (7.05)	$C_{44}H_{42}N_6P_2PdCl_8 \cdot CH_2Cl_2$
172	36.80 (37.06)	3.15 (3.04)	5.22 (5.76)	$C_{44}H_{42}N_6P_2Br_6PdCl_2 \cdot CH_2Cl_2$
173	51.75 (51.63)	4.29 (4.16)	8.15 (8.16)	$C_{44}H_{42}N_6P_2F_6PdCl_2 \cdot 0.25CH_2Cl_2$
174	59.93 (60.02)	6.07 (6.06)	8.07 (8.36)	$C_{50}H_{60}N_6P_2PdCl_2 \cdot 0.25CH_2Cl_2$
175	62.00 (62.00)	6.85 (6.71)	7.42 (7.71)	$C_{56}H_{72}N_6P_2PdCl_2 \cdot 0.25CH_2Cl_2$
176	63.43 (63.69)	7.42 (7.26)	7.39 (7.16)	$C_{62}H_{84}N_6P_2PdCl_2 \cdot 0.25CH_2Cl_2$
177	63.54 (63.49)	7.36 ((7.56)	6.44 (6.80)	$C_{68}H_{96}N_6P_2PdCl_2 \cdot 0.75CH_2Cl_2$

[a] Calculated values in parentheses.

Coprecipitation of the solvent is possible in these complexes; this is in agreement with the microanalytical data given in Table 2.22. Agreements between the observed and calculated CHN values are consistent with the formulations of the palladium complexes **169–177.**

The $^{31}P\{^{1}H\}$ NMR spectra of the complexes recorded in d^6-DMSO gave a major phosphorus resonance in the range 5.99–9.75 ppm and minor phosphorus resonances (**171–173**) in the range 12.61–16.54 ppm as given in Table 2.23. In all cases significant downfield ^{31}P resonances in comparison to the corresponding free ligands were observed. For example the δ(P) value for **169** is 8.21 ppm, but the value for the corresponding free ligand, **152** was –49.77 ppm (Table 2.11). This indicates that coordination or complexation has taken place, but does not give any clue as to whether the complex is *cis* or *trans*.

In **171–173**, where there were two ^{31}P resonances [range 5.99–9.75 and 12.61–16.54 ppm], the possibility of the complexes existing as a mixture of *cis* and *trans* isomers in solution cannot be ruled out even though in the solid state only the *cis* isomer was observed as supported by IR spectroscopy. A similar result was obtained in the case of $[PdCl_2\{Ph_2N(H)C_5H_3(Cl\text{-}5)N\}_2$ which gave two singlets, δ(P) 29.7 and 15.4 ppm in $CDCl_3$ solution consistent with presence of *cis* and *trans* isomers in solution, but solid state IR spectrum indicated only the presence of the *cis* isomer (ν_{PdCl} 306, 282 cm^{-1})].[200] The two Pd–Cl stretches in the infrared spectra of these complexes (Table 2.21) is indicative of the formation of the *cis* isomer in all cases, had *trans* isomer been obtained, only one Pd–Cl stretch would have been expected. The reaction of $PtCl_2$(COD) with two equivalents of these ligands (**156** and **158**) in $CDCl_3$ at room temperature (NMR scale) gave a product whose $^{31}P\{^{1}H\}$ spectrum showed a single $^{31}P\{^{1}H\}$ resonance flanked by two ^{195}Pt satellites [$^{1}J_{PPt}$, *ca.* 3400 Hz] indicative of the *cis* disposition of the diazaphosphorinane ligands. Thus the diazaphosphorinane ligands readily displace labile ligands from Pd or Pt complexes such as MCl_2(COD) to form *cis* MCl_2L_2 complexes [M = Pd, Pt; L = diazaphosphorinane ligand].

Table 2.23 Selected NMR data (in ppm or Hz)[a] for **169–177**.

	δ(P)	Other ^{31}P signals	δ(H)/arom.[b]	δ(H)/NH[c]	δ(H)/CH_2[d]	δ(H)/CH_2[e]	δ(H)/CH_2[f]	δ(H)/CH_2[g]	δ(H)/CH_2[h]
169	8.21		6.92–7.35	6.61 (14.4)	5.18 (13.6)	4.38 (13.6)	3.856 (4.8)	3.70 (6.4)	3.34
170	8.54		6.85–7.17	6.59 (14.4)	5.03 (13.6)	4.26 (12.0)	3.96 (4.8)	3.71 (6.8)	3.33
171	9.37	16.54	6.65–7.52	6.21 (14.6)	5.14 (13.2)	4.27 (13.2)	3.72 (5.6)	3.39 (6.4)	3.30
172	9.75	15.96	6.68–7.59	6.38 (16.0)	5.13 (13.6)	4.28 (13.2)	3.71 (6.4)	3.62 (6.0)	3.45
173	5.99	12.61	6.61–7.32	6.32 (16.0)	4.69 (12.4)	4.27 (14.4)	3.86 (4.8)	3.72 (6.0)	3.40
174	8.59		6.78–7.12	6.29 (16.0)	5.02 ((13.6)	4.23 (14.2)	3.81 (4.8)	3.65 (6.0)	3.42
175	11.19		6.83–7.27	6.81 (16.0)	4.82 (13.2)	4.33 (13.2)	3.48 (4.8)	3.06 (6.4)	2.60
176	9.01		6.72–7.54	6.43 (14.0)	5.07 (13.2)	4.28 (13.6)	3.83 (4.8)	3.65 (6.4)	3.39
177	7.18		6.91–7.35	6.53 (14.4)	5.12 (12.8)	4.35 (13.2)	3.73 (5.6)	3.12 (6.4)	2.67

[a] All NMR recorded in d^6-DMSO; [b]Aromatic H, m, (15 H, C_6H_5 for **169** or 12 H, C_6H_4 for **170–177**)

[c] NH proton signals, (t, 1H, $^3J_{PH}$ coupling in brackets); [d] NCH_2N protons, (d, 1 H, $^2J_{HH}$ coupling in brackets)

[e] PCH_2N protons, (dd, 2 H, $^3J_{HH}$ coupling in brackets); [f] $N(CH_2)N$ protons, (dd, 1 H, $^2J_{HH}$ coupling in brackets)

[g] PCH_2N protons, (d, 2 H, $^2J_{PH}$, coupling in brackets); [h] PCH_2N protons, 2 H, multiplicity obscured by solvent signals

Further confirmation for the *cis* arrangement comes from single crystal X-ray diffraction analyses of **169** and **170**, obtained in both cases by the slow vapour diffusion of Et_2O into solutions of the complexes in CH_2Cl_2 over several days. The crystal data and structure refinement details for **169** and **170** are shown in Appendices 8.6 and 8.7 respectively.

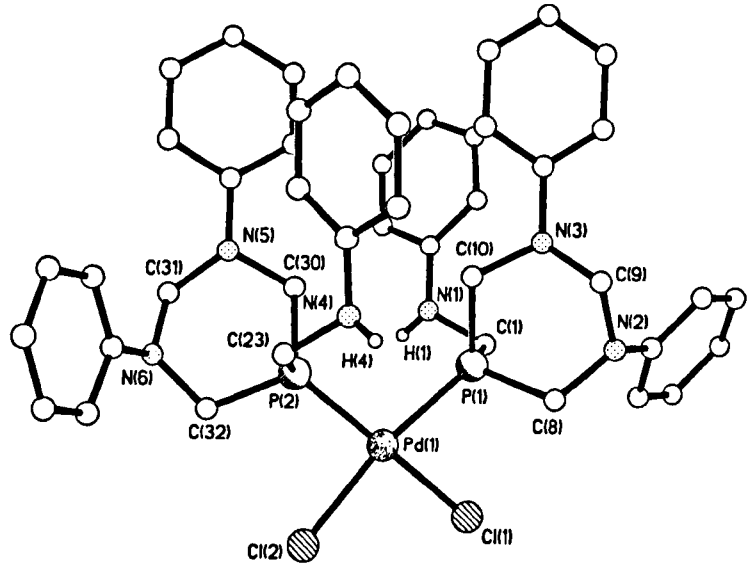

Figure 2.9 Molecular structure of **169**. CH_2Cl_2 solvent molecule of crystallisation has been omitted for clarity.

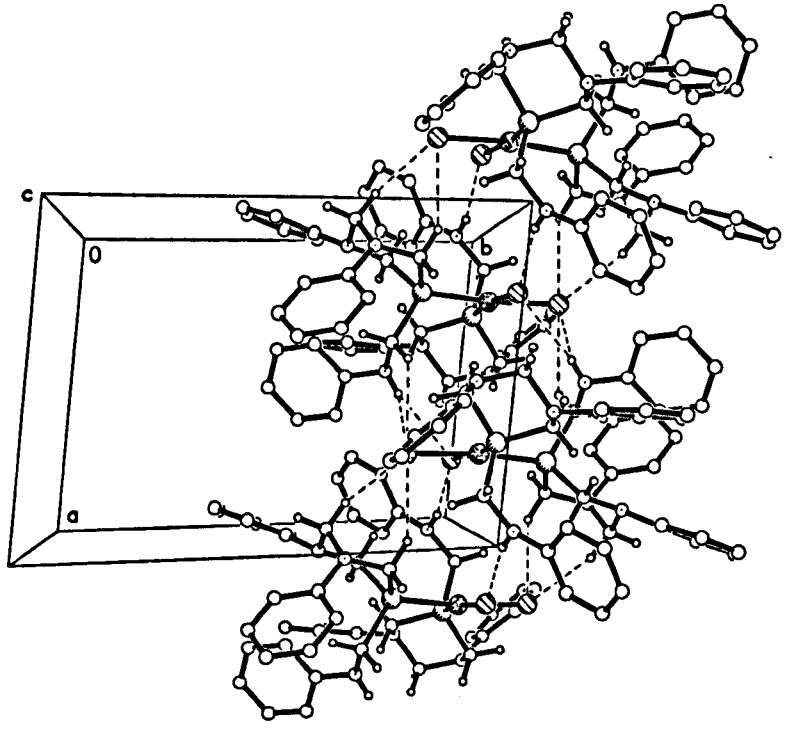

Figure 2.10 Packing plot for compound **169** showing N–H···Cl and C–H_2···Cl interactions between molecules forming a chain parallel to *a*.

Table 2.24 Selected bond lengths and angles for **169**.[a]

Bond lengths (Å)		Bond lengths (Å)		Bond angles (°)	
Pd(1)–P(1)	2.2519(11)	P(1)–C(1)	1.851(4)	P(1)–Pd(1)–P(2)	99.65(4)
Pd(1)–P(2)	2.2607(10)	P(2)–C(23)	1.851(4)	P(1)–Pd(1)–Cl(1)	81.79(4)
Pd(1)–Cl(1)	2.3710(10)	N(1)–C(1)	1.450(5)	P(2)–Pd(1)–Cl(2)	89.18(4)
Pd(1)–Cl(2)	2.3778(10)	N(4)–C(23)	1.445(5)	Cl(1)–Pd(1)–Cl(2)	89.83(4)

Hydrogen bonds

D–H···A	d(H···A) (Å)	d(D···A) (Å)	<(DHA) (°)
N(1)–H(1)···Cl(2A)	2.75(5)	3.532(4)	166(4)
N(4)–H(4)···Cl(1B)	2.75(4)	3.310(4)	127(4)
N(4)–H(4)···Cl(2B)	2.81(4)	3.578(4)	158(4)

[a] Estimated standard deviations in parentheses.

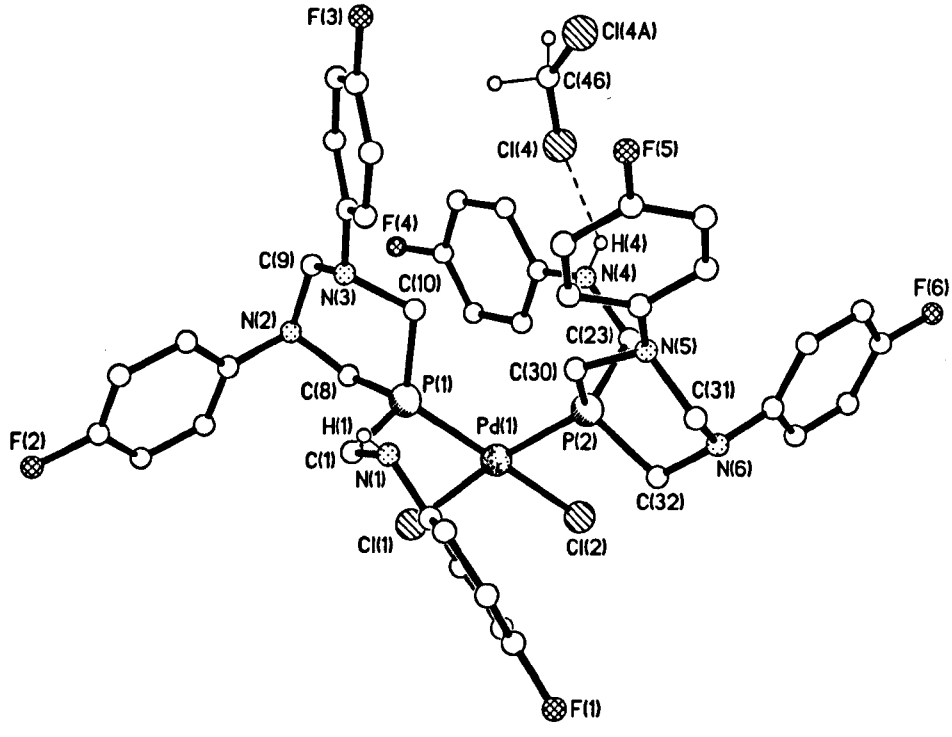

Figure 2.11 Molecular structure of **170** showing H-bond to CH_2Cl_2 solvent molecule of crystallisation. Second CH_2Cl_2 solvent molecule of crystallisation has been omitted for clarity.

In both cases, the complex adopts a *cis* configuration, with the Pd(II) in a distorted square-planar coordination environment as shown in Figures 2.9 and 2.11. In **169**, the

bond angles around palladium(II) centre (Table 2.24), confirm an approximate square-planar geometry with the two diazaphosphorinane ligands *cis* to each other. The Pd–P and Pd–Cl bond lengths are given in Table 2.24 and are comparable to other previously reported compounds.[201,202] There were intermolecular N–H···Cl hydrogen bonding interactions as shown in Figure 2.10 and Table 2.24.

Table 2.25 Selected bond lengths and angles for **170**.[a]

Bond lengths (Å)		Bond lengths (Å)		Bond angles (°)	
Pd(1)–P(1)	2.2527(13)	P(1)–C(1)	1.838(5)	P(1)–Pd(1)–P(2)	100.45(5)
Pd(1)–P(2)	2.2448(13)	P(2)–C(23)	1.843(5)	P(1)–Pd(1)–Cl(1)	84.36(5)
Pd(1)–Cl(1)	2.3641(12)	N(1)–C(1)	1.452(6)	P(2)–Pd(1)–Cl(2)	85.72(5)
Pd(1)–Cl(2)	2.3653(13)	N(4)–C(23)	1.441(6)	Cl(1)–Pd(1)–Cl(2)	90.10(5)

Hydrogen bonds

D–H···A	d(H···A) (Å)	d(D···A) (Å)	<(DHA) (°)
N(1)–H(1)···Cl(2C)	2.70(5)	3.377(4)	149(5)
N(4)–H(4)···Cl(4)	2.92(6)	3.483(4)	133(5)

[a] Estimated standard deviations in parentheses.

The X-ray structure of **170** (Figure 2.11) reveals a similar pattern, with the bond angles around palladium(II) centre (Table 2.25), confirm an approximate square-planar geometry with the two diazaphosphorinane ligands *cis* to each other. The Pd–P and Pd–Cl bond lengths are given in Table 2.25, similar to those of **169** and comparable to other previously reported compounds.[146,201] As was in the case of **169**, intermolecular N–H···Cl hydrogen bonding was evident in **170** (Table 2.25). In addition, there was intermolecular hydrogen bonding involving CH_2Cl_2 solvent molecule of crystallisation (Figure 2.11 and Table 2.25).

2.4.4. SYNTHESIS OF PLATINUM(II) DIAZAPHOSPHORINANE COMPLEXES 178 AND 179

Two platinum(II) complexes were synthesised by reacting **156** or **158** with $PtCl_2$(COD), in CH_2Cl_2 at room temperature under aerobic conditions, followed by precipitation with Et_2O upon concentration of the solution under reduced pressure.

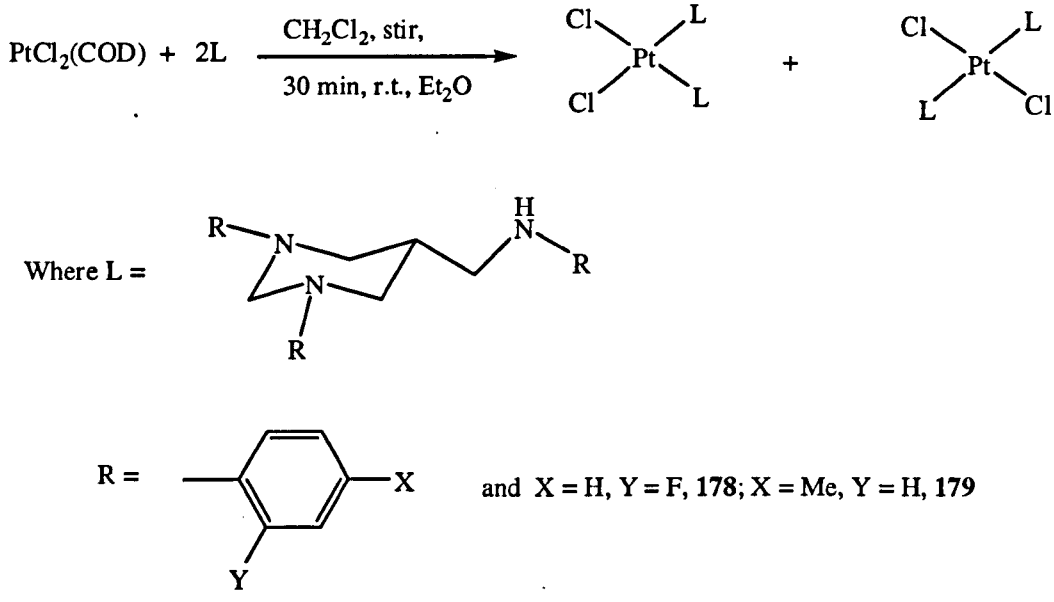

Equation 2.7.

In both cases the ligands readily react to form either the *cis* or *trans* platinum(II) complex in good yield (Table 2.26), according to Equation 2.7; all the products are colourless solids.

2.4.4.1 CHARACTERISATION OF COMPOUNDS 178 AND 179

As in the previous cases characterisation was achieved by MS, microanalysis, IR and NMR, the results are given in Tables 2.26–2.28. Furthermore, the structure of **178** has been elucidated by single crystal X-ray crystallography.

The infrared spectra were recorded as pressed KBr disks (Table 2.26), in both cases the ν(NH) stretches of the ligands slightly increased on coordination to the metal centre. For example in the precursor **156**, the ν(NH) stretch for the precursor was 3302 cm^{-1} but on coordination in **178**, it was increased to 3426 cm^{-1}.

Table 2.26 Percentage yield (isolated), FAB-MS and selected FT-IR data[a] (in cm^{-1}) for **178** and **179**.

Platinum(II) complex	% yield	*m/z* $[M]^+$	ν(NH)	ν(PtCl)
178	74	1096	3426 (s)	287, 311
179	84	1073	3345 (s)	287, 311

[a] Recorded as a pressed KBr disk.

There was a similar increase in the case of **179** from 3301 cm^{-1} in the precursor ligand **158** to 3345 cm^{-1}. In both cases, two Pt–Cl stretches were observed, indicating the formation of a *cis* isomer.

The FAB-MS data in Table 2.26 as well as the microanalytical data in Table 2.27 were consistent with the molecular formulae of compounds **178** and **179**. Coprecipitation of solvent is possible in these complexes; this is in agreement with the microanalytical data.

Table 2.27 Microanalysis (%) and molecular formulae for compounds **178** and **179**.[a]

	C	H	N	Molecular formula
178	47.97 (48.18)	3.88 (3.86)	7.27 (7.66)	$C_{44}H_{42}N_6P_2F_6PtCl_2$
179	55.05 (55.15)	5.59 (5.57)	7.51 (7.68)	$C_{50}H_{60}N_6P_2PtCl_2 \cdot 0.25CH_2Cl_2$

[a] Calculated values in parentheses.

The solution $^{31}P\{^1H\}$ NMR spectra of **178** and **179** in $CDCl_3$ showed single $^{31}P\{^1H\}$ resonances flanked by two ^{195}Pt satellites separated by $^1J_{PPt}$ coupling constant of *ca.* 3300 Hz as given in Table 2.28. Thus the $^{31}P\{^1H\}$ NMR and IR spectroscopic data are supportive of the *cis* configuration. In both complexes, the phosphorus resonances were downfield of the precursor ligands **156** and **158** observed at about −50.00 ppm as given in Table 2.11.

Table 2.28 Selected NMR data (in ppm or Hz) for **178** and **179**.[a]

	δ(P)	$^1J_{PPt}$	δ(H)/arom.[b]	δ(H)/NH[c]	δ(H)/CH_2
178	−11.44	3363	6.71–7.31	6.69 (8.4)	3.05–4.57
179	−6.58	3398	6.34–7.26	6.78 (6.8)	3.44–4.82

[a]All ^{31}P NMR recorded in $CDCl_3$, [b]Aromatic H, m, (12 H, C_6H_4),
[c]NH proton signals, (d, 1H, $^3J_{PH}$ coupling in brackets).

The ^{1}H NMR spectra were not significantly different from the analogous palladium(II) complexes discussed in Section 2.4.3. The CH_3 protons in **179** were observed as a triplet at 1.24 ppm with a $^4J_{HH}$ coupling of 14.0 Hz.

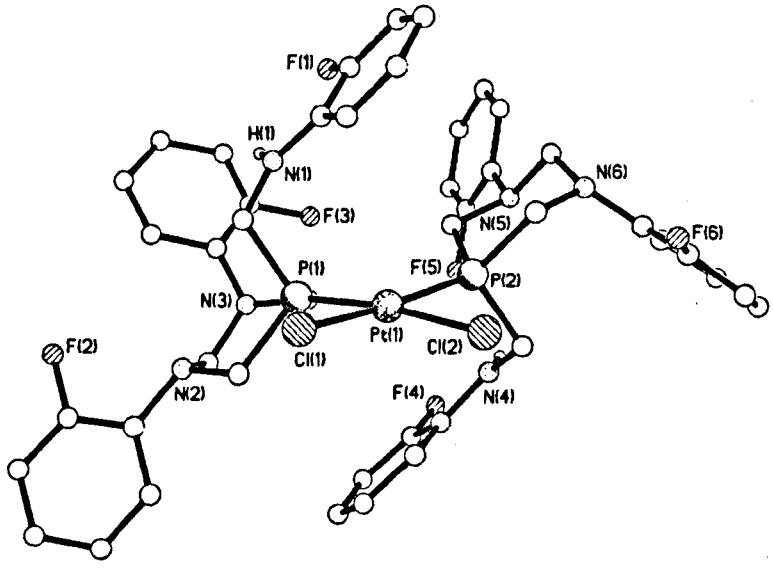

Figure 2.12 Molecular structure of **178**.

A further confirmation of the *cis* configuration for these complexes was achieved when a few X-ray quality crystals were obtained by layering petroleum ether (b.p. 40–60 °C) on a CH_2Cl_2 solution of **178** kept for several days. The single X-ray crystal determination of this confirms the *cis* configuration as shown in Figure 2.12.

Table 2.29 Selected bond lengths and angles for **178**.[a]

Bond lengths (Å)		Bond lengths (Å)		Bond angles (°)	
Pt(1)–P(1)	2.2287(7)	P(1)–C(1)	1.842(3)	P(1)–Pt(1)–P(2)	87.29(3)
Pt(1)–P(2)	2.2325(7)	P(2)–C(23)	1.852(3)	P(1)–Pt(1)–Cl(1)	84.81(3)
Pt(1)–Cl(1)	2.3551(7)	N(1)–C(1)	1.446(4)	P(2)–Pt(1)–Cl(2)	84.28(2)
Pt(1)–Cl(2)	2.3652(7)	N(4)–C(23)	1.481(4)	Cl(1)–Pt(1)–Cl(2)	89.68(2)

Hydrogen bonds

D–H···A	d(H···A) (Å)	d(D···A) (Å)	<(DHA) (°)
N(4)–H(4A)···Cl(1A)	2.96	3.487(3)	119.8
N(4)–H(4A)···F(5)	2.55	3.220(4)	133.4

[a] Estimated standard deviations in parentheses.

The platinum(II) complex, **178** displays a *cis* configuration with respect to the diazaphosphorinane ligands, the Pt(II) centre being in a near square-planar geometry as shown by the bond angles around the Pt(II) centre given in Table 2.29.

Selected bond lengths and angles are given in Table 2.29, the Pt–P and Pt–Cl bond lengths are comparable to those of other previously reported compounds.[200,203] There are intermolecular N–H···Cl hydrogen bonds (Table 2.29). The crystal data and structure refinement details for **178** are shown in Appendix 8.8.

The H-bonds here are bifurcated, hence are likely to be weak. This is supported by the relatively non-linear nature of the bond angles (Table 2.29). It is worthy of note that formation of N–H···F hydrogen bonding rarely observed in covalently bound fluorine compounds[193] was evident in **178** as revealed by the X-ray diffraction analysis. The H···F bond length and N–H···F bond angle however, were longer and relatively non-linear hence not comparable to typical values for N–H···F intermolecular hydrogen bonds in the literature which are in the range [2.25–2.33 Å; 155–166°].[193]

2.5 CONCLUSIONS

Two new classes of phosphonium salts have been synthesised from THPC and aniline or phenylenediamine precursors as aniline and phenylenediamine derivatives of THPC respectively. The new aniline derivatives (**128–146**) of THPC represented as $[P(CH_2NHR)_4]Cl$, where R = phenyl or a substituted phenyl group were synthesised by reacting THPC with different aniline precursors in EtOH at room temperature following the procedure first published by Frank *et al.*[10] The new phenylenediamine derivatives of THPC, $[P\{(CH_2NH)_2R\}_2]Cl$, [R = C_6H_4, **147**; R = C_6H_3Me, **148**; R = C_6H_3COPh, **149**; R = $C_6H_2C_4H_4$, **150**] were also synthesised by reacting THPC with phenylenediamine precursors in EtOH in ethanol at room temperature following a similar procedure first published by Frank *et al.*[10]

Selected aniline derivatives of THPC were reacted with Et_3N in acetone at room temperature following a procedure first published by Frank *et al.*[10] to give the corresponding diazaphosphorinane ligands cyclo-$\{CH_2N(R)CH_2N(R)CH_2\text{-}P\}$-$CH_2N(H)R$, **152–161** where R = phenyl or a substituted phenyl group. The reactivity of

the diazaphosphorinane ligands towards late transition metals including Ru(II), Rh(III), Ir(III), Pd(II) and Pt(II) has been evaluated.

The phosphonium salts, diazaphosphorinane ligands and metal complexes were characterised by a combination of conventional techniques: MS, microanalysis, FT–IR, NMR [^{1}H and ^{31}P{^{1}H}], and in several cases by single crystal X-ray crystallography. Furthermore, *P*-coordination bonding modes have been observed in the complexes and verified by spectroscopic and single X-ray diffraction analyses. The Ru(II), Rh(III) and Ir(III) complexes showed a classic "piano-stool" geometry, while the Pd(II) and Pt(II) complexes showed square-planar geometries with *cis*-configurations and illustrate a range of intra- and intermolecular hydrogen-bonding contacts as confirmed by single X-ray diffraction analyses. These interesting coordination properties may have useful future implications in homogeneous catalysis.

CHAPTER THREE

NEW CATIONIC CYCLIC PHOSPHORUS(III) LIGANDS

3.0 INTRODUCTION

Cationic phosphorus(III) ligands are very useful in organometallic and coordination chemistry because of the lone pair of electrons on the phosphorus as well as the availability of the positive and negative ions which enhance other useful properties such as ion exchange and hydrogen-bonding. The ready availability of THPC coupled with its use as a precursor to phosphines makes it a potential candidate for the synthesis of cationic phosphorus(III) ligands as tertiary phosphine ammonium salts.

In this chapter, the reaction of THPC with benzylamine precursors in ethanol at room temperature under aerobic conditions following a similar procedure first published by Frank *et al.*[10] will be explored in anticipation of reducing the P(V) compound, THPC to a tertiary phosphine ammonium chloride, (cationic cyclic P(III) ligand). The benzylamines are of relatively higher basicity than the aniline precursors used previously (Chapter 2) which could not effect a reduction of THPC, but required Et_3N in a second and final step to give a cyclic P(III) compound. Anion metathesis of the resulting chlorides with $Na[BPh_4]$, $Na[SbF_6]$ or $K[PF_6]$ in methanol at room temperature under aerobic conditions will be performed to give the corresponding metathesised salts. The coordination chemistry of these P(III) salts will then be explored by reacting them with Ru(II), Rh(I), Rh(III), Ir(III), Pd(II), Pt(II) and Au(I) precursors to form the corresponding transition metal complexes.

The cationic phosphorus(III) salts and metal complexes will be characterised by a combination of conventional techniques: MS, microanalysis, FT–IR, NMR [^1H and $^{31}P\{^1H\}$], and in several cases by single crystal X-ray crystallography. The structural and stereoelectronic relationship between these salts and complexes with other phosphorus(III) compounds and their complexes in the literature will be described also.

3.1 SYNTHESIS OF TERTIARY PHOSPHINE AMMONIUM CHLORIDES (180–184) FROM THPC

A range of new tertiary phosphine ammonium chlorides [cyclo-$\{CH_2N(R')CH_2N(R')CH_2\text{-}P\}\text{-}CH_2N(H_2)R']^+Cl^-$, [R′ = $C_6H_5CH_2$, **180**; R′ = 4-

$FC_6H_4CH_2$, **181**; R′ = 4-$ClC_6H_4CH_2$, **182**; R′ = 4-$MeC_6H_4CH_2$, **183**; R′ = 4-$MeOC_6H_4CH_2$, **184**] were synthesised by reacting THPC with different benzylamine precursors in ethanol using a similar procedure first published by Frank *et al.*[10] THPC readily reacts with the benzylamine precursors in a 1:4 molar ratio in ethanol at room temperature under aerobic conditions (Equation 3.1).

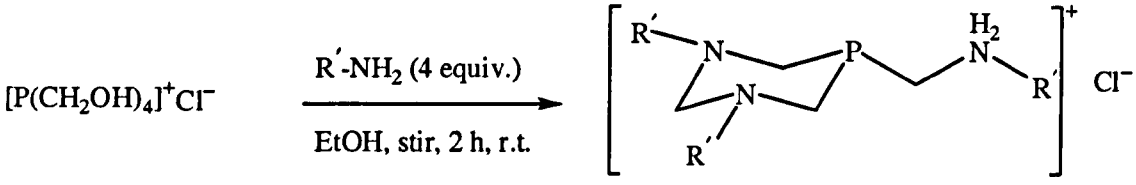

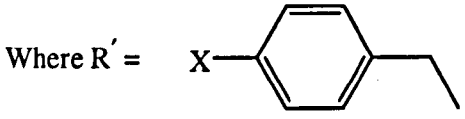

; X = H, **180**; X = F, **181**
X = Cl, **182**; X = Me, **183**
X = MeO, **184**

Equation 3.1.

The reactions afforded the desired products in excellent yields (Table 3.1). All the precursors were liquids, but the products were crystalline colourless solids.

3.1.1 CHARACTERISATION OF COMPOUNDS 180–184

Characterisation was achieved by MS, microanalysis, FT–IR, NMR and single crystal X-ray crystallography as in the previous cases (Section 2.1.1).

Table 3.1 Percentage yield (isolated), FAB-MS and selected FT-IR data[a] (in cm^{-1}) for compounds **180–184**.

Compound	% yield	*m/z* $[M–Cl]^+$	ν (NH_2^+)	ν (CH)
180	86	404	3028 (vs)	2781 (vs)
181	83	458	3044 (m)	2821 (vs)
182	82	506	3023 (vs)	2785 (vs)
183	87	446	2916 (s)	2780 (vs)
184	93	494	3028 (m)	2954 (m)

[a] Recorded as a pressed KBr disk.

The MS data with the *m/z* values given in Table 3.1 are in agreement with the loss of the chloride ion, *m/z* $[M-Cl]^+$ in the respective compounds **180–184**. The FT–IR spectra of these compounds were run as pressed KBr disks. In **180–184**, the $\nu(NH_2^+)$ stretches were observed at about 3000 cm^{-1} (Table 3.1) and are higher than the expected range of 2250–2700 cm^{-1}, probably due to hydrogen-bonding.[190] The peaks resulting from these vibrations were sharp, hence easily distinguished from the broad OH peaks also observed at about 3000 cm^{-1} when the precursor THPC infrared spectrum was run as a pressed KBr disk. The benzyl CH vibrations were observed in the range 2780–2954 cm^{-1}.

The microanalytical data (Table 3.2), were within acceptable limits hence are consistent with the formulations of **180–184**. There was evidence of coprecipitation of water in the case of **184**.

Table 3.2 Microanalysis (%) and molecular formulae for compounds **180–184**.[a]

Compound	C	H	N	Molecular formula
180	68.25 (68.25)	7.10 (7.10)	9.58 (9.55)	$C_{25}H_{31}N_3PCl$
181	60.56 (60.79)	5.58 (5.71)	8.41 (8.51)	$C_{25}H_{28}N_3F_3PCl$
182	55.20 (55.27)	5.15 (5.19)	7.62 (7.73)	$C_{25}H_{28}N_3PCl_4$
183	69.79 (69.77)	7.71 (7.74)	8.70 (8.72)	$C_{28}H_{37}N_3PCl$
184	61.89 (61.87)	6.91 (7.37)	7.72 (7.37)	$C_{28}H_{37}N_3O_3PCl{\cdot}0.75H_2O$

[a] Calculated values in parentheses.

The $^{31}P\{^1H\}$ NMR spectra of these compounds recorded in d^6–DMSO showed single ^{31}P resonances around –55.00 ppm (Table 3.3), significantly different from the single phosphorus resonance of the precursor THPC [δ(P) = 26.50 ppm] also recorded in d^6–DMSO, and was some 40.00 ppm downfield with respect to PTA [δ(P) = –96.20 ppm, D_2O].[102] This suggests the transformation of a phosphorus(V) compound, THPC to a phosphorus(III) compound, in this case a tertiary phosphine ammonium salt.

Selected ^1H NMR data are given in Table 3.3. The aromatic protons were observed as multiplets in the range 6.68–7.62 ppm, while the resonances of the various CH_2 protons

were observed as singlets, doublets or multiplets as given in Table 3.3. The resonances for the NH_2 protons were broad and weak, not observed in some cases (**181** and **182**), but were observed in **180**, **183** and **184**, significantly downfield at 9.55, 8.24 and 8.32 ppm respectively when compared to the NH resonances of the diazaphosphorinane compounds (Table 2.11), due to the positive charge on the quaternary nitrogen atom. The ^1H NMR spectrum of **183** with CH_3 at the 4-position showed the characteristic CH_3 proton resonance as a singlet at 2.25 ppm,[190] while in the ^1H NMR spectrum of **184**, the CH_3O resonance for the protons also at the 4-position were observed relatively downfield, probably due to the electronegativity of the oxygen atom, as a singlet at 3.40 ppm.

Table 3.3 Selected NMR data (in ppm or Hz) for **180–184**.[a]

Compound	δ(P)	δ(H)/arom.	δ(H)/CH_2	δ(H)/CH_2	δ(H)/CH_2	δ(H)/CH_2	δ(H)/CH_2	δ(H)/NH_2
180	–55.08	7.01–7.59, m	4.21, s	3.38–3.42, m	3.18 (13.6)[b]	2.65, t		9.55, br
181	–54.72	6.93–7.62, m	4.21, s	4.02, s	3.29[c]	3.18 (13.8)[b]	2.67, t	n.o.
182	–54.31	7.06–7.60, m	4.22, s	4.03, s	3.34[c]	3.17 (14.0)[b]	2.09, t	n.o.
183	–54.85	6.95–7.41, m	4.14, s	3.34–3.89, m	3.13 (13.6)[b]	2.67, t		8.24, br
184	–54.90	6.68–7.51, m	4.13, s	3.48–3.64, m	3.21 (14.0)[b]	2.68, t		8.32, br

[a] All NMR recorded in d^6-DMSO

[b] CH_2 protons, d, $^2J_{PH}$ coupling in brackets

[c] CH_2 protons, multiplicity could not be fully assigned due to overlap with residual solvent resonances

n.o. = not observed

The compounds were highly crystalline, with X-ray quality crystals of **181** obtained from the ethanol filtrate kept for more than 24 h. The single crystal X-ray structure of **181** has been determined (Figure 3.1) and reveals a pyramidal configuration with the phosphorus atom at the apex of the pyramid. The lone pair of electrons on the phosphorus(III) centre qualifies **181** as a potential ligand.

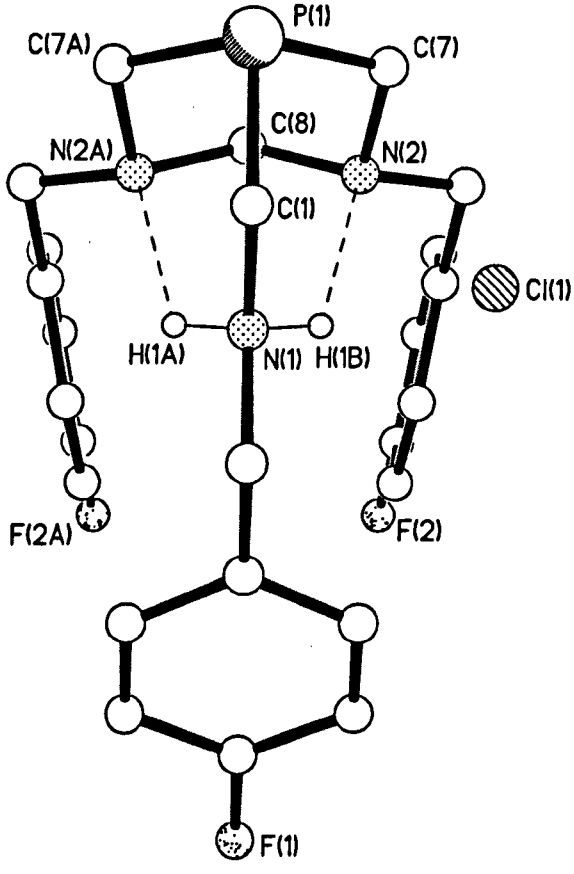

Figure 3.1 Molecular structure of **181**.

The crystal structure also reveals a P–C–N–C–N–C six-membered ring with a chair conformation, exhibiting crystallographic mirror symmetry, whose axis bisects the ammonium group of the cation, the methylene diamine bridge and the 4-FC_6H_4 ring. A close examination of the intracage P–C bond lengths and P–C–N bond angles of **181** reveals close similarities with PTA.[204,205] The C–P–C angle within the P–C–N–C–N–C ring is 99.4 (2)° slightly longer than the analogous C–P–C angle in PTA [96.1(1)°].[204,205] Selected bond lengths and angles of **181** are given in Table 3.6. The P–C bond lengths of 1.847(3) and 1.841(5) Å are similar to those of **129** and comparable to other previously reported organophosphorus compounds.[33,185–187] The crystal data and structure refinement details for **181** are given in Appendix 8.9.

The most important structural feature of **181** is the presence of a pair of intramolecular H-bonds originating from the ammonium group of the cation at N(1) linking the two N atoms in the ring *via* the H atoms at the methylene diamine bridge shown as N(1)–H(1A)···N(2A) and N(1)–H(1B)···N(2) in Figure 3.1. The pair of N–H···N intramolecular H-bonds forms a conformationally locked phosphine framework in the solid state. Thus **181** can be regarded as a charged variant of the well-known PTA ligand as illustrated in Figure 3.2. The X-ray diffraction analysis also reveals the existence of additional weak intermolecular bonding contacts between the cations and the chloride counterions leading to infinite 2-D sheets as shown in Figure 3.3.

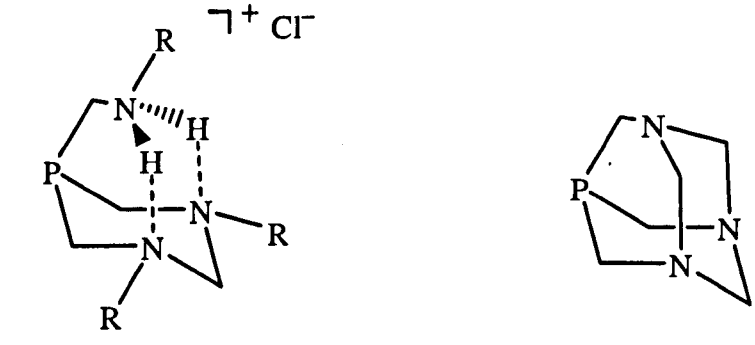

Where R = 4-$FC_6H_4CH_2$

181

PTA

Figure 3.2 Structures of **181** and PTA.

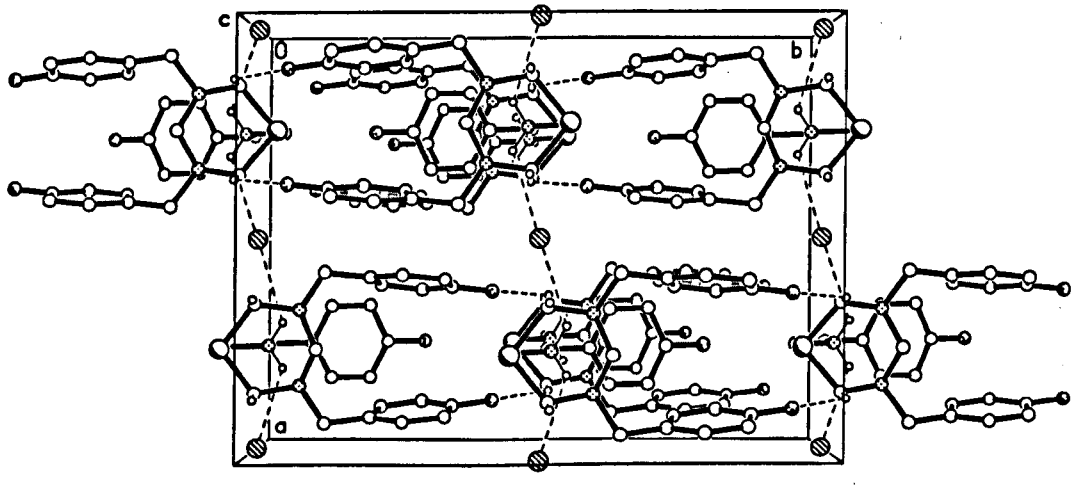

Figure 3.3 Packing plot of **181** showing the H-bonded sheet pattern.

Table 3.4 Selected bond lengths and angles for **181**.[a]

Bond lengths (Å)		Bond angles (°)		Bond angles (°)	
P(1)–C(7)	1.847(3)	P(1)–C(1)–N(1)	116.2(3)	C(1)–P(1)–C(7)	101.21(15)
P(1)–C(1)	1.841(5)	P(1)–C(7)–N(2)	113.8(2)	C(7)–P(1)–C(7A)	99.4(2)

Selected hydrogen bonding contacts

D–H···A	d(H···A) (Å)	d(D···A) (Å)	<(DHA) (°)
N(1)–H(1B)···N(2)	2.27	2.915(5)	126.4

[a] Estimated standard deviations in parentheses.

3.2 SYNTHESIS OF TERTIARY PHOSPHINE AMMONIUM SALTS (185–196) WITH $[BPh_4]^-$, $[SbF_6]^-$ or $[PF_6]^-$ COUNTERIONS

Anion metathesis of some of the tertiary phosphine ammonium chlorides (**180–183**), synthesised in Section 3.1, with some alkali metal salts in methanol was performed resulting in the formation of new tertiary phosphine ammonium salts. Reaction of the chlorides **180–183** with $Na[BPh_4]$, $Na[SbF_6]$ or $K[PF_6]$ in methanol followed by addition of H_2O (Equation 3.2) gave the compounds **185–196** as colourless solids in high yields (Table 3.5).

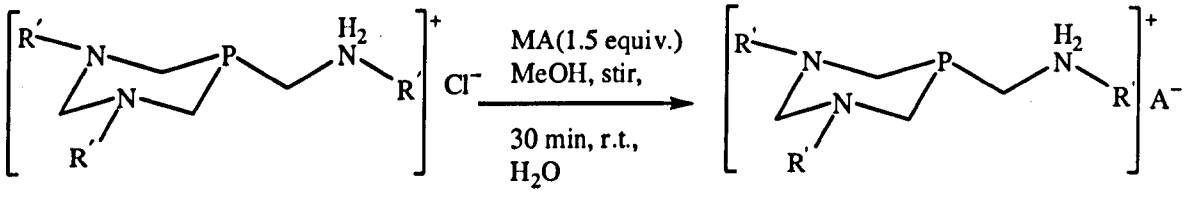

Where R' = 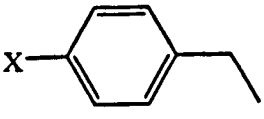

M = Na, K; A = BPh_4, SbF_6, PF_6

X = H, A = BPh_4, **185**; X = Cl, A = SbF_6, **191**

X = F, A = BPh_4, **186**; X = Me, A = SbF_6, **192**

X = Cl, A = BPh_4, **187**; X = H, A = PF_6, **193**

X = Me, A = BPh_4, **188**; X = F, A = PF_6, **194**

X = H, A = SbF_6, **189**; X = Cl, A = PF_6, **195**

X = F, A = SbF_6, **190**; X = Me, A = PF_6, **196**

Equation 3.2.

3.2.1 CHARACTERISATION OF COMPOUNDS 185–196

Characterisation was achieved by MS, microanalysis, FT–IR, NMR and single crystal X-ray crystallography in some cases. The FAB–MS data (Table 3.5) for the compounds are in agreement with the loss of the respective counterion (*m/z* $[M–X]^+$).

Table 3.5 Percentage yield (isolated), FAB-MS and selected FT-IR data[a] (in cm^{-1}) for compounds **185–196**.

	% yield	*m/z* $[M–X]^+$ [b]	$\nu(NH_2^+)$	ν(CH)	ν(SbF)	ν(PF)
185	92	404	3053 (vs)	2969 (vs)		
186	93	458	3053 (m)	2970 (vs)		
187	90	508	3030 (vs)	2980 (vs)		
188	90	446	3050 (s)	2998 (vs)		
189	92	404	3031 (vs)	2952 (vs)	654 (vs)	
190	73	458	3052 (m)	2954 (vs)	653 (vs)	
191	91	508	3029 (vs)	2933 (vs)	657 (vs)	
192	85	446	3023 (s)	2921 (vs)	662 (vs)	
193	72	404	3032 (vs)	2948 (s)		842 (vs)
194	82	458	3055 (vs)	2956 (m)		848 (vs)
195	75	508	3071 (s)	2938 (s)		846 (vs)
196	78	446	3023 (vs)	2920 (s)		844 (vs)

[a] Recorded as a pressed KBr disk; [b] X = BPh_4^-, SbF_6^- or PF_6^-.

The FT–IR spectra of these compounds were run as pressed KBr disks. In **185–196**, the $\nu(NH_2^+)$ stretches observed at about 3000 cm^{-1} (Table 3.5) were not significantly different from those observed for the precursor tertiary phosphine ammonium chlorides, **180–183**. They were also higher than the expected values probably due to hydrogen bonding. The benzyl CH vibrations were also similar to those of the precursor chlorides. A strong SbF vibration at about 650 cm^{-1} indicates the presence of SbF_6^- in **189–192**, while a strong band at about 840 cm^{-1} in **193–196** can be ascribed to PF vibration indicating the presence of PF_6^-.

The microanalytical data are given in Table 3.6. There was evidence of coprecipitation of water in most of the salts as supported by the microanalytical data. The agreement between the observed and calculated CHN data is consistent with the formulation of compounds **185–196**.

Table 3.6 Microanalysis (%) and molecular formulae for compounds **185–196**.[a]

Compound	C	H	N	Molecular formula
185	80.85 (81.32)	6.80 (7.10)	5.69 (5.81)	$C_{49}H_{51}N_3PB$
186	74.28 (73.96)	6.06 (6.33)	5.39 (5.28)	$C_{49}H_{48}N_3F_3PB{\cdot}H_2O$
187	69.77 (69.64)	5.75 (5.96)	5.04 (4.97)	$C_{49}H_{48}N_3Cl_3PB{\cdot}H_2O$
188	81.22 (81.55)	7.52 (7.50)	5.53 (5.49)	$C_{52}H_{57}N_3PB$
189	46.35 (46.35)	4.80 (4.92)	6.46 (6.52)	$C_{25}H_{31}N_3PSbF_6{\cdot}0.25H_2O$
190	42.46 (42.70)	3.90 (4.16)	5.87 (5.98)	$C_{25}H_{28}N_3PSbF_9{\cdot}0.5H_2O$
191	40.43 (40.38)	4.01 (3.80)	6.00 (5.65)	$C_{25}H_{28}N_3Cl_3PSbF_6$
192	48.25 (48.65)	5.10 (5.54)	5.94 (6.08)	$C_{28}H_{37}N_3PSbF_6{\cdot}0.5H_2O$
193	55.03 (54.65)	5.61 (5.69)	7.68 (7.65)	$C_{25}H_{31}N_3P_2F_6$
194	48.21 (48.32)	4.51 (4.87)	6.72 (6.76)	$C_{25}H_{28}N_3P_2F_9{\cdot}H_2O$
195	45.86 (46.00)	4.18 (4.32)	6.36 (6.44)	$C_{25}H_{28}N_3Cl_3P_2F_6$
196	56.80 (56.42)	6.65 (6.34)	7.54 (7.05)	$C_{28}H_{37}N_3P_2F_6{\cdot}0.25H_2O$

[a] Calculated values in parentheses.

The $^{31}P\{^1H\}$ NMR spectra of **185–196** recorded in d^6–DMSO showed single ^{31}P resonances around –55.00 ppm (Table 3.7) not significantly different from those of the precursor tertiary phosphine ammonium chlorides, **180–183**. In the case of **193–196**, containing the hexafluorophosphate(V), PF_6^- anion, apart from the phosphorus(III) resonances around –55.00 ppm mentioned above, the $^{31}P\{^1H\}$ NMR spectra showed the characteristic septet splitting pattern [average $\delta(P) = -144.00$ ppm], significantly upfield of the pyramidal P atom, due to the six NMR-active ^{19}F atoms coupling to the P(V) atom of the PF_6^- ion, symmetrically separated by average $^1J_{PF}$ coupling constant of 713 Hz (Table 3.7).

Selected ^{1}H NMR data are given in Table 3.7. The resonances for aromatic protons were in the range 6.68–7.95 ppm, while the resonances of the various CH_2 protons, as in the case of the precursor chlorides, were observed as singlets, doublets or multiplets as given in Table 3.7. The resonances for the NH_2 protons were very weak, and not seen in some cases but were observed in some, downfield (8.10–9.02 ppm) due to the charge on the N atom (ammonium species, $[NR_4]^+$). The ^{1}H NMR spectra of **188**, **192** and **196** all with CH_3 at the 4-position showed the characteristic CH_3 proton resonances at about 2.24 ppm.

Table 3.7 Selected NMR data (in ppm or Hz) for **185–196**.[a]

	δ(P)	δ(P)	δ(H)/arom.	δ(H)/CH_2	δ(H)/CH_2[b]	δ(H)/CH_2[c]	δ(H)/CH_2	δ(H)/NH_2	$^1J_{PF}$
185	–54.84		6.78–7.54, m	4.23, s	3.35–3.85	3.10 (13.6)	2.67, t	8.56, br	
186	–54.84		6.78–7.58, m	4.21, s	3.33–3.84	3.11 (13.6)	2.67, t	n.o.	
187	–54.45		6.78–7.60, m	4.22, s	3.50–3.84	3.11 (13.6)	2.64, t	n.o.	
188	–54.81		6.78–7.36, m	4.16, s	3.46–3.99	3.08 (14.0)	2.65, t	8.10, br	
189	–55.20		6.92–7.49, m	4.22, s	3.41–3.57	3.10 (12.0)	2.66 , t	9.01, br	
190	–54.92		6.98–7.57, m	4.22, s	3.50–3.84	3.10 (13.6)	2.67, t	8.95, br	
191	–54.24		7.00–7.59, m	4.23, s	3.50–3.90	3.12 (14.0)	2.68, t	8.14, br	
192	–54.65		6.90–7.43, m	4.18, s	3.43–3.98	3.13 (13.6)	2.67, t	8.18 , br	
193	–54.61	–144.20, sept.	7.01–7.49, m	4.23, s	3.41–3.85	3.10 (14.0)	2.67, t	9.02, br	711
194	–54.42	–144.20, sept.	6.98–7.58, m	4.22, s	3.51–3.84	3.12 (13.6)	2.67, t	9.00, br	714
195	–54.30	–144.19, sept.	6.99–7.95, m	4.23, s	3.48–3.98	3.11 (14.0)	2.67, t	8.13, br	713
196	–55.35	–144.20, sept.	6.92–7.38, m	4.28, s	3.43–3.79	3.13 (14.0)	2.67, t	n.o.[d]	713

[a] All NMR spectra were recorded in d^6-DMSO

[b] CH_2 protons, multiplicity could not be fully assigned due to overlap with residual solvent resonances

[c] CH_2 protons, d, $^2J_{PH}$ coupling in brackets

n.o. = not observed

The compounds as in the case of the tertiary phosphine ammonium chlorides, **180–184**, were highly crystalline. Suitable crystals of **185** and **193** were obtained by vapour diffusion of Et_2O into their CH_2Cl_2 solutions over the course of several days. Similarly, suitable crystals of **190** were obtained when petroleum ether (40–60°C) was layered on CH_2Cl_2 solution kept for several days. The single crystal X-ray structures of **185**, **190** and **193** have been determined (Figures 3.4, 3.5 and 3.9) and showed pyramidal configurations with the phosphorus atom at the top of the pyramid. The crystal structures of the cations also reveal a P–C–N–C–N–C six-membered ring with a chair conformation in all the compounds similar to that of **181**. The lone pair of electrons on the phosphorus atoms again qualifies these compounds as potential ligands. As in the case of **181**, the intracage P–C bond lengths and P–C–N bond angles of **190** and **193** also reveal close similarities with PTA.[204,205] The C–P–C angles within the P–C–N–C–N–C rings are 99.84(12)° and 97.78(5)° for **190** and **193** respectively, slightly longer than the analogous C–P–C angle in PTA [96.1(1)°].[204,205] The bond lengths and angles of **185**, **190** and **193** are given in Tables 3.8, 3.9 and 3.10. The P–C bond lengths are also similar to those of **129** and comparable to other previously reported compounds.[33,185–187] The crystal data and structure refinement details for **185**, **190** and **193** are given in Appendices 8.10, 8.11 and 8.12.

The compounds are H-bonded and unlike in the case of **181**, only one N–H···N intramolecular H-bond, N(1)–H(1A)···N(2) was observed in **185** as shown in Figure 3.4. The inability of forming the second N–H···N intramolecular H-bond, N(1)–H(1B)···N(3) is caused by the N–H···π and C–H···π interactions between the cation and the anion (BPh_4^-) as shown in Figure 3.4. The H(1B) hydrogen at N(1) in the cation has an interaction with a phenyl group in the anion [N(1)–H(1B)···C(30)] hence cannot flip over to form the N(1)–H(1B)···N(3) H-bond as in the case of **181**. Therefore no cage structure was formed in this case. However, in compounds **190** and **193** as was the case in **181**, a pair of N–H···N intramolecular H-bonds forming conformationally locked phosphine frameworks in the solid state was evident. Thus compounds **190** and **193** can also be regarded as charged variants of PTA. The existence of additional weak intermolecular bonding contacts between the cations and the counterions in **190** and **193** leading to infinite 2-D sheets was also revealed by the X-ray diffraction analyses (Figures 3.7 and 3.8).

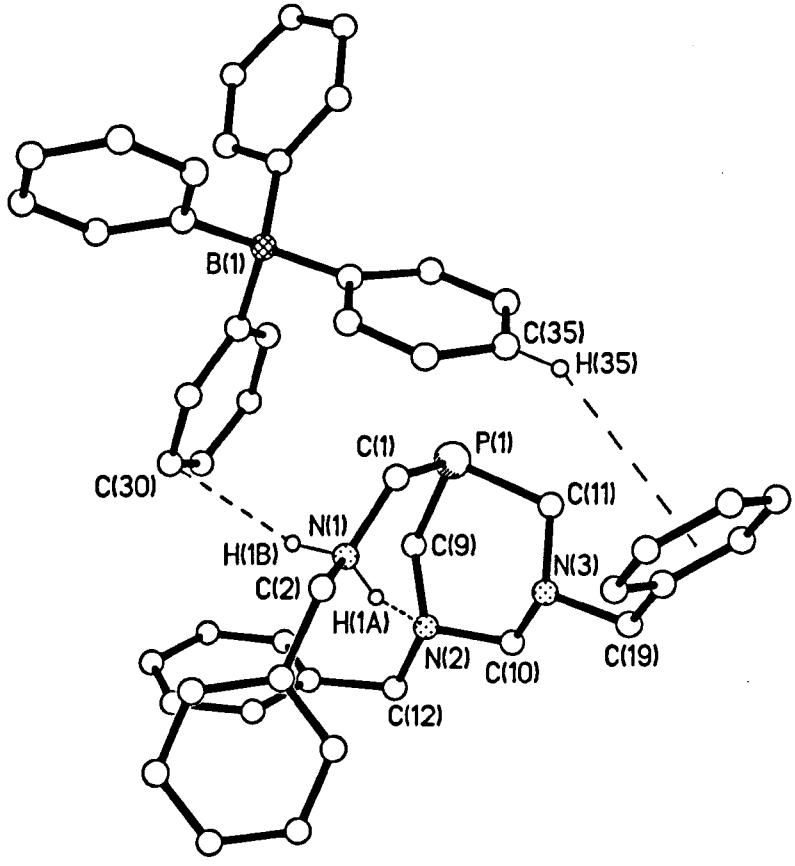

Figure 3.4 Molecular structure of **185** showing N–H···π and C–H··π interactions between cation and anion (BPh_4^-).

Table 3.8 Selected bond lengths and angles for **185**.[a]

Bond lengths (Å)		Bond lengths (Å)		Bond angles (°)	
P(1)–C(11)	1.8407(14)	C(1)–N(1)	1.4816(19)	C(11)–P(1)–C(9)	97.38(6)
P(1)–C(9)	1.8457(13)	C(9)–N(2)	1.4772(17)	C(11)–P(1)–C(1)	98.39(7)
P(1)–C(1)	1.8581(16)	C(11)–N(3)	1.4664(17)	C(9)–P(1)–C(1)	100.54(6)

Selected hydrogen bonding contacts

D–H···A	d(H···A) (Å)	d(D···A) (Å)	<(DHA) (°)
N(1)–H(1A)···N(2)	1.887(18)	2.7393(17)	148.4(16)

[a] Estimated standard deviations in parentheses.

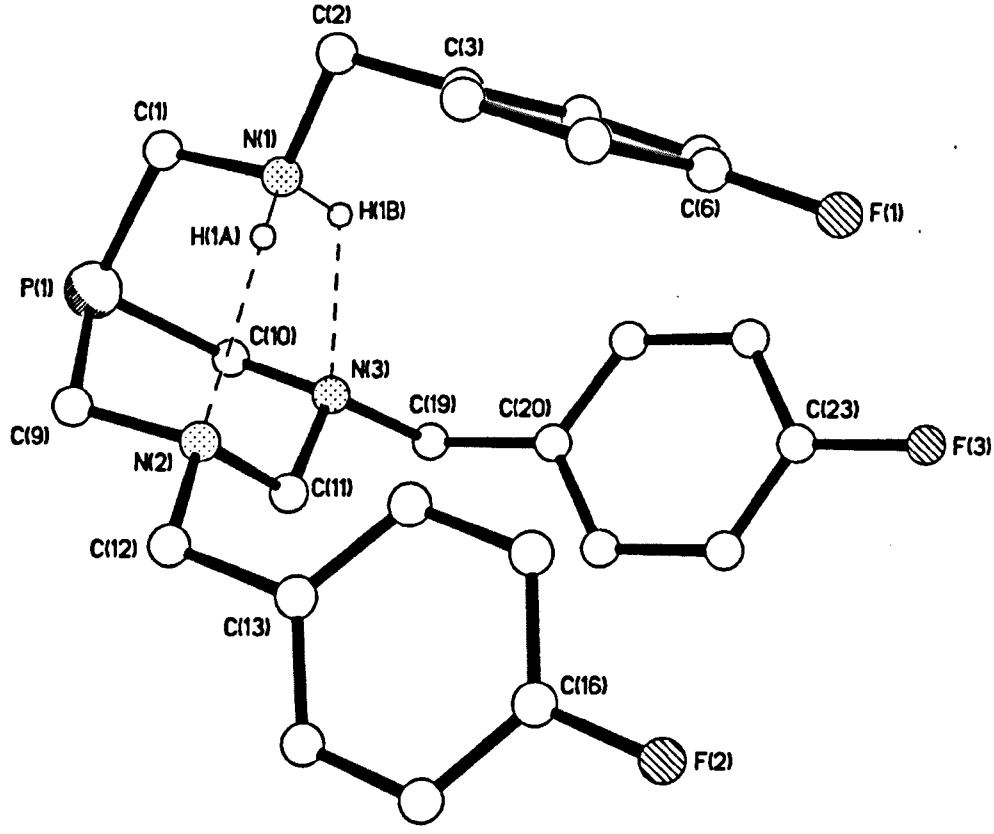

Figure 3.5 Molecular structure of **190**. The SbF_6^- counterion has been omitted for clarity.

The apical P–C and C–N bond lengths as well as C–P–C bond angles for **190** are given in Table 3.9. In addition to the intramolecular N–H···N H-bonding mentioned earlier, **190** also exhibits intermolecular N–H···F H-bonding, involving, the six SbF_6^- fluorines as shown in Figure 3.6.

The X-ray diffraction analyses also reveal that there is intermolecular π–π stacking of the molecules. Phenyl···phenyl groups are stacked down the *c*-axis of the unit cells in these compounds as shown by the packing plot for **190** (Figure 3.7). The average C–C distance of 3.484 Å between the phenyl groups separating two molecules of **190** was similar to the interplanar distance of *ca.* 3.354 Å involving carbon atoms in the structure of graphite.[206]

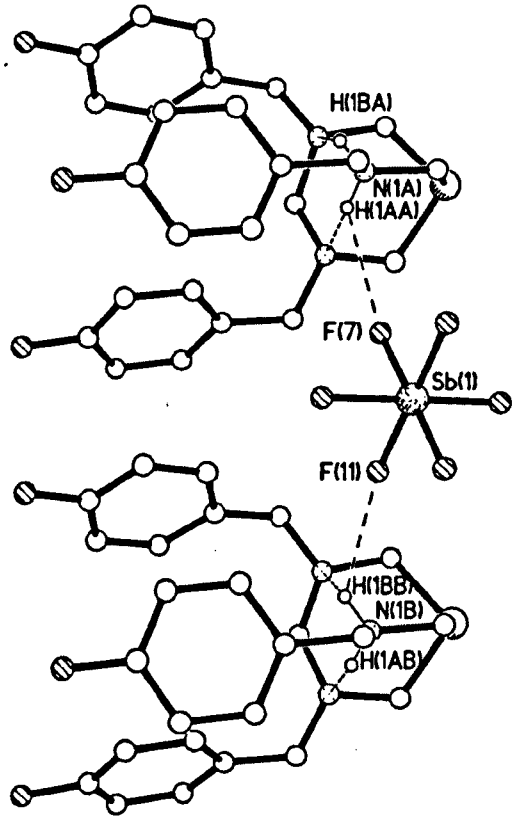

Figure 3.6 Molecular structure of **190** showing intermolecular H-bonding contacts between the $[SbF_6]^-$ counterion and cations.

Table 3.9 Selected bond lengths and angles for **190**.[a]

Bond lengths (Å)		Bond angles (°)		Bond angles (°)	
P(1)–C(1)	1.850(3)	P(1)–C(1)–N(1)	115.47(17)	C(10)–P(1)–C(1)	101.96(12)
P(1)–C(9)	1.843(3)	P(1)–C(9)–N(2)	114.39(17)	C(9)–P(1)–C(1)	99.84(12)
P(1)–C(10)	1.841(3)	P(1)–C(10)–N(3)	113.91(17)	C(10)–P(1)–C(9)	98.03(12)

Selected hydrogen bonding contacts

D–H···A	d(H···A) (Å)	d(D···A) (Å)	<(DHA) (°)
N(1)–H(1A)···N(2)	2.14(3)	2.804(3)	138(3)
N(1)–H(1B)···N(3)	2.20(3)	2.841(3)	130(2)
N(1)–H(1A)···F(7A)	2.63(3)	3.166(3)	125(2)
N(1)–H(1B)···F(11B)	2.46(3)	3.021(3)	123(2)

[a] Estimated standard deviations in parentheses.

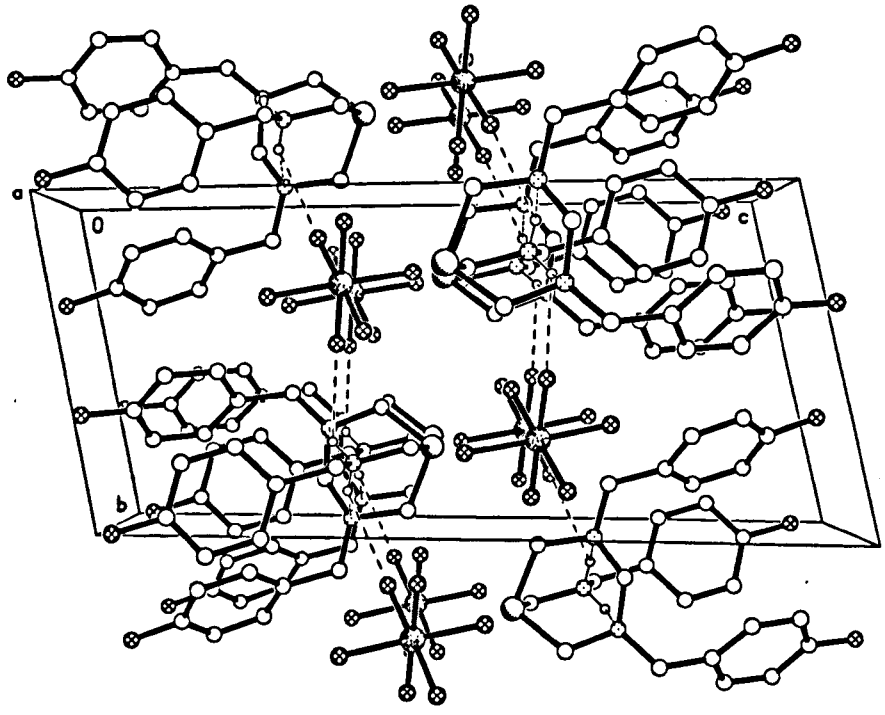

Figure 3.7 Packing plot for compound **190**, parallel to *a* showing H-bonded chains of cations and anions.

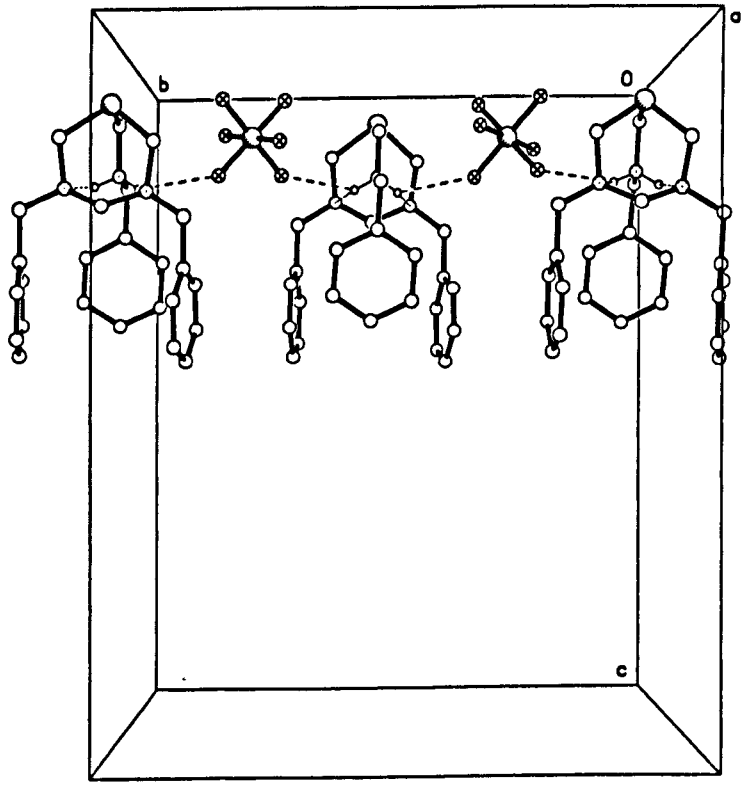

Figure 3.8 Packing plot for compound **193**.

Compounds **190** and **193** have similar cation/anion arrangements as shown in Figures 3.6 and 3.10. The packing plots for **190** and **193** are also similar involving stacking of phenyl···phenyl groups down the *c*-axis of the unit cell in each case although Figures 3.7 and 3.8 do not clearly show this.

The P–C bond lengths and the apical C–P–C angles of **193** are given in Table 3.10, and are comparable to **181, 185, 190** and other similar compounds.[33,185–187] The crystal data and the structure refinement details for **193** are shown in Appendix 8.12.

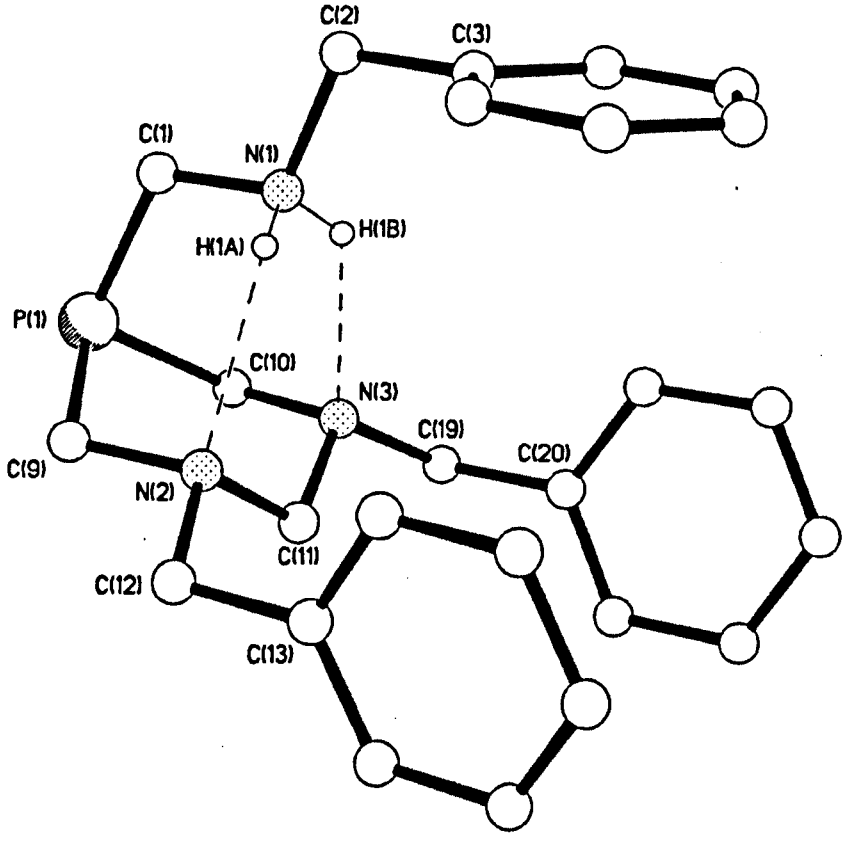

Figure 3.9 Molecular structure of **193**. The PF_6^- counterion has been omitted for clarity.

Compound **193** as in the case of **190**, exhibits both intramolecular (N–H···N) and intermolecular (N–H···F) hydrogen bonding involving the PF_6^- counterions as shown in Figure 3.10 and Table 3.10. In both cases the cations are linked together by H-bonding with the $[SbF_6]^-$ or $[PF_6]^-$ counterions. The highly electronegative six F atoms in these ions are involved in intermolecular hydrogen bonding by linking two or more cationic

parts of the salts together. Such intermolecular hydrogen bonding was not found in the case of **185** probably due to the absence of highly electronegative atoms in the $[BPh_4]^-$ counterion.

There are three important findings pertaining to the N–H···N H-bonded framework from compounds **190** and **193** together with **181** mentioned earlier. Firstly, there was no apparent disruption of the N–H···N intramolecular H-bonded motif in spite of the fact that polar solvents (alcohols/H_2O) were used in the synthesis and crystallisation. Compound **185** was odd in this sense, in that only one N–H···N intramolecular H-bond instead of two was observed due to N–H···π and C–H···π interactions between the cation and the anion (BPh_4^-) mentioned previously.

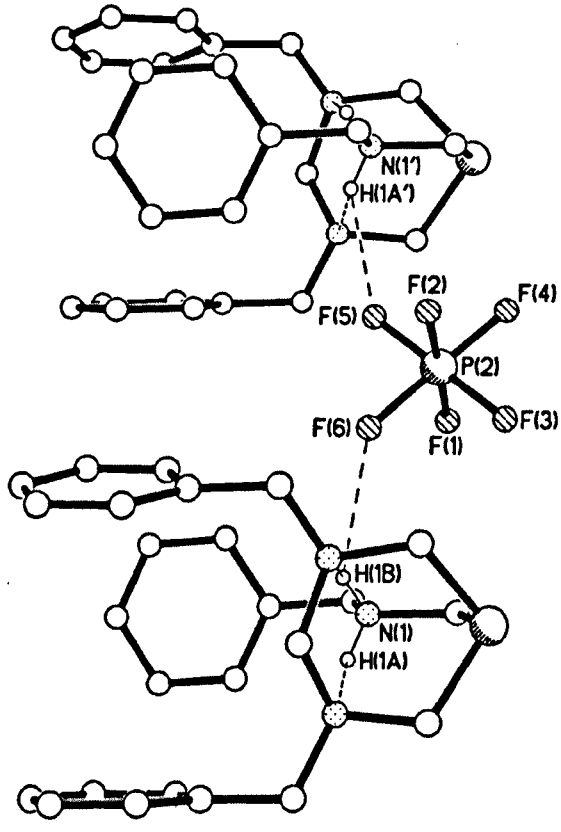

Figure 3.10 Molecular structure of **193** showing intermolecular H-bonding contacts between the $[PF_6]^-$ counterion and cations.

Secondly, alternate H-bonding arrangements involving the anions were not important; hence the core structure of the cation was maintained regardless of the counter anion (Cl^-, SbF_6^- or PF_6^-) present. Thirdly, N–H···F contacts involving the three electronegative fluorine atoms in the 4-positions (**181** and **190**) were absent, hence do

not disrupt the N–H···N H-bonding arrangement found in the aforementioned compounds, consistent with the difficulty in forming hydrogen bonds from organic fluorines.[193] Thus the single crystal X-ray structures of **181, 190** and **193** have shown that simple modification of the PTA core can be achieved in which non-covalent interactions such as H-bonds generally maintain the structure in the solid state.

Table 3.10 Selected bond lengths and angles for **193**.[a]

Bond lengths (Å)		Bond angles (°)		Bond angles (°)	
P(1)–C(9)	1.8359(12)	P(1)–C(1)–N(1)	116.70(7)	C(9)–P(1)–C(10)	97.78(5)
P(1)–C(10)	1.8366(13)	P(1)–C(9)–N(2)	114.09(7)	C(9)–P(1)–C(1)	101.28(5)
P(1)–C(1)	1.8490(12)	P(1)–C(10)–N(3)	113.53(7)	C(10)–P(1)–C(1)	101.32(5)

Selected hydrogen bonding contacts

D–H···A	d(H···A) (Å)	d(D···A) (Å)	<(DHA) (°)
N(1)–H(1A)···N(2)	2.241(15)	2.8506(13)	128.7(12)
N(1)–H(1B)···N(3)	2.154(15)	2.8234(13)	132.9(12)
N(1)–H(1A)···F(5)	2.372(15)	3.0045(13)	131.6(12)
N(1)–H(1B)···F(6)	2.473(15)	3.0414(13)	123.2(12)

[a] Estimated standard deviations in parentheses.

The tertiary phosphine ammonium salts, though structurally related to the water-soluble PTA, as confirmed by single crystal X-crystallography were found to be insoluble in water. At ambient temperatures, they were however soluble in CH_2Cl_2, CH_3OH and DMSO. The average solution conductivity measurements of **180, 181, 189, 190, 193** and **194** in water–methanol (20:80) recorded with a Jenway Model 4510 conductivity meter was 10.06 μs at 20.85 °C close to that of a 1:1 electrolyte (KCl), 6.79 μs measured under similar conditions. In the solid state, the salts were air stable but slowly oxidise in d^6-DMSO solution over *ca.* 24 h, for instance, the solution $^{31}P\{^1H\}$ NMR spectra of **180** recorded in d^6-DMSO within 24 h period showed that the purity of **180** as indicated by the ^{31}P resonances decreased from δ(P) = –54.30 ppm, 68% to –54.88 ppm, 44%. There was almost a corresponding percentage purity of another phosphorus compound as shown by a second ^{31}P resonance at δ(P) = 26.70 ppm, 18% in the

spectrum recorded after 24 h, suggestive of slow oxidation of the P(III) compound to its corresponding tertiary phosphine oxide.

3.3 COORDINATION STUDIES OF TERTIARY PHOSPHINE AMMONIUM SALTS

Having established the fact that the tertiary phosphine ammonium salts are structurally related to the versatile PTA ligand, their coordination potential was explored by reacting them with relevant ruthenium(II), rhodium(I), rhodium(III), iridium(III), palladium(II), platinum(II) and gold(I) compounds forming the corresponding transition metal complexes in high yields.

3.3.1 SYNTHESIS OF RUTHENIUM(II) COMPLEXES 197–202

The synthesis of half-sandwich organometallic ruthenium(II) compounds of PTA have been reported previously by Dyson and co-workers.[110,125]

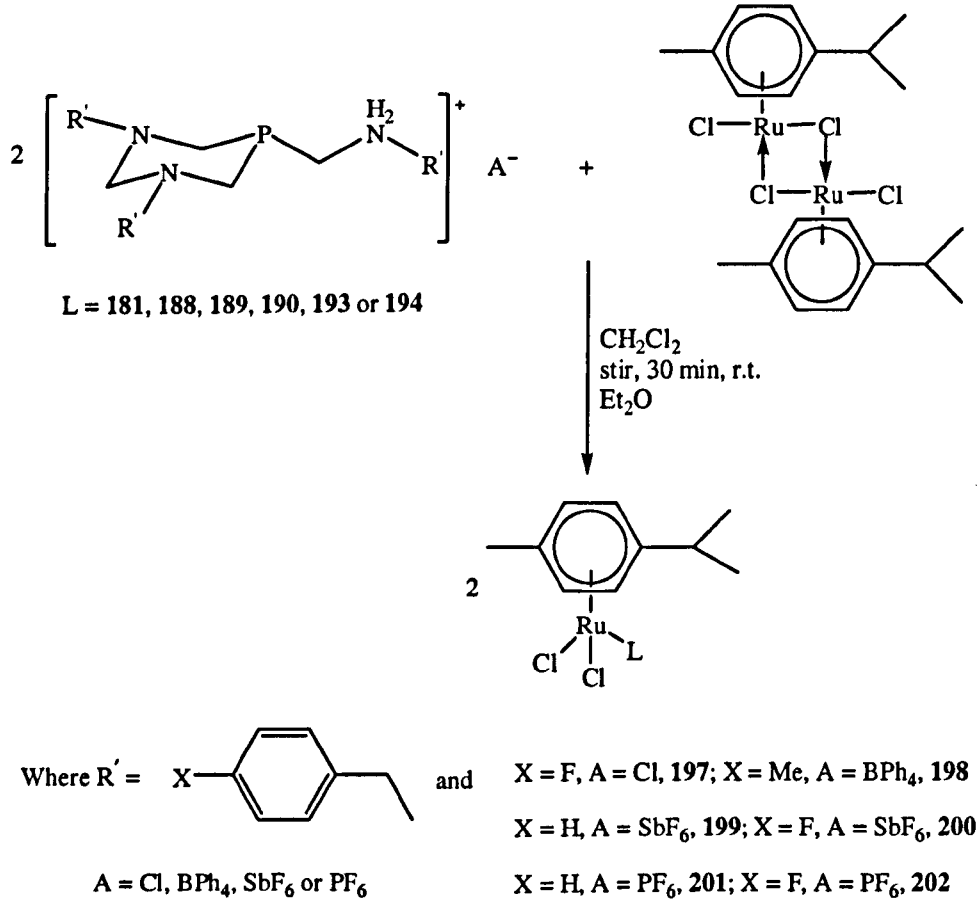

Equation 3.3.

In order to assess whether these tertiary phosphine ammonium salts could function as similar *P*-monodentate ligands, a range of cationic organometallic ruthenium(II) complexes were synthesised by reacting some of the tertiary phosphine ammonium salts with $\{RuCl_2(\eta^6\text{-}p\text{-cymene})\}_2$ in CH_2Cl_2 under aerobic conditions at room temperature. This was followed by precipitation with diethyl ether upon concentration of the solution under reduced pressure. In all cases the ligands readily react to form the desired ruthenium(II) complex in excellent yields (Table 3.11). In each case, two equivalents of the ligand react by standard bridge cleavage of the ruthenium dimer to form two moles of orange coloured ruthenium(II) complex according to Equation 3.3.[198]

3.3.1.1 CHARACTERISATION OF COMPOUNDS 197–202

MS, microanalysis, FT–IR, NMR and X-ray diffraction techniques in some cases were used in the characterisation of the complexes; the results are given in Tables 3.11–3.13. The FAB–MS data (Table 3.11) for compounds **197–202** are in agreement with the loss of the respective counterion (*m/z* $[M-X]^+$).

Table 3.11 Percentage yield (isolated), FAB-MS and selected FT-IR data[a] (in cm^{-1}) for compounds **197–202.**

	% yield	*m/z* $[M-X]^+$ [b]	$\nu(NH_2^+)$	ν(CH)	ν(RuCl)	ν(SbF)	ν(PF)
197	98	764	3044 (w)	2966 (m)	294 (w)		
198	97	752	3053 (w)	2956 (m)	281 (w)		
199	91	710	3060 (w)	2967 (m)	290 (s)	654(vs)	
200	90	764	3068 (w)	2968 (m)	290 (m)	663(vs)	
201	90	710	3068 (w)	2967 (w)	295 (w)		842 (vs)
202	91	764	3068 (w)	2970 (m)	293 (w)		846 (vs)

[a] Recorded as a pressed KBr disk; [b] X = Cl^-, BPh_4^-, SbF_6^- or PF_6^-.

Selected diagnostic FT–IR spectral data are given in Table 3.11. The $\nu(NH_2^+)$ stretches were observed in the range 3044–3068 cm^{-1}, not significantly different from the range 3031–3055 cm^{-1} for the precursor ligands. The NH_2^+ infrared absorptions were generally weak but the strong single bands at *ca.* 845 cm^{-1} in compounds **201** and **202**

indicate the presence of the PF_6^- ion. This is consistent with other ruthenium complexes containing the PF_6^- counterion,[207] while the SbF bands of *ca.* 655 cm^{-1} confirm the presence of the SbF_6^- counterion (**199** and **200**). The terminal stretching vibration of the ν(Ru-Cl) bands of the complexes were observed at between 281 and 295 cm^{-1} (Table 3.11). The values for these infrared absorptions are comparable to other previously reported ruthenium(II) phosphine complexes.[208]

The microanalytical data are given in Table 3.12; the values agree within acceptable limits and are consistent with the formulae of the ruthenium(II) complexes **197–202.** Coprecipitation of solvent molecules was evident as shown in the microanalytical data.

Table 3.12 Microanalysis (%) and molecular formulae for compounds **197–202.**[a]

	C	H	N	Molecular formula
197	47.88 (48.04)	5.05 (4.95)	4.58 (4.64)	$C_{35}H_{42}N_3PF_3RuCl_3 \cdot 1.25CH_2Cl_2$
198	65.46 (65.40)	6.46 (6.36)	3.61 (3.63)	$C_{62}H_{71}N_3PBRuCl_2 \cdot CH_2Cl_2$
199	36.99 (36.95)	4.10 (4.39)	3.19 (3.69)	$C_{35}H_{45}N_3PSbF_6RuCl_2 \cdot 2.25CH_2Cl_2$
200	39.32 (39.80)	4.01 (4.09)	3.74 (3.87)	$C_{35}H_{42}N_3PSbF_9RuCl_2 \cdot CH_2Cl_2$
201	48.19 (48.28)	5.17 (5.23)	4.77 (4.79)	$C_{35}H_{45}N_3P_2F_6RuCl_2 \cdot 0.25CH_2Cl_2$
202	44.94 (44.78)	4.61 (4.55)	4.51 (4.41)	$C_{35}H_{42}N_3P_2F_9RuCl_2 \cdot 0.5CH_2Cl_2$

[a] Calculated values in parentheses.

The $^{31}P\{^1H\}$ NMR spectra of these complexes recorded in d^6-DMSO, showed single phosphorus signals in the range δ(P) 6.18–8.18 ppm as given in Table 3.13, suggestive of the presence of a single phosphorus containing compound. These phosphorus signals are significantly downfield of the values [δ(P) ≈ −55.00 ppm] for the corresponding precursor tertiary phosphine ammonium salt ligands as given in Tables 3.3 and 3.7 and are in good agreement with *P*-monodentate coordination. The average coordination chemical shifts for compounds **197–202** ($\Delta\delta_P$ 62 ppm) was not significantly different from that for $RuCl_2(\eta^6$-*p*-cymene)(PTA) ($\Delta\delta_P$ 60 ppm) suggesting similar stereoelectronic properties.[110] The $^{31}P\{^1H\}$ NMR spectra of **201** and **202,** in addition to the single ^{31}P signals at 7.97 and 8.13 ppm respectively, showed the characteristic septet splitting quite upfield of these signals at an average of about −144 ppm. In both

cases, the separation in the characteristic septet splitting pattern from the coupling between the ^{31}P and ^{19}F nuclei was symmetrically separated by an average $^{1}J_{PF}$ coupling constant of 711 Hz (Table 3.13).

Selected ^{1}H NMR spectral data are given in Table 3.13. The signals of the *p*-cymene protons in compounds **197–202** were similar to those of the ruthenium(II) diazaphosphorinane complexes(**163** and **164**) discussed in Section 2.4.1.1 regardless of the different ligands used as given in Tables 2.15 and 3.13. For examples, in both cases, the arene protons of the *p*-cymene were observed at *ca.* between 5.70 and 5.90 ppm, with similar $^{3}J_{PH}$ coupling constants. The $-C\underline{H}(CH_3)_2$ protons in the *p*-cymene displayed a characteristic septet at *ca.* 2.60 ppm in both cases indicating that it is adjacent to 6 protons [$-(CH_3)_2$], while the CH_3 protons were observed at *ca.* 1.90 ppm. These proton signals were comparable to those of other related ruthenium(II) complexes.[198]

Table 3.13 Selected NMR data (in ppm or Hz)[a] for compounds **197–202.**

	δ(P)	δ(P)[b]	δ (H)/ NH_2	δ(H)/arom.	δ(H) /CH_2	δ(H) /CH_2[c]	δ(H) /CH_2	δ(H)/ CH_2[d]	δ(H)/*p*-$CH_3C_6H_4CH(CH_3)_2$[e]
197	6.18		9.00	6.87–7.65, m	4.30, s	4.01 (4.8)	3.78–3.85, m	3.21	1.97, 5.80 (6.0), 2.62 (6.4), 1.15 (6.4)
198	7.18		8.84	6.61–7.53, m	4.20, s	3.98[f]	3.65–3.84, m	3.10	1.95, 5.78 (6.0), 2.62 (6.4), 1.09 (7.6)
199	7.30		8.89	6.99–7.53, m	4.29, s	4.02 (4.8)	3.71–3.80, m	3.45	1.96, 5.94 (8.0), 2.62 (6.8), 1.14 (6.8)
200	8.11		8.65	6.90–7.57, m	4.26, s	4.01, (4.6)	3.61–3.75, m	3.41	1.97, 5.78 (6.4), 2.62 (6.4), 1.15 (6.8)
201	8.13	–144.20	n.o.	7.02–7.48, m	4.27, s	4.00[f]	3.49–3.50, m	3.21	1.96, 5.82 (6.8), 2.59 (6.8), 1.14 (6.8)
202	7.97	–144.19	8.83	6.84–7.56, m	4.30, s	3.98[f]	3.61–3.85, m	3.40	1.97, 5.85 (6.8), 2.62 (6.8), 1.15 (6.8)

[a] All NMR spectra were recorded in d^6-DMSO

[b] δ(P) PF_6^- counterion;

[c] CH_2 protons, d, $^2J_{PH}$ coupling in brackets

[d] CH_2 protons multiplicity could not be fully assigned due to overlap with residual solvent signals

[e] *p*-Cymene resonances: CH_3 (s), C_6H_4 (dd), CH (sept.) and $(CH_3)_2$ (d) protons respectively, $^3J_{PH}$ couplings in brackets

[f] Not resolved

n.o. = not observed

Crystals of **199** and **200** suitable for X-ray diffraction study were obtained by layering of petroleum ether (b.p. 40–60 °C) on $CDCl_3/CH_2Cl_2$ solution, and by slow vapour diffusion of Et_2O into CH_2Cl_2 solution respectively. The X-ray structures have been determined (Figures 3.12 and 3.14), all the hydrogen atoms except those on N(1), have been omitted for clarity. The η^6-coordination is illustrated by thick dashed lines between the Ru atoms and the centroid of the aromatic ring of the *p*-cymene ligands(Figures 3.12 and 3.14). The structures of **199** and **200** confirm a classic "piano-stool" geometry formed by the ancillary *p*-cymene (η^6-4-$MeC_6H_4{}^iPr$) ligand and the three "legs" being the phosphorus donor of the *P*-monodentate cationic tertiary phosphine ammonium moiety and the two chlorides. There are no significant differences observed in the Ru–P and Ru–Cl bonds lengths for **199** and **200**, and both are comparable to analogous complexes with PTA.[104,110] Furthermore, upon coordination there are minimal differences in the P–C and P–C–N metric parameters between the complexes and the precursor ligands. The crystal structures reveal that the pair of intramolecular N–H···N H-bonds maintain the rigid cage structures of the precursors in the solid state even upon complexation in both complexes. Additional weak intermolecular H-bonding interactions linking the molecules into dimer pairs was also observed (Figures 3.13 and 3.15), similar to what has been recently observed in cationic dimeric Ru^{II} PTA complexes (Figure 3.11).[121]

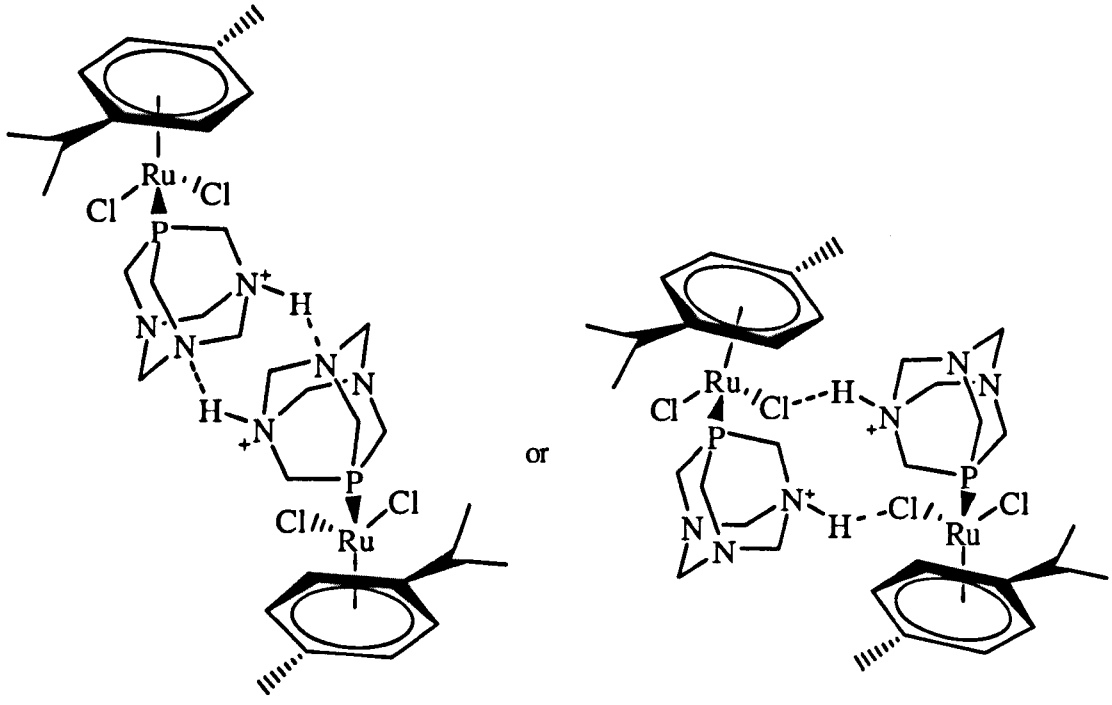

Figure 3.11 Structures of cationic dimeric Ru^{II} PTA complexes.[121]

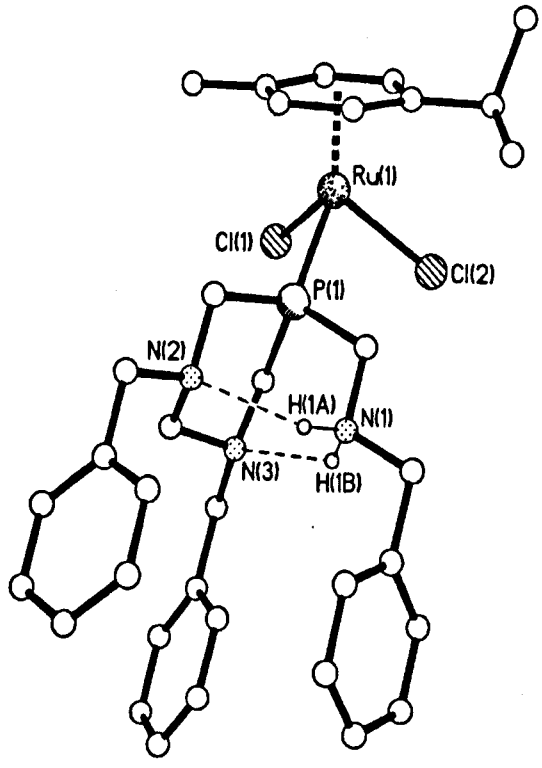

Figure 3.12 Molecular structure of **199**. The SbF_6^- counterion and $1.67CH_2Cl_2$ solvent molecules of crystallisation have been omitted for clarity.

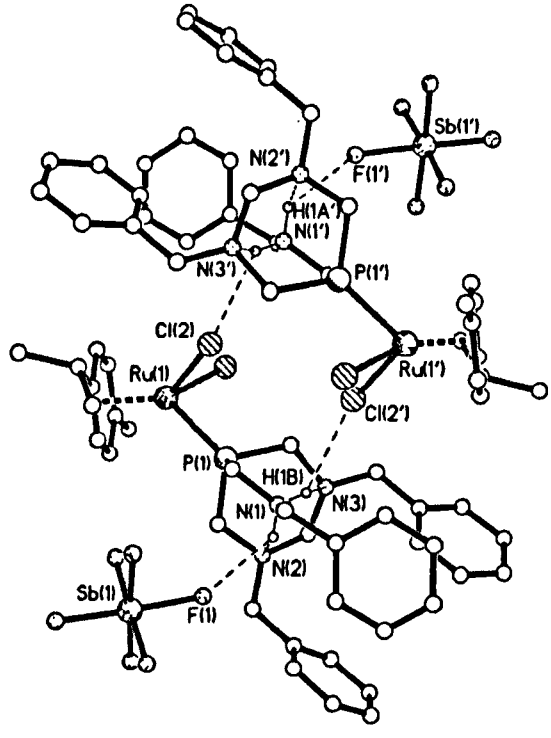

Figure 3.13 Molecular structure of **199**, showing H-bonding forming dimer pairs.

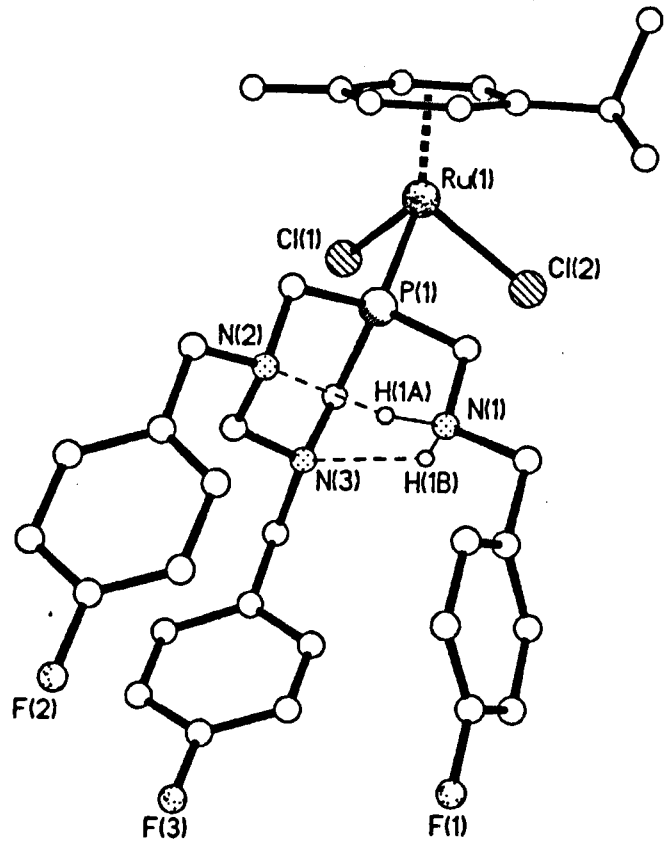

Figure 3.14 Molecular structure of **200**. The SbF_6^- counterion and $0.33CH_2Cl_2$ solvent molecule of crystallisation have been omitted for clarity.

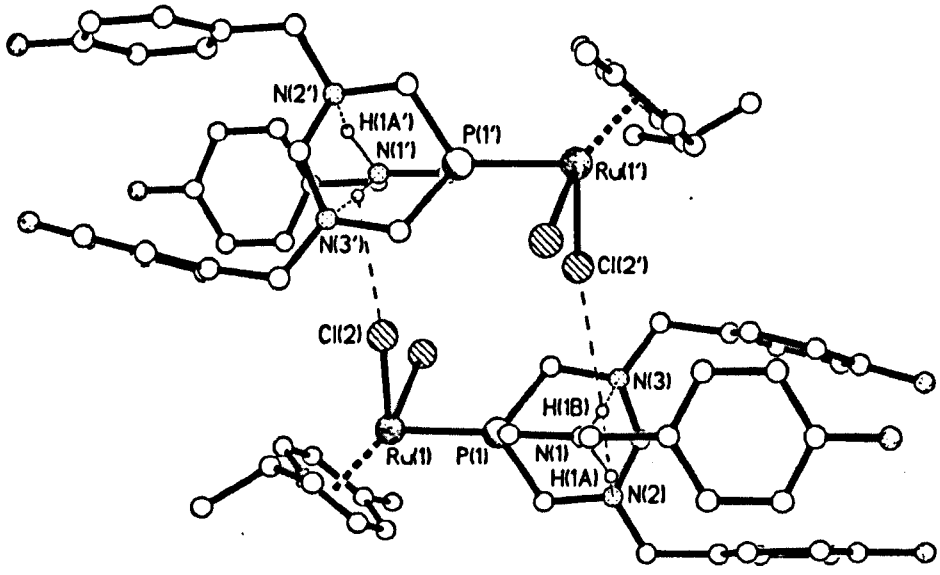

Figure 3.15 Molecular structure of **200**, showing H-bonding forming dimer pairs.

Selected bond lengths and angles are given in Tables 3.14 and 3.15 for compounds **199** and **200** respectively. The crystal data and structure refinement details for **199** and **200** are shown in Appendices 8.13 and 8.14.

Table 3.14 Selected bond lengths and angles for **199**.[a]

Bond lengths (Å)		Bond lengths (Å)		Bond angles (°)	
Ru(1)–P(1)	2.3293(6)	C(1)–N(1)	1.506(3)	P(1)–Ru(1)–Cl(1)	87.60(2)
Ru(1)–Cl(1)	2.4064(7)	C(9)–N(2)	1.474(3)	P(1)–Ru(1)–Cl(2)	83.75(2)
Ru(1)–Cl(2)	2.4103(6)	C(11)–N(3)	1.471(3)	Cl(1)–Ru(1)–Cl(2)	88.00(2)
Ru(1)–C_{av}	2.210(3)	C(19)–N(3)	1.470(3)	C(1)–P(1)–C(11)	104.69(11)
P(1)–C(1)	1.843(2)	C(12)–N(2)	1.486(3)	C(9)–P(1)–C(1)	102.68(12)
P(1)–C(9)	1.831(3)			C(9)–P(1)–C(11)	99.85(11)
P(1)–C(11)	1.828(2)				

Selected hydrogen bonding contacts

D–H···A	d(H···A) (Å)	d(D···A) (Å)	<(DHA) (°)
N(1)–H(1A)···F(1)	2.35(3)	2.914(3)	120(3)
N(1)–H(1B)···Cl(2A)	2.64(3)	3.225(2)	127(3)
N(1)–H(1A)···N(2)	2.22(3)	2.894(3)	130(3)
N(1)–H(1B)···N(3)	2.24(3)	2.840(3)	128(3)

[a] Estimated standard deviations in parentheses.

There is evidence of intra- and intermolecular hydrogen bonding in these complexes as in the case of the precursor ligands (for example **190**) as shown in Figures 3.13 and 3.15. It is interesting to note that in **199**, apart from N–H···N and N–H···Cl intra- and intermolecular hydrogen bonding respectively, there is intermolecular N–H···F hydrogen bonding (Figure 3.13) observed between the SbF_6^- counterion and N(1) atom with the N···F bond distance and N–H···F bond angle as shown in Table 3.14 comparable to other previously reported compounds.[207] Such hydrogen bonding interactions involving the SbF_6^- ions in the case of **200**, though observed in the precursor ligand (**190**, Figure 3.5) are either diminished or absent, hence not seen (Figure 3.15) probably due to repulsion between the F atoms from the SbF_6^- ion and the

three F atoms in the cationic moiety of the ligand now at the ruthenium coordination sphere.

Table 3.15 Selected bond lengths and angles for **200**.[a]

Bond lengths (Å)		Bond lengths (Å)		Bond angles (°)	
Ru(1)–P(1)	2.319(17)	C(1)–N(1)	1.501(8)	P(1)–Ru(1)–Cl(1)	87.29(7)
Ru(1)–Cl(1)	2.388(2)	C(9)–N(2)	1.467(8)	P(1)–Ru(1)–Cl(2)	84.46(6)
Ru(1)–Cl(2)	2.420(17)	C(11)–N(3)	1.472(8)	Cl(1)–Ru(1)–Cl(2)	86.85(7)
Ru(1)–C_{av}	2.212(7)	C(19)–N(3)	1.479(9)	C(1)–P(1)–C(11)	104.3(3)
P(1)–C(1)	1.839(7)	C(12)–N(2)	1.491(8)	C(9)–P(1)–C(1)	103.3(3)
P(1)–C(9)	1.824(6)			C(9)–P(1)–C(11)	99.9(3)
P(1)–C(11)	1.823(7)				

Selected hydrogen bonding contacts

D–H···A	d(H···A) (Å)	d(D···A) (Å)	<(DHA) (°)
N(1)–H(1A)···N(2)	2.05(6)	2.891(8)	129(5)
N(1)–H(1B)···N(3)	2.39(8)	2.893(8)	132(8)
N(1)–H(1B)···Cl(2A)	2.85(8)	3.273(6)	123(8)

[a] Estimated standard deviations in parentheses.

3.3.2 SYNTHESIS OF RHODIUM(I) COMPLEXES 203 AND 204

Two square-planar rhodium(I) carbonyl complexes were synthesised by reacting $Rh_2(CO)_4(\mu\text{-}Cl)_2$ with the tertiary phosphine ammonium chlorides **180** or **181** in CH_2Cl_2 under aerobic conditions at room temperature. This was followed by precipitation with Et_2O upon concentration of the solution under reduced pressure. In both cases, the desired Rh(I) complex was obtained in good to excellent yield (> 80%) as given in Table 3.16. Four equivalents of the tertiary phosphine ammonium chlorides (ligand) react with the dimer to form two moles of the square planar Rh(I) complex according to Equation 3.4. Both complexes were pale orange solids.

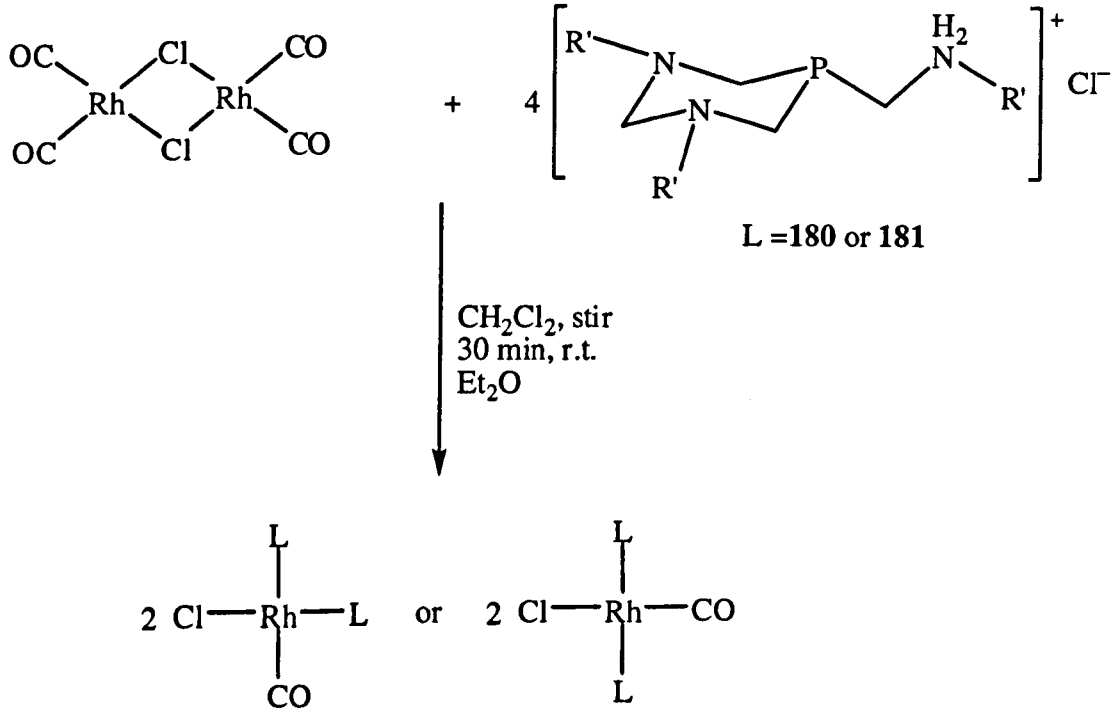

Equation 3.4.

3.3.2.1 CHARACTERISATION OF COMPOUNDS 203 AND 204

Compounds **203** and **204** were characterised by LSI–MS, microanalysis and FT–IR, the results are given in Tables 3.16 and 3.17. Compounds **203** and **204** were extremely insoluble in both non polar and polar solvents; hence no meaningful NMR [^{1}H, ^{31}P{^{1}H}] spectral data could be obtained.

Table 3.16 Percentage yield (isolated), LSI–MS and selected FT-IR data[a] (in cm^{-1}) for compounds **203** and **204**.

	% yield	*m/z* [M–2H–Cl]$^{+}$	ν(NH$_2^{+}$)	ν(CH)	ν(CO)	ν(RhCl)
203	88	1009	3034(w)	2928 (w)	1979 (s)	n.o.
204	93	1117	3044 (m)	2939 (m)	1979 (s)	n.o.

[a] Recorded as pressed KBr disk; n.o. = not observed.

The LSI–MS data (Table 3.16), for compounds **203** and **204** are in agreement with the loss of two H and one Cl, *m/z* $[M–2H–Cl]^+$. In both cases, the complexes precipitated with some amount of solvent as shown by the microanalysis results (Table 3.17).

The FT–IR spectra for **203** and **204** were recorded in the solid state as pressed KBr disks; selected data are given in Table 3.16. The ν(CH) stretches were similar to those of the free ligands. Similarly, the $\nu(NH_2^+)$ stretches were also not significantly different from those of the free ligands and were observed at *ca.* 3030 cm^{-1}. There was an intense CO stretch observed at 1979 cm^{-1} in each case. Although no direct comparisons between the FT–IR data for **203** and **204** with the known neutral complexes *trans*-$Rh(CO)Cl(PTA)_2$ [ν_{CO} = 1963 cm^{-1} (chloroform)][209] and *trans*-$Rh(CO)Cl(PTAR_3)_2$ where R = "lower rim" PTA substituent, C_6H_5, C_6H_4OMe, C_6H_4CN [ν_{CO} = 1978–1987 cm^{-1} (chloroform)] [210] can be drawn, **180** and **181** can be regarded as having similar electron donating properties to this class of PTA ligands. The Rh–Cl vibrations normally observed below 300 cm^{-1} were not seen because of the relatively shorter range (4000–500 cm^{-1}) of FT–IR spectrometer used.

The microanalytical data are given in Table 3.17; the values agree within acceptable limits and are consistent with the formulae of the rhodium(I) complexes **203** and **204**.

Table 3.17 Microanalysis (%) and molecular formulae for compounds **203** and **204**.[a]

	C	H	N	Molecular formula
203	54.28 (54.45)	5.40 (5.65)	7.46 (7.29)	$C_{51}H_{62}N_6OP_2RhCl_3 \cdot 1.25CH_2Cl_2$
204	50.63 (50.40)	4.70 (4.72)	6.94 (6.78)	$C_{51}H_{56}N_6OP_2F_6RhCl_3 \cdot CH_2Cl_2$

[a] Calculated values in parentheses.

As mentioned earlier, no meaningful NMR [^1H, $^{31}P\{^1H\}$] spectral data could be obtained for **203** and **204** due to insolubility in common solvents, hence direct elucidation of their geometry by NMR spectroscopy is not possible. However, the solution $^{31}P\{^1H\}$ NMR spectra of the known analogous complexes $Rh(CO)Cl(PTA)_2$, $Rh(CO)Cl(PTAR_3)_2$ [R = "lower rim" PTA substituent, C_6H_5, C_6H_4OMe, C_6H_4CN] gave single doublets in the range –54.4 to –60.1 ppm with $^1J_{PRh}$ values between 117

and 127 Hz indicative of the formation of the *trans* isomer only in all cases.[209,210] From the literature highlighted, it can therefore be suggested that the complexes **203** and **204** also exhibit *trans* configuration.

3.3.3 SYNTHESIS OF RHODIUM(III) AND IRIDIUM(III) COMPLEXES 205–210

The dimeric chloro bridged complexes $[MCl_2(\eta^5\text{-}Cp^*)]_2$ M = Rh or Ir are known to undergo chloro bridge cleavage reactions leading to the formation of series of interesting neutral and cationic mononuclear complexes.[196] It has been demonstrated by Dyson and co-workers[51] and Erlandsson *et al.*[211] that half-sandwich organometallic Rh(III) and Ir(III) complexes respectively of PTA could be synthesised using these chloro bridged complexes.

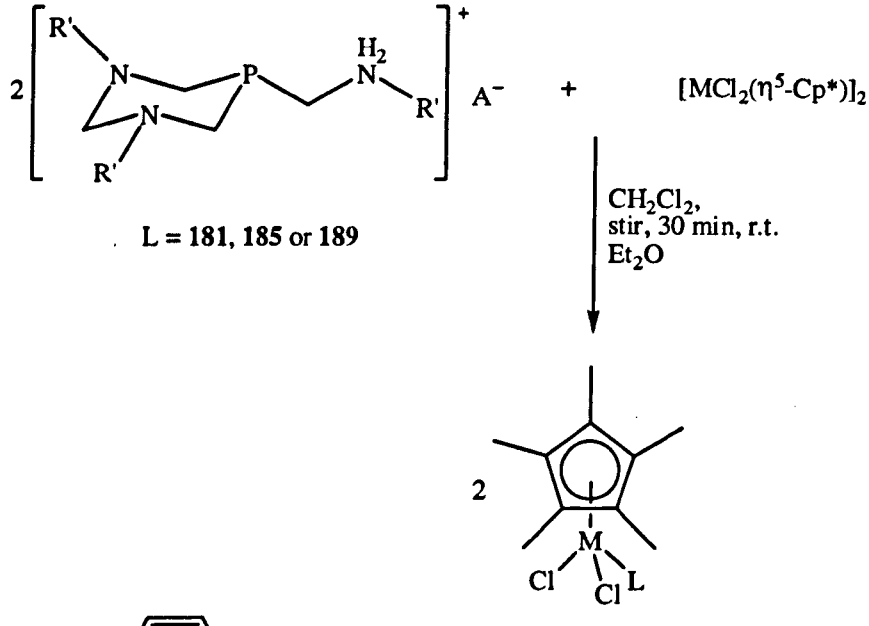

Where R' = 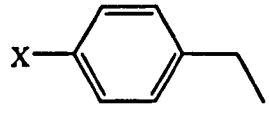 and M = Rh, X = F, A = Cl, **205**; M = Rh, X = H, A = BPh_4, **206**
M = Rh, X = H, A = SbF_6, **207**; M = Ir, X = F, A = Cl, **208**
M = Ir, X = H, A = BPh_4, **209**; M = Ir, X = H, A = SbF_6, **210**

Equation 3.5.

In order to assess whether the tertiary phosphine ammonium salts could function as similar *P*-monodentate ligands to further establish the relationship between the tertiary phosphine ammonium salts and PTA, three complexes each of rhodium(III) and iridium(III) were synthesised by reacting **181**, **185** or **189** with $[MCl_2(\eta^5\text{-}Cp^*)]_2$, M =

Rh or Ir respectively in CH_2Cl_2 under aerobic conditions at room temperature. This was followed by precipitation with Et_2O after concentration of the solution under reduced pressure. In all the cases, the desired M(III) complexes were obtained as orange solids in good to excellent yield (> 80%) as given in Table 3.18. Two equivalents of the ligand react with the dimer to form two moles of the corresponding M(III) complex according to Equation 3.5.

3.3.3.1 CHARACTERISATION OF COMPOUNDS 205–210

The complexes were characterised as in the previous cases by conventional techniques namely MS, microanalysis, FT–IR, NMR; the results are given in Tables 3.18–3.20. Single crystal X-ray crystallography was also used for **207** and **208** where suitable crystals were obtained.

Table 3.18 Percentage yield (isolated), FAB-MS and selected FT-IR data[a] (in cm^{-1}) for compounds **205–210**.

	% yield	*m/z*[M–X]$^{+}$ [b]	ν(NH_2^+)	ν(CH)	ν(MCl)	ν(SbF)
205	88	766	3040 (w)	2920 (w)	290 (w)	
206	96	712	3029 (m)	2981 (m)	279 (w)	
207	98	712	3031 (m)	2950 (w)	290 (vs)	660 (vs)
208	96	857	3050 (w)	2921 (w)	296 (w)	
209	85	802	3054 (w)	2981 (w)	295 (w)	
210	77	802	3019 (w)	2923 (w)	290 (vs)	662 (vs)

[a] Recorded as a pressed KBr disk; [b] X = Cl^-, BPh_4^-, SbF_6^-; MCl = RhCl or IrCl.

The FAB–MS data (Table 3.18) for compounds **205–210** were in agreement with the loss of the respective counterion (*m/z* [M–X]$^+$). The FT–IR spectra for **205–210** were recorded in the solid state as pressed KBr disks. The ν(CH) stretches were similar to those of the free ligands, similarly, the ν(NH_2^+) stretches were also not significantly different from those of the free ligands and were observed in the range 3019–3054 cm^{-1}. The M–Cl vibrations were very weak unlike in the case of the ruthenium(II) complexes **197–202**; there was however, a very strong ν(MCl) band at 290 cm^{-1} in the

case of compounds **207** and **210**. The very strong bands at 660 and 662 cm^{-1} due to Sb–F support the presence of the SbF_6^- counterions in the case of compounds **207** and **210**.

The microanalytical data are given in Table 3.19; the values agree within acceptable limits and are consistent with the proposed molecular formulae of the rhodium(III) and iridium(III) complexes **205–210**. In all except **210**, the complexes precipitated with some amount of solvent as shown by the microanalysis results (Table 3.19).

Table 3.19 Microanalysis (%) and molecular formulae for compounds **205–210**.[a]

	C	H	N	Molecular formula
205	49.47 (49.54)	5.13 (5.17)	4.86 (4.85)	$C_{35}H_{43}N_3F_3PRhCl_3 \cdot 0.75CH_2Cl_2$
206	60.70 (60.92)	5.95 (5.87)	3.32 (3.49)	$C_{59}H_{66}N_3PBRhCl_2 \cdot CH_2Cl_2$
207	41.46 (41.81)	4.50 (4.68)	4.07 (4.07)	$C_{35}H_{46}N_3PRhCl_2SbF_6 \cdot CH_2Cl_2$
208	41.09 (41.29)	4.37 (4.42)	4.04 (3.88)	$C_{35}H_{43}N_3F_3PIrCl_3 \cdot 2.25CH_2Cl_2$
209	60.23 (60.52)	5.89 (5.74)	3.71 (3.54)	$C_{59}H_{66}N_3PBIrCl_2 \cdot 0.75CH_2Cl_2$
210	40.60 (40.48)	4.58 (4.46)	4.05 (4.05)	$C_{35}H_{46}N_3PIrCl_2SbF_6$

[a] Calculated values in parentheses.

The NMR spectral data recorded in d^6-DMSO are given in Table 3.20. In compounds **205–207**, the $^{31}P\{^1H\}$ NMR spectra showed a doublet with δ(P) values between 3.24 and 4.75 ppm and an average $^1J_{PRh}$ coupling constant of *ca.*145 Hz comparable to what was found for other Rh(III) compounds reported previously.[199] On the other hand, the spectra of **208–210** showed singlets with δ(P) values between –25.34 and –26.35 ppm. In both cases as was observed in the ruthenium(II) complexes **197–202** mentioned in (Section 3.3.1), the ^{31}P resonances were significantly downfield compared with the precursor salts given in Tables 3.3 and 3.7 and are in good agreement with *P*-monodentate coordination.

The average coordination chemical shifts for the rhodium(III) compounds **205–207** ($\Delta\delta_P$ 59 ppm) were also not significantly different from the analogous rhodium(III)(PTA) compound, $RhCl_2(\eta^5\text{-}Cp^*)(PTA)$ ($\Delta\delta_P$ 65 ppm) suggesting similar stereoelectronic properties.[51] Similarly, the average coordination chemical shifts for the

Ir(III) compounds, **208–210** ($\Delta\delta_P$ 29 ppm) were the same as what was obtained in the analogous Ir(III)(PTA) compound, $IrCl_2(\eta^5\text{-}Cp^*)(PTA)$ ($\Delta\delta_P$ 29 ppm) suggesting similar stereoelectronic properties.[211]

In the ^1H NMR spectra of the complexes, the ring methyl protons were observed as singlets in the range 1.65–1.70 ppm, possibly not resolved, except **205** which showed a doublet, indicative of long range coupling between phosphorus and the ring methyl protons of the pentamethylcyclopentadienyl moiety [$^4J_{PH}$, 3.2 Hz] (Table 3.20) similar to what was found in the analogous PTA complexes, $RhCl_2(\eta^5\text{-}Cp^*)(PTA)$ [$\delta(H)$ = 1.69 ppm, d, $^4J_{PH}$ = 3.5 Hz, $CDCl_3$][51] and $IrCl_2(\eta^5\text{-}Cp^*)(PTA)$ [δ = 1.79 ppm, d, $^4J_{PH}$ = 2.0 Hz, $CDCl_3$].[211] There were singlet CH_2 resonances between 4.08 and 4.40 ppm (Table 3.20) which were also similar to 4.33 and 4.51 ppm and 4.20 and 4.70 ppm assigned to the methylene protons within the PTA ligand in the analogous rhodium(III)[51] and iridium(III) PTA complexes[211] respectively.

Table 3.20 Selected NMR data (in ppm or Hz) for **205–207.**[a]

	δ(P)	δH/(arom.)	δH/(CH_2)	δH/(CH_2)	δH/(CH_2)[c]	δH/(CH_2)[d]	δH/(η^5-Cp*)[e]
205	3.24(146)[b]	6.53–7.93, m	4.37, s	4.08, s	3.77 (12.4)	3.23	1.70 (3.2)
206	4.75(146)[b]	6.74–7.51, m	4.37, s	4.10, s	3.76 (12.0)	3.21	1.66[f]
207	4.61(144)[b]	6.93–7.51, m	4.37, s	4.10, s	3.76 (12.4)	3.22	1.65[f]
208	–26.35	6.70–6.89, m	4.38, s	4.08, s	3.77 (12.0)	3.13	1.67[f]
209	–25.34	6.79–7.52, m	4.40, s	4.10, s	3.77 (12.0)	3.15	1.70[f]
210	–25.34	6.86–7.52, m	4.40, s	4.10, s	3.78 (12.8)	3.14	1.70[f]

[a] All NMR spectra were recorded in d^6-DMSO; [b] Doublets $^1J_{PRh}$ coupling in brackets

[c] (CH_2) protons, d, $^2J_{PH}$ coupling in brackets

[d] (CH_2) protons, multiplicity could not be fully assigned due to overlap with residual solvent resonances

[e] (η^5-Cp*) protons, d, $^4J_{PH}$ coupling in brackets

[f] Not resolved, s

A few X-ray quality crystals of compounds **207** and **208** were obtained in each case from a solution in acetone and by vapour diffusion of Et_2O into a $DMSO/CH_2Cl_2/MeOH$ solution kept over several days and the X-ray structures have been determined, though not completed in the case of **208** is supportive of *P*-monodentate coordination and a typical "piano-stool" geometry around the metal centre (Figure 3.16).

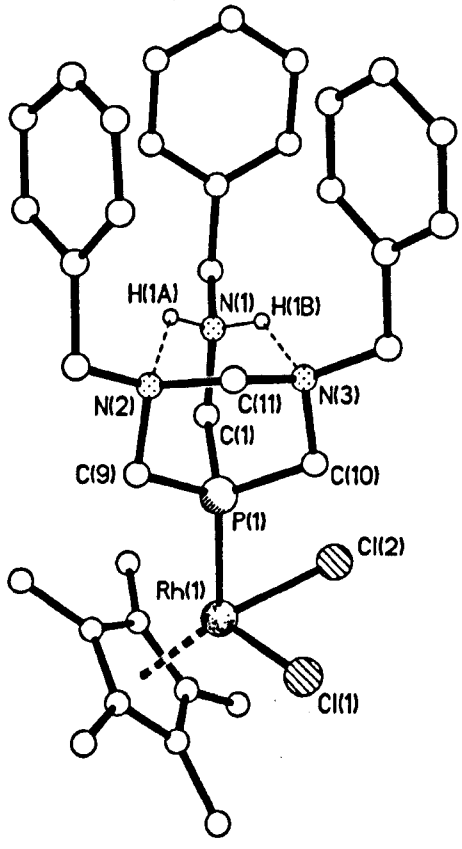

Figure 3.16 Molecular structure of **207**. The SbF_6^- counterion and $2CH_2Cl_2$ solvent molecules of crystallisation have been omitted for clarity.

The structure confirms a classic "piano-stool" geometry formed by the ancillary η^5-Cp* ligand and the three "legs" being the phosphorus donor of the *P*-monodentate cationic tertiary phosphine ammonium moiety and the two chlorides. The Rh–P and Rh–Cl bond lengths for **207** [Rh–P = 2.2851(19) Å; $(Rh–Cl)_{av}$ = 2.415(2) Å] are comparable to analogous complexes with PTA [Rh–P = 2.286(1) Å; $(Rh–Cl)_{av}$ = 2.417(1) Å].[51] The two P–Rh–Cl bond angles in **207** are also comparable to those found in the analogous PTA complex, $RhCl_2(\eta^5$-Cp*)(PTA).[51] Furthermore, upon coordination as in the case of the ruthenium(II) complexes discussed in Section 3.3.1, there are minimal differences

in the P–C and P–C–N metric parameters between the complex and its precursor ligand. The crystal structure reveals that, again the pair of intramolecular N–H···N H-bonds maintain the rigid cage structure of the precursor salt in the solid state even upon complexation.

Selected bond lengths and angles for compound **207** are given in Table 3.21. The crystal data and structure refinement details for **207** are shown in Appendix 8.15.

Table 3.21 Selected bond lengths and angles for **207**.[a]

Bond lengths (Å)		Bond lengths (Å)		Bond angles (°)	
Rh(1)–P(1)	2.2851(19)	C(1)–N(1)	1.497(8)	P(1)–Rh(1)–Cl(1)	88.85(7)
Rh(1)–Cl(1)	2.406(2)	C(9)–N(2)	1.476(10)	P(1)–Rh(1)–Cl(2)	83.37(7)
Rh(1)–Cl(2)	2.424(2)	C(10)–N(3)	1.482(9)	Cl(1)–Rh(1)Cl(2)	92.67(8)
Rh(1)–C_{av}	2.189(7)	P(1)–C(9)	1.836(8)	P(1)–C(1)–N(1)	115.4(5)
P(1)–C(1)	1.834(7)	P(1)–C(10)	1.830(7)	P(1)–C(9)–N(2)	110.1(5)
				P(1)–C(10)–N(3)	110.0(5)

Selected hydrogen bonding contacts

D–H···A	d(H···A) (Å)	d(D···A) (Å)	<(DHA) (°)
N(1)–H(1B)···Cl(2')	2.65	3.291(6)	127.8
N(1)–H(1A)···N(2)	2.34	2.952(9)	123.8
N(1)–H(1A)···F(1)	2.40	3.022(9)	124.4
N(1)–H(1A)···F(1X)	2.89	3.35(3)	112.2
N(1)–H(1B)···N(3)	2.18	2.851(8)	128.6

[a] Estimated standard deviations in parentheses.

The intramolecular N–H···N hydrogen bonding parameters involving the N(1) and N(2); N(1) and N(3) for **207** are given in Table 3.21.

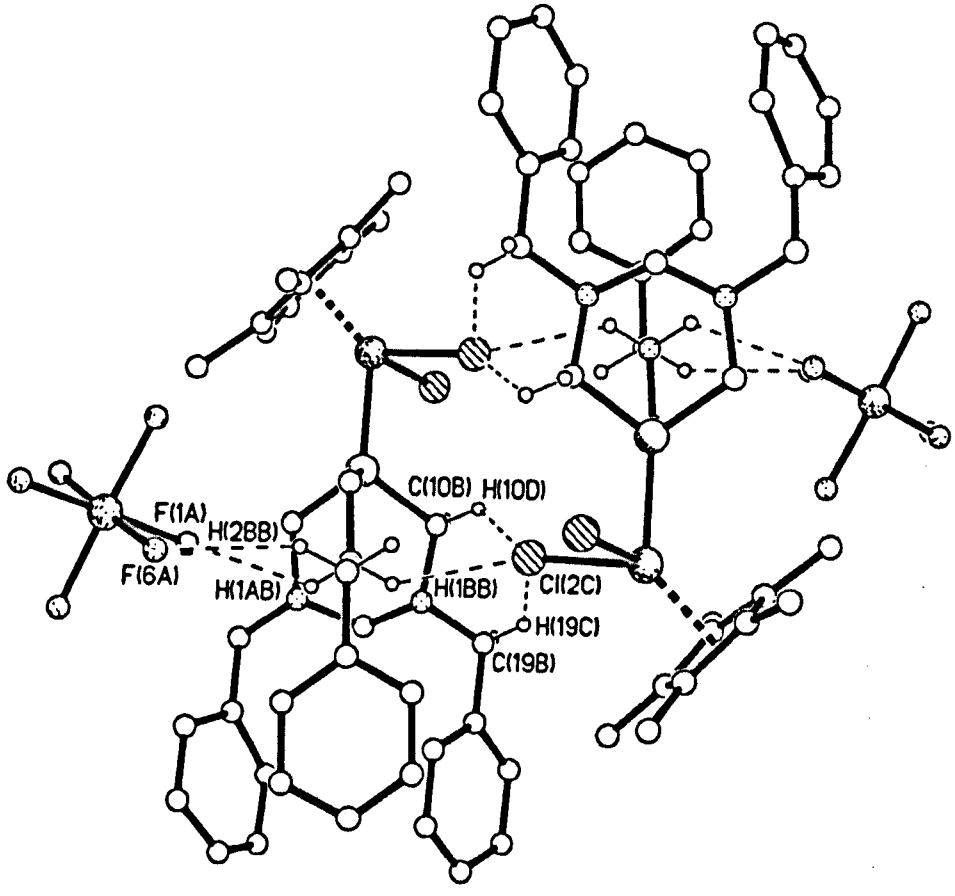

Figure 3.17 Molecular structure of **207**, showing H-bonding forming dimer pairs.

Additional weak intermolecular H-bonding interactions involving the chlorides, linking molecules into dimer pairs as well as H-bonding between the F atoms from the SbF_6^- ion and N(1) atom was evident (Figure 3.17, Table 3.21).

3.3.4 COORDINATION OF MONOMERIC PALLADIUM(II) PRECURSORS WITH 180, 181, 189 OR 190

The coordination potential of the tertiary phosphine ammonium salts was also evaluated by reacting **180**, **181**, **189** or **190** with various monomeric palladium(II) precursors namely $PdCl_2(COD)$, $PdCl_2(CH_3CN)_2$ and Pd(Me)Cl(COD). The reactions were performed under various reaction conditions in order to obtain $PdCl_2L_2$ type complexes (L = Ligand) after displacing the labile COD or CH_3CN ligands.

3.3.4.1 SYNTHESIS AND CHARACTERISATION OF PALLADIUM(II) COMPLEX 211

Reaction of two equivalents of **180** with $PdCl_2(COD)$ in $CHCl_3$, refluxed at 90 °C under N_2 for 2 h, gave a yellow solid **210** in 65% yield as shown in Equation 3.6.

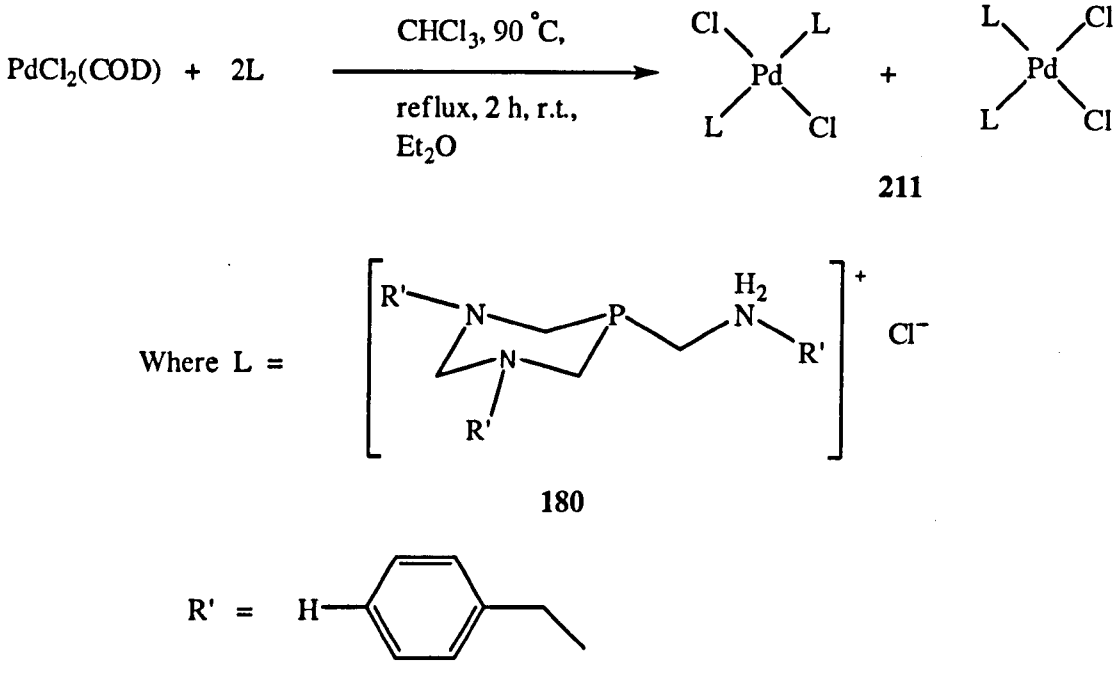

Equation 3.6

The solution $^{31}P\{^1H\}$ NMR spectrum of compound **211**, recorded in d^6-DMSO, showed a phosphorus resonance at δ(P) −0.65 ppm significantly downfield of the value for the free ligand at δ(P) −55.08 ppm. The ^1H NMR spectrum gave multiplets in the range 6.60–7.80 and 3.71–3.80 ppm, for the aromatic and CH_2 protons respectively. There was coprecipitation of solvent consistent with the microanalytical data for **211**: $C_{50}H_{62}N_6P_2PdCl_4 \cdot 0.5CHCl_3$ requires: C, 54.31; H, 5.64; N, 7.52. Found: C, 54.77; H, 5.72; N, 7.60 %. The FT–IR spectrum of **211** was run as a pressed KBr disk. The NH_2^+ vibrations were at a slightly lower wave number, 2920 cm^{-1} compared with the value for the precursor ligand observed at 3028 cm^{-1}. Two Pd–Cl stretches were observed at 291 and 319 cm^{-1} in the IR spectrum indicative of *cis* disposition of the chloride ligands.

Some X-ray quality crystals were obtained by slow vapour diffusion of Et_2O into a chloroform solution of **211** over several days and the structure has been determined. The X-ray diffraction analysis on one of these crystals gave a novel unexpected six-membered chelate complex **211'** (Figure 3.18) which was not consistent with the other characterising data for **211**.

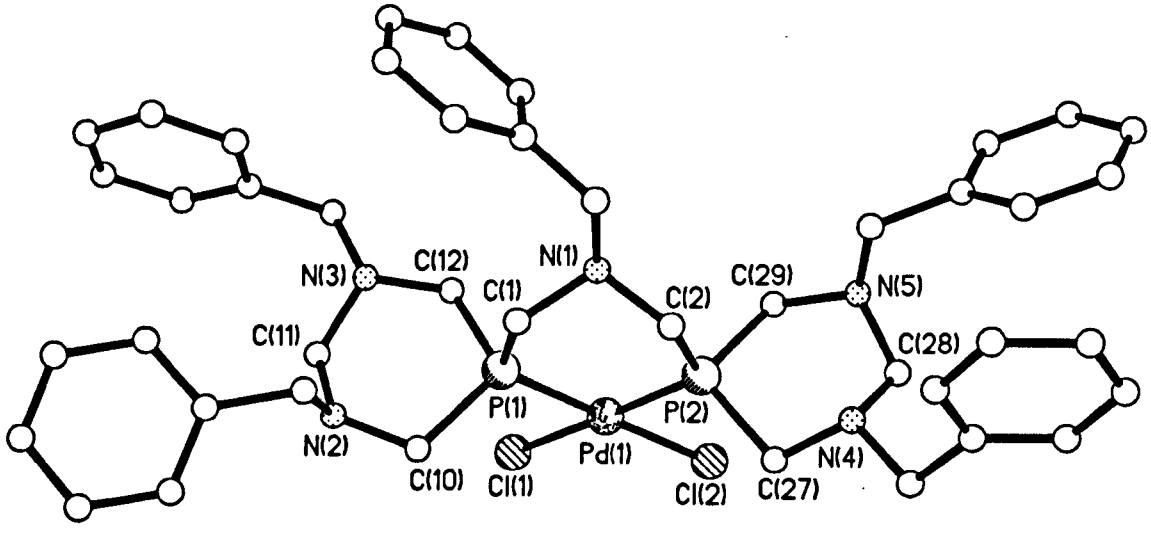

Figure 3.18 Molecular structure of **211'**.

The structure of **211'** reveals an approximate square-planar geometry with the Pd–Cl and Pd–P bond lengths and angles about the palladium(II) centre were within the expected range for other square-planar Pd(II) phosphine chloride complexes [146,201] as well **169** and **170** in Section 2.4.3. The only exception being that the P(1)–Pd(1)–P(2) bond angle [92.60(7)°] was smaller than the P(1)–Pd(1)–P(2) bond angle [100.45(5)°] in **169** probably due to the constraint caused by the six-membered Pd–P–C–N–C–P chelate ring. The X-ray diffraction analysis does not indicate the presence of H-bonding supportive of the absence of donor/acceptor groups. Selected bond lengths and angles are given in Table 3.22. This structural motif is supported by the absence of any hits from a CSD search.[191,192] The crystal data and structure refinement for **211'** are shown in Appendix 8.16.

Table 3.22 Selected bond lengths and angles[a] for **211′**.

Bond lengths (Å)		Bond lengths (Å)		Bond angles (°)	
Pd(1)–P(1)	2.226(2)	P(1)–C(10)	1.836(7)	P(1)–Pd(1)–P(2)	92.60(7)
Pd(1)–P(2)	2.223(2)	P(1)–C(12)	1.817(7)	P(1)–Pd(1)–Cl(1)	88.51(7)
Pd(1)–Cl(1)	2.371(2)	P(2)–C(27)	1.826(7)	P(2)–Pd(1)–Cl(2)	87.97(7)
Pd(1)–Cl(2)	2.353(19)	P(2)–C(29)	1.856(7)	Cl(1)–Pd(1)–Cl(2)	90.87(7)
P(1)–C(1)	1.836(7)	C(1)–N(1)	1.457(8)	Cl(1)–Pd(1)–P(2)	177.37(8)
P(2)–C(2)	1.813(7)	C(2)–N(2)	1.455(8)	Cl(2)–Pd(1)–P(1)	178.82(8)

[a] Estimated standard deviations in parentheses.

A plausible explanation for the transformation from **211** to the chelate complex **211′**, as observed in the X-ray diffraction analysis, is given below (Equation 3.7).

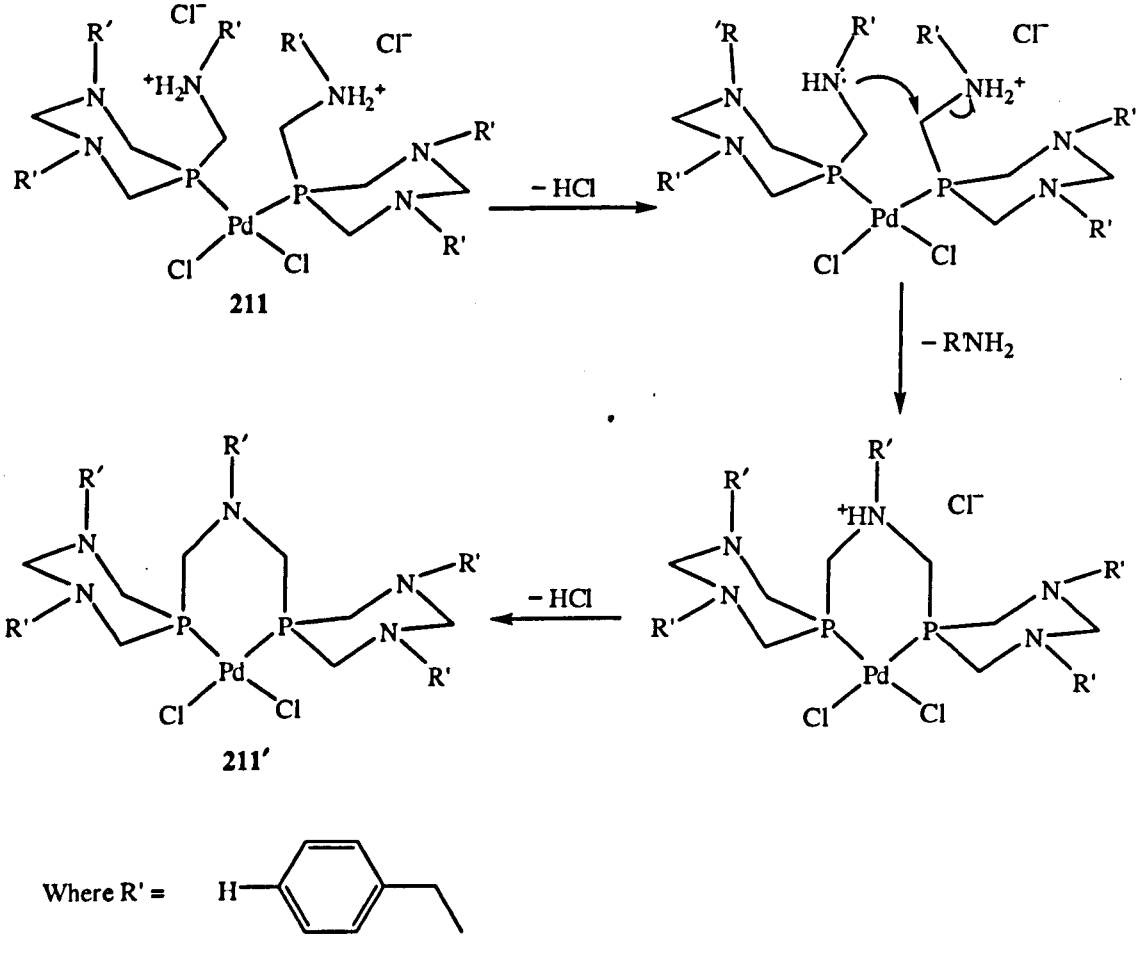

Equation 3.7.

This transformation might primarily be due to the bulky nature of the two phosphine ligands not fitting into the coordination sphere of the metal in a *cis* arrangement or the driving force may be formation of a six-membered ring (chelate effect). During the crystallisation process, there is probable intramolecular rearrangement involving the two exocyclic fragments in the two phosphine ligands at the Pd(II) centre. There is loss of a proton from the ammonium group in the exocylic fragment in one phosphine ligand which is eliminated as HCl resulting in the formation of a lone pair of electrons on the ammonium N atom. The lone pair of electrons is then donated to the carbon in the P–C–N fragment of the exocyclic fragment in the second phosphine ligand. This leads to the loss of a molecule of benzylamine in the second phosphine ligand and the formation of an ionic six-membered Pd–P–C–N–C–P chelate compound, which loses a molecule of HCl to form the new neutral six-membered Pd–P–C–N–C–P chelate complex **211′**, as proposed in Equation 3.7. This mechanism is similar to the transformation of $[P(CH_2NHPh)_4]Cl$ to a six-membered P–C–N–C–N–C ring compound (diazaphosphorinane) aided by Et_3N probably *via* an intramolecular mechanism shown in Scheme 1.2.[10]

3.3.4.2 SYNTHESIS AND CHARACTERISATION OF PALLADIUM(II) COMPLEX 212

The reaction of $PdCl_2(COD)$ with **181** was attempted under a different reaction condition. Two equivalents of **181** were reacted with $PdCl_2(COD)$ in CH_2Cl_2 at room temperature under aerobic conditions for 24 h. This was followed by precipitation with Et_2O upon concentration of the solution under reduced pressure and the resulting yellow solid, **212** was obtained in high yield. The product conforms to the expected $PdCl_2L_2$ complex as supported by the microanalytical data. The solution $^{31}P\{^1H\}$ NMR spectrum of compound **212** in d^6-DMSO showed a major phosphorus resonance (>70 %) at δ(P) –0.88 ppm significantly downfield of the δ(P) value for the free ligand, –54.72 ppm, while the ^1H NMR spectrum showed the following proton resonances: 9.14 (br, NH_2), 6.80–7.70 (m, arom. H) and 3.71–4.80 (m, CH_2), ppm. The microanalytical data for **212** is consistent with the formula, $C_{50}H_{56}N_6P_2F_6PdCl_4{\cdot}0.25CH_2Cl_2$ requires: C, 50.87; H, 4.80; N, 7.08. Found: C, 50.56; H, 4.89; N, 7.02 %. The FT–IR spectrum of **212** run as pressed KBr disk showed a sharp NH_2^+ vibration at 2988 cm^{-1} slightly different from the value for the precursor

ligand **181** observed at 3044 cm^{-1} and a single Pd–Cl vibration at 307 cm^{-1}, indicative of *trans* disposition of the two coordinated chloride ligands in this case. Attempts to obtain suitable crystals for X-ray diffraction analysis were unsuccessful.

3.3.4.3 SYNTHESIS AND CHARACTERISATION OF PALLADIUM(II) COMPLEXES 213–215

Palladium compounds with higher lability and *trans*-directing propensity such as $PdCl_2(CH_3CN)_2$, were also used as suitable sources of Pd(II) in the coordination reactions of the tertiary phosphine ammonium salts. In these reactions, there is greater probability of forming the expected ML_2Cl_2 type complexes in which the bulky ligands fit around the metal coordination sphere in a *trans* arrangement. Reaction of $PdCl_2(CH_3CN)_2$ with **181**, **189** or **190** in CH_2Cl_2 at room temperature followed by precipitation with Et_2O upon concentration of the solution under reduced pressure gave the yellow compounds **213–215**. In all cases, the ligands readily react to form the desired palladium(II) complex in excellent yields (Table 3.23). Two equivalents of the ligand react with $PdCl_2(CH_3CN)_2$ to form the Pd(II) complexes according to Equation 3.8.

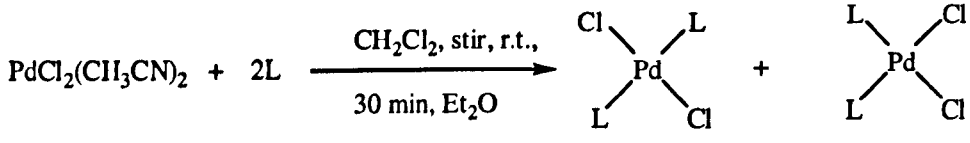

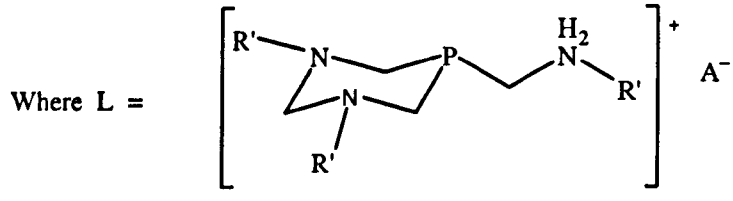

181, 189 or 190

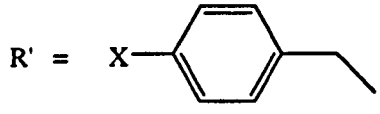

and X = F, A = Cl, **213**;
X = H, A = SbF_6, **214**;
X = F, A = SbF_6, **215**

Equation 3.8.

Characterisation was achieved by microanalysis, FT-IR and NMR spectroscopy. The results are given in Tables 3.23–3.25.

Table 3.23 Percentage yield (isolated) and selected FT-IR data[a] (in cm^{-1}) for compounds **213–215**.

Compound	% yield	$\nu(NH_2^+)$	ν(CH)	ν(SbF)	ν(PdCl)
213	94	2941 (s)	2811 (m)		308 (w)
214	91	3030 (s)	2820 (m)	661	290 (vs)
215	84	3044 (s)	2827 (m)	661	292 (vs)

[a] Recorded as a pressed KBr disk.

The FT–IR spectra for **213–215** were also run as pressed KBr disks; selected data are given in Table 3.23. The $\nu(NH_2^+)$ stretches of the palladium(II) complexes were in the range 2941–3044 cm^{-1} and were not significantly different from those of the precursor ligands. On the other hand, the ν(CH) stretches were slightly lowered on coordination to the palladium(II) centre, for example in **215** the ν(CH) stretch in the precursor ligand, **190** was 2954 cm^{-1} but on coordination in compound **215**, the band was shifted to 2827 cm^{-1}. The strong infrared Sb–F bands at 661 cm^{-1} in compounds **214** and **215** confirm the presence of the SbF_6^- counterions in these complexes. The infrared spectra of the palladium(II) complexes showed single ν(Pd–Cl) stretches in the range 290 to 308 cm^{-1}, that of **213** was weak, while those of **214** and **215** very strong, indicating in all cases that a *trans* isomer was formed.

There was evidence of coprecipitation of the solvent in these complexes; this is in agreement with the microanalytical data given in Table 3.24. The agreement between the observed and calculated CHN values in Table 3.24 is consistent with the formulation of the palladium(II) complexes **213–215**.

Table 3.24 Microanalysis (%) and molecular formulae for compounds **213–215**.[a]

	C	H	N	Molecular formula
213	49.96 (49.60)	4.84 (4.72)	6.95 (6.84)	$C_{50}H_{56}N_6P_2F_6PdCl_4 \cdot 0.75CH_2Cl_2$
214	36.80 (37.17)	4.03 (4.00)	5.08 (4.91)	$C_{50}H_{62}N_6P_2Sb_2F_{12}PdCl_2 \cdot 3CH_2Cl_2$
215	37.27 (37.72)	3.43 (3.57)	5.17 (5.23)	$C_{50}H_{62}N_6P_2Sb_2F_{18}PdCl_2 \cdot 0.5CH_2Cl_2$

[a] Calculated values in parentheses.

The solution $^{31}P\{^{1}H\}$ NMR spectra of these complexes, recorded in d^6-DMSO, showed multiple signals; in all cases the major signal being significantly downfield of the corresponding value for the ligand. For example the major δ(P) value for **215** was at –0.67 ppm (Table 3.25), while the δ(P) for the corresponding ligand was at –54.92 ppm. The multiple signals could be due to a mixture of *P*-containing species or possible decomposition of phosphorus containing products in the NMR solvent.

Table 3.25 Selected NMR data (in ppm) for **213–215**.[a]

	Major δ(P)	Other ^{31}P Signals	δ(H)/arom.	δ(H)/CH_2	δ(H)/NH_2^+
213	–0.47	–20.69, –30.24	7.07–7.69	3.86–4.82	8.37
214	–0.62	–20.32, –30.74	7.15–7.55	3.56–4.84	8.18
215	–0.67	–20.36, –30.22	6.92–7.45	3.52–4.73	8.16

[a] All NMR spectra were recorded in d^6-DMSO.

Two of these multiple ^{31}P signals in these spectra could also indicate the presence of both the *cis* and *trans* isomers in solution. This not withstanding, in the solid state the FT–IR spectra indicated the presence of the *trans* isomer. The fact that in all cases the major signal falls within the narrow range –0.47 to –0.67 ppm coupled with strong single ν(Pd–Cl) stretches in the IR spectra strongly suggest *P*-coordination and formation of the *trans* isomer.

Selected ^{1}H NMR resonances of the complexes are given in Table 3.25; the aromatic and the CH_2 proton signals fall within the expected values. The δ(H) values for the NH_2^+ protons are downfield (8.16–8.37 ppm) indicative of being adjacent to the electronegative N atom of the ammonium salt. Attempts to obtain X-ray quality crystals were unsuccessful.

3.3.4.4 SYNTHESIS AND CHARACTERISATION OF PALLADIUM(II) COMPLEXES 216 AND 217

The palladium(II) precursor Pd(Me)Cl(COD) was also reacted with the tertiary phosphine ammonium salts in order to evaluate their coordination potential.

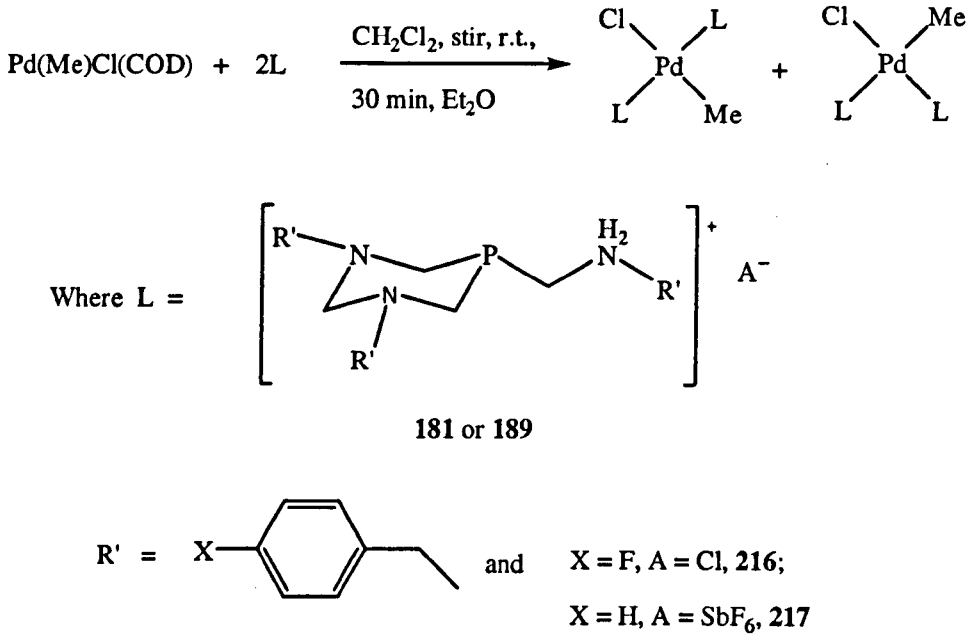

Equation 3.9.

Reaction of Pd(Me)Cl(COD) with **181** or **189** under similar reaction conditions as for $PdCl_2(CH_3CN)_2$, as described in Section 3.3.4.3, gave the orange solids **216** and **217**. In both cases, the ligands readily react to form the desired palladium(II) complex in excellent yields (Table 3.26). Two equivalents of the ligand react with Pd(Me)Cl(COD) to form the complexes **216** and **217** according to Equation 3.9 in high yield (Table 3.26).

Characterisation as in the previous cases was achieved by MS, microanalysis, FT–IR and NMR, the results are given in Tables 3.26–3.28. The FAB–MS data (Table 3.26), for compounds **216** and **217** are in agreement with the loss of two anions (*m/z* $[M-2X]^+$) per mole of the respective palladium(II) complexes.

Table 3.26 Percentage yield (isolated), FAB-MS and selected FT-IR data[a] (in cm^{-1}) for compounds **216** and **217**.

	% yield	*m/z* $[M-2X]^+$ [b]	ν(NH_2^+)	ν(CH)	ν(SbF)	ν(PdCl)
216	88	1073	3029 (w)	2932 (m)		279 (w)
217	82	965	3030 (w)	2920 (m)	650 (vs)	290 (w)

[a] Recorded as a pressed KBr disk; [b] $X = Cl^-, SbF_6^-$.

The FT–IR spectra were run as pressed KBr disks, selected spectral data are given in Table 3.26. The $\nu(NH_2^+)$ stretches of the palladium(II) complexes were in the range 3029–3030 cm^{-1} and not significantly different from those of the precursor ligands, but the ν(CH) stretches were slightly decreased on coordination to the palladium(II) centre, for example in **217** the ν(CH) stretch in the precursor ligand **189** was 2952 cm^{-1} but on coordination the infrared band was observed at 2920 cm^{-1}. The infrared spectra of complexes **216** and **217** showed single ν(Pd–Cl) stretches at 279 and 290 cm^{-1} respectively, indicative of *trans* configuration in both cases.

The microanalytical data are given in Table 3.27. The agreement between the observed and calculated CHN values is consistent with the formulation of the palladium(II) complexes **216** and **217**. There was evidence of coprecipitation of the solvent in the case of compound **216** as confirmed by the microanalytical data.

Table 3.27 Microanalysis (%) and molecular formulae for compounds **216** and **217**.[a]

	C	H	N	Molecular formula
216	52.43 (52.79)	5.30 (5.14)	7.09 (7.21)	$C_{51}H_{59}N_6P_2F_6PdCl_3 \cdot 0.25CH_2Cl_2$
217	42.58 (42.62)	4.72 (4.56)	5.85 (5.85)	$C_{51}H_{65}N_6P_2Sb_2F_{12}PdCl$

[a] Calculated values in parentheses.

The solution $^{31}P\{^1H\}$ NMR spectra of these complexes, recorded in d^6-DMSO (Table 3.28) showed a single resonance at –0.68 ppm (>80%) in the case of **216** supportive of the formation of the *trans* isomer, significantly downfield of the value for the precursor ligand. In the case of **217**, the $^{31}P\{^1H\}$ NMR spectrum showed multiple signals as was observed in **213–215**, these could also be due to a mixture of *P*-containing species or possible decomposition of phosphorus containing products in the NMR solvent. Two of these multiple ^{31}P signals could also indicate the presence of both the *cis* and *trans* isomers in solution. This not withstanding, the single ν(Pd–Cl) stretches observed in the FT–IR spectra of both complexes strongly suggest the presence of the *trans* isomer in the solid state.

Table 3.28 Selected NMR data (in ppm) for **216** and **217**.[a]

	Major δ(P)	Other ^{31}P Signals	δ(H)/arom.	δ(H)/CH_2	δ(H)/NH_2^+
216	–0.68		7.01–7.58	3.64–4.78	n.o.
217	–0.63	–20.76, –30.34	7.32–7.86	3.53–4.98	n.o.

[a] All NMR spectra were recorded in d^6-DMSO; n.o. = not observed.

Selected ^{1}H NMR signals of the complexes are given in Table 3.28; the aromatic and the CH_2 proton signals fall within the expected values. However, unlike in the case of the palladium(II) complexes synthesised from $PdCl_2(CH_3CN)_2$, mentioned earlier, (Table 3.25), the NH_2^+ proton signals were not observed. Attempts to obtain X-ray quality crystals of **216** and **217** were unsuccessful.

3.3.5 COORDINATION OF CYCLOMETALLATED PALLADIUM(II) DIMERS WITH 181 OR 190

Coordination studies of **181** or **190** with cyclometallated palladium(II) dimers namely $[Pd(C\sim N)(\mu\text{-}Cl)]_2$, where (C~N = $C_9H_{12}N$ or $C_{12}H_{12}N$) were also performed in order to obtain the corresponding arylpalladium complexes as shown in Scheme 3.1. Ruiz *et al.*[143] have shown that the cyclopalladated monomeric complex $Pd(C_9H_{12}N)Cl(PTA)$ **75** could be synthesised from the cyclopalladated dimeric complex, $[Pd(C_9H_{12}N)(\mu\text{-}Cl)]_2$ and PTA. In order to assess whether the tertiary phosphine ammonium salts could form similar monomeric complexes, the salts were reacted with the palladium(II) dimers $[Pd(C\sim N)(\mu\text{-}Cl)]_2$, where (C~N = $C_9H_{12}N$ or $C_{12}H_{12}N$) under similar reaction conditions. The palladium(II) dimer $[Pd(C_9H_{12}N)(\mu\text{-}Cl)]_2$ was reacted with two equivalents **181** or **190** in CH_2Cl_2, followed by precipitation with hexane upon concentration of the solution under reduced pressure (Scheme 3.1), to give the desired cyclometallated palladium(II) complexes **218** and **219** as white solids in high yields (Table 3.29).

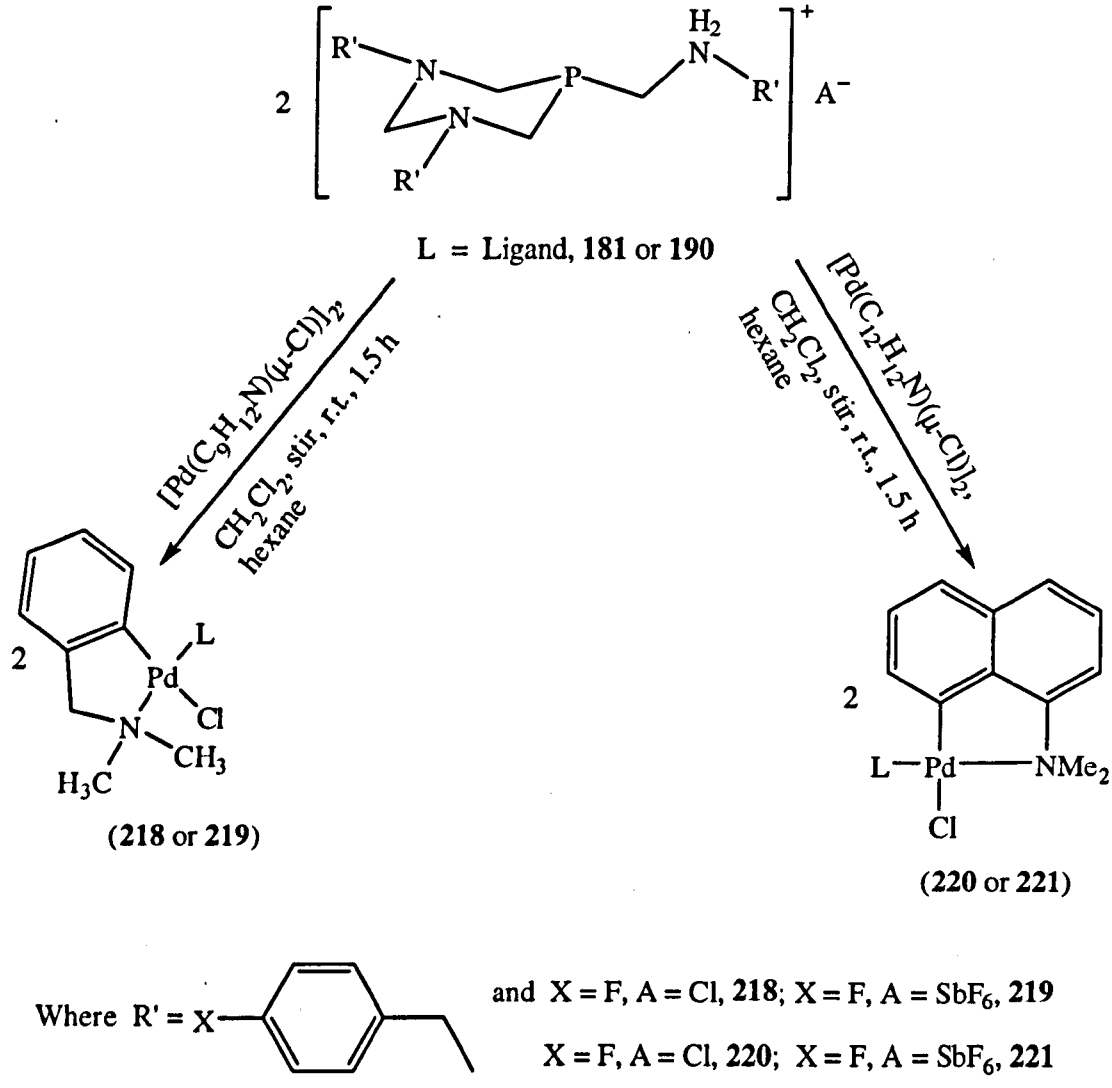

Scheme 3.1.

Similarly, the analogous palladium(II) dimer $[Pd(C_{12}H_{12}N)(\mu\text{-}Cl)]_2$ was reacted with **181** or **190** using the same procedure (Scheme 3.1) to give the desired cyclometallated palladium(II) complexes **220** and **221** as pale-yellow solids in high yields (Table 3.29).

3.3.5.1 CHARACTERISATION OF COMPOUNDS 218–221

Characterisation was achieved as in the previous cases by MS, microanalysis as well as FT–IR and NMR spectroscopy. The results are given in Tables 3.29–3.31. The FAB–MS data (Table 3.29) for compounds **218–221** are in agreement with the loss of one anion (*m/z* $[M-X]^+$).

Table 3.29 Percentage yield (isolated), FAB-MS and selected FT-IR data[a] (in cm^{-1}) for compounds **218–221.**

	% yield	*m/z* $[M-X]^{+}$ [b]	$\nu(NH_2^+)$	ν(CH)	ν(SbF)
218	81	735	3048 (m)	2929 (m)	
219	79	735	2970 (s)	2721 (m)	633 (s)
220	78	771	3044 (m)	2955 (m)	
221	89	771	3055 (m)	2928 (m)	660 (vs)

[a] Recorded as a pressed KBr disk; [b] $X = Cl^-, SbF_6^-$

The FT–IR spectra of the Pd(II) complexes **218–221,** run as pressed KBr disks, showed that the NH_2^+ vibrations at *ca.* 3000 cm^{-1} as well as the ν(CH) stretches (Table 3.29), were not significantly different from those of the precursor ligands though the ν(CH) stretches were at slightly higher wavenumbers upon coordination to the Pd(II) centre. For example the ν(CH) stretch in the precursor ligand (**181**) was 2821 cm^{-1}, but on coordination the vibration was observed at 2929 cm^{-1}(**218**) and 2955 cm^{-1}(**220**). The Sb–F bands at 633 and 660 cm^{-1} confirm the presence of the SbF_6^- counterions in **219** and **221** respectively.

Table 3.30 Microanalysis (%) and molecular formulae for compounds **218–221.**[a]

	C	H	N	Molecular formula
218	52.41 (51.99)	5.37 (5.16)	7.00 (7.08)	$C_{34}H_{40}N_4PF_3PdCl_2 \cdot 0.25CH_2Cl_2$
219	41.49 (41.49)	4.21 (4.12)	5.63 (5.65)	$C_{34}H_{40}N_4PSbF_9PdCl \cdot 0.25CH_2Cl_2$
220	53.74 (54.08)	4.98 (4.93)	6.48(6.77)	$C_{37}H_{40}N_4PF_3PdCl_2 \cdot 0.25CH_2Cl_2$
221	44.23 (44.16)	4.05 (4.01)	5.57 (5.37)	$C_{37}H_{40}N_4PSbF_9PdCl$

[a] Calculated values in parentheses.

The microanalytical data (Table 3.30) are within acceptable limits, hence are consistent with the formulations of the cyclometallated palladium(II) complexes **218–221.** There was evidence of coprecipitation of solvent in the complexes (**218–220**) with the exception of **221,** this is consistent with the microanalytical data (Table 3.30).

The solution $^{31}P\{^{1}H\}$ NMR spectra of these complexes recorded in d^6-DMSO showed two or three ^{31}P signals with the major (> 60%) at between δ(P) −3.83 and −5.03 ppm in **218**, **219** and **221** though **220** showed a single signal (> 90%) at 4.13 ppm (Table 3.31), in all cases these were significantly downfield of the corresponding δ(P) values [*ca.* δ(P) −55.00 ppm] for the free ligands. The average coordination chemical shifts for the Pd(II) complexes [$\Delta\delta_P$ 50.50 ppm] were very similar to what was obtained in the analogous PTA complex, **75** [$\Delta\delta_P$ 50.00 ppm],[143] again suggesting comparable stereoelectronic properties.

Table 3.31 Selected NMR data (in ppm) for compounds **218–221**.[a]

	Major δ(P)	Other ^{31}P Signals	δ(H)/arom.	δ(H)/CH_2	δ(H)/NH_2
218	−5.03	−1.77	6.80–7.01	3.60–4.01	8.91
219	−5.00	−1.60, −13.92	6.34–7.76	3.68–4.99	n.o.
220	−4.13		6.80–7.80	3.70–4.50	n.o.
221	−3.83	2.60	6.34–7.76	3.68–4.99	n.o.

[a] All NMR spectra were recorded in d^6-DMSO; n.o. = not observed.

The ^{1}H NMR signals of the Pd(II) complexes are given in Table 3.31; the aromatic and CH_2 proton signals are in line with expected values. The NH_2^+ proton signal for **218** was weak and observed as expected at a downfield position [*ca.* δ(P) 8.90 ppm], indicative of being adjacent to the electronegative N atom of the ammonium salt, this was however not observed in compounds **219–221**.

Some X-ray quality crystals of **218** and **220** were obtained by slow vapour diffusion of hexane into an acetone solution; in each case over the course of several days and the X-ray structures determined (Figures 3.19 and 3.20). As in the case of the analogous cyclopalladated PTA complex **75**, coordination at palladium resulted in a square-planar geometry with bond angles that deviate from 90° due to the bite angle of the cyclometallated ligand.[143] Selected bond lengths and angles are given in Tables 3.32 and 3.33.

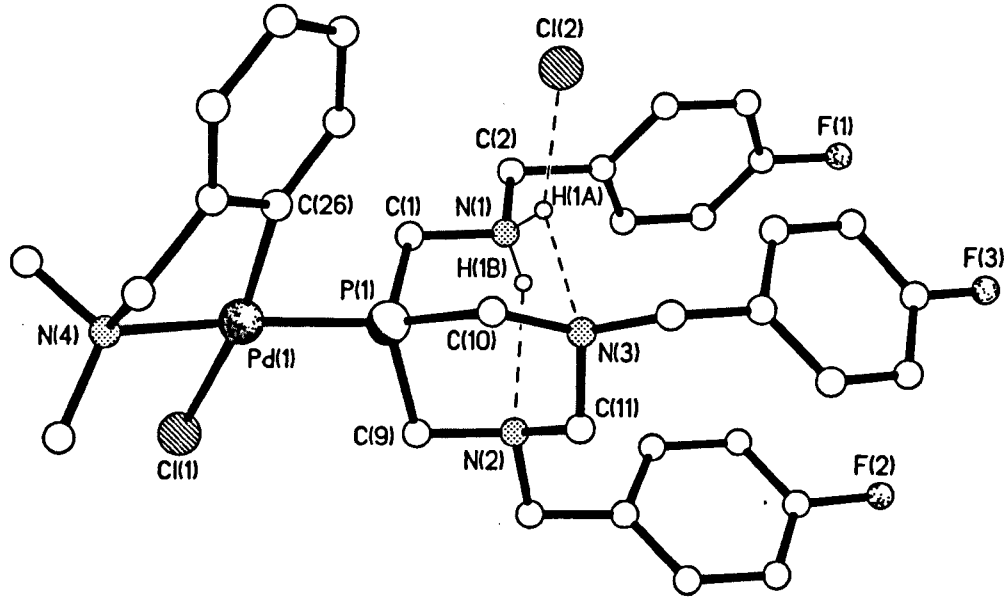

Figure 3.19 Molecular structure of **218**.

The Pd–C, Pd–Cl, Pd–N and Pd–P bond lengths for **218** (Table 3.32) and **213** (Table 3.33) were similar to those reported for **75** [Pd–C = 2.0086(16); Pd–Cl = 2.3983(4); Pd–N = 2.1467(14); Pd–P = 2.2260(4) Å].[143]

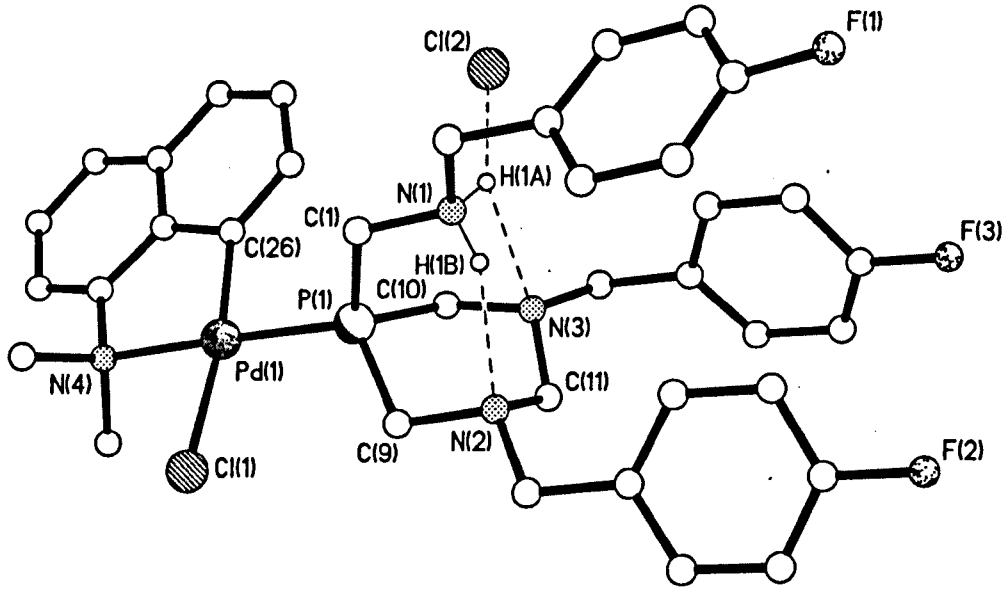

Figure 3.20 Molecular structure of **220**.

The bond angles about the palladium(II) centres in **218** and **220** were also similar to those found for complex **75** [C–Pd–N = 80.82(6); C–Pd–P = 97.27(5); P–Pd–Cl = 86.621(15); N–Pd–Cl = 95.01(4); P–Pd–N = 172.84(4); C–Pd–Cl = 175.84(4)°].[143] The C(26)–Pd(1)–N(4) bond angles of 82.01(9)° and 83.54(6)° for **218** and **220** respectively are in agreement with the normal range for such complexes.[143,212,213]

Table 3.32 Selected bond lengths and angles for **218**.[a]

Bond lengths (Å)		Bond lengths (Å)		Bond angles (°)	
Pd(1)–C(26)	1.997(2)	C(1)–N(1)	1.494(3)	C(26)–Pd(1)–N(4)	82.01(9)
Pd(1)–N(4)	2.156(2)	C(9)–N(2)	1.470(3)	C(26)–Pd(1)–P(1)	92.98(7)
Pd(1)–P(1)	2.2247(6)	N(2)–C(11)	1.468(3)	N(4)–Pd(1)–Cl(1)	93.43(6)
Pd(1)–Cl(1)	2.3955(6)	C(11)–N(3)	1.457(3)	P(1)–Pd(1)–Cl(1)	93.16(2)
P(1)–C(1)	1.836(2)	N(3)–C(10)	1.458(3)	N(4)–Pd(1)–P(1)	167.34(6)
P(1)–C(9)	1.826(2)			C(26)–Pd(1)–Cl(1)	170.31(7)
P(1)–C(10)	1.828(2)			C(9)–P(1)–C(10)	100.70(11)
				C(9)–N(2)–C(11)	110.79(18)
				C(10)–N(3)–C(11)	111.54(18)

Selected hydrogen bonding contacts

D–H···A	d(H···A) (Å)	d(D···A) (Å)	<(DHA) (°)
N(1)–H(1B)···N(2)	2.31(3)	2.944(3)	137(2)
N(1)–H(1A)···Cl(2)	2.35(3)	3.084(2)	138(2)
N(1)–H(1A)···N(3)	2.43(3)	2.895(3)	111.8(19)

[a] Estimated standard deviations in parentheses.

In both cases, the X-ray structures reveal that the phosphine ligand is *trans* to the *N*-donor due to the difficulty of coordinating mutually *trans* phosphine and aryl ligands which is related to the *trans* influence of the ligands in palladium complexes (*i.e.* the destabilising effect known as *transphobia*).[143,214] This is in agreement with the fact that most reported structures of arylpalladium complexes do not have the phosphine *trans* to the aryl group [*e.g.* $Pd(C_9H_{12}N)Cl(PTA)$; $Pd(C_{12}H_{12}N)Cl(P)$, where P = $Ph_2PCH_2N(H)C_5H_3(Cl\text{-}5)N$].[143,200] In the few complexes that do, the *trans* coordination

of phosphine and carbon donor ligands is forced by the nature of the phosphine, the complex or the aryl group.[214] Furthermore, upon coordination the P–C and P–C–N metric parameters of the precursor ligand were not changed. In both complexes, there was evidence of intermolecular N–H···Cl H-bonding involving the chloride counterions and one of the two H atoms on the ammonium group of the cation at N(1) as given in Tables 3.32 and 3.33. The crystal structures again reveal that a pair of intramolecular N–H···N H-bonds maintain the rigid cage structure of the precursor **181** in the solid state even upon complexation, as was seen in the case of the Ru(II) and Rh(III) complexes discussed in Sections 3.3.1 and 3.3.3 respectively. The crystal data and structure refinement details for **218** and **220** are shown in Appendices 8.17 and 8.18 respectively.

Table 3.33 Selected bond lengths and angles for **220**.[a]

Bond lengths (Å)		Bond lengths (Å)		Bond angles (°)	
Pd(1)–C(26)	2.0019(18)	C(1)–N(1)	1.490(2)	C(26)–Pd(1)–N(4)	83.54(6)
Pd(1)–N(4)	2.1469(15)	C(9)–N(2)	1.474(2)	C(26)–Pd(1)–P(1)	95.35(5)
Pd(1)–P(1)	2.2280(5)	N(2)–C(11)	1.463(2)	N(4)–Pd(1)–P(1)	174.90(4)
Pd(1)–Cl(1)	2.4008(5)	C(11)–N(3)	1.455(2)	C(26)–Pd(1)–Cl(1)	172.34(5)
P(1)–C(1)	1.8298(18)	N(3)–C(10)	1.459(2)	N(4)–Pd(1)–Cl(1)	91.99(4)
P(1)–C(9)	1.8336(18)			P(1)–Pd(1)–Cl(1)	89.638(16)
P(1)–C(10)	1.8349(17)			C(9)–P(1)–C(10)	99.92(8)
				C(9)–N(2)–C(11)	110.15(14)
				C(10)–N(3)–C(11)	111.56(14)

Selected hydrogen bonding contacts

D–H···A	d(H···A) (Å)	d(D···A) (Å)	<(DHA) (°)
N(1)–H(1B)···N(2)	2.21(2)	2.932(2)	142.7(19)
N(1)–H(1A)···N(3)	2.59(2)	2.997(2)	107.3(15)
N(1)–H(1A)···Cl(2)	2.19(2)	2.9741(16)	143.3(18)

[a] Estimated standard deviations in parentheses.

It has been shown that the electronic and structural properties of **218** and **220** are similar to those of the analogous water-soluble PTA complex **75**, which has been shown to successfully catalyse the reaction of aryl halides with terminal alkynes (Sonoghashira reaction) with excellent results in the absence of amine and CuI.[143] Thus **218** and **220** could be useful as potential catalysts or catalyst precursors for this type of reaction.

3.3.5.2 SYNTHESIS AND CHARACTERISATION OF PALLADIUM(II) COMPLEX 222

Following a similar procedure for the synthesis of **218**, $[Pd(C_9H_{12}N)(\mu\text{-}Cl)]_2$ was again reacted with **181** in CH_2Cl_2 but stirred for 30 min instead of 1.5 h, followed by precipitation with Et_2O instead of hexane to give a pale-yellow solid **222**. Analysis of complex **222** show that it was identical with the Pd(II) complex **218**, as suggested by the microanalytical data, consistent with the formula $C_{34}H_{40}N_4PF_3PdCl_2 \cdot 1.25CH_2Cl_2$, requires: C, 48.32; H, 4.89; N, 6.39. Found: C, 48.68; H, 4.83; N, 6.65%. This indicates coprecipitation with 1.25 moles of CH_2Cl_2 as against 0.25 moles in the case of **218** as shown in Table 3.30. The solution $^{31}P\{^1H\}$ NMR spectrum of **222** in d^6-DMSO showed a major phosphorus resonance (> 60 %) at $\delta(P)$ −5.00 ppm, similar to the ^{31}P signal for **218**, significantly downfield of the $\delta(P)$ value obtained for the free ligand, −54.72 ppm, while the ^1H NMR spectrum showed the following proton resonances: 6.34–7.76 (m, arom. H), 3.68–4.58 (m, CH_2) ppm. The FT–IR spectrum of the solid run as a pressed KBr disk showed bands at 2970 and 2721 cm^{-1} different from the NH_2^+ and CH vibrations of the precursor ligand observed at 3044 and 2821 cm^{-1} respectively. These bands in **222** were slightly lower than the NH_2^+ and CH vibrations observed at 3048 and 2929 cm^{-1} respectively in **218**.

Single crystals of **222** were obtained by vapour diffusion of Et_2O into a $DMSO/CH_2Cl_2$ solution over the course of several days and the X-ray structure has been determined which gave an unexpected novel dimeric palladium(II) complex **222'** (Figure 3.21). The molecular formula from the X-ray diffraction analysis was not consistent with the other characterising data. The X-ray structure of **222'** was quite different from the monomeric complex **218** shown in Figure 3.19. The structure of **222'** reveals an approximate square-planar geometry at both Pd(II) centres with typical Pd–P and Pd–Cl bond lengths and angles about the palladium(II) centres. Selected bond lengths and angles for

compound **222′** are given in Table 3.34. The bond lengths were typical but the bond angles about the Pd(II) centres were larger or smaller than those of non-chelated monomeric Pd(II) phosphine chloride complexes previously reported[146,201] as well as **169** and **170** in Section 2.4.3. For example, the P(1)–Pd(1)–P(1A) bond angle in **222′** [73.84(5)°] was smaller than the P(1)–Pd(1)–P(2) bond angle [100.45(5)°] in **170**. As was in the case of **211′**, the pronounced smaller P–Pd–P bond angle was due to the constraint caused by the small four-membered Pd–P–Pd–P ring in **222′**. The X-ray diffraction analysis does not show the presence of H-bonding indicative of the absence of typical donor/acceptor groups in **222′**. The crystal structure of **222′** also reveals an inversion centre, between the two Pd(II) centres making the two six-membered P–C–N–C–N–C rings identical. Unlike in the case of **218** and **220** where all the C–N bonds in the rings were *ca.* 1.463(3) Å comparable to typical values of between 4.336(8) and 1.452(3) Å previously reported involving sp^3 hybridised carbon atoms,[194] only two were within this range (Table 3.34). The other two carbon-nitrogen bond lengths of *ca.* 1.32(6) Å in the ring were within the typical range for C=N double bonds with sp^2 carbon atoms as reported in some pyridylphosphine complexes [C=N, 1.338(3) Å].[201]

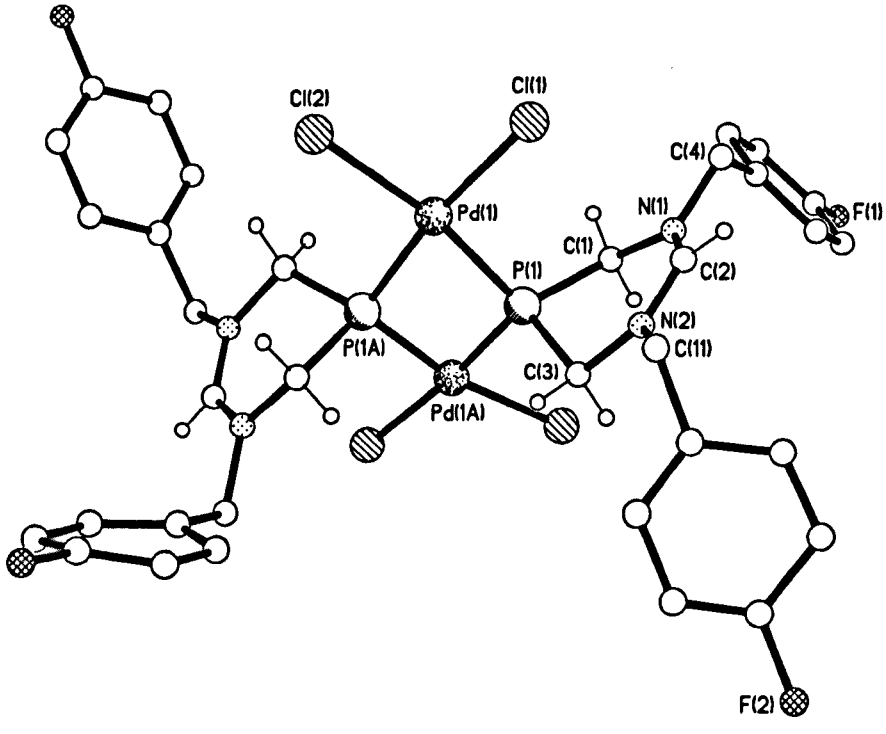

Figure 3.21 Molecuar structure of **222′** showing all H atoms in equivalent P–C–N–C–N–C rings. $(CH_3)_2SO$ solvent molecule of crystallisation has been omitted for clarity.

Therefore there is some electron delocalisation involving saturated and unsaturated bonds in the six-membered P–C–N–C–N–C rings, this is consistent with the presence of only one H atom at the C atom in the N–C–N fragment, instead of two in both rings (two H atoms on C(1) and C(3) but only one on C(2) as shown in one of the equivalent rings in Figure 3.21).

Table 3.34 Selected bond lengths and angles[a] for **222′**.

Bond lengths (Å)		Bond lengths (Å)		Bond angles (°)	
Pd(1)–P(1)	2.2418(18)	P(1)–C(1)	1.825(5)	P(1)–Pd(1)–P(1A)	73.84(5)
Pd(1)–P(1A)	2.2350(12)	P(1)–C(3)	1.835(4)	P(1)–Pd(1)–Cl(1)	98.62(4)
Pd(1)–Cl(1)	2.3736(12)	C(1)–N(1)	1.469(6)	P(1A)–Pd(1)–Cl(2)	93.60(4)
Pd(1)–Cl(2)	2.3842(13)	N(1)–C(2)	1.311(6)	Cl(1)–Pd(1)–Cl(2)	94.00(5)
		C(2)–N(2)	1.320(6)	C(1)–P(1)–C(3)	96.9(2)
		N(2)–C(3)	1.475(6)	C(1)–N(1)–C(2)	124.4(4)
				C(2)–N(2)–C(3)	123.2(4)

[a] Estimated standard deviations in parentheses.

Thus each P–C–N–C–N–C ring in **222′** is contracted compared to those of **218** and **220**. The novelty of this structural motif is supported by the absence of any hits from a CSD search.[191,192] The crystal data and structure refinement details for **222′** are shown in Appendix 8.19.

The X-ray diffraction analysis of **222** as was observed in **211** was not consistent with the results from the other characterising data on the bulk complex. During the crystallisation process, there is probable intramolecular rearrangement involving the phosphine and C~N ($C_9H_{12}N$) ligands. A lone electron pair from one of the ring N atoms in the phosphine ligand (**181**) is lost which affords a radical cation, stabilised by loss of a proton from the N–CH_2–N fragment. This is followed by rearrangement of the exocylic arm of the phosphine ligand in **222**. Firstly, a proton from the ammonium group is lost, followed by donation of an electron pair from the N atom to the carbon in the P–C–N fragment resulting in the cleavage of the P–C bond and subsequent formation of an sp^2 hybridised compound as shown in Scheme 3.2. There are also

decomplexation and complexation processes involving the bidentate, C~N ($C_9H_{12}N$) ligand and the Cl^- counterion respectively at the Pd(II) centre of the resulting intermediate complex to give reactive 14 electron zwitterionic "$PdCl_2P$" groups which dimerise to form the novel zwitterionic Pd(II) dimer **222'** as proposed in Scheme 3.2. This is similar to the mechanism proposed by Zagumennov *et al.*[13] which also involves the removal of the lone electron pair from a ring N atom and the formation of a carbocation in the transformation of cyclo-{$CH_2N(R)CH_2N(R)CH_2$-P}-$CH_2N(H)R$, R = 4-MeC_6H_4 by electrochemical oxidation to compound **6** (Equation 1.9).

A close examination of the X-ray structure of **222'** with an imaginary line bisecting the structure through the Pd(1)···Pd(1A) axis reveal that for each half, the P–C–N–C–N–C ring present in the precursor ligand is retained as was the case of **218** and **220**. On the other hand, the bidentate C~N ($C_9H_{12}N$) ligand as well as the exocyclic arm of **181** bearing the pair of N–H···N intramolecular H-bonds that forms a conformationally locked phosphine framework were lost. This is in contrast to retention of the entire structural framework of the precursor ligand **181** even after coordination in the case of **218** and **220**. It can be inferred therefore that the repeat reaction of $[Pd(C_9H_{12}N)(\mu\text{-}Cl)]_2$ with **181** in CH_2Cl_2 with variation of the reaction time gave a similar product to **218** as confirmed by the characterising data such as microanalysis on the bulk complex. The structural difference between **218** and **222'** can therefore be attributed to intramolecular rearrangements during the crystallisation process which gave rise to the zwitterionic novel palladium(II) dimeric complex, **222'** as shown in Scheme 3.2.

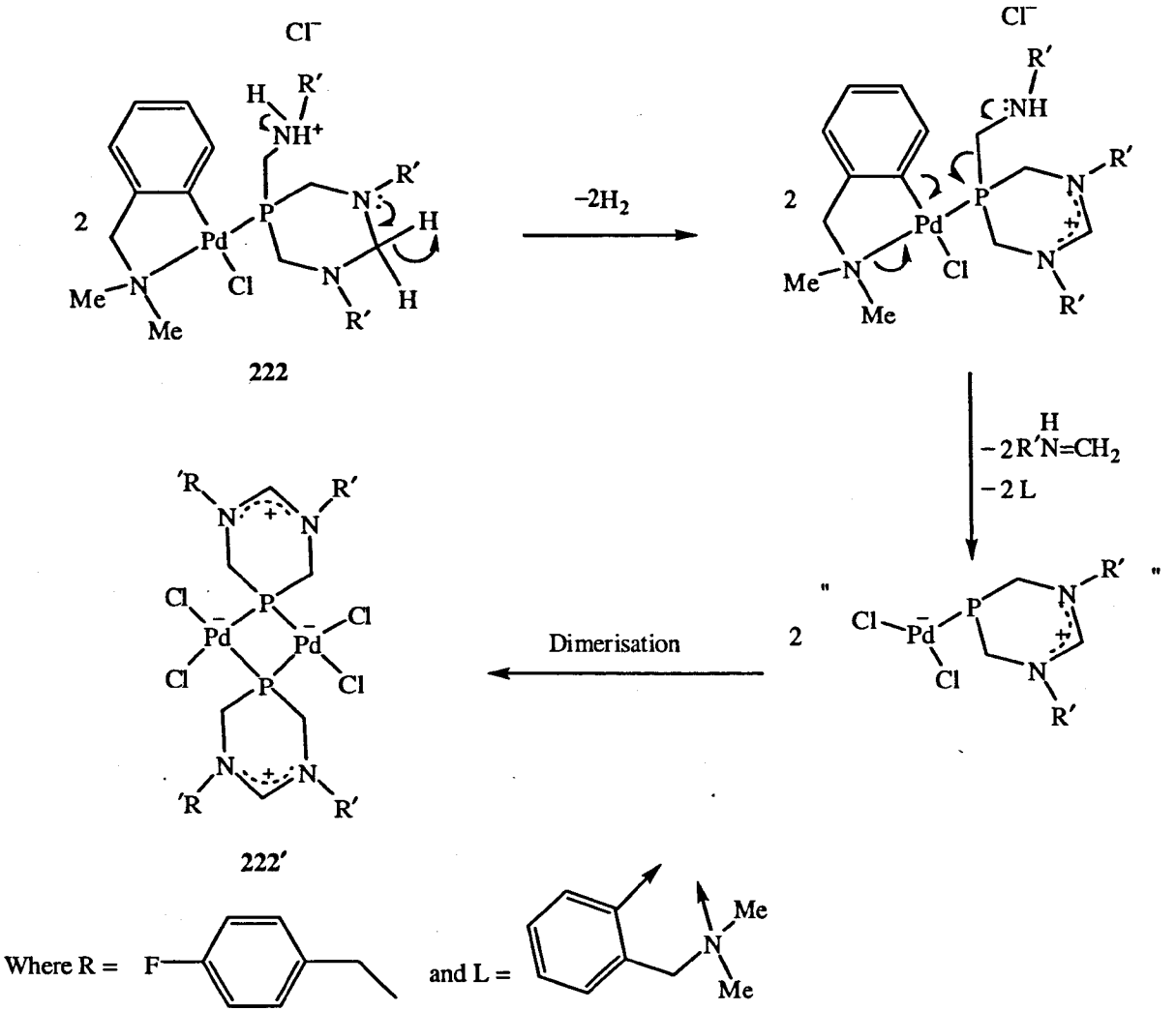
Cl⁻
2
Pd
Cl
Me
N
Me
P
N
R′
NH⁺
H
H
H
R′
222
−2H2
Cl⁻
R′
NH
2
Pd
Cl
Me
N
Me
P
N
R′
N
R′
−2R′N=CH2
−2L
2
Cl
Pd
Cl
P
N
R′
N
R′
Dimerisation
'R
N
N
R′
Cl
Pd
Pd
Cl
Cl
Cl
P
P
N
N
'R
R′
222′
Where R =
F
and L =
Me
N
Me

Scheme 3.2

3.3.6 SYNTHESIS OF PLATINUM(II) COMPLEXES 223 AND 224

The ligating potential of the tertiary phosphine ammonium salts was also explored by reacting **189** or **190** with $PtCl_2(CH_3CN)_2$ as shown in Equation 3.10. Reaction of $PtCl_2(CH_3CN)_2$ with two equivalents of **189** or **190** in CH_2Cl_2 at room temperature followed by precipitation with Et_2O upon concentration of the solution under reduced pressure gave the off-white compounds **223** and **224**. In both cases, the ligands readily react to form the desired platinum(II) complex in good yield (Table 3.35).

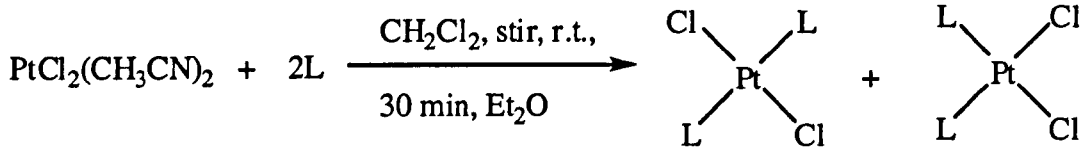

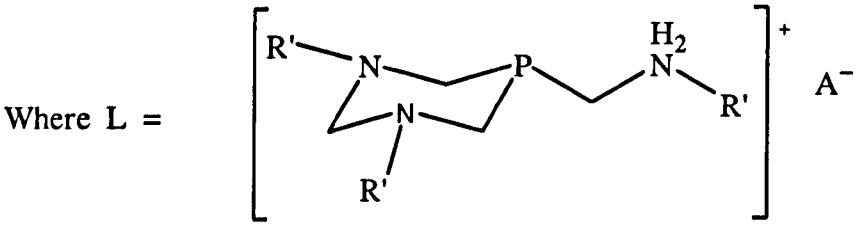

189 or **190**

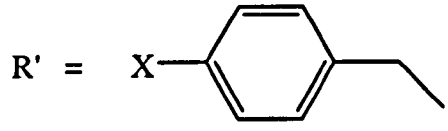

and X = H, A = SbF_6, **223**;

X = F, A = SbF_6, **224**

Equation 3.10.

3.3.6.1 CHARACTERISATION OF COMPOUNDS 223 AND 224

Characterisation was achieved by microanalysis and FT–IR spectroscopy. The results are given in Tables 3.35 and 3.36. The solubility of the complexes was poor in DMSO and $CDCl_3$ hence no meaningful NMR [^1H, $^{31}P\{^1H\}$] spectral data could be obtained in these solvents.

The FT–IR spectra were run on the bulk material, as pressed KBr disks and are given in Table 3.35. The $\nu(NH_2^+)$ stretches of 3031 and 3036 cm^{-1} for **223** and **224** respectively were not significantly different from those of the precursor ligands; the $\nu(CH)$ stretches at about 2930 cm^{-1} were also similar to those of the corresponding precursor ligands. The Sb–F stretches were observed at about 660 cm^{-1} while the

single strong ν(Pt–Cl) stretches at 290 cm^{-1} were indicative of *trans* configuration for both platinum(II) complexes.

Table 3.35 Percentage yield (isolated) and selected FT-IR data[a] (in cm^{-1}) for compounds **223** and **224**.

Compound	% yield	$\nu(NH_2^+)$	ν(CH)	ν(SbF)	ν(PtCl)
223	59	3031 (w)	2932 (m)	661 (vs)	290 (vs)
224	68	3036 (w)	2935 (w)	662 (vs)	290 (vs)

[a] Recorded as a pressed KBr disk.

There was evidence of coprecipitation of solvent, in the case of **217**; this is supported by the microanalytical data given in Table 3.36. The agreement between the observed and calculated CHN values in Table 3.36 is consistent with the formulation of the platinum(II) complexes **223** and **224**.

Table 3.36 Microanalysis (%) and molecular formulae for compounds **223** and **224**.[a]

	C	H	N	Molecular formula
223	39.33 (38.83)	3.98 (4.04)	5.39 (5.43)	$C_{50}H_{62}N_6P_2Sb_2F_{12}PtCl_2$
224	35.31 (35.22)	3.44 (3.36)	5.11 (4.83)	$C_{50}H_{56}N_6P_2Sb_2F_{18}PtCl_2{\cdot}CH_2Cl_2$

[a] Calculated values in parentheses.

As a result of the poor solubility in available NMR solvents mentioned above, NMR spectroscopy was not useful in elucidating their geometry unlike the case of the diazaphosphorinane platinum(II) complexes **178** and **179** (Section 2.4.4). This not withstanding, the strong single ν(Pt–Cl) IR signals were indicative of *trans* configuration in both cases. X-ray quality single crystals of **223** were obtained by layering petroleum ether (b.p. 40–60 °C) on a CH_2Cl_2 solution kept for several days and the X-ray structure has been determined which gave a novel dimeric platinum(II) complex **223′** (Figure 3.22). As was the case in **222′**, the molecular formula from the X-ray diffraction analysis was not consistent with the other characterising data which support a monomeric $PtCl_2L_2$ type complex.

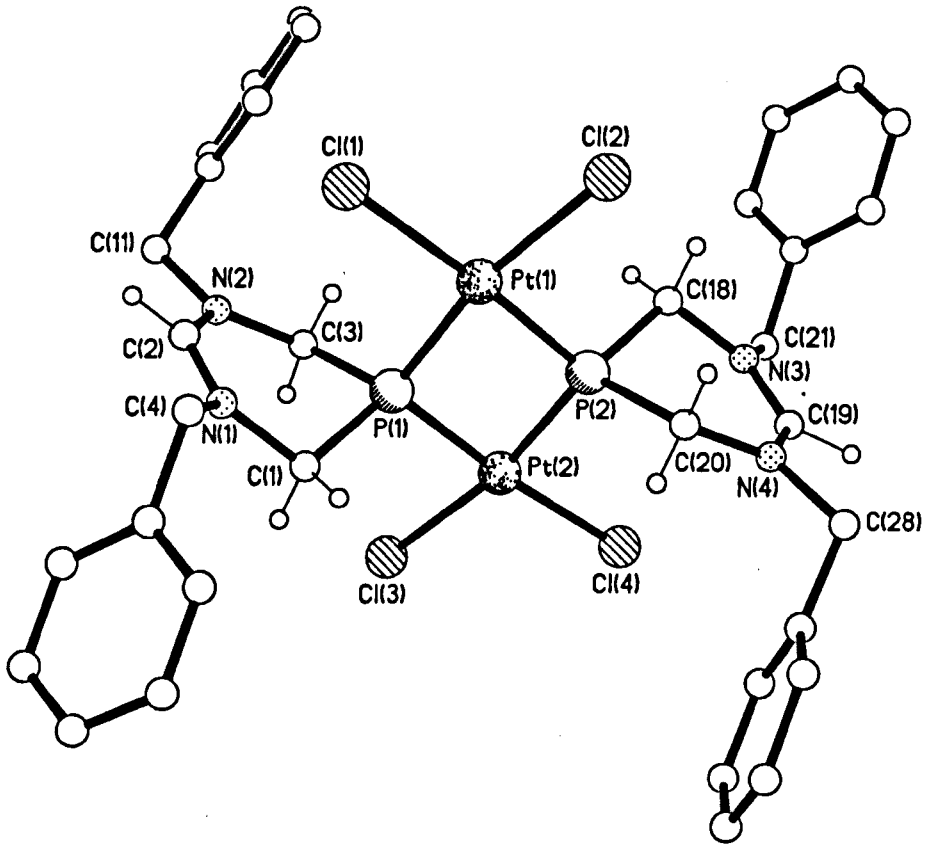

Figure 3.22 Molecular structure of **223′** showing H atoms in the two P–C–N–C–N–C rings. CH_2Cl_2 solvent molecule of crystallisation has been omitted for clarity.

The novelty of this structural motif is supported by the absence of any hits from a CSD search.[191,192] The crystal data and structure refinement details for **223′** are shown in Appendix 8.20.

The geometry about each Pt(II) centre reveal distorted square-planar with the chlorides and phosphines having a *cis* disposition in each case. Selected bond lengths and angles for compound **223′** are given in Table 3.37. The P–Pt–P bond angles were severely compressed in **223′** [75.57(4), 75.58(4)°] comparable to the identical analogous P–Pd–P angles in **222′** [73.84(5) °] due to the constraint caused by the 4-membered P–Pt–P–Pt rings, while the Cl–Pt–Cl angles were slightly expanded [91.75(4), 92.13(4)°] also not significantly different from the analogous Cl–Pd–Cl angles in **222′** [94.00(5)°]. The X-ray diffraction analysis does not show the presence of H-bonding in **223′** indicative of the absence of H-bonding capabilities in **223′**.

Table 3.37 Selected bond lengths and angles[a] for **223'**.

Bond lengths (Å)		Bond lengths (Å)		Bond angles (°)	
Pt(1)–P(1)	2.2316(11)	Pt(2)–Cl(3)	2.3825(11)	P(1)–Pt(1)–P(2)	75.57(4)
Pt(1)–P(2)	2.2235(10)	Pt(2)–Cl(4)	2.3716(10)	Cl(1)–Pt(1)–Cl(2)	91.75(4)
Pt(1)–Cl(1)	2.3752(10)	P(1)–C(1)	1.836(4)	Cl(1)–Pt(1)–P(1)	99.73(4)
Pt(1)–Cl(2)	2.3721(10)	P(1)–C(3)	1.834(4)	Cl(2)–Pt(1)–P(2)	92.94(4)
Pt(2)–P(1)	2.2266(10)	P(2)–C(18)	1.828(4)	P(1)–Pt(2)–P(2)	75.58(4)
Pt(2)–P(2)	2.2279(11)	P(2)–C(20)	1.828(4)	P(1)–Pt(2)–Cl(3)	93.54(4)
C(1)–N(1)	1.472(5)	C(18)–N(3)	1.458(5)	P(2)–Pt(2)–Cl(4)	98.71(4)
N(1)–C(2)	1.302(5)	N(3)–C(19)	1.316(6)	Cl(3)–Pt(2)–Cl(4)	92.13(4)
C(2)–N(2)	1.303(5)	C(19)–N(4)	1.312(6)	C(1)–P(1)–C(3)	95.8(2)
N(2)–C(3)	1.460(5)	N(4)–C(20)	1.468(5)	C(1)–N(1)–C(2)	122.9(4)
				C(2)–N(2)–C(3)	124.0(4)
				C(18)–P(2)–C(20)	96.3(2)
				C(18)–N(3)–C(19)	123.1(4)
				C(19)–N(4)–C(20)	124.3(4)

[a] Estimated standard deviations in parentheses.

From the X-ray diffraction analysis, it is evident that the two P–C–N–C–N–C rings in **223'** were also contracted compared to those of **218** and **220** with evidence of electron delocalisation as observed in the case of **222'**. The carbon-nitrogen bond distances comprising of the shorter C=N and longer C–N bonds in the P–C–N–C–N–C rings in **223'** were identical with those of **222'** as shown in Tables 3.34 and 3.37. Therefore there is also some electron delocalisation involving saturated and unsaturated bonds in the six-membered P–C–N–C–N–C rings as observed in **222'**, this is consistent with the presence of two H atoms on C(1) and C(3) but only one on C(2) in one ring and a similar pattern repeated in the second ring with C(18) and C(20) having two H atoms each and only one H atom on C(19) as shown in Figure 3.22.

Although the X-ray diffraction analysis of **223'**, did not reveal an inversion centre as was the case in **222'**, drawing an imaginary line through the Pt(1)···Pt(2) axis show the following point. On either side of the Pt(1)···Pt(2) axis in **223'** the

"$CH_2NH_2CH_2C_6H_5$" fragment (the exocylic arm), in the precursor ligand **189** is lost but the P–C–N–C–N–C ring retained. This is again in contrast to the retention of the entire structural framework of the precursor ligand **181** even upon coordination in the case of **218** and **220**. The CHN analysis of **223** is supportive of the expected monomeric platinum(II) complex, $PtCl_2L_2$ and the FT–IR spectrum supportive of *trans* disposition. The structural difference between **223** and **223′** can therefore again be attributed to similar intramolecular pattern of rearrangements. During the crystallisation process, one of the two phosphine ligands in **223**, follows the same pattern of rearrangements in both the ring and the exocyclic arm as proposed in the case of **222** (Scheme 3.2), while the second phosphine ligand was lost and eliminated as shown in Scheme 3.3 similarly forming reactive 14 electron zwitterionic "$PtCl_2P$" groups which dimerise to form the novel zwitterionic Pt(II) dimer **223′** as tentatively proposed in Scheme 3.3.

Alternatively, both phosphine ligands at the Pt(II) centre in **223** may simultaneously undergo the intramolecular rearrangement mentioned previously to form the reactive zwitterionic "$PtCl_2P$" groups which dimerise to form the novel zwitterionic Pt(II) dimer **223′**.

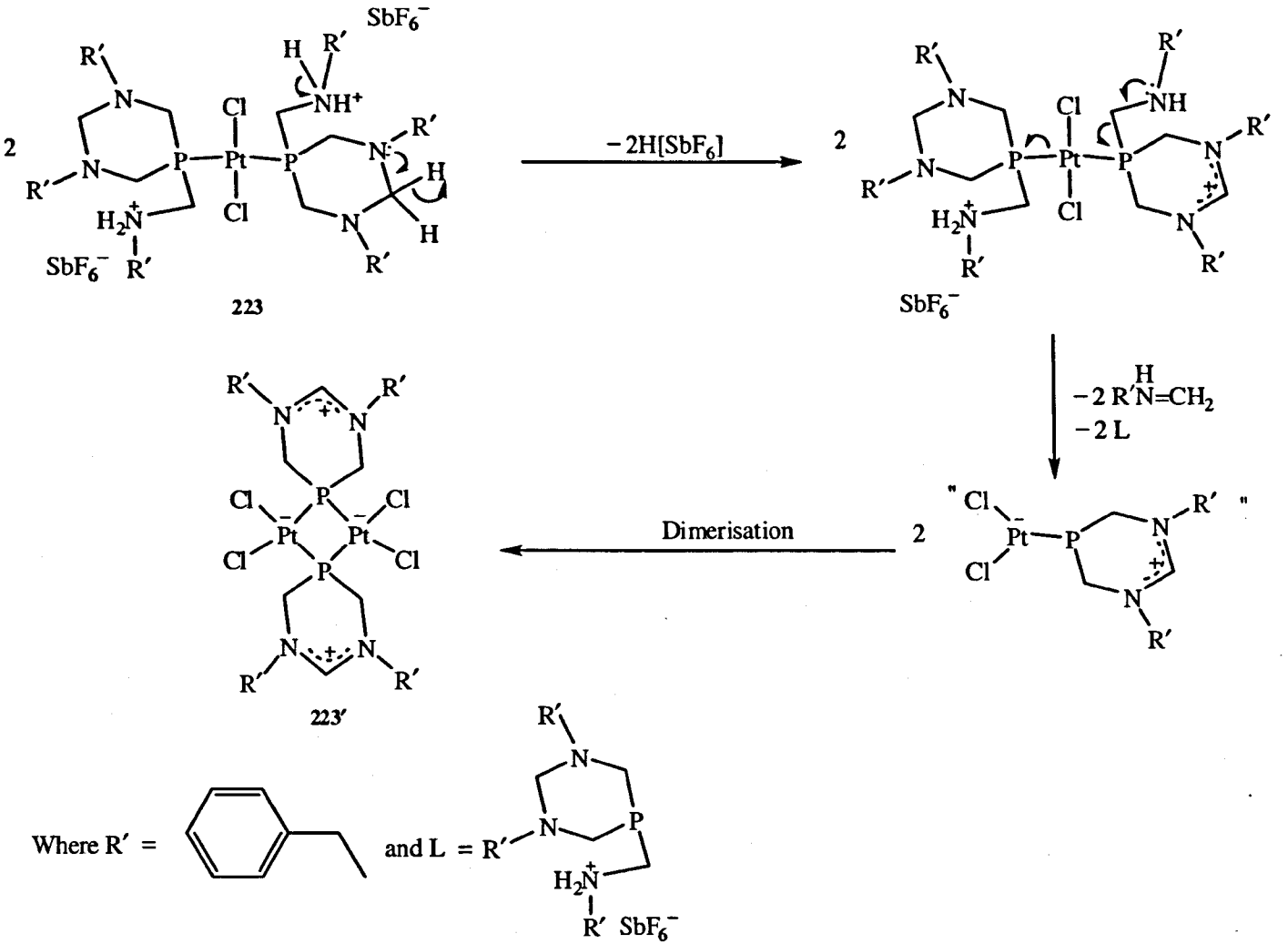
SbF6−
223
−2H[SbF6]
SbF6−
−2 R′N=CH2
−2 L
Dimerisation
223′
Where R′ =
and L =
SbF6−

Scheme 3.3

3.3.7. SYNTHESIS OF GOLD(I) COMPLEXES 225–228

Fackler Jr. and co-workers[168] have demonstrated that gold(I) complexes of PTA could be synthesised from PTA and the labile gold(I) chlorides $(Me_2S)AuCl$ or (THT)AuCl.

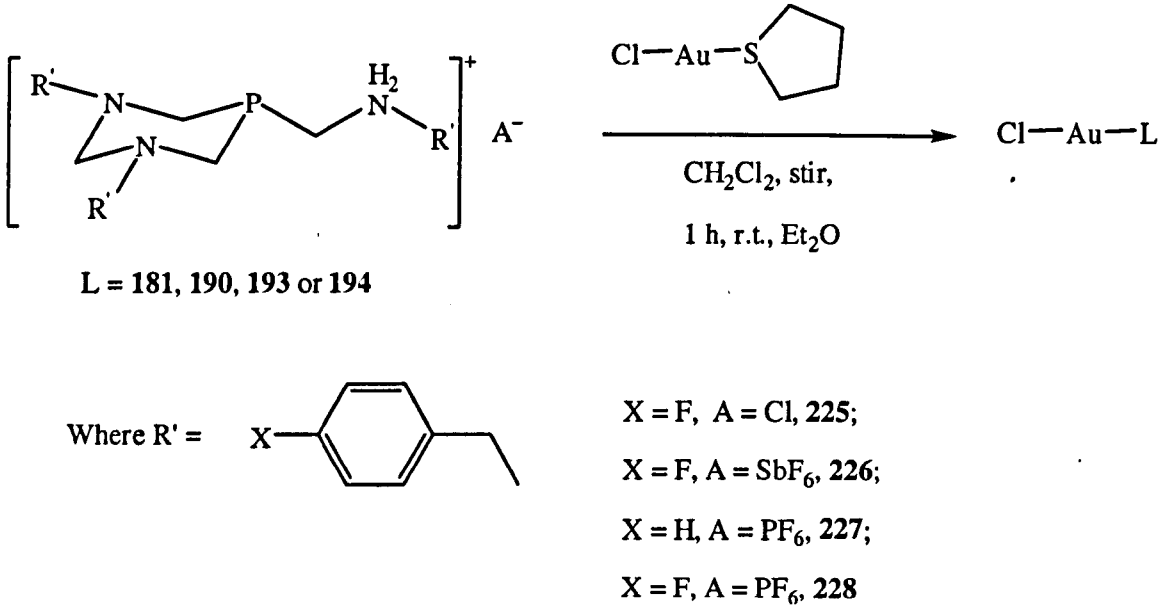

Equation 3.11.

To further explore the coordination potential of the tertiary phosphine ammonium salts as similar *P*-monodentate ligands, **181**, **190**, **193** or **194** were reacted with (THT)AuCl in CH_2Cl_2 at room temperature under aerobic conditions. Four gold(I) complexes were synthesised using a slightly different procedure by reacting **181**, **190**, **193** or **194** with (THT)AuCl in a 1:1 molar ratio in CH_2Cl_2 followed by addition of Et_2O to induce precipitation upon concentration under reduced pressure as shown in Equation 3.11. The desired Au(I) complexes **225–228** were obtained as off-whitish solids in high yields (Table 3.38) and stored in the dark.

3.3.7.1 CHARACTERISATION OF COMPOUNDS 225–228

Characterisation was achieved as in the previous cases by MS, microanalysis as well as FT–IR and NMR spectroscopies; the results are given in Tables 3.38–3.40. The FAB–MS data (Table 3.38), for compounds **225–228** were in agreement with the loss of the respective counterions (*m/z* $[M-X]^+$). The FT–IR spectra of the Au(I) complexes, run as pressed KBr disks, showed NH_2^+ vibrations in the range 3009–3080 cm^{-1}, while the ν(CH) stretches were observed at between 2829 and 2962 cm^{-1} as given in Table 3.38.

Both infrared stretches were not significantly different from those of the precursor ligands as given in Tables 3.1 and 3.5. The ν(Au–Cl) vibrations expected at [*ca.* 300 cm^{-1}][200] were not seen because of the shorter frequency range (4000–500 cm^{-1}) of the FT-IR spectrometer used. The strong vibrations at 662 cm^{-1} were indicative of the presence of SbF_6^- in the case of complex **226**, while the similar strong IR bands at 841 and 849 cm^{-1} are assigned to the P–F vibrations in compounds **227** and **228** respectively, confirming the presence of the PF_6^- counterion.

Table 3.38 Percentage yield (isolated), FAB-MS and selected FT-IR data[a] (in cm^{-1}) for compounds **225–228**.

	% yield	*m/z* $[M-X]^{+}$ [b]	ν(NH_2^+)	ν(CH)	ν(SbF)	ν(PF)
225	81	690	3041 (w)	2928 (m)		
226	86	690	3009 (w)	2829 (m)	662 (vs)	
227	78	636	3032 (m)	2947 (m)		841 (vs)
228	83	690	3080 (m)	2962 (m)		849 (vs)

[a] Recorded as a pressed KBr disk; [b] X = Cl^-, SbF_6^- or PF_6^-.

The microanalytical data in Table 3.39 were within acceptable limits, hence are consistent with the formulations of the gold(I) complexes, and there was evidence of coprecipitation of solvent in all the complexes.

Table 3.39 Microanalysis (%) and molecular formulae for compounds **225–228**.[a]

	C	H	N	Molecular formula
225	39.44 (39.84)	3.71 (3.80)	5.48 (5.47)	$C_{25}H_{28}N_3F_3PAuCl_2 \cdot 0.5CH_2Cl_2$
226	30.98 (30.87)	2.90 (2.99)	4.40 (4.15)	$C_{25}H_{28}N_3F_9SbPAuCl \cdot CH_2Cl_2$
227	35.25 (35.00)	3.73 (3.77)	4.82 (4.62)	$C_{25}H_{31}N_3F_6P_2AuCl \cdot 1.5CH_2Cl_2$
228	34.73 (34.87)	3.16 (3.33)	4.58 (4.78)	$C_{25}H_{28}N_3F_9P_2AuCl \cdot 0.5CH_2Cl_2$

[a] Calculated values in parentheses.

The solution $^{31}P\{^1H\}$ NMR spectra of the complexes were recorded in d^6-DMSO. Upon coordination to gold(I), the ^{31}P NMR signals of the precursor ligands [δ(P) ≈ −55.00

ppm] shifted significantly downfield, in the range between −12.41 and −14.53 ppm (Table 3.40), an indication of the ligation of the phosphorus atom to the gold atom.

Table 3.40 Selected $^{31}P\{^{1}H\}$ NMR data (in ppm or Hz) for **225–228**.[a]

Compound	δ(P)	Other ^{31}P Signals	$^{1}J_{PF}$
225	−12.41		
226	−12.99		
227	−14.53	−144.19 sept	711
228	−12.87	−144.18 sept	713

[a] All NMR spectra were recorded in d^6-DMSO.

The average coordination chemical shifts for the Au(I) complexes ($\Delta\delta_P$ 42.00 ppm) were similar to what was obtained in the analogous (PTA)Au(I) complex, (PTA)AuCl ($\Delta\delta_P$ 45.00 ppm)[169] again suggesting similar stereoelectronic properties.

The ^{1}H NMR signals of the Au(I) complexes were generally very weak. However the aromatic protons in the case of **227** were observed between 7.22 and 7.49 ppm, while the CH_2 protons resonated between 3.74 and 4.80 ppm, similar to what was obtained in the analogous (PTA)AuCl complex.[169]

Single crystals of **225** suitable for structure determination by X-ray diffraction were obtained by slow vapour diffusion of Et_2O into CH_2Cl_2/MeOH solution kept over the course of several days and the structure has been determined (Figure 3.23). The structure of **225** reveals an approximate linear geometry with the Au–Cl and Au–P bond lengths and the P–Au–Cl bond angles given in Table 3.41. This data is similar to those reported for analogous linear gold(I) PTA complex AuCl(PTA)·CH_3CN [Au–Cl = 2.304(2) Å; Au–P = 2.226(2) Å; P–Au–Cl = 175.8(1)°].[168] Selected bond lengths and angles are given in Tables 3.41. The crystal data and structure refinement details for **225** are shown in Appendix 8.21. The crystal structure reveals that the pair of intramolecular N–H···N H-bonds observed in the precursor salt, forming the rigid cage structure in the solid state, was not maintained upon complexation unlike in the case of the Ru(II), Rh(III) and Pd(II) complexes previously discussed. The crystal structure instead reveals intermolecular H-

bonding contacts involving the Au(I) cations and the Cl^- counterions forming H-bonded chains. Molecules are linked together *via* the chloride counterions forming a zigzag chain involving the Au(I) cations and the N(1) hydrogens as shown in Figure 3.23.

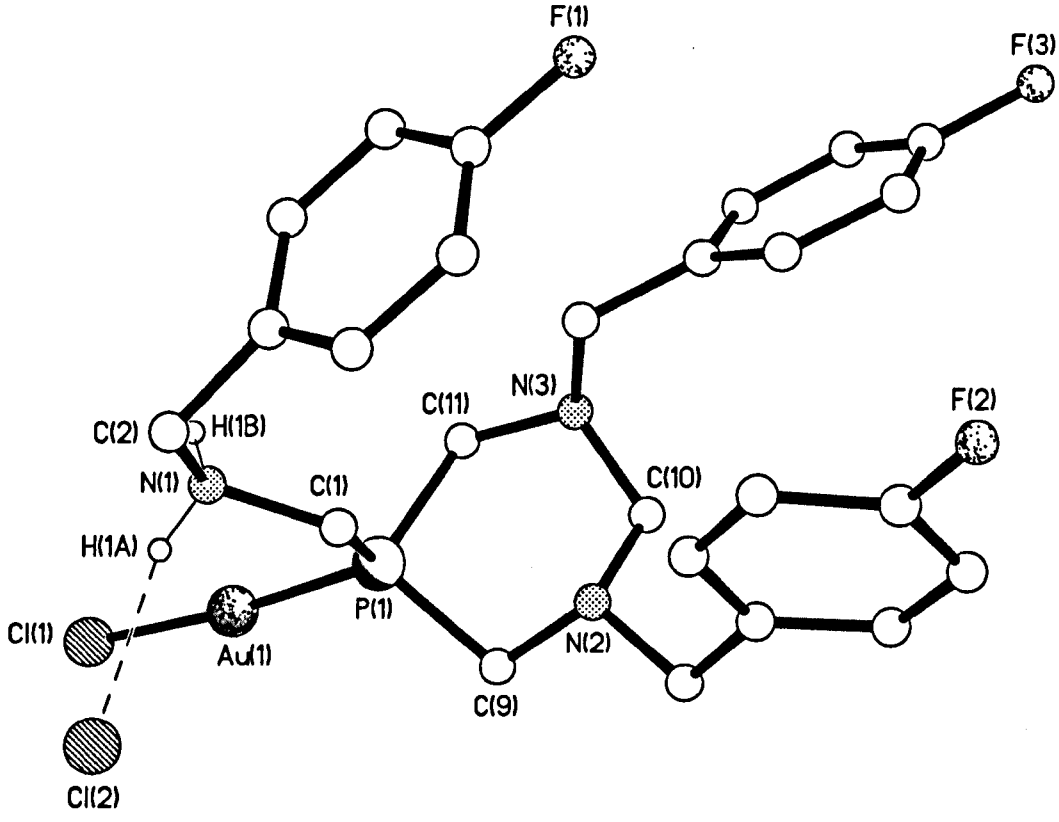

Figure 3.23 Molecular structure of **225**.

Table 3.41 Selected bond lengths and angles for **225**.[a]

Bond lengths (Å)		Bond lengths (Å)		Bond angles (°)	
Au(1)–P(1)	2.2191(5)	C(1)–N(1)	1.487(3)	P(1)–Au(1)–Cl(1)	175.37(2)
Au(1)–Cl(1)	2.2959(5)	C(9)–N(2)	1.467(3)	P(1)–C(1)–N(1)	113.59(14)
P(1)–C(1)	1.842(2)	C(11)–N(3)	1.456(3)	P(1)–C(9)–N(2)	106.7(14)
P(1)–C(9)	1.824(2)	P(1)–C(11)	1.848(2)	P(1)–C(11)–N(3)	117.42(14)

Selected hydrogen bonding contacts

D–H···A	d(H···A) (Å)	d(D···A) (Å)	<(DHA) (°)
N(1)–H(1B)···Cl(2A)	2.21(3)	3.099(2)	174(2)
N(1)–H(1A)···Cl(2)	2.23(3)	3.068(2)	162(2)

[a] Estimated standard deviations in parentheses.

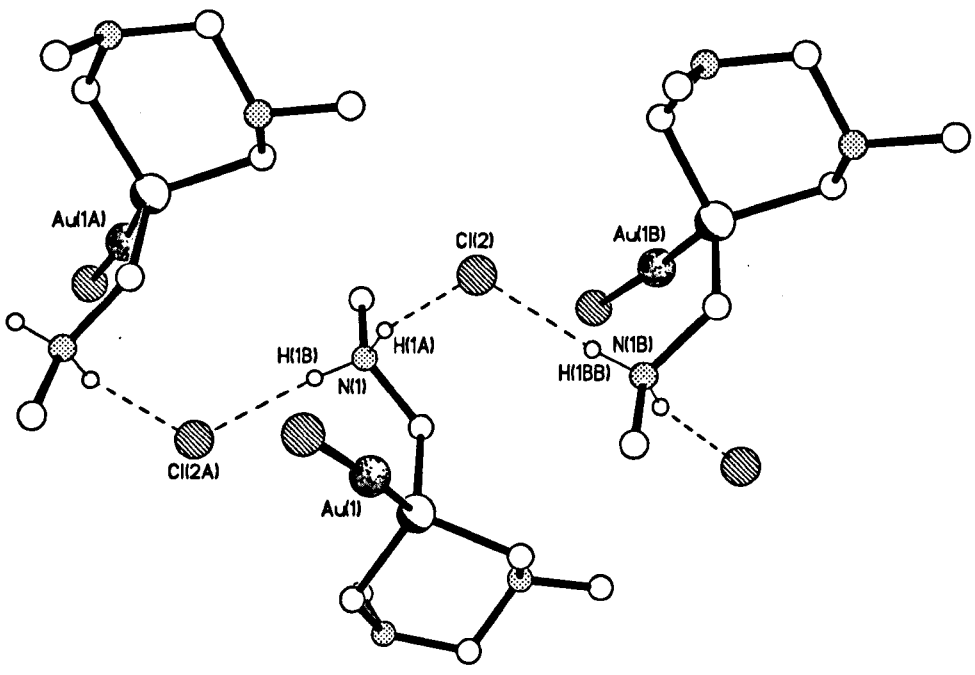

Figure 3.24 Molecular structure of **225** showing intermolecular H-bonding linking molecules together (4-FC_6H_4 groups omitted).

It is evident from this H-bonding arrangement with a chloride counterion between two cationic species, that the Au(I) species are effectively separated from one another (neighbouring N···N distances shown to be 5.35 Å). The X-ray diffraction analysis has shown that the actual Au···Au distance in **225** is 4.10 Å, hence aurophilic interaction was not evident; this can be explained by the intermolecular H-bonding arrangement mentioned previously, coupled with the bulky nature of the phosphine ligand. Aurophilic, Au···Au interactions with bond lengths of *ca.* 3.0 Å are commonly observed crystallographically for Au(I) compounds with sterically undemanding ligands.

3.4 CONCLUSIONS

New cyclic cationic phosphorus(III) ligands, [cyclo-{$CH_2N(R')CH_2N(R')CH_2$-P}-$CH_2N(H_2)R']^+Cl^-$, [R′ = $C_6H_5CH_2$, **180**; R′ = 4-$FC_6H_4CH_2$, **181**; R′ = 4-$ClC_6H_4CH_2$, **182**; R′ = 4-$MeC_6H_4CH_2$, **183**; R′ = 4-$MeOC_6H_4CH_2$, **184**] were prepared by reacting benzylamine precursors with THPC in ethanol at room temperature following a similar procedure first published by Frank *et al.*[10] Anion metathesis of **180–183** with $Na[BPh_4]$, $Na[SbF_6]$ or $K[PF_6]$ in methanol at room temperature under aerobic conditions was performed to give the corresponding phosphorus(III) salts **185–196** in good to excellent

yields: [cyclo-{$CH_2N(R')CH_2N(R')CH_2$-P}-$CH_2N(H_2)R']^+X^-$, [R' = $C_6H_5CH_2$, 4-$FC_6H_4CH_2$, 4-$ClC_6H_4CH_2$, 4-$MeC_6H_4CH_2$; X = BPh_4, SbF_6, PF_6]. The new phosphorus(III) ligands undergo complexation to a range of late transition metals [Ru(II), Rh(I), Rh(III), Ir(III), Pd(II), Pt(II) and Au(I)] to form the corresponding complexes.

The cyclic cationic phosphorus(III) ligands and complexes were characterised by a combination of conventional techniques: MS, microanalysis, FT–IR, NMR [^1H and $^{31}P\{^1H\}$], and in several cases by single crystal X-ray crystallography. Furthermore, *P*-coordination bonding modes have been observed in all the complexes and verified by spectroscopic and single crystal X-ray diffraction analyses. The crystal structures of various examples have been determined and illustrate a range of intra- and intermolecular H-bonding contacts. The X-ray structures of the new cationic phosphorus(III) ligands reveal that the phosphine framework is conformationally locked in the solid state through pairs of intramolecular N–H···N hydrogen bonds forming an analogous cage framework to the well-known water-soluble PTA ligand with similar metric parameters, although only one N–H···N hydrogen bond was evident in one case due to H-bonding interactions involving its BPh_4^- counterions. These ligands though found to be insoluble in water can therefore be considered as charged variants of PTA and their metal complexes were found to have similar stereoelectronic properties to those of analogous complexes with PTA. The cage frameworks formed by the intramolecular N–H···N hydrogen bonds in the these ligands are maintained in the Ru(II), Rh(III) and the cyclopalladated Pd(II) complexes. The cage framework was, however, not maintained in the case of the Au(I) complex. The coordination studies of the cyclic cationic phosphorus(III) ligands has given rise to interesting novel complexes: a monomeric Pd(II) chelate complex as well as two structurally similar zwitterionic Pd(II) and Pt(II) dimeric complexes probably *via* intamolecular rearrangements. Plausable mechanisms have been proposed for the observations.

Further studies directed towards understanding the properties of these ligands in aqueous and organic media may have useful future implications in homogeneous catalysis as well as medicinal applications for which the analogous PTA metal complexes are known. The mechanistic aspects of the reactions that led to the novel complexes obtained in this work could also be critically examined.

CHAPTER FOUR

CATALYSIS

4.0 INTRODUCTION

Catalysis is the phenomenon of changing the rate of a chemical reaction by use of a catalyst. A catalyst is a substance that alters the rate of a chemical reaction without itself undergoing any permanent chemical change; it may speed up or slow down a reaction. For a reversible reaction, a catalyst alters the rate at which equilibrium is attained but does not alter the position of equilibrium. A catalyst is generally associated with increasing the rate of a reaction hence are referred to as positive catalysts, while those that slow down a reaction are called negative catalysts. The increase in the rate of a chemical reaction is achieved by the catalyst aiding to attain chemical equilibrium faster by reducing the potential energy barriers in the reaction path. The primary focus of this work was to evaluate the catalytic potential of the new phosphorus(III) ligands and or their transition metal complexes. Very little was done in this regard due to time constraints, only a demonstration of the catalytic potential of the neutral phosphorus(III) ligands (diazaphosphorinane ligands) is described in this chapter. The structural and stereoelectronic relationship between the transition metal complexes of the cationic phosphorus(III) ligands and known analogous PTA complexes used in various catalytic applications is also described.

4.1 CATALYTIC APPLICATIONS

Catalysis has wide ranging applications in the chemical industry and has a major impact on the quality of human life as well as economic development. In recent years, catalysis is also looked upon as a solution to eliminate or replace polluting processes due to the inherent characteristics of most catalytic processes as clean technologies. The search for new catalysts is one of the major driving forces behind organometallic research and hence most catalytic processes involve the use of transition metal complexes in one form or the other. Homogeneous and heterogeneous catalysis are two main types of industrial catalytic processes depending on their relationship to the phase of the reaction in which they are involved. A homogeneous catalyst is in the same phase as the components of the reaction it is catalysing, while a heterogeneous catalyst is in a different phase from the components of the reaction for which it is acting. The former has a high catalytic efficiency but also has difficulty separating the used catalyst from the product after the

reaction. Adopting a heterogeneous catalyst could solve the problem of catalyst recovery and reuse, but in most cases, the catalyst's low utility and the complexity of the reaction mechanism become new problems in its application. Both types of catalysts have their advantages and disadvantages, though heterogeneous catalysis has been more widely applied. Therefore achieving a combination of the advantages of both the homogeneous and heterogeneous processes is always the focus in catalysis.[215,216] The Heck coupling reaction is considered important in such explorations, not only for its significance in C–C coupling reaction between aryl halides and olefins,[217–219] but also for its characteristic "quasi-homogeneous" mechanism.[220–224] Tang and co-workers,[225] proposed a new strategy of heterogenising homogeneous catalysts by encaging a quasi-homogeneous catalytic reaction into a zeolitic microcapsular reactor represented as Pd@S1 (Figure 4.1).

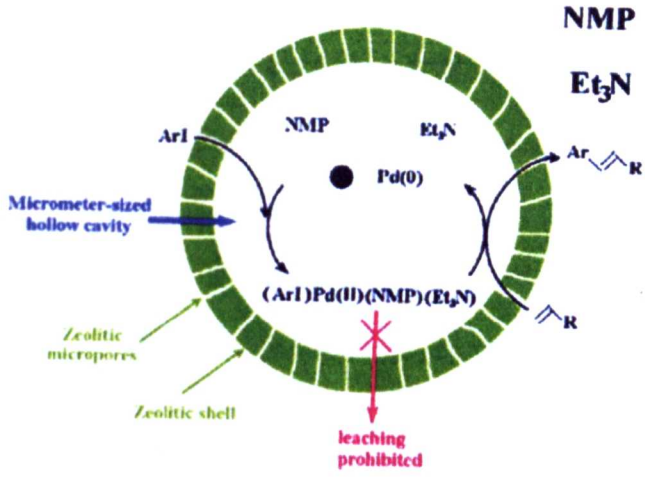

Figure 4.1 Schematic illustrations for the encaged quasi-homogeneous Heck-coupling in Pd@S1 catalyst.[225]

It has been reported that the palladium-catalysed Heck reaction is essentially a quasi-homogeneous catalytic process occurring *via* either a palladium complex intermediate[221] or solvated palladium clusters[220,223] in the system of aryl iodides and aprotic polar solvents. Heck coupling on the Pd@S1 catalyst may follow a similar mechanism but within the micrometer-sized hollow cavities as illustrated in Figure 4.1. Addition of the aryl halide to the reaction solution triggers an oxidative addition to palladium atoms in the Pd nanoparticles with the aid of *N*-methylpyrrolidone [NMP] and Et_3N, thus forming a soluble active Pd(II) complex, [Pd(II)(ArI)(NMP)(Et_3N)] as an intermediate.[219] The

active intermediate then reacts with olefin to complete the catalytic cycle. The palladium(II) complex returns to its metallic state, Pd(0) and redeposits onto the surface of the support once all of the aryl halides are consumed. Importantly, unlike in the case of the classical supported palladium catalyst, the formed active [Pd(II)(ArI)(NMP)(Et_3N)] intermediate in this catalyst is encaged in the micrometer-sized hollow cavities of the zeolitic microcapsular reactor, because its molecular diameter is relatively larger than the pore size in the zeolitic shell (silicalite-1). With the protective effect of the surrounding zeolitic shell, this catalyst exhibited antileaching properties. Excellent reactivity was achieved even under a relatively low Pd adopted amount (Pd/ArI = 0.0025) during the reaction, but was reused for more than 10 runs with negligible loss of activity, in contrast to rapid decay of activity of conventional Pd/C catalysts. It was concluded that this heterogenization of a homogeneous catalyst which entails encapsulation of homogeneous catalytic microenvironment in a porous inorganic shell combines the efficiency of the homogeneous catalyst and the durability of the heterogeneous catalyst. This strategy could provide a novel and beneficial route for the rational design of catalysts in this domain, which may be useful in the synthesis of complex industrial and fine-chemicals.[225]

Catalysed reaction pathways are usually represented by catalytic cycles. A catalytic cycle consists of series of stoichiometric reactions (usually reversible) that form a closed loop; the catalyst must be regenerated so that it can participate in the cycle of reactions more than once. The catalytic cycle of the Heck reaction which is basically the palladium-catalysed C-C coupling between aryl halides or vinyl halides and activated alkenes in the presence of a base is shown below (Figure 4.2). There are four steps in the catalytic cycle: oxidative addition, carbometallation, β-hydride elimination and reductive elimination. The reaction probably involves the initial reduction of Pd(II) to Pd(0), followed by oxidative addition of RX to generate an R–Pd(II) intermediate. R normally has to be an aryl or vinyl group otherwise, β-elimination which is the major decomposition pathway for alkyls can disrupt the required R–Pd intermediate species.[3] The Pd(II) intermediate species undergoes an insertion with the alkene, followed by β-hydride elimination to give the desired product. Polar solvents such as DMF or CH_3CN are required and a base (commonly Et_3N, KOAc or NaOAc) is required to recycle the palladium catalyst by removing HX in the last step (reductive elimination).

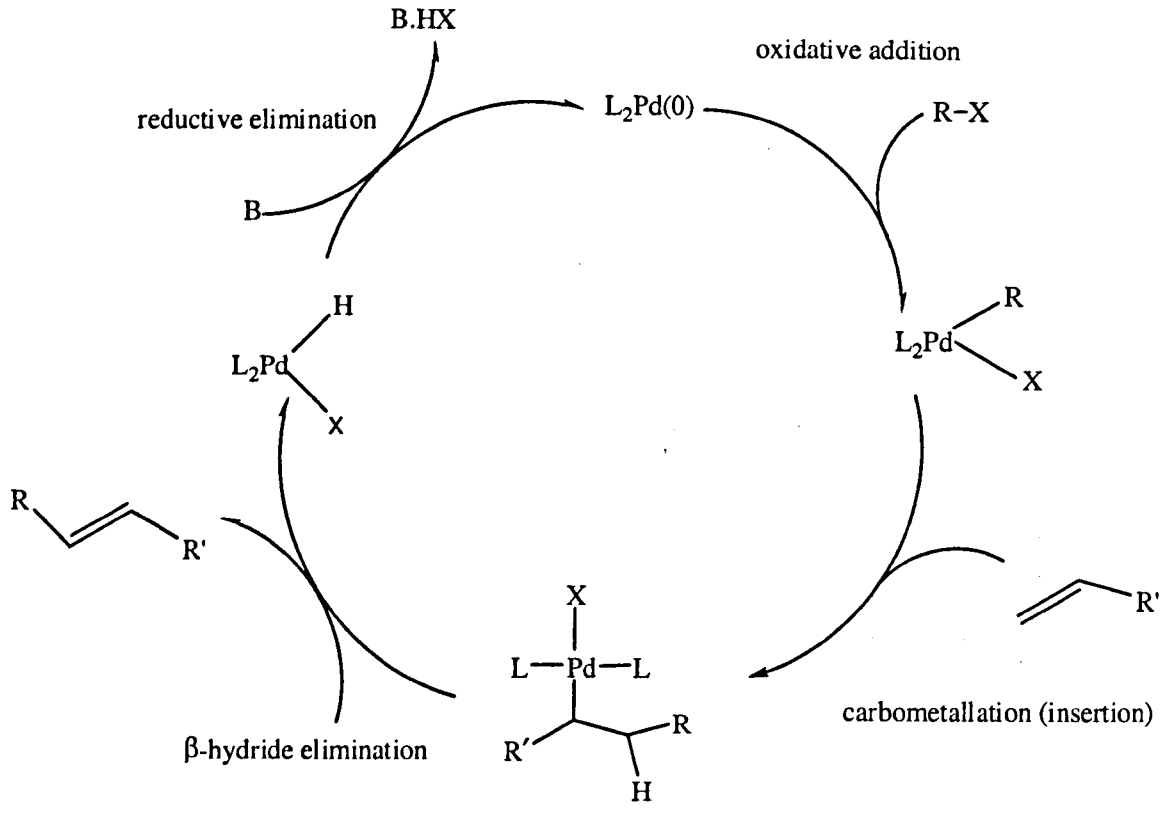

Figure 4.2 The Heck cycle (R′ = electron-withdrawing group).

The role of the electron-withdrawing group, R′ on the alkene is to ensure that the insertion step takes place in the direction shown, to give R′CH=CHR and not RR′C=CH_2. The Pd–R bond in the oxidative addition product seems to be polarised in the direction [Pd^{+}–R^{-}] so that the R group attacks the positive end of the C=C double bond of the alkene, which is the one remote from the electron-withdrawing group R′.

In choosing a catalyst for use especially for a commercial process, apart from the changes in reaction conditions that the use of a catalyst may bring about (*e.g.* pressure and temperature), other factors of importance include; the concentration of the catalyst required, the catalytic turnover, the selectivity of the catalyst to the desired product and how often the catalyst needs renewing. Two catalytic turnover parameters used are the catalytic turnover number (TON) and the catalytic turnover frequency (TOF). The TON is the number of moles of product per mole of catalyst; this number indicates the number of catalytic cycles for a given process, *e.g.* after 3 h the TON was 2500. While the TOF is the catalytic turnover per unit time: the number of moles of product per mole of catalyst per unit time, *e.g.* the TOF was 30 min^{-1}.

4.1.1 HOMOGENEOUS CATALYSIS

In homogeneous catalysis, the catalysts used are of the same phase as the reactants *e.g.* enzymes in biochemical reactions or transition metal complexes used in the liquid phase in organic reactions. Homogeneous catalysis by soluble metal complexes has wide ranging applications in the chemical industry. Important examples include hydrogenation, carbonylation, hydroformylation, polymerisation, oxidation, isomerisation, etc. These catalysts have several advantages over the conventional heterogeneous catalyst systems such as high activity and selectivity under mild operating conditions. Catalytic mechanisms are considerably easier to study in homogeneous systems, where such powerful methods as NMR can be used to assign structures and follow reaction kinetics. In spite of these, the application of homogeneous catalysis has been limited due to the difficulties in separation of catalysts from products and their economic utilisation. Sometimes special techniques are involved to easily separate the catalyst from the product, when homogeneous catalysts must be utilised because of their superior high activity and selectivity among other advantages. For example homogeneous catalysts can be chemically grafted on to solid supports for greater ease of separation of the catalyst from the reaction products. Although such catalyst systems are technically called heterogeneous, they often retain the characteristic reactivity patterns that they showed as homogeneous catalysts, and the properties are usually different from those of classical heterogeneous catalysts; these are sometimes called "heterogenised" homogeneous catalysts.

Another way to address the problem of catalyst separation is to apply biphasic catalysis. One strategy uses a water-soluble catalyst. This is retained in an aqueous layer that is immiscible with the organic medium in which the reaction takes place. Intimate contact between the two solutions is achieved during the catalytic reaction, after which the two liquids are allowed to settle and the layer containing the catalyst is separated by decantation. Many homogeneous catalysts are hydrophobic; hence it is necessary to introduce ligands that will bind to the metal that carry hydrophilic substituents. Much work has been carried out with the *P*- donor ligand, **229** which can be introduced into a variety of organometallic complexes by carbonyl or alkene displacement.[226] For example, the water-soluble complex $HRh(CO)(\mathbf{229})_3$ is a hydroformylation catalyst precursor; conversion of hex-1-ene to heptanal proceeds with 93% selectivity for the *n*-isomer, a

higher selectivity than is shown by $HRh(CO)(PPh_3)_3$ under conventional homogeneous catalytic conditions.[226]

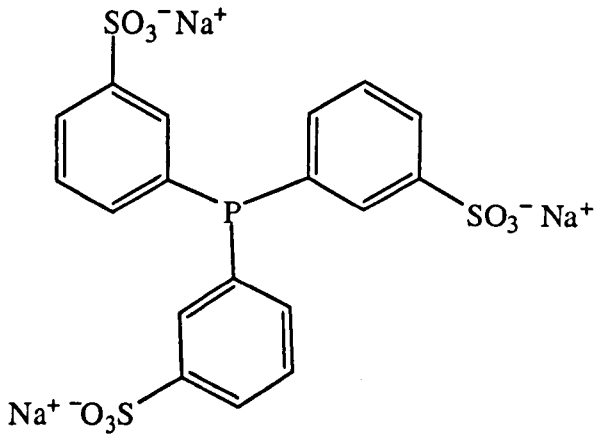

229

A range of alkene hydrogenations are catalysed by $HRh(CO)(\mathbf{229})_3$ and it is particularly selective and efficient for the hydrogenation of hex-1-ene.[226]

Similarly, PTA-organometallic compounds have been successfully used as water-soluble catalysts. The water-solubility of such catalysts is usually imparted by the highly water-soluble PTA ligand. Examples of PTA transition metal complexes used as water-soluble catalysts include those of Ru, Ir and Pd. The respective analogous Ru, Ir and Pd complexes synthesised in this work using the tertiary phosphine ammonium salts shown to be charged variants of PTA could be similarly used as water-soluble catalysts if the properties of the ligands (tertiary phosphine ammonium salts) are understood in aqueous and organic media and made to form water-soluble complexes.

The hydrogenation of benzene and other arenes under aqueous-organic biphasic conditions using the ruthenium(II) complexes $RuCl_2(p^6$-cymene)(PTA) **45**, $[RuCl(p^6$-cymene)$(PTA)_2]BF_4$ **46** and $[RuCl_2(p^6$-cymene)(TPPMS)] has been reported.[128] They were shown to be homogeneous catalysts for this reaction. The analogous $[RuCl_2(p^6$-cymene)(TPPMS)] complex was found to have significantly higher activity than both **45** and **46**. The active catalysts formed during the hydrogenation reactions correspond to a trinuclear cluster, a colloid and mononuclear complexes respectively.[128] The analogous ruthenium(II) complexes synthesised in this work such as **199** and **200** discussed in Section 3.3.1 and shown to have similar stereoelectronic properties with **45** could

function as similar water-soluble catalysts if made water soluble by attachment of appropriate polar functional groups.

The water-soluble iridium(III) complexes η^5-Cp*Ir(PTA)Cl_2 and [η^5-Cp*Ir(PTA)$_2$Cl]Cl have also been evaluated as catalyst precursors for the hydrogenation of CO_2 and hydrogen carbonate in aqueous solutions under relatively mild conditions.[211] The catalytically active species was shown to be [η^5-Cp*Ir(PTA)$_2$H]$^+$ by multinuclear NMR spectroscopy and its nature confirmed by independent synthesis. Although, these catalyst precursors showed only moderate activity on CO_2 hydrogenation compared to analogous Rh and Ru complexes,[211] they gave mechanistic insight into the reactions, thus contributing to catalyst design and reaction optimisations. As in the case of the ruthenium(II) complexes, the analogous iridium(III) complexes synthesised (**208–210**) were shown to have similar stereoelectronic properties with the analogous PTA complex and these could be evaluated as similar hydrogenation catalysts if made water-soluble by using versions of the precursor ligands attached with highly polar functional groups such as $-SO_3Na$, $-CO_2Na$, $-OH$ etc.

Similarly, the water-soluble monomeric palladium(II) PTA complex **75** together with Pd(OAc)$_2$/PTA has been shown to be an efficient copper- and amine-free Sonogashira catalyst system.[143] This catalyst system employed relatively low palladium catalyst loadings in the Sonogashira reaction of aryl bromides and chlorides with terminal alkynes with excellent results in the absence of amine and CuI. The results were better than those obtained in systems based on P(*t*-Bu)$_3$ such as [Pd(allyl)Cl]$_2$/P(*t*-Bu)$_3$ and **75** is one of the few palladacycle complexes that are more active in this type of cross-coupling reaction, being able to catalyse Sonogashira reactions with aliphatic alkynes and even aryl chlorides.[143] The analogous monomeric cyclometallated Pd(II) complexes synthesised in this work from the tertiary phosphine ammonium salts and cyclometalated dimers [Pd(C~N)(μ-Cl)]$_2$, where (C~N = $C_9H_{12}N$ or $C_{12}H_{12}N$), **[218–221]** have been shown to have similar stereoelectronic properties with the analogous Pd(II)PTA complex **75**. Thus the palladium(II) complexes **218–221** could be evaluated as similar Sonogashira catalysts if made water soluble by the use of versions of the precursor ligands attached or grafted with highly polar functional groups.

Apart from the use of water-soluble catalysts in biphasic catalysis involving aqueous and organic phases, fluorous *i.e* a perfluoroalkane phase instead of an aqueous phase could be used. Higher C_n perfluoroalkanes are used in fluorous biphasic catalysis; the low-boiling related chlorofluorocarbons (CFC's) have been phased out under the Montreal Protocol[227] due to their adverse effect on the ozone layer. At room temperature most fluorous solvents are immiscible with other organic solvents, but an increase in temperature typically renders the solvents miscible. The reactants are initially dissolved in a non-fluorinated, organic solvent and the catalyst is present in the fluorous phase. Raising the temperature of the system creates a single phase in which the catalysed reaction occurs. On cooling, the solvents, along with the products and catalyst, separate. Catalysts with suitable solubility properties can be designed by incorporating fluorophilic substituents such as C_6F_{13} or C_8F_{17}. For example, the hydroformylation catalyst $HRh(CO)(PPh_3)_3$ has been adapted for use in fluorous media by using the phosphine ligand **230** in place of PPh_3.[226]

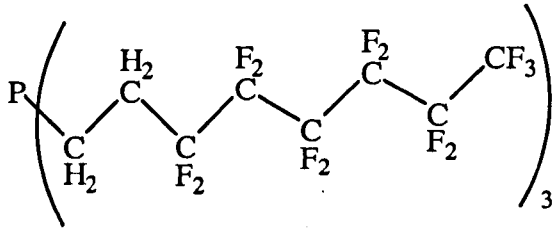

230

Introducing fluorinated solvents obviously alters the electronic properties of the ligand. If the metal centre in the catalyst 'feels' this change, its catalytic properties are likely to be affected. These effects can be minimized by placing a spacer between the metal and the fluorinated substituent.

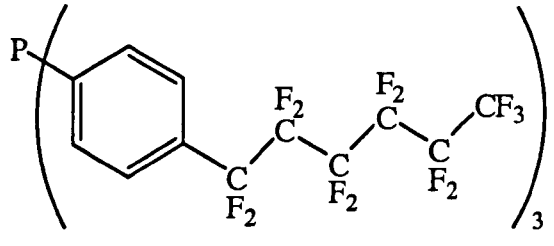

231

Thus in the phosphine ligand **231**, which is a derivative of PPh_3, the aromatic ring helps to shield the P atom from the effects of the electronegative F atoms.[226] Although the use

of the biphasic system allows the catalyst to be recovered and recycled, leaching of the Rh into the non-fluorous phase does occur over a number of catalytic cycles.

4.1.1.1 CATALYTIC POTENTIAL OF THE NEW DIAZAPHOSPHORINANE LIGANDS

The catalytic potential of most of the ligands and complexes synthesised (Chapters two and three) were not evaluated due to time constraints. However, the catalytic potential of the diazaphosphorinane ligands was evaluated at Sasol Technology, St Andrews, UK for the homogeneous ruthenium-based hydrogenation of esters.

In contrast to the hydrogenation of carbonyl compounds, the hydrogenation of esters is troublesome.[228] The hydrogenation of esters to alcohols is a conversion of industrial importance (Equation 4.1). This conversion is usually employed in the production of fatty alcohols and is a potential route to ethylene glycol, an important industrial compound *via* dimethyl oxalate.[229]

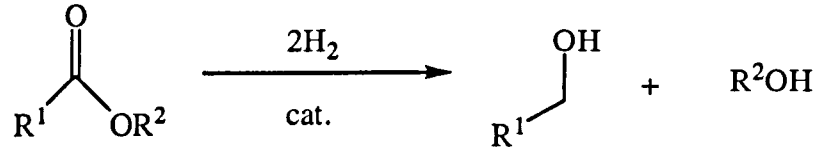

Equation 4.1.

Homogeneous ester hydrogenations, in comparison to its heterogeneous counterpart are not common. The homogeneous hydrogenation of ester to alcohols is indeed a difficult process and this is illustrated by the relatively few cases reported.[230–233] Anionic ruthenium hydride catalysts have been described by Grey *et al.* [230] and neutral ruthenium catalysts were reported by Matteoli *et. al.*[231,232] Generally, drastic conditions are required for the efficient conversion of an ester to the corresponding alcohol, unless the ester is activated by electron-withdrawing substituents. For example Matteoli *et. al.*[231] used a ruthenium-based catalyst $Ru(CO)_2(CH_3COO)_2(PBu_3)_2$ for the hydrogenation of dimethyl oxalate **232** to methyl glycolate **233**, which was subsequently reduced at a much slower rate to ethylene glycol **234** under drastic conditions according to Scheme 4.1. The conversion of **232** to **233** was relatively easy, while the conversion of **233** to **234** requires drastic conditions [$p(H_2)$ 200 bar; 180 °C].[231]

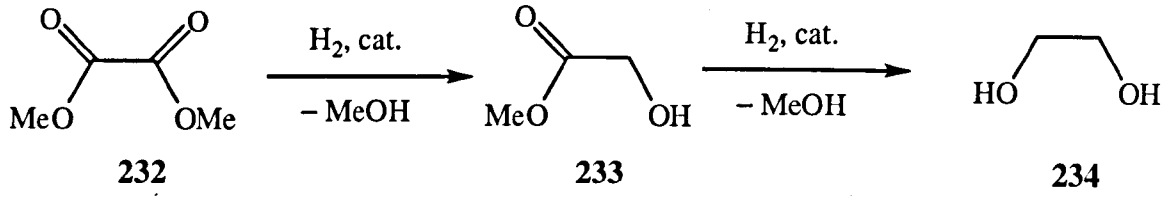

232 **233** **234**

Scheme 4.1

In order to achieve the conversion of dimethyl oxalate to ethylene glycol under milder reaction conditions with improved activity a search towards more active catalyst systems was initiated by Elsevier and co-workers.[233] Interest was directed towards the use of ruthenium complexes having an increased electron density on the ruthenium centre, which would enhance the nucleophilicity of the intermediate hydride towards the carbonyl function of the ester. They described the selection of suitable ruthenium complexes and ligands as catalyst precursors for the hydrogenation of dimethyl oxalate to ethylene glycol.[228] It was shown that dimethyl oxalate was efficiently hydrogenated to ethylene glycol under mild conditions [$p(H_2)$ 75 bar; 100 °C],[233] using a ruthenium catalyst prepared *in situ* from $Ru(acac)_3$ and a tripodal ligand $MeC(CH_2PPh_2)_3$ ($Triphos^{Ph}$).[228,233] This catalyst was far more active than any known homogeneous catalyst for this conversion. The first homogeneous ester hydrogenation catalyst utilising a sulfur-based ligand $MeC(CH_2SBu)_3$ ($TriSulf^{Bu}$) for the selective hydrogenation of dimethyl oxalate to methyl glycolate has also been reported,[229] the $TriSulf^{Bu}$ system was shown to be the most active catalyst that is selective towards the formation of methyl glycolate.[229] As mentioned earlier, the use of ruthenium complexes with increased electron density at the ruthenium centre would enhance the attack of the catalyst on the electrophilic carbonyl carbon atom of the dimethyl oxalate.[228] This will lead to an increase in the rate of conversion to the alcohol. The diazaphosphorinane ligands with the lone pair of electrons on the P atom are therefore suitable ligands for this reaction, which like other phosphines would generate an active ruthenium catalyst for this reaction. Thus cyclo-{$CH_2N(Ph)CH_2N(Ph)CH_2$-P}-$CH_2N(H)Ph$, **152** was used for the ruthenium-based ester hydrogenation of dimethyl oxalate in MeOH, 1.3 equivalents of **152** gave a conversion of 20.3% methyl glycolate. When 4 equivalents were used together with a variation of the pressure and run time, 76.9% methyl glycolate conversion was achieved

which was comparable to using 6 equivalents of P(n-Oct)$_3$, the best known monodentate phosphine to achieve a conversion of 100% methyl glycolate under similar conditions.[229]

4.1.2 HETEROGENEOUS CATALYSIS

This is where the catalysts used are in a different phase to the reactants and products. Heterogeneous catalysis has been the basis for most of the commercial processes, where the active catalytic species are usually on a solid support. Several such heterogeneous catalysts have been developed in order to overcome the typical problems of homogeneous catalysis. The most frequent motivation given is: recovery, recycling, and re-use of the catalyst. However, major drawbacks of heterogeneous catalysis include relatively lower activity and selectivity. Reaction conditions are harsh and mechanistic understanding is more or less impossible.

Several solid supports have been used to achieve heterogeneous catalysis. These include: Suzuki cross-coupling reactions using palladium on hydrotalcite as a catalyst (Figure 4.3),[234] Stille coupling reactions catalysed by a polymer supported palladium complex[235] and Sonogashira coupling reactions using a cellulose supported palladium(0) catalyst.[236] Others are the Heck reaction using Pd-complexes entrapped into zeolites to catalyse the reactions between aryl halides and olefins,[237] ligand-protected palladium nanoparticles,[238,239] palladium on active carbon (Pd/C),[240–242] and the use of Pd supported on activated carbon to catalyse Heck reactions of bromoarenes to control Pd leaching.[243]

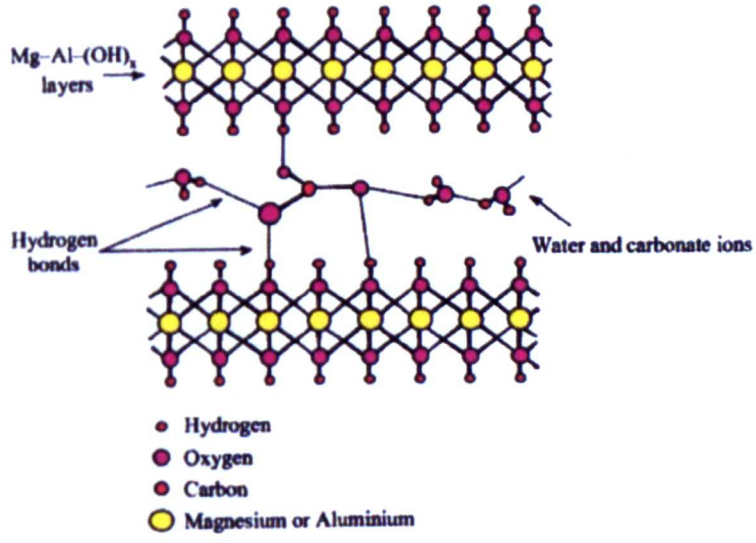

Figure 4.3 Structure of hydrotalcite.[234]

Hydrotalcite is a naturally occurring mineral with double hydroxide layer. Hydrotalcites form a major class of the anionic clay materials. Structurally, the geometry is octahedral with Mg^{2+} ions at the centre and the vertices occupied by OH groups forming stacks. Some of the Mg^{2+} ions are replaced by Al^{3+} ions, which results in charge deficiency in the layers. In order to ensure electroneutrality in the overall structure, the excess positive charge is balanced by CO_3^{2-} ions present in a disorderly manner in the interlayer spacing, which also contains water of crystallisation as shown in Figure 4.3.

4.2 SUPPORTED CATALYSTS

It is a well known fact that most coupling reactions are very attractive for industrial applications; however, the homogeneous variant in most cases has no practical application in industry due to the problems of separation, recovery and regeneration of the catalyst. In principle, heterogeneous catalysts can be used to minimise some of the problems faced by homogeneous catalysts. Among such heterogeneous catalysts are: supported metal catalysts, zeolite encapsulated catalysts, colloid-nanoparticles and intercalated metal compounds.

4.2.1 ZEOLITES

Zeolites are minerals with open aluminosilicate frameworks, hence easily take up loosely bound water and small molecules in their structure. The term zeolite was originally coined by a Swedish mineralogist named, A.F. Cronstedt in 1756, who observed, upon rapid heating, the constituent stones began to dance about as the water evaporated. Using the Greek words which mean "stone that boils," he called the mineral zeolite. They have three-dimensional structures arising from a framework of $[SiO_4]^{4-}$ and $[AlO_4]^{5-}$ tetrahedra forming coordination polyhedra linked by all their corners *via* the oxygen atoms. Collective polyhedra form frameworks that are generally open and contain pores (channels) and cavities in which are located cations and water molecules which have considerable freedom of movement, permitting ion exchange and reversible dehydration. The pores and cavities are of molecular dimensions and typically have diameters in the range 4–12 Å, hence are called micropores according to the IUPAC classification of porous materials.[244,245] The microscopically small zeolitic pores or channels of molecular dimensions are often called "molecular sieves". The size and shape of the channels have extraordinary effects on the properties of these materials for adsorption processes, and this property leads to their use in separation processes. Molecules can be separated *via*

shape and size effects related to their possible orientation in the pore, or by differences in strength of adsorption.

Since silicon typically exists in a 4+ oxidation state, the silicon-oxygen tetrahedra are electrically neutral. However, in zeolites, aluminium typically exists in 3+ oxidation states so that aluminium-oxygen tetrahedra form centres that are electrically deficient of an electron. Thus zeolite frameworks are typically anionic, and charge compensating cations populate the pores to maintain electrical neutrality. These cations can participate in ion-exchange processes, and this yields some important properties for zeolites. When charge compensating ions are "soft" cations such as sodium, zeolites are excellent water softeners because they can pick up the "hard" magnesium and calcium ions in water leaving behind the "soft" cations. When the zeolitic cations are protons, the zeolite becomes a strong solid acid. Such solid acids form the foundations of zeolite catalysis applications including the fluidized bed cat-cracking in petroleum refineries. Other types of reactive metal cations can also populate the pores to form catalytic materials with unique properties. Thus, zeolites are also commonly used in catalytic operations and catalysis with zeolites is often called "shape selective catalysis".

More than 150 zeolites have been synthesised and 40 naturally occurring zeolites are known. One major advantage of zeolites is that since they are naturally occurring, they are often cheap. Additionally, since they are largely composed of silicon, a major component of the earth's crust, they find many uses in an environmentally aware society. Zeolites form in nature under high pressure/temperature conditions at pH typically between 9 and 10. Nature requires 50 to 50,000 years to complete these reactions. Naturally occurring zeolites are rarely phase-pure, and are contaminated to varying degrees by other species *e.g.* Fe^{3+}, SO_4^{2-}, quartz etc. Thus naturally occurring zeolites are excluded from many important commercial applications where uniformity and purity are essential. Many of the uses of natural zeolites are environmentally related. For example, natural zeolites are used for the treatment of radioactive waste as well as municipal waste water treatment. They are also effective in adsorbing ammonia and hydrogen sulfide. These properties make natural zeolites ideal for use in pet litter to prevent emanation of irritating odours. For similar reasons, natural zeolites can also be used for effective control of irritating gases in horse stalls, kennels, barns, etc.

Initial efforts to synthesise zeolites were carried out under high pressure/temperature conditions in order to simulate those natural zeolites first discovered from volcanic deposits. Significant progress was made when synthesis was started under normal atmospheric conditions (<100 °C and atmospheric pressure). Synthesis was also focused on recreating natural zeolites, however, it was soon realised that many new structures could be easily synthesised. General synthesis starts from crystallisation from an inhomogeneous gel, obtained from a silica source and an aluminium source combined with water. Some of the parameters that control the type of zeolite formed are pH of the solution, temperature, pressure and the crystallisation time. The crystals of synthetic zeolites are very small compared to natural zeolites. This is due to the very long crystallisation time of natural zeolites in the earth.

Synthetic zeolites hold some key advantages over their natural analogues. The synthetics can be synthesised in a uniform phase-pure state. It is also possible to synthesise desirable structures which do not occur in nature *e.g.* Zeolite A. Since the principal raw materials are silica and alumina which are among the most abundant minerals on earth, the potential to synthesise zeolites is virtually unlimited. Finally, zeolite synthesis requires significantly less time than the 50 to 50,000 years in the case of natural zeolites. All commercially useful zeolites owe their value to one or more of three properties: adsorption, ion-exchange and catalysis.

Adsorption: Zeolites are used to adsorb a variety of materials. This includes applications in drying, purification and separation. They are used as very effective desiccants and can remove volatile organic chemicals from air streams, separate isomers and mixtures of gases. The most fundamental consideration regarding the adsorption of chemical species by zeolites is molecular sieving. Species with a kinetic diameter which makes them too large to pass through a zeolite pore are effectively "sieved". This "sieve effect" can be utilised to produce sharp separations of molecules by size and shape. The particular affinity a species has for an internal zeolite cavity depends on electronic considerations. The strong electrostatic field within a zeolite results in very strong interaction with polar molecules such as water. Non-polar molecules are also strongly adsorbed due to the polarising power of these electric fields. Thus excellent separations can be achieved by zeolites even when steric hindrance occurs. Adsorption based on molecular sieving, electrostatic fields and polarisability are always reversible. This allows the zeolite to be

reused many times, cycling between adsorption and desorption. This accounts for the considerable economic value of zeolites in adsorptive applications.

Ion-exchange: The presence of the counter balancing cations in the zeolite framework which are mobile, present the possibility for ion-exchange. This ion-exchange ability accounts for one of the greatest volume uses of zeolites. For example, zeolite A, a synthetic zeolite with sodium as a cation has widely replaced environmentally harsh phosphates as detergent water softeners. Unlike phosphates, zeolite A cannot contribute to the eutrophication of lakes, streams and rivers.

Catalysis: It is possible to say that zeolites are the most widely used catalysts in industry.[246] They have become extremely useful as catalysts for oil refining, petrochemistry, and organic synthesis in the production of fine and speciality chemicals, particularly when dealing with molecules having kinetic diameters below 10 Å. The reason for their success in catalysis is related to the following specific features:[246,247] (1) They have very high surface area and adsorption capacity. (2) The adsorption properties of the zeolites can be controlled, and they can be varied from hydrophobic to hydrophilic type materials. (3) Active sites, such as acid sites for instance, can be generated in the framework and their strength and concentration can be tailored for a particular application. (4) The size of their channels and cavities are in the range typical for many molecules of interest (5–12 Å), and the strong electric fields[248] existing in those micropores together with an electronic confinement of the guest molecules[249] are responsible for the preactivation of the reactants. (5) Their intricate channel structure allows the zeolites to present types of shape selectivity, *i.e.*, product, reactant, and transition state, which can be used to direct a given catalytic reaction toward the desired product avoiding undesired side reactions. (6) All of these properties of zeolites, which are of paramount importance in catalysis, are ultimately dependent on the thermal and hydrothermal stability of these materials. Zeolites can be activated to produce very stable materials resistant to heat, steam and chemical attacks. The acidity and acid strength of a zeolite can be modified by exchanging the cations or by modifying the Si/Al ratio.

Despite these catalytically desirable properties of zeolites they became inadequate when reactants with sizes above the dimensions of the pores have to be processed. In this case, the rational approach to overcome such a limitation would be to maintain the porous

structure, which is responsible for the benefits described above, but to increase their diameter to bring them into the mesoporous region. Attempts made using larger organic templates, resulting in large voids did not give positive results because these organic templates affect the gel chemistry and void fillers in the growing porous solids. Other methods to produce zeolites that retain the desirable properties but can accommodate reactants with larger dimensions are also prone to one drawback or the other. For example, when cacoxenite mineral[250] is used in this context as a catalyst, it was found to be thermally unstable and thus not suitable as a catalyst. Cacoxenite is a naturally occurring iron(III) phosphate compound, $[Fe^{3+}Al]_{25}[PO_4]_{17}O_6[OH]_{12}\cdot 75H_2O$ with an open frame-work containing cylindrical tunnels occupied by water molecules with a free diameter of *ca.* 15 Å. Thus the best strategy to produce larger pore molecular sieves/zeolites for catalytic processes is to increase the activity of the existing microporous materials for processing large molecules. This approach involves the generation of mesopores in the crystallites of the microporous zeolites.[249]

Zeolite-supported catalysts have been used for the Heck reaction. Djakovitch *et al.*[237] have studied the capability of palladium complex-loaded zeolites for catalysing the Heck reaction of aryl bromides with olefins using standard reaction conditions as mentioned earlier. It may be stated that the most studied NaY zeolites utilise low amounts of Pd (0.1 mol %) which can be easily separated and re-used after washing. The advantages derivable from this system are that the immobilised complexes in the zeolite super-cages should have almost the same activity as the free complexes in solution; secondly the zeolite microstructure (micro-reactor) could help to overcome the problems of leaching using heterogeneous catalysts in solution. Zeolites are also capable of stabilising intermediate active species retained in their cavities and combine shape selectivity. It is worthy of note that even aryl chlorides can be activated by this type of catalyst.

4.2.1.1 SYNTHESIS AND CHARACTERISATION OF ZEOLITE A, 235

Zeolite-A **235** was synthesised from NaOH using published procedures,[251,252] by adding $Na[AlO_2]$ to an aqueous solution of NaOH, heated to boiling point, followed by the slow addition of hot aqueous solution of $Na_2[SiO_3]$. The reactants were stirred vigorously, at 90°C for 4 h and the resulting white suspension (Zeolite-A) separated by filtration, washed with water and dried at 105°C for 16 h. The product was characterised by powder

X-ray diffraction. The experimental diffraction pattern was in excellent agreement with that expected with the reflections from the product in black perfectly matching those expected in red as shown in Figure 4.4.

4.2.1.2 SYNTHESIS AND CHARACTERISATION OF PERMANGANATE SODALITE, 236

Permanganate sodalite **236** another zeolite was synthesised also from NaOH using published procedures[251,252] by the addition of Zeolite-A to an aqueous solution of NaOH. This was followed by the addition of $Na[MnO_4]$ and refluxed for 24 h at 100°C and the resulting purple solid filtered on a glass sinter and dried at 105°C for 16 h. The product was also characterised by powder X-ray diffraction, the experimental diffraction pattern again was in excellent agreement with that expected with the reflections from the product in black perfectly matching those expected in red as shown in Figure 4.5.

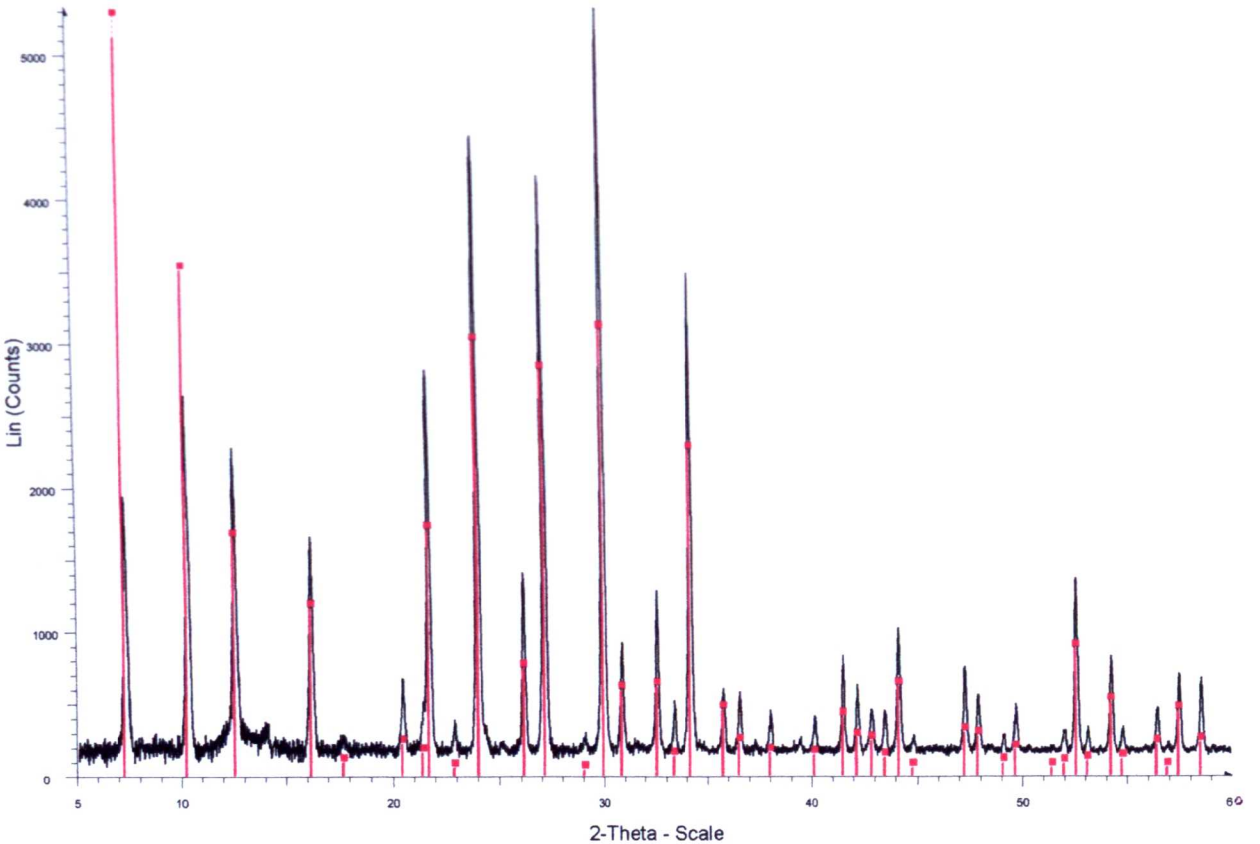

Figure 4.4 Powder X-ray diffraction pattern for **235**, RED lines = Sodium Aluminium Silicon Oxide Hydrate $Na_{92.71}(Si_{96.96}Al_{95.04}O_{384})(H_2O)$[observed] ; BLACK curves = Zeolite A [calculated].

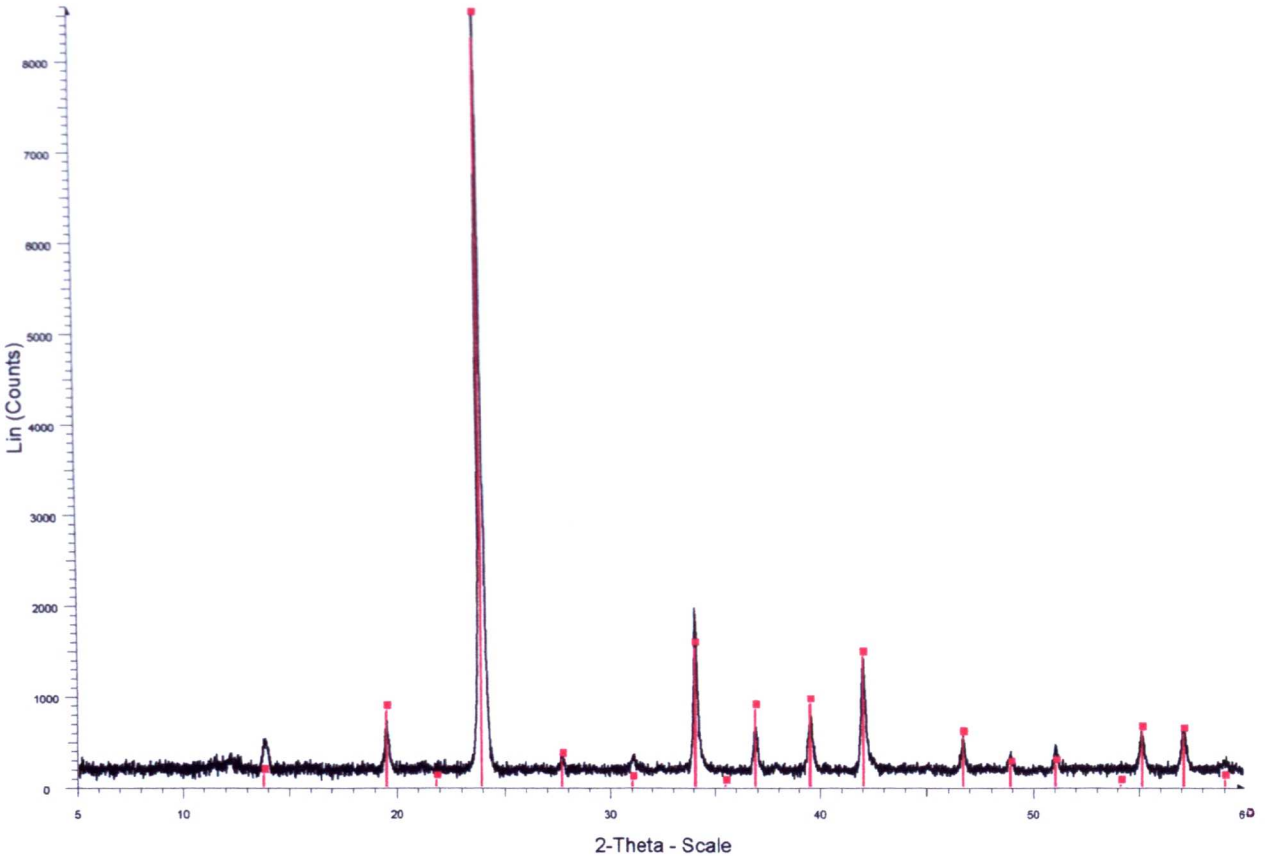

Figure 4.5 Powder X-ray diffraction pattern for **236**, RED lines = Sodalite $Na_2(Al_6Si_6O_{24}(MnO_4)1.46(OH)$[observed] ; BLACK curves = MnO_4 sodalite [calculated].

4.3 CONCLUSIONS

It has been shown that both the neutral and cationic phosphorus(III) ligands readily react with a range of late transition metals including Ru, Rh, Ir, Pd, Pt and Au to form complexes that could be useful in catalysis. In all the complexes *P*-coordination has been observed and verified by spectroscopy and crystallography. The high catalytic potential of the diazaphosphorinane ligands was proved when **152** was used for a ruthenium-based ester hydrogenation of dimethyl oxalate to achieve comparable result with P(*n*-Oct)$_3$, the best known monodentate phosphine. The complexes of the cationic phophorus(III) ligands found to be structurally and stereoelectronically related to analogous PTA complexes used in various catalytic organic transformations may therefore have useful future implications in catalysis.

CHAPTER FIVE

EXPERIMENTAL

5.1 MATERIALS

All reactions and manipulations were carried out under aerobic conditions unless otherwise stated. Dichloromethane was previously distilled over CaH_2 and THPC was recrystallised from 2-propanol before use.[10] The following starting materials were prepared according to literature methods: $[RuCl_2(\eta^6\text{-}p\text{-cymene})]_2$,[253] $[RhCl_2(\eta^5\text{-Cp*})]_2$,[254] $[IrCl_2(\eta^5\text{-Cp*})]_2$,[254] $PdCl_2(COD)$,[255] $Pd(Me)Cl(COD)$,[256] $[Pd(C\sim N)(\mu\text{-}Cl)]_2$ where (C~N = $C_9H_{12}N$ or $C_{12}H_{12}N$),[257,258] $PtCl_2(COD)$[259] and $[AuCl(THT)]$.[260] All other solvents and chemicals were obtained from commercial suppliers and used without further purification.

5.2 INSTRUMENTATION

Infrared spectra were recorded as KBr pellets in the range 4000–200 cm^{-1} on a Perkin-Elmer System 2000 Fourier-transform spectrometer, or in the range 4000–500 cm^{-1} on SHIMADZU FT–IR-8400S/FT–IR-8300 Fourier-transform spectrometers. ^1H NMR spectra were recorded on a Bruker DPX-400 FT spectrometer with chemical shifts (δ) in ppm to high frequency of $SiMe_4$, and coupling constants (J) in Hz. The $^{31}P\{^1H\}$ NMR spectra were also recorded on the same spectrometer with chemical shifts (δ) in ppm to high frequency of 85% H_3PO_4. All NMR spectra were recorded in d^6-DMSO or $CDCl_3$ unless otherwise stated. Microanalyses (Perkin-Elmer 2400 CHN/Exeter Analytical Inc. CE 440 Elemental Analyzer) were performed within the Department. Mass spectra were recorded on a JEOL SX102 instrument as Fast Atom Bombardment (FAB), in a positive ionization mode using a 3-nitrobenzyl alcohol (NOBA) matrix or on a Finnigan MAT 95XP as low-resolution FAB (LSIMS) in positive ionization mode using CH_2Cl_2 as the solvent and a NOBA matrix. Powder diffraction data were recorded on a Bruker D8 powder diffractometer using monochromated copper radiation over the 2θ range 5–60° using a 0.0147° 2θ step.

The crystallographic data were collected within the Department at 150 K on a Bruker SMART 1000 CCD diffractometer using graphite monochromated Mo–Kα radiation (λ = 0.71073 Å) or on a Bruker Apex 2 CCD diffractometer using graphite monochromated radiation from a sealed tube Mo–Kα source. Crystallographic data for much smaller crystals were collected at Daresbury using the synchrotron radiation source.

The crystal structures were solved by direct methods or Patterson synthesis. Programmes used were COLLECT[261] or Bruker AXS APEX 2[262] for diffractometer control and DENZO[263] or SAINT[264] for frame integration, Bruker SHELXTL[265,266] for structure solution, refinement and molecular graphics and local programmes. Conductivity measurements were recorded with a Jenway Model 4510 conductivity meter.

5.3 SYNTHESIS OF ANILINE DERIVATIVES (128–146) OF THPC

A range of aniline derivatives $[P(CH_2NHR)_4]Cl$ where R = phenyl or a substituted phenyl group were synthesised by reacting THPC with aniline precursors in a 1:4 molar ratio in ethanol using the procedure first published by Frank *et al.*[10]

5.3.1 SYNTHESIS OF COMPOUNDS 128, 129, 132, 138, 143–145

A typical procedure where the aniline precursor is a liquid is given here for compound $[P(CH_2NHC_6H_5)_4]Cl$, **128**. The amount of THPC used was 3.38 g in all cases except in **138**, **143** and **145** where the amount was different; **138** (2.85 g), **143** (0.75 g) and **145** (0.75 g), in all cases the THPC was reacted with the aniline precursor in a 1:4 molar ratio. A solution of THPC (3.83 g, 20.10 mmol) in 100% EtOH (75 cm^3) was prepared. Aniline (7.78 g, 83.41 mmol) was added dropwise to the THPC solution and the mixture stirred for 2 h at room temperature. There was a mild exotherm followed by precipitation of a white solid **128**. Compound **128** is known to be light sensitive (turns yellowish on exposure to light) hence was kept in the dark. The precipitate was filtered on a glass sinter and dried under vacuum and kept in the dark. Yield: 8.91 g, 90%. Yields for other compounds synthesised in this study are given in parentheses: **129** (9.39 g, 83%), **132** (11.00 g, 97%), **138** (9.47 g, 83%), **143** (2.26 g, 90%), **144** (11.32 g, 93%) and **145** (2.20 g, 85%).

5.3.2 SYNTHESIS OF COMPOUNDS 130, 131, 133–137, 139–142, 146

A typical procedure where the aniline precursor is a solid is given here for compound $[P(CH_2NH\text{-}4\text{-}ClC_6H_4)_4]Cl$, **130**. The amount of THPC used was 3.38 g in all cases except in **133**, **141** and **142** where the amount was different; **133** (3.00 g), **141** (2.83 g) and **142** (2.83 g). In all cases THPC was reacted with the aniline precursor in a 1:4 molar ratio in ethanol and stirred for 2 h at room temperature except in the case of **146** where the reaction was stirred for 24 h. A solution of THPC (3.83 g, 20.10 mmol) in 100% EtOH (25 cm^3) was prepared. A solution of 4-chloroaniline (10.64 g, 83.41 mmol) in 100% EtOH (50 cm^3) was also prepared and added dropwise to the THPC solution and the mixture stirred for 2 h

at room temperature. There was a mild exotherm followed by precipitation of a white solid. The yield was improved upon concentration of the solution under reduced pressure. The resulting solid **130** was filtered on a glass sinter and dried under vacuum. Yield: 11.37 g, 90%. Yields for other compounds synthesised in this study are given in parentheses: **131** (13.45 g, 83%), **133** (15.25 g, 97%), **134** (10.25 g, 95%), **135** (11.48 g, 86%), **136** (11.92 g, 97%), **137** (7.92 g, 71%), **139** (10.25 g, 76%), **140** (11.16 g 94%), **141** (8.38 g, 84%), **142** (9.02 g, 86%) and **146** (10.03 g, 69%).

5.4 SYNTHESIS OF PHENYLENEDIAMINE DERIVATIVES (147–150) OF THPC

A range of phenylenediamine derivatives $[P\{(CH_2NH)_2R\}_2]Cl$, [R = C_6H_4, **147**; R = C_6H_3Me, **148**; R = C_6H_3COPh, **149**; R = $C_6H_2C_4H_4$, **150**] were synthesised by reacting THPC with phenylenediamine precursors in 1:4 or 1: 2 molar ratio in ethanol, using a similar procedure first published by Frank *et al.*[10]

5.4.1 SYNTHESIS OF COMPOUND 147

Four equivalents of 1,2-phenylenediamine were reacted with THPC in the synthesis of $[P\{(CH_2NH)_2C_6H_4\}_2]Cl$, **147**; the use of two equivalents gave practically the same product as confirmed by the characterising data. A solution of THPC (3.83 g, 20.10 mmol) in 100% EtOH (75 cm^3) was prepared. Phenylenediamine (9.02 g, 83.41 mmol) was added dropwise to the THPC solution and the mixture stirred for 2 h at room temperature. The resulting white solid **147** was filtered on a glass sinter and dried under vacuum. Yield: 10.12 g, 91%.

5.4.2 SYNTHESIS OF COMPOUNDS 148–150

For compounds **148–150**, two equivalents of the phenylenediamine precursor was reacted with THPC. A typical procedure is given here for $[P\{(CH_2NH)_2C_6H_3Me\}_2]Cl$, **148**. A solution of THPC (1.96 g, 10.30 mmol) in 100% EtOH (20 cm^3) was prepared. A solution of 3,4-diaminotoluene (2.52 g, 2.59 mmol) in 100% EtOH (50 cm^3) was also prepared and added dropwise to the THPC solution and the mixture stirred for 2 h at room temperature. The resulting light brown solid **148** was filtered on a glass sinter and dried under vacuum. Yield: 3.11 g, 83%. Yields for other compounds synthesised in this study are given in parentheses: **149** (2.48 g, 87%) and **150** (0.30 g, 74%).

5.4.3 SYNTHESIS OF COMPOUND $[P\{(CH_2NH)_2C_6H_4\}_2]BPh_4$, 151

Compound $[P\{(CH_2NH)_2C_6H_4\}_2]BPh_4$, **151** was synthesised by anion metathesis of **147** using 1.5 equivalents of $Na[BPh_4]$. A solution of **147** (0.20 g, 0.45 mmol) in HPLC grade MeOH (5 cm^3) was prepared. $Na[BPh_4]$ (0.23 g, 0.68 mmol) was dissolved in the minimum volume of MeOH, this was added dropwise to the previous solution and the mixture stirred for 30 min at room temperature. Concentration under reduced pressure and addition of distilled water (*ca.* 5 cm^3) gave a white solid **151** which was filtered on a glass sinter and dried under vacuum. Yield: 0.23 g, 81%. Selected data: $^{31}P\{^1H\}$ NMR: 24.53 ppm. ^1H NMR: 6.70–7.18 (m, arom. H), 4.09–4.13 (m, CH_2), 5.78 ppm (d, $^3J_{PH}$ 17 Hz, NH). FT–IR: 3360 (vs, NH) cm^{-1}. FAB–MS: *m/z* 299 [M–BPh_4]. Anal. Calcd. for $C_{40}H_{40}N_4PB{\cdot}H_2O$: C, 75.47; H, 6.65; N, 8.80. Found: C, 75.13; H, 6.19; N, 9.09.

5.5 SYNTHESIS OF DIAZAPHOSPHORINANE LIGANDS

A range of diazaphosphorinane ligands were synthesised by reacting the phosphonium salts, **128–134**, **143–145** with 1.56 equivalents of triethylamine in acetone at room temperature using the procedure first published by Frank *et al.*[10]

5.5.1 SYNTHESIS OF COMPOUNDS 152–161

A typical procedure is given here for cyclo-$\{CH_2N(Ph)CH_2N(Ph)CH_2\text{-}P\}\text{-}CH_2N(H)Ph$ **152**. The amount of phosphonium salt used was 5.00 g in all cases except in **153**, **157**, **159**, **160** and **161** where the amount was different; **153** (4.50 g), **157** (1.25 g), **159** (2.50 g), **160** (1.00 g) and **161** (0.75 g), in all cases the phosphonium salt was reacted with 1.56 equivalents of triethylamine. A solution of $[P(CH_2NHC_6H_5)_4]Cl$, **128** (5.00 g, 10.2 mmol) in 99.9% acetone (70 cm^3) was prepared. To this was added triethylamine (1.63 g, 16.1 mmol). The mixture was stirred for 1 h after which the resulting white solid (triethylamine hydrochloride) was filtered on a glass sinter and dried under vacuum. The filtrate was concentrated under reduced pressure to *ca.* 1–2 cm^3. To the resulting oil was added 100% EtOH (50 cm^3) and stirred for 2 h at room temperature. The resulting white solid **152** was filtered on a glass sinter and dried under vacuum. Yield: 2.88 g, 78%. Yields for other compounds synthesised in this study are given in parentheses: **153** (2.26 g, 68%), **154** (2.24 g, 61%), **155** (2.30 g, 62%), **156** (2.86 g, 78%), **157** (0.75 g, 81%), **158** (3.39 g, 92%), **159** (1.39 g, 75%), **160** (0.65 g, 88%) and **161** (0.46 g, 83%).

5.5.2 SYNTHESIS OF COMPOUND $P(CH_2NHC_6H_5)_3$ 162

Compound $P(CH_2NHC_6H_5)_3$, **162** was synthesised by bubbling ammonia into **128** in acetone, using the procedure first published by Frank *et al.*[10] Ammonia was bubbled into a slurry of **128** (4.90 g, 10.0 mmol) in HPLC grade acetone (50 cm^3) for 5 mins at room temperature, during which time **128** dissolved and was replaced by a finely divided white solid, NH_4Cl. The mixture was stirred for 30 mins and the white solid separated from the resulting yellow solution by filtration. The solution was concentrated under reduced pressure and upon work-up and recrystallisation using benzene gave a white solid **162** which was filtered and dried under vacuum. Yield: 2.10 g, 60%. Selected data: $^{31}P\{^1H\}$ NMR: −38.75 ppm. ^1H NMR: 6.46–7.37 (m, arom. H), 5.79 (s, NH), 3.62 (d, $^2J_{HH}$ 12.0 Hz, CH_2), 3.45 (d, $^2J_{HH}$ 9.6 Hz, CH_2) ppm. FT–IR: 3024 (s, NH) cm^{-1}. Anal. Calcd. for $C_{21}H_{24}N_3P{\cdot}0.25C_3H_6O$: C, 71.78; H, 7.06; N, 11.55. Found: C, 71.88; H, 7.08; N, 11.51.

5.6 COORDINATION STUDIES OF DIAZAPHOSPHORINANE LIGANDS

The diazaphosphorinane ligands were reacted with ruthenium(II), rhodium(III), iridium(III), palladium(II) and platinum(II) precursors to form new metal complexes.

5.6.1 SYNTHESIS OF RUTHENIUM(II) COMPLEXES 163 AND 164

Two ruthenium(II) complexes were synthesised by reacting $[RuCl_2(\eta^6\text{-}p\text{-cymene})]_2$ with the diazaphosphorinane ligands **152** or **153** in a 1:2 molar ratio. A typical procedure is given here for compound $RuCl_2(\eta^6\text{-}p\text{-cymene})$(**152**), **163**. To a stirred solution of $[RuCl_2(\eta^6\text{-}p\text{-cymene})]_2$ (0.03 g, 0.05 mmol) in CH_2Cl_2 (10 cm^3) was added **152** (0.04 g, 0.11 mmol) as a solid in one portion. After stirring the solution for 30 min, the volume was reduced to *ca.* 1–2 cm^3 and Et_2O (10 cm^3) added and stirred for 30 min. The resulting orange solid **163** was filtered on a glass sinter and dried under vacuum. Yield: 0.06 g, 92%. Yield for the other compound synthesised in this study is given in parenthesis: **164** (0.06 g, 86%).

5.6.2 SYNTHESIS OF RHODIUM(III) AND IRIDIUM(III) COMPLEXES 165–168

Two complexes each of rhodium(III) and iridium(III) were synthesised by reacting $[MCl_2(\eta^5\text{-}Cp^*)]_2$, M = Rh or Ir with the diazaphosphorinane ligands **152** or **153** in a 1:2 molar ratio. Typical procedures are given for compounds $RhCl_2(\eta^5\text{-}Cp^*)$(**152**), **165** and $IrCl_2(\eta^5\text{-}Cp^*)$(**152**), **167**. To a stirred solution of $\{RhCl_2(\eta^5\text{-}Cp^*)\}_2$ (0.03 g, 0.05 mmol) in

CH_2Cl_2 (10 cm^3) was added **152** (0.04 g, 0.11 mmol) as a solid in one portion. After stirring the solution for 30 min, the volume was reduced to *ca.* 1–2 cm^3 under reduced pressure followed by addition of Et_2O (10 cm^3) and stirred for 30 min. The resulting orange solid **165** was filtered on a glass sinter and dried under vacuum. Yield: 0.06 92%. Yield for the other compound synthesised in this study is given in parenthesis: **166** (0.06 g, 85%).

Similarly, to a stirred solution of $\{IrCl_2(\eta^5\text{-}Cp^*)\}_2$ (0.03 g, 0.04 mmol) in CH_2Cl_2 (10 cm^3) was added **152** (0.03 g, 0.08 mmol) as a solid in one portion. After stirring the solution for 30 min, the volume was reduced to *ca.* 1–2 cm^3 followed by addition of Et_2O (10 cm^3) and stirred for 30 min. The resulting orange/yellow solid **167** was filtered on a glass sinter and dried under vacuum. Yield: 0.04 g, 74%. Yield for the other compound synthesised in this study is given in parenthesis: **168** (0.05 g, 84%).

5.6.3 SYNTHESIS OF PALLADIUM(II) COMPLEXES 169–177

A range of palladium(II) complexes were synthesised by reacting some of the diazaphosphorinane ligands **152–156** and **158–161** with $PdCl_2$(COD) in CH_2Cl_2 in a 2:1 molar ratio at room temperature to give the complexes **169–177**. A typical procedure is given for $PdCl_2$(**152**)$_2$ **169**. To a stirred solution of $PdCl_2$(COD) (0.10 g, 0.35 mmol) in CH_2Cl_2 (20 cm^3) was added **152** (0.25 g, 0.70 mmol) as a solid in one portion. After stirring the solution for 30 min the volume was reduced to *ca* 1–2 cm^3 under reduced pressure and Et_2O (20 cm^3) added. The resulting yellow solid **169** was filtered on a glass sinter and dried under vacuum. Yield: 0.29 g, 93%. Yields for other compounds synthesised in this study are given in parentheses: **170** (0.27 g, 75%), **171** (0.35 g, 89%), **172** (0.38 g, 79%), **173** (0.29 g, 82%), **174** (0.27 g, 77%), **175** (0.34 g, 92%), **176** (0.17 g, 75%) and **177** (0.23 g, 77%).

5.6.4 SYNTHESIS OF PLATINUM(II) COMPLEXES 178 AND 179

Two platinum(II) complexes were synthesised by reacting the diazaphosphorinane ligands **156** or **158** with $PtCl_2$(COD) in CH_2Cl_2 in a 2:1 molar ratio at room temperature. A typical procedure is given for $PtCl_2$(**156**)$_2$, **178**. To a stirred solution of $PtCl_2$(COD) (0.10 g, 0.27 mmol) in CH_2Cl_2 (20 cm^3) was added **156** (0.22 g, 0.53 mmol) as a solid in one portion. After stirring the solution for 30 min the volume was reduced to *ca.* 1–2 cm^3 under reduced pressure and Et_2O (20 cm^3) added. The resulting off-white or cream solid **178** was filtered

on a glass sinter and dried under vacuum. Yield: 0.22 g, 76%. Yield for the other compound synthesised in this study is given in parenthesis: **179** (0.25 g, 86%).

5.7 SYNTHESIS OF TERTIARY PHOSPHINE AMMONIUM SALTS

A range of new tertiary phosphine ammonium chlorides [cyclo-{$CH_2N(R')CH_2N(R')CH_2$-P}-$CH_2N(H_2)R']^+Cl^-$, where R′ = $C_6H_5CH_2$, 4-$FC_6H_4CH_2$, 4-$ClC_6H_4CH_2$, 4-$MeC_6H_4CH_2$, 4-$MeOC_6H_4CH_2$ were synthesised by reacting THPC with benzylamine precursors in a 1:4 molar ratio in ethanol at room temperature using a similar procedure first published by Frank *et al.*[10] Anion metathesis of some of the chlorides with different alkali metal salts in methanol was performed to give new tertiary phosphine ammonium salts.

5.7.1 SYNTHESIS OF COMPOUNDS 180–184

Five new tertiary phosphine ammonium chlorides (**180–184**) were synthesised by reacting THPC with benzylamine precursors as stated above. A typical procedure is given for [cyclo-{$CH_2N(R')CH_2N(R')CH_2$-P}-$CH_2N(H_2)R']^+Cl^-$ **180**, where R′ = $C_6H_5CH_2$. To a solution of THPC (3.83 g, 20.10 mmol) in 100% EtOH (75 cm^3) was added dropwise benzylamine, $C_6H_5CH_2NH_2$ (8.94 g, 83.40 mmol). A slight exotherm and thick white fumes were observed, and after *ca.* 5 mins, the solution became clear. The mixture was stirred for 2 h at room temperature (frequently some unwanted "sticky" material was formed which was separated from the solution by decantation). The solution was concentrated under reduced pressure to approximately a quarter of the original volume. The resulting crystalline colourless solid **180** was filtered on a glass sinter and dried under vacuum. Yield: 7.60 g, 86%. Using 2.85 g of THPC and the corresponding amount of the benzylamine precursors, 4-$FC_6H_4CH_2NH_2$, 4–$ClC_6H_4CH_2NH_2$ or 4–$MeC_6H_4CH_2NH_2$ gave the compounds **181–183**, while using 3.40 g of THPC with 4 equivalents of 4-$MeOC_6H_4CH_2NH_2$ gave **184**. Yields for other compounds synthesised in this study are given in parentheses: **181** (6.11 g, 83%), **182** (6.67g, 82%), **183** (6.27 g, 87%) and **184** (2.95 g, 93%).

5.7.2 REACTION OF TERTIARY PHOSPHINE AMMONIUM CHLORIDES WITH $Na[BPh_4]$, $Na[SbF_6]$ or $K[PF_6]$

Anion metathesis of the tertiary phosphine ammonium chlorides (**180–183**) with $Na[BPh_4]$, $Na[SbF_6]$ or $K[PF_6]$ in methanol was performed to give various tertiary phosphine

ammonium salts **185–196**, [cyclo-{$CH_2N(R')CH_2N(R')CH_2$-P}-$CH_2N(H_2)R']^+X^-$, [R′ = $C_6H_5CH_2$, 4-$FC_6H_4CH_2$, 4-$ClC_6H_4CH_2$, 4-$MeC_6H_4CH_2$; X = BPh_4, SbF_6, PF_6].

5.7.2.1 SYNTHESIS OF COMPOUNDS 185–188

Four new tertiary phosphine ammonium tetraphenylborates **185–188** were synthesised by reacting the tertiary phosphine ammonium chlorides **180–183** with 1.5 equivalents of $Na[BPh_4]$ in HPLC grade MeOH. A typical procedure is given for [cyclo-{$CH_2N(R')CH_2N(R')CH_2$-P}-$CH_2N(H_2)R']^+BPh_4^-$ **185**, where R′ = $C_6H_5CH_2$. A solution of $Na[BPh_4]$ (0.23 g, 0.67 mmol) in the minimum volume of HPLC grade MeOH was added to a solution of **180**, (0.20 g, 0.45 mmol) in HPLC grade MeOH (10 cm^3). The solution was stirred for 30 min at room temperature. Concentration of the solution under reduced pressure and addition of distilled water gave a colourless precipitate **185** which was filtered and dried under vacuum. Yield: 0.29 g, 89%. Similarly using **181**, **182** or **183** and $Na[BPh_4]$, the salts **186–188** were obtained. Yields for other compounds synthesised in this study are given in parentheses: **186** (0.27 g, 86%), **187** (0.27 g, 90%) and **188** (0.29 g, 90%).

5.7.2.2 SYNTHESIS OF COMPOUNDS 189–192

Four new tertiary phosphine ammonium hexafluoroantimonates **189–192**, were synthesised by reacting the tertiary phosphine ammonium chlorides **180–183** with 1.5 equivalents of $Na[SbF_6]$ in HPLC grade MeOH. A typical procedure is given for [cyclo-{$CH_2N(R')CH_2N(R')CH_2$-P}-$CH_2N(H_2)R']^+SbF_6^-$ **189**, where R′ = $C_6H_5CH_2$. A solution of $Na[SbF_6]$ (0.18 g, 0.69 mmol) in the minimum volume of HPLC grade MeOH was added to a solution of **180**, (0.20 g, 0.45 mmol) in HPLC grade MeOH (10 cm^3). The solution was stirred for 30 min at room temperature. Concentration of the solution under reduced pressure and addition of distilled water gave a colourless precipitate **189** which was filtered and dried under vacuum. Yield: 0.28 g, 97%. Similarly using **181**, **182** or **183** and $Na[SbF_6]$, the salts **190–192** were obtained. Yields for other compounds synthesised in this study are given in parentheses: **190** (0.21 g, 73%), **191** (0.24 g, 78%) and **192** (0.24 g, 86%).

5.7.2.3 SYNTHESIS OF COMPOUNDS 193–196

Four new tertiary phosphine ammonium hexafluorophosphates, **193–196**, were synthesised by reacting the tertiary phosphine ammonium chlorides **180–183** with 1.5 equivalents of

$K[PF_6]$ in HPLC grade MeOH. A typical procedure is given for [cyclo-$\{CH_2N(R')CH_2N(R')CH_2$-P$\}$-$CH_2N(H_2)R']^+PF_6^-$ **193**, where R′ = $C_6H_5CH_2$. A solution of $K[PF_6]$ (0.13 g, 0.71 mmol) in the minimum volume of HPLC grade MeOH was added to a solution of **180**, (0.20 g, 0.45 mmol) in HPLC grade MeOH (10 cm^3). The solution was stirred for 30 min at room temperature. Concentration of the solution under reduced pressure and addition of distilled water gave a colourless precipitate **186** which was filtered and dried under vacuum. Yield: 0.18 g, 72%. Similarly using **181**, **182** or **183** and $K[PF_6]$, the salts **186–189** were obtained. Yields for other compounds synthesised in this study are given in parentheses: **194** (0.20 g, 83%), **195** (0.18 g, 75%) and **196** (0.19 g, 78%).

5.8 COORDINATION STUDIES OF TERTIARY PHOSPHINE AMMONIUM SALTS

The tertiary phosphine ammonium salts were coordinated to some transition metal precursors: ruthenium(II), rhodium(I), rhodium(III), iridium(III), palladium(II), platinum(II) and gold(I) in order to access their ligating potential.

5.8.1 SYNTHESIS OF RUTHENIUM(II) COMPLEXES 197–202

A range of ruthenium(II) complexes were synthesised by reacting $[RuCl_2(\eta^6$-*p*-cymene$)]_2$ with the tertiary phosphine ammonium salts **181**, **188–190**, **193** and **194** in a 1:2 molar ratio. A typical procedure is given for $RuCl_2(\eta^6$-*p*-cymene$)$(**181**), **197**. To a stirred solution of $[RuCl_2(\eta^6$-*p*-cymene$)]_2$ (0.03 g, 0.05 mmol) in CH_2Cl_2 (10 cm^3) was added **181** (0.05 g, 0.10 mmol) as a solid in one portion. After stirring the solution for 30 min, the volume was reduced to *ca.* 1–2 cm^3 under reduced pressure followed by addition of Et_2O (10 cm^3) and stirred for 30 min. The resulting orange solid **197** was filtered on a glass sinter and dried under vacuum. Yield: 0.08 g, 98%. Similarly, using **188**, **189**, **190**, **193** or **194** and $[RuCl_2(\eta^6$-*p*-cymene$)]_2$ the complexes **198–202** were obtained. Yields for other compounds synthesised in this study are given in parentheses: **198** (0.09 g, 97%), **199** (0.08 g, 91%), **200** (0.08 g, 90%), **201** (0.09 g, 91%) and **202** (0.08 g, 91%).

5.8.2 SYNTHESIS OF RHODIUM(I) COMPLEXES 203 AND 204

Two rhodium(I) complexes were synthesised by reacting $Rh_2(CO)_4(\mu$-$Cl)_2$ with the tertiary phosphine ammonium salts **180** or **181** in a 1:4 molar ratio. A typical procedure is given for Rh(CO)Cl(**180**)$_2$, **203**. To a stirred solution of $Rh_2(CO)_4(\mu$-$Cl)_2$ (0.03 g, 0.08 mmol) in CH_2Cl_2 (10 cm^3) was added **180** (0.14 g, 0.32 mmol) as a solid in one portion. The dark

orange solution immediately went pale and a yellow solid precipitated within *ca.* 10 min. After stirring the solution for 30 min, the volume was reduced to *ca.* 1–2 cm^3 under reduced pressure, followed by addition of Et_2O (10 cm^3) and stirred for about 30 min. The resulting solid **203** was filtered on a glass sinter and dried under vacuum. Yield: 0.14 g, 88%. Similarly, using **181** and $Rh_2(CO)_4(\mu\text{-}Cl)_2$ the complex $Rh(CO)Cl(\mathbf{181})_2$, **204** was obtained. Yield: **204** (0.16 g, 93%.

5.8.3 SYNTHESIS OF RHODIUM(III) AND IRIDIUM(III) COMPLEXES 205–210

A range of rhodium(III) and iridium(III) complexes were synthesised by reacting $[MCl_2(\eta^5\text{-}Cp^*)]_2$, M = Rh or Ir with the tertiary phosphine ammonium salts **181**, **185** or **189** in a 1:2 molar ratio. Typical procedures are given for $RhCl_2(\eta^5\text{-}Cp^*)(\mathbf{181})$, **205** and $IrCl_2(\eta^5\text{-}Cp^*)(\mathbf{181})$, **208**. To a stirred solution of $[RhCl_2(\eta^5\text{-}Cp^*)]_2$ (0.03 g, 0.05 mmol) in CH_2Cl_2 (10 cm^3) was added **181** (0.05 g, 0.10 mmol) as a solid in one portion. After stirring the solution for 30 min, the volume was reduced to *ca.* 1–2 cm^3 under reduced pressure and Et_2O (10 cm^3) added. The resulting suspension was stirred for *ca.* 30 min and the resulting orange solid **205** was filtered on a glass sinter and dried under vacuum. Yield: 0.07 g, 88%. Using **185** or **189** and $[RhCl_2(Cp^*)]_2$ the complexes **206** and **207** were obtained. Yields for other compounds synthesised in this study are given in parentheses: **206** (0.09 g, 96%) and **207** (0.09 g, 98%).

Similarly, to a stirred solution of $[IrCl_2(\eta^5\text{-}Cp^*)]_2$ (0.03 g, 0.05 mmol) in CH_2Cl_2 (10 cm^3) was added **181** (0.05 g, 0.10 mmol) as a solid in one portion. After stirring the solution for 30 min, the volume was reduced to *ca.* 1–2 cm^3 under reduced pressure and diethyl ether (10 cm^3) added. The resulting suspension was stirred for *ca.* 30 min and the resulting yellow solid **208** filtered on a glass sinter and dried under vacuum. Yield: 0.06 g, 96%. Using **185** or **189** and $[IrCl_2(Cp^*)]_2$ the complexes **209** and **210** were obtained. Yields for other compounds synthesised in this study are given in parentheses: **209** (0.07 g, 85%) and **210** (0.06 g, 77%).

5.8.4 SYNTHESIS OF PALLADIUM(II) COMPLEXES

The tertiary phosphine ammonium salts were reacted with various palladium(II) precursors: $PdCl_2(COD)$, $PdCl_2(CH_3CN)_2$, Pd(Me)Cl(COD) and $[Pd(C\sim N)(\mu\text{-}Cl)]_2$, where C~N = $C_9H_{12}N$, $C_{12}H_{12}N$.

5.8.4.1 SYNTHESIS OF PALLADIUM(II) COMPLEX 211

A palladium(II) complex was prepared by reacting $PdCl_2(COD)$ with the tertiary phosphine ammonium salt **180** in a 1:2 molar ratio in $CHCl_3$. To a stirred solution of $PdCl_2(COD)$ (0.10 g, 0.35 mmol) in $CHCl_3$ (10 cm^3) was added a solution of **180** (0.31 g, 0.70 mmol) in $CHCl_3$ (10 cm^3) and refluxed under nitrogen at 90 °C for 2 h. The yellow palladium solution briefly turned orange and became yellow again with the characteristic smell of cycloocta-1,5-diene (COD) signalling its displacement by the phosphine ligand **180**. On cooling, the volume was reduced to *ca.* 1–2 cm^3 under reduced pressure and diethyl ether (10 cm^3) added. The resulting yellow precipitate **211** was filtered on a glass sinter and dried under vacuum. Yield: 0.24 g, 64%.

5.8.4.2 SYNTHESIS OF PALLADIUM(II) COMPLEX 212

To a stirred solution of $PdCl_2(COD)$ (0.05 g, 0.175 mmol) in CH_2Cl_2 (20 cm^3) was added **181** (0.17 g, 0.350 mmol) as a solid in one portion. After stirring the solution for 24 h, the volume was reduced to *ca.* 1-2 cm^3 under reduced pressure and Et_2O (10 cm^3) added. The resulting suspension was stirred for *ca.* 30 min and the resulting yellow solid **212** filtered on a glass sinter and dried under vacuum. Yield: 0.19 g, 92%.

5.8.4.3 SYNTHESIS OF PALLADIUM(II) COMPLEXES 213–215

Reaction of $PdCl_2(CH_3CN)_2$ with the tertiary phosphine ammonium salts **181**, **189** or **190** in CH_2Cl_2 at room temperature followed by precipitation with Et_2O upon concentration of the solution under reduced pressure gave the yellow compounds **213–215**. A typical procedure is given for $PdCl_2(181)_2$, **213**. To a stirred solution of $PdCl_2(CH_3CN)_2$ (0.05 g, 0.19 mmol) in CH_2Cl_2 (10 cm^3) was added **181** (0.19 g, 0.38 mmol) as a solid in one portion. After stirring the solution for 30 min, the volume was reduced to *ca.* 1–2 cm^3 under reduced pressure and Et_2O (10 cm^3) added and stirred for 30 min. The resulting yellow solid **213** was filtered on a glass sinter and dried under vacuum. Yield: 0.21 g, 94%. Yields for other compounds synthesised in this study are given in parentheses: **214** (0.26 g, 91%) and **215** (0.25 g, 84%).

5.8.4.4 SYNTHESIS OF PALLADIUM(II) COMPLEXES 216 AND 217

Reaction of Pd(Me)Cl(COD) with the tertiary phosphine ammonium salts **181** or **189** in CH_2Cl_2 at room temperature followed by precipitation with Et_2O upon concentration of the

solution under reduced pressure gave the yellow compounds **216** and **217**. A typical procedure is given for Pd(Me)Cl(**181**)$_2$, **216**. To a stirred solution of Pd(Me)Cl(COD) (0.05 g, 0.19 mmol) in CH_2Cl_2 (10 cm^3) was added **181** (0.19 g, 0.38 mmol) as a solid in one portion. After stirring the solution for 30 min, the volume was reduced to *ca.* 1–2 cm^3 under reduced pressure followed by addition of Et_2O (10 cm^3) and stirred for 30 min. The resulting yellow/orange solid **216** was filtered on a glass sinter and dried under vacuum. Yield: 0.19 g, 88%. Similarly using **189** and Pd(Me)Cl(COD) complex **217** was obtained. Yield: 0.16 g, 93%.

5.9 COORDINATION STUDIES OF TERTIARY PHOSPHINE AMMONIUM SALTS WITH CYCLOMETALLATED PALLADIUM DIMERS

The Pd dimers namely [Pd(C~N)(μ-Cl)]$_2$, where C~N = $C_9H_{12}N$, $C_{12}H_{12}N$ were reacted with **181** or **190** in a 2:1 molar ratio in CH_2Cl_2 at room temperature, following the procedure by Ruiz *et al.*[143]

5.9.1 SYNTHESIS OF COMPOUNDS 218 AND 219

A typical procedure is given for compound Pd(Cl)$C_6H_4CH_2NMe_2$(**181**), **218**. To a stirred solution of [PdCl($C_9H_{12}N$)(μ-Cl)]$_2$ (0.030 g, 0.05 mmol) in CH_2Cl_2 was added **181** (0.05 g, 0.10 mmol) as a solid in one portion. The solution was stirred for 1.5 h and the volume reduced to *ca.* 1–2 cm^3 under reduced pressure and hexane (10 cm^3) added. The resulting suspension was stirred for 20 min and the off-white solid **218** collected on a glass sinter and dried under vacuum. Yield: 0.07 g, 81%. Similarly, using **190** and [PdCl($C_9H_{12}N$)(μ-Cl)]$_2$ complex **219** was obtained. Yield: 0.08 g, 79%.

5.9.2 SYNTHESIS OF COMPOUNDS 220 AND 221

A typical procedure is given for Pd(Cl)$C_{10}H_6NMe_2$(**181**), **220**. To a stirred solution of [PdCl($C_{12}H_{12}N$)(μ-Cl)]$_2$ (0.030 g, 0.05 mmol) in CH_2Cl_2 was added **181** (0.05 g, 0.10 mmol) as a solid in one portion. The solution was stirred for 1.5 h and the volume reduced to *ca.* 1–2 cm^3 under reduced pressure and hexane (10 cm^3) added. The resulting suspension was stirred for 20 min and the pale-yellow solid **220** collected on a glass sinter and dried under vacuum. Yield: 0.06 g, 78%. Similarly, using **190** and [PdCl($C_{12}H_{12}N$)(μ-Cl)]$_2$, complex **221** was obtained. Yield: 0.09 g, 89%.

5.9.3 SYNTHESIS OF COMPOUND 222

To a stirred solution of $[PdCl(C_9H_{12}N)(\mu\text{-}Cl]_2$ (0.03 g, 0.05 mmol) in CH_2Cl_2 (10 cm^3) was added **181** (0.070 g, 0.11 mmol) as a solid in one portion. After stirring the solution for 30 min the volume was reduced to *ca.* 1–2 cm^3 under reduced pressure followed by addition of diethyl ether (10 cm^3) and stirred for 20 min. The resulting pale yellow solid **222** was filtered on a glass sinter and dried under vacuum. Yield: 0.08 g, 80%.

5.10 SYNTHESIS OF PLATINUM(II) COMPLEXES 223 AND 224

Reaction of $PtCl_2(CH_3CN)_2$ with two equivalents of the tertiary phosphine ammonium salts **189** or **190** in CH_2Cl_2 at room temperature followed by precipitation with Et_2O upon concentration of the solution under reduced pressure gave the off-white compounds **223** and **224**. A typical procedure is given for $PtCl_2$(**189**)$_2$, **223**. To a stirred solution of $PtCl_2(CH_3CN)_2$ (0.05 g, 0.14 mmol) in CH_2Cl_2 (20 cm^3) was added **189** (0.18 g, 0.28 mmol) as a solid in one portion. After stirring the solution for 30 min the volume was reduced to *ca.* 1–2 cm^3 under reduced pressure and Et_2O (10 cm^3) added. The resulting pale-yellow solid **223** was filtered on a glass sinter and dried under vacuum. Yield: 0.13 g, 59%. Similarly, using **190** and $PtCl_2(CH_3CN)_2$, complex **224** was obtained. Yield: 0.16 g, 68%.

5.11 SYNTHESIS OF GOLD(I) COMPLEXES 225–228

Four gold(I) complexes **225–228** were synthesised by reacting AuCl(THT) with the tertiary phosphine ammonium salts **181**, **190**, **193** or **194** in a 1:1 molar ratio in CH_2Cl_2 at room temperature. A typical procedure is given for compound AuCl(**181**), **225**. To a stirred solution of AuCl(THT) (0.030 g, 0.09 mmol) in CH_2Cl_2 (10 cm^3) in a flask wrapped with foil, was added **181** (0.046 g, 0.09 mmol) as a solid in one portion. After stirring the solution for 1 h, the volume was reduced to *ca.* 1–2 cm^3 under reduced pressure and Et_2O (10 cm^3) added and stirred for 20 min. The resulting off-whitish solid **225** was filtered on a glass sinter and dried under vacuum and kept in the dark. Yield: 0.055 g, 81%. Similarly, using **190**, **193** or **194** with AuCl(THT), the complexes **226**, **227** and **228** respectively were obtained. Yields for other compounds synthesised in this study are given in parentheses: **226** (0.075 g, 86%), **227** (0.057 g, 78%) and **228** (0.065 g, 83%).

5.12 SYNTHESIS OF ZEOLITE A AND PERMANGANATE SODALITE

Zeolite A and permanganate sodalite were synthesised from NaOH using published procedures,[251,252] and characterised by powder X-ray diffraction.

5.12.1 SYNTHESIS OF ZEOLITE A 235

To a solution of NaOH (25.030 g, 625.00 mmol) in H_2O (300 cm^3) in a beaker (exothermic, beaker was immersed in water to cool), was added $Na[AlO_2]$ (13.50 g, 137.80 mmol) as a solid and heated to boiling point on a hot plate. This was followed by slow addition of a hot solution of $Na_2[SiO_3]$ (10.60 g, 86.82 mmol) in H_2O (200 cm^3) with rapid stirring for 4 h with the temperature maintained at 90 °C, the beaker covered with a watch glass to prevent water loss. The resulting white suspension (Zeolite-A) was separated by filtration, washed with water and dried at 105°C for 16 h in the oven. Yield: 14.26 g. The product was characterised by powder X-ray diffraction, the experimental diffraction pattern was in excellent agreement with the expected, the reflections from the product in black matching the expected in red as shown in Figure 4.4.

5.12.2 SYNTHESIS OF PERMANGANATE SODALITE 236

To a solution of NaOH (28.21 g, 705.25 mmol) in H_2O (63 cm^3) in a beaker (exothermic, beaker was immersed in water to cool), followed by addition of more H_2O (30 cm^3) and Zeolite A (4.00 g) as a solid. The mixture was transferred to a 3-neck flask followed by addition of $Na[MnO_4]$ (45.00 g, 317.06 mmol) and refluxed for 24 h, with the temperature maintained at *ca.* 100 °C. The resulting purple solid was filtered on a glass sinter and dried at 105°C for 16 h in the oven. Yield: 4.26 g. The product was characterised by powder X-ray diffraction, the experimental diffraction pattern was in excellent agreement with the expected, the reflections from the product in black matching the expected in red as shown in Figure 4.5.

6.0 GENERAL CONCLUSIONS

As set out in the aims of the research, the preparation and characterisation of new phosphonium salts and phosphorus(III) ligands from THPC was achieved. Two new classes of phosphonium salts synthesised were aniline derivatives of THPC and phenylenediamine derivatives of THPC. While two new classes of cyclic phosphorus(III) ligands synthesised were diazaphosphorinanes and tertiary phosphine ammonium salts as neutral and cationic phosphorus(III) ligands respectively. The primary focus of the preparation and characterisation of new transition metal complexes with phosphorus(III) ligands was also achieved. However, only very little was done in the evaluation of the phosphorus(III) ligands or complexes, in selected cases, as potential catalysts for organic transformations due to time constraints.

A range of new aniline derivatives of THPC were synthesised by reacting THPC with different aniline precursors in ethanol at room temperature following the procedure first published by Frank *et al.*[10] Phenylenediamine derivatives of THPC were also synthesised by reacting THPC with phenylenediamine precursors in ethanol at room temperature following a similar procedure first published by Frank *et al.*[10] The resulting solids were characterised by conventional techniques. Single crystal X-ray diffraction analyses confirmed the proposed molecular formulae exhibiting tetrahedral configuration with evidence of intermolecular H-bonding in one of the aniline derivatives of THPC and one of phenylenediamine derivative of THPC. The crystal structure of the phenylenediamine derived salt showed a phosphorus based spirocycle. This represents the first crystallographic example of a spirocyclic compound with a phosphorus atom at the centre. This is supported by the absence of any hits from a CSD search.[191,192]

Diazaphosphorinanes were also synthesised by reaction of the corresponding aniline derivatives of THPC with triethylamine in acetone using the procedure first published by Frank *et al.*[10] The resulting colourless solids were obtained in good yields, and similarly characterised. Single crystal X-ray diffraction analysis in one case showed a pyramidal geometry with the phosphorus atom at the apex. The lone pair of electrons on the phosphorus atom qualifies this compound as a potential ligand. The catalytic ability of the diazaphosphorinane ligands was demonstrated in a ruthenium-based ester hydrogenation of dimethyloxalate to methylglycolate to achieve 76.9% conversion when 4 equivalents were used. This was comparable to using 6 equivalents of P(*n*-Oct)$_3$, the best known

monodentate phosphine to achieve 100% methylglycolate conversion under similar conditions.[229]

Apart from the diazaphosphorinane ligands, the preparation of a range of new tertiary phosphines of the type $P(CH_2NHR)_3$ where R = phenyl or substituted phenyl group by bubbling ammonia gas into solutions of selected aniline derivatives of THPC earlier prepared was attempted, using the procedure first published by Frank *et al.*[10] The known compound $P(CH_2NHC_6H_5)_3$ was successfully synthesised and characterised.

Coordination studies of the diazaphosphorinane ligands was carried out with relevant ruthenium(II), rhodium(III), iridium(III), palladium(II) and platinum(II) precursors to form the expected complexes in good to excellent yields. The metal complexes were characterised using conventional techniques and single X-ray crystallography in several cases. In the case of the Rh(III) and Ir(III) complexes, confirmations of the structures were achieved by single crystal X-ray diffraction analysis. The complexes showed a classic "piano-stool" geometry with evidence of intramolecular N–H···Cl hydrogen bonding, involving one of the metal bound chlorides and the diazaphosphorinane ligand in each case. While the Pd(II) and Pt(II) complexes were shown to exhibit *cis* configuration as supported by the infrared spectra having two M–Cl stretches in the range 263–316 cm^{-1}. In the case of the platinum(II) complexes the *cis* configuration was further supported by $^{31}P\{^1H\}$ NMR [$^1J_{PPt} \approx 3600$ Hz]. Further confirmation of the *cis* configuration comes from the X-ray structures of two palladium(II) complexes and a platinum(II) complex where crystals were obtained. The structures confirm the *cis* arrangement and show approximate square planar geometry with bond lengths and angles comparable to those of other reported compounds.[201,202]

A range of tertiary phosphine ammonium chlorides were prepared by reacting THPC with benzylamine precursors using a similar procedure first published by Frank *et al.*[10] The reactions gave good to excellent yields of the desired colourless products, characterised and shown to exhibit monodentate *P*-coordination. The X-ray crystal structure of one of the chlorides showed a pyramidal configuration and reveals a P–C–N–C–N–C six-membered ring with a chair conformation, exhibiting mirror plane symmetry. There was a pair of N–H···N intramolecular H-bonds which form a conformationally locked phosphine

framework in the solid state similar to the well-known PTA cage. This can be regarded as a charged variant of the PTA ligand with related P–C bond lengths and P–C–N, C–P–C bond angles.[204,205]

Anion metathesis of the tertiary phosphine ammonium chlorides with $Na[BPh_4]$, $Na[SbF_6]$ or $K[PF_6]$ in methanol at room temperature under aerobic conditions, gave the corresponding colourless tertiary phosphine ammonium salts in high yields. All the salts were similarly characterised, and the structures were consistent with the molecular formulae of the salts.

The crystal structures of some of these metathesised salts have similar structures to that of the structure of the precursor chloride which has been crystallographically determined, although only one N–H···N intramolecular H-bond was observed in one case due to H-bonding interactions involving the π systems in the BPh_4^- counterions present. Thus from the single crystal X-ray structures of these cyclic cationic phosphorus(III) ligands, it is evident that simple modification of the PTA core can be achieved in which non-covalent interactions such as H-bonds maintain the structure in the solid state.

The coordination potential of the tertiary phosphine ammonium salts was evaluated by reacting selected examples with relevant Ru(II), Rh(I), Rh(III), Ir(III), Pd(II), Pt(II) and Au(I) precursors and the corresponding transition metal complexes were obtained in high yields, similarly characterised and shown to exhibit *P*-monodentate coordination. In the Ru(II) complexes, the $^{31}P\{^1H\}$ NMR spectra of the complexes showed average coordination chemical shifts similar to that obtained for $RuCl_2(\eta^6$-*p*-cymene)(PTA) ($\Delta\delta_P$ 60 ppm) suggesting similar stereoelectronic properties.[110] The crystal structures of the Ru(II) complexes obtained show classic "piano-stool" geometry with the metric parameters comparable to analogous complexes with PTA.[104,110] Furthermore, upon coordination there were minimal differences in the P–C and P–C–N metric parameters between the complexes and the precursor ligands with retention of the rigid cage crystal structure even upon complexation in each case. There was evidence of dimer pairs formed by intermolecular H-bonding interactions similar to what has been recently observed in cationic dimeric Ru^{II}PTA complexes.[121]

Two square planar rhodium(I) carbonyl complexes were synthesised by reacting $Rh_2(CO)_4(\mu\text{-}Cl)_2$ with two of the tertiary phosphine ammonium chlorides to give the corresponding Rh(I)carbonyl complexes. Characterisation was similarly achieved by conventional techniques, except that in both complexes, meaningful NMR data could not be obtained due to poor solubility in common solvents. The CO vibrations in the FT–IR spectral data of these complexes were similar to those of analogous *trans*-rhodium(I) carbonyl PTA complexes suggestive of the Rh(I) complexes probably exhibiting a *trans* configuration in each case.

Rhodium(III) and iridium(III) complexes were prepared by reacting some of the tertiary phosphine ammonium salts in each case with $[RhCl_2(\eta^5\text{-}Cp^*)]_2$ or $[IrCl_2(\eta^5\text{-}Cp^*)]_2$ respectively and similarly characterised. A combination of microanalytical and spectroscopic data of the products confirms the formulae of the compounds exhibiting *P*-monodentate coordination.

In the case of the rhodium(III) complexes the $^{31}P\{^1H\}$ NMR spectral data showed a doublet in all the complexes with an average $^1J_{PRh}$ coupling constant of *ca.* 145 Hz comparable to other rhodium(III) complexes reported previously.[199] While in the case of the analogous iridium(III) complexes, the $^{31}P\{^1H\}$ NMR spectra showed singlets. The average coordination chemical shifts for the rhodium(III) and iridium(III) complexes were also not significantly different from those found for the analogous rhodium(III)(PTA) and irdium(III)(PTA) complexes respectively suggesting similar stereoelectronic properties.[51,211]

Single crystals of a rhodium(III) and iridium(III) complex were obtained and the structures have been determined, though that of the iridium complex not completed are supportive of mononuclear *P*-coordination and a typical "piano-stool" geometry around the metal centre. In the case of the completed rhodium(III) complex, the metric parameters were comparable to analogous Rh(III)PTA complexes.[51] Furthermore, upon coordination as in the case of the ruthenium(II) complexes there were minimal differences in the P–C and P–C–N metric parameters between the rhodium(III) complex and the precursor phosphorus(III) ligand and the rigid cage structure was maintained. An additional weak intermolecular H-bonding interaction linking the molecules into dimer pairs was also observed.

The coordination potential of the tertiary phosphine ammonium salts was also explored by reacting some of these ligands with various monomeric palladium(II) precursors namely $PdCl_2(COD)$, $PdCl_2(CH_3CN)_2$ and Pd(Me)Cl(COD) and characterised. The characterising data in all the complexes supports the proposed molecular formula of the expected monomeric $PdCl_2L_2$ complex indicative of *P*-coordination and *trans* configuration except the one synthesised from $PdCl_2(COD)$ which support a *cis* configuration. Attempts to obtain suitable crystals for X-ray diffraction analysis were unsuccessful in most cases. However, in the case of the reaction between $PdCl_2(COD)$ and one of the tertiary phosphine ammonium salts, attempts to obtain crystals for X-ray diffraction analysis gave a novel six-membered chelate Pd(II) complex with an approximate square-planar geometry about the palladium(II) centre not consistent with the other charactering data obtained from the bulk complex. The structural motif for this novel Pd(II) complex is supported by the absence of any hits from a CSD search.[191,192] A plausible mechanism for the transformation from $PdCl_2L_2$ type complex to the chelate complex has been proposed.

The coordination potential of the tertiary phosphine ammonium salts was further evaluated by reacting them with cyclometallated palladium(II) dimers namely $[Pd(C\sim N)(\mu\text{-}Cl)]_2$, where (C~N = $C_9H_{12}N$ or $C_{12}H_{12}N$) using the procedure by Ruiz *et al.*[143] The resulting cyclometallated palladium(II) complexes were characterised and shown to exhibit *P*-monodentate coordination. The $^{31}P\{^1H\}$ NMR spectra have shown that the average coordination chemical shifts for the cyclometallated Pd(II) complexes [$\Delta\delta_P$ 50.00 ppm] were the same as what was obtained in the analogous PTA complex, $Pd(C_9H_{12}N)Cl(PTA)$, **75** [$\Delta\delta_P$ 50.00 ppm],[143] again suggesting similar stereoelectronic properties. The X-ray structures of two of these complexes have been determined and reveal an approximate square-planar geometry with metric parameters similar to those reported for the analagous cyclometallated palladium(II) PTA complexes.[143,212,213] Furthermore, upon coordination the P–C and P–C–N metric parameters of the precursor ligand were not changed and the rigid cage structure of the precursor ligand formed by a pair of intramolecular N–H···N H-bonds was maintained in the solid state even upon complexation, as was seen previously in the case of the Ru(II) and Rh(III) complexes.

One of the reactions involving $[Pd(C_9H_{12}N)(\mu\text{-}Cl)]_2$ was repeated with variation of the time and precipitant to obtain a pale-yellow solid. The NMR [^1H, $^{31}P\{^1H\}$], CHN and FT–IR data involving the bulk complex were identical with similar data obtained for the complex

obtained earlier. However, X-ray diffraction analysis of crystals obtained gave an unexpected novel zwitterionic palladium(II) dimeric complex. The molecular formula from the X-ray diffraction analysis was not consistent with the other characterising data obtained on the bulk complex which is in agreement with the monomeric $PdCl_2L_2$ type complex. A mechanism involving intramolecular rearrangements during the crystallisation process leading to this transformation has been proposed.

Similarly, the ligating potential of the tertiary phosphine ammonium salts was also explored by reacting them with $PtCl_2(CH_3CN)_2$. Characterisation was similarly achieved except that due to extreme insolubility in common solvents no meaningful NMR [^1H, $^{31}P\{^1H\}$] spectral data could be obtained. As was in the case of the Pd(II) complex forming an unexpected zwitterionic Pd(II) dimeric complex, X-ray diffraction analysis of crystals obtained gave an unexpected novel zwitterionic platinum(II) dimeric complex. The molecular formula from the X-ray diffraction analysis was also not consistent with the other characterising data obtained on the bulk complex which is in agreement with the monomeric $PtCl_2L_2$ type complex. A mechanism involving a similar intramolecular rearrangement as in the case of the novel Pd(II) complex during the crystallisation process leading to this transformation has also been proposed. The novelty of the structural motifs in the zwitterionic Pd(II) and Pt(II) dimeric complexes are supported by the absence of any hits from CSD searches.[191,192] In both cases, there was no evidence of H-bonding, indicative of the absence of typical donor/acceptor groups in these complexes.

To further explore the coordination potential of the cationic phosphorus(III) ligands, they were reacted with [AuCl(THT)] and the resulting Au(I) complexes similarly characterised and shown to exhibit monodendate *P*-coordination. The average coordination chemical shifts for the Au(I) complexes ($\Delta\delta_P$ 42.00 ppm) were similar to what was obtained in the analogous (PTA)Au(I) complex, (PTA)AuCl ($\Delta\delta_P$ 45.00 ppm)[169] also suggesting similar stereoelectronic properties. The crystal structure of one of the complexes has been determined and reveal an approximate linear geometry with simlar metric parameters to analogous linear gold(I) PTA complexes.[168,169] Furthermore, upon coordination as in the case of the ruthenium(II), rhodium(III) and palladium(II) complexes, there were minimal differences in the P–C and P–C–N metric parameters between the complex and its precursor ligand, but the rigid cage structure of the precursor ligand formed by a pair of intramolecular N–H···N H-bonds in the solid state was not maintained in this case upon

complexation unlike in the case of the ruthenium(II), rhodium(III) and palladium(II) complexes. There was evidence of intermolecular H-bonding involving the Au(I)PCl cations and the Cl^- counterions. The X-ray diffraction analysis revealed that the Au···Au distance between neighbouring molecules was 4.10 Å. Aurophilic Au···Au interactions with bond lengths of *ca.* 3.0 Å commonly observed crystallographically for Au(I) compounds with sterically undemanding ligands that usually link Au^+ species together were not observed in this Au(I) complex.

Two zeolite types, Zeolite-A (**235**) and permanganate sodalite (**236**) were also prepared according to published procedures,[251,252] and characterised by powder X-ray diffraction. The experimental diffraction pattern in each case was in excellent agreement with the expected.

6.1 FURTHER WORK

Further work should be directed towards optimising the catalytic potential of the new diazaphosphorinane ligands whose catalytic abilities were demonstrated in a ruthenium-based ester hydrogenation of dimethyloxalate to methylglycolate. The preparation of tertiary phosphines of the type $P(CH_2NHR)_3$, where R is phenyl or phenyl substituent by bubbling NH_3 into solutions of the aniline derivatives of THPC prepared using the procedure first published by Frank *et al.*[10] could also be looked into as potential new class of tertiary phosphine ligands.

The tertiary phosphine ammonium salts synthesised in this work are structurally related to the well-known water-soluble PTA ligand as confirmed by single crystal X-crystallography, but were found to be insoluble in water. They have also been shown to have similar stereoelectronic properties with PTA. The renewed interest in PTA is due to its high solubility in water which together with its derivatives has had numerous applications in medicine, coordination and organometallic chemistry and catalysis especially in aqueous media. Therefore further studies should also be directed towards understanding the properties of the tertiary phosphine ammonium salts in aqueous and organic media. They could be made water soluble by attaching highly polar functional groups such as $-SO_3^-$, $-CO_2^-$, –OH etc and their coordination chemistry as well as potential medicinal and catalytic applications of their transition metal complexes explored. As mentioned in Section 4.1.1, water-soluble ruthenium(II) complexes including $RuCl_2(p^6$-

cymene)(PTA) **45**, were used as homogeneous catalysts in the hydrogenation of benzene and other arenes under aqueous-organic biphasic conditions.[128] The analogous ruthenium(II) complexes synthesised in this work such as **199** and **200** discussed in Section 3.3.1 shown to be structurally and stereoelectronically related to **45** could function as similar water-soluble catalysts if made water soluble by attachment of appropriate polar functional groups.

Water-soluble iridium(III) complexes including η^5-Cp*Ir(PTA)Cl_2 have also been evaluated as catalyst precursors for the hydrogenation of CO_2 and hydrogen carbonate in aqueous solutions under relatively mild conditions.[211] The analogous iridium(III) complexes synthesised such as η^5-Cp*$IrCl_2$(**181**) shown to have similar stereoelectronic properties to the analogous PTA complex could be evaluated as hydrogenation catalysts if made water-soluble by the attachment of highly polar functional groups grafted into the precursor ligands in the complexes.

Similarly, the water-soluble monomeric palladium(II) PTA complex **75** together with $Pd(OAc)_2$/PTA has been shown to be an efficient copper- and amine-free Sonogashira catalyst system.[143] Analogous monomeric cyclometallated Pd(II) complexes **218–221** were synthesised in this work from the tertiary phosphine ammonium salts and cyclometallated Pd dimers $[Pd(C\sim N)(\mu\text{-}Cl)]_2$, where (C~N = $C_9H_{12}N$ or $C_{12}H_{12}N$). For example, **218** or **220** shown to be structurally related to **75** and having similar stereoelectronic properties to **75** could be evaluated as similar Sonogashira catalysts if made water soluble by the attachment of highly polar functional groups to the precursor ligands in the complexes.

The new interest in PTA apart from its coordination chemistry and utility as a ligand in catalysis, has been due to reports that ruthenium complexes of PTA have displayed anticancer properties.[104] Dyson and co-workers have shown that the water-soluble complex $RuCl_2(p^6$-cymene)(PTA) **45**, exhibits pH dependent DNA damage; the pH at which damage is greatest correlates to the pH environment of cancer cells.[110] The molecular structure of this complex determined by single crystal X-ray diffraction was very similar to the structures of the ruthenium(II) complexes **199** and **200** synthesised in this work. Therefore further work should also be directed towards obtaining water soluble derivatives of these new ruthenium(II) complexes followed by the evaluation of their anticancer properties.

The water-soluble rhodium(III)PTA complex $RhCl_2(\eta^5\text{-}Cp^*)(PTA)$ together with the osmium RAPTA analogue have demonstrated very similar cytotoxicity profiles to the ruthenium(II) complex **45**. The X-ray structure of $RhCl_2(\eta^5\text{-}Cp^*)(PTA)$ has been determined[51] and the Rh–P and Rh–Cl bond lengths as well as the P–Rh–Cl bond angles are comparable to those of the analogous rhodium(III) complex **207** synthesised in this work. As in the case of the ruthenium(II) complexes therefore further work should also be directed towards obtaining water soluble derivatives of the rhodium(III) complexes followed by the evaluation of their anticancer properties.

Lastly, the mechanistic aspects of the reactions that led to the interesting novel crystal structures of the palladium(II) complexes **211′** and **222′** as well as the platinum(II) complex **223′** obtained in this work could also be critically examined.

7.0 REFERENCES

1. G. O. Spessard and G. L. Miessler, *Organometallic Chemistry*, Prentice-Hall, New Jersey, 1997.
2. M. J. Clarke, *Coord. Chem. Rev.*, 2003, **236**, 209.
3. R. H. Crabtree, *The Organometallic Chemistry of the Transition Metals*, 3rd Edn., John Wiley and Sons, Inc., 2001.
4. P. T. Anastas and M. M. Kirchhoff, *Acc. Chem. Res.*, 2002, **35**, 686.
5. D. Duraczynska, E. M. Serwicka, A. Waksmundzka-Gora, A. Drelinkiewicz and Z. Olejniczak, *J. Organomet. Chem.*, 2008, **693**, 510.
6. D. E. C. Corbridge, *Phosphorus: An Outline of its Chemistry, Biochemistry and Technology*, Elsevier, 1978.
7. G. V. Rao and G. C. Reddy, *Tetrahedron Lett.*, 2008, **49**, 824.
8. J. Uziel, N. Riegel, B. Aka, P. Figuiè and S. Jugé, *Tetrahedron Lett.*, 1997, **38**, 3405.
9. M. J. Winter, *d-Block Chemistry*, Oxford University Press, 1999.
10. A. W. Frank and G. L. Drake Jr., *J. Org. Chem.*, 1972, **37**, 2752.
11. A. W. Frank and G. L. Drake Jr., *J. Org. Chem.*, 1977, **42**, 4125.
12. G. N. Nikonov, A. A. Karasik, E. V. Malova and K. M. Enikkeev, *Heteroatom Chem.* 1992, **4**, 439.
13. V. A. Zagumennov, A. A. Karasik, E. V. Nikitin and G. N. Nikonov, *Russ. Chem. Bull.*, 1997, **46**, 1154.
14. M. T. Reetz, G. Lohmer and R. Schwickardi, *Angew. Chem. Int. Ed.*, 1998, **37**, 481.
15. A. Tewari, M. Hein, A. Zapf and M. Belle, *Tetrahedron*, 2005, **61**, 9705.
16. Y. Abe, K. Kude, S. Hayase, M. Kawatsura, K. Tsunashima and T.Itoh, *J. Mol. Catal. B: Enzym.* 2008, **51**, 81.
17. M-C. Tseng, H-C. Kan and Y-H. Chu, *Tetrahedron Lett.*, 2007, **48**, 9085.
18. P. Ludley and N. Karodia, *Tetrahedron Lett.*, 2001, **42**, 2011.
19. D. A. Gerritsma, A. Robertson, J. McNulty and A. Capretta, *Tetrahedron Lett.*, 2004, **45**, 7629.
20. N. Karodia, S. Guise, C. Newlands and J. Anderson, *Chem. Commun.*,1998, 2341.
21. C. Comyns, N. Karodia, S. Zeler and J. Anderson, *J. Catal. Lett.*, 2000, **67**, 113.

22. C. L. Johnson, R. E. Donkor, W. Nawaz and N. Karodia, *Tetrahedron Lett.*, 2004, **45**, 7359.

23. F. Stazi, D. Marcoux, J-C. Popon, D. Latassa and A. B. Charette, *Angew Chem., Int. Ed.*, 2007, **46**, 5011.

24. A. Kanazawa and T. Ikeda, *Coord. Chem. Rev.*, 2000, **198**, 117.

25. W. Xie, Y. Ye, A. Shen, L. Zhou, Z. Lou, X. Wang and J. Hu, *Vib. Spectrosc.*, 2008, **47**, 119.

26. E. J. Delikatny, W. A. Cooper, S. Brammah, N. Sathasivam and D. C. Rideout, *Cancer Res.*, 2002, **62**, 1394.

27. W. A. Cooper, W. A. Bartier, D. C. Rideout and E. J. Delikatny, *Mag. Reson. Med.*, 2001, **45**, 1001.

28. F. Ouenadio, N. Walchshofer, C. Trentesaux, R. Barret and J. Paris, *Anti-Cancer Drugs*, 2001, **12**, 603.

29. X. Wang and S-K. Tian, *Tetrahedron Lett.*, 2007, **48**, 6010.

30. A. Hamdi, K. C. Nam, B. J. Ryu, J. S. Kim and J. Vicens, *Tetrahedron Lett.*, 2004, **45**, 4689.

31. H. M. Yeo, B. J. Ryu and K. C. Nam, *Org. Lett.*, 2008, **10**, 2931.

32. D. J. Daigle in: M. Y. Darensbourg (Ed.), *Inorg. Synth.*, 1988, **32**, 40.

33. D. Moiseev, B. R. James, B. O. Patrick and T. Q. Hu, *Inorg. Chem.*, 2006, **45**, 2917.

34. A. D. Philips, L. Gonsalvi, A. Romerosa, F. Vizza and M. Peruzzini, *Coord. Chem. Rev.*, 2004, **248**, 955.

35. J. W. Ellis, K. N. Harrison, P. A. T. Hoye, A. G. Orpen, P. G. Pringle and M. B. Smith, *Inorg. Chem.*, 1992, **31**, 3026.

36. J. C. Jeffery, B. Odell, N. Stevens and R. E. Talbot, *Chem. Commun.*, 2000, 101.

37. C. A. McAulife, *Comprehensive Coordination Chemistry,* G.Wilkinson, R. D. Gillard and J. A. McCleverty Eds., Pergamon Press, Oxford, UK, 1987, Vol. 2, pp 89–1066.

38. D. G. Gilheany and C. M. Mitchell, *The Chemistry of Organophosphorus Compounds,* F. R. Hartley, Ed., Wiley, New York, 1990, Vol. 1, pp 150–190 and references therein.

39. L. D. Quin, *A Guide to Organophosphorus Chemistry,* New York, 2000.

40. G. W. Parshall, *Homogeneous Catalysis*: *The Application and Chemistry of Catalysis by Soluble Transition Metal Complexes.* Wiley New York, 1980.

41. I. Ojima (Ed.), *Catalytic Asymmetric Synthesis*, Verlag VCH, Weinheim, 1993.
42. R. Noyori, *Asymmetric Catalysis in Organic Synthesis*, John Wiley, New York, 1994.
43. C. A. Tolman, *Chem. Rev.*, 1977, **77**, 313.
44. D. Michoss, X. L. Luo, J. A. K. Howard and R. H. Crabtree, *Inorg. Chem.*, 1992, **31**, 3914.
45. A. C. Cooper, W. E. Streib, O. Eisenstein and K. G. Caulton, *J. Am. Chem. Soc.*, 1997, **119**, 9069.
46. A. S. C. Chan, C. C. Chen, R. Cao, M. R. Lee, S. M. Peng and G. H. Lee, *Organometallics*, 1997, **16**, 3469.
47. A. Buhling, P. C. J. Kamer, P. W. N. M. van Leeuwen and J. W. Elgersma, *J. Mol. Catal. A: Chemical*, 1995, **98**, 69.
48. A. Buhling, P. C. J. Kamer, P. W. N. M. van Leeuwen and J. W. Elgersma, *J. Mol. Catal. A: Chemical*, 1997, **116**, 297.
49. M. Tanaka, T. Hayashi and I. Ogata, *Bull. Chem. Soc., Japan*, 1997, **50**, 2351.
50. W. Geortz, W. Keim, D. Vogt, U. Englert, M. D. K. Boele, L. A. van der Veen, P. C. J. Kamer and P. W. N. M. van Leeuwen, *J. Chem. Soc. Dalton Trans.*, 1998, 2981.
51. A. Dorcier, W. H. Ang, S. Balano, L. Gonsalvi, L. Juillerat-Jeannerat, G. Laurenczy, M. Peruzzini, A. D. Phillips, F. Zanobini and P. J. Dyson, *Organometallics*, 2006, **25**, 4090.
52. Y. K. Yan, M. Melchart, A. Habtermariam and P. J. Sadler, *Chem. Commun.*, 2005, 4764.
53. D. J. Daigle, A. B. Pepperman Jr. and S. L. Vail, *J. Heterocycl. Chem.*, 1974, **11**, 407.
54. B. Dutta, C. Scolaro, R. Scopelliti, P. J. Dyson and K. Severin, *Organometallics*, 2008, **27**, 1355.
55. T. Brenstrum, J. Clattenburg, J. Britten, S. Zavorine, J. Dyck, A. J. Robertson, J. McNulty and A. Capretta, *Org. Lett.*, 2006, **8**, 103.
56. J. McNulty and Y. Zhou, *Tetrahedron Lett.*, 2004, **45**, 407.
57. N. E. Leadbeater and M. Marco, *Chem. Rev.*, 2002, **102**, 3217.
58. M. Benaglia, A. Puglisi and F. Cozzi, *Chem. Rev.*, 2003, **103**, 3401.
59. H. Han and S. A. Johnson, *Organometallics*, 2006, **25**, 5594.

60. B. Bosnich, *Inorg. Chem.*, 1999, **38**, 2554.

61. H. Suzuki, *Eur. J. Inorg. Chem.*, 2002, 1009.

62. E. Y. Fung, M. M. Olmstead, J. C. Vickery and A. L. Balch, *Coord. Chem., Rev.*, 1998, **171**, 151.

63. R. D. Cannon and R. P. White, *Prog. Inorg. Chem.*, 1998, **36**, 195.

64. B. Cage, F. A. Cotton, N. S. Dalal, E. A. Hillard, B. Rakvin and C. M. Ramsey, *J. Am. Chem. Soc.*, 2003, **125**, 5270.

65. J. F. Berry, F. A. Cotton, C. Y. Liu, T. Lu, C. A. Murillo, B. S. Tsukerblat, D. Villagran and X. Wang, *J. Am. Chem. Soc.*, 2005, **127**, 4895.

66. J. Yoon, L. M. Mirica, T. P. D. Stack and E. I. Solomon, *J. Am. Chem. Soc.*, 2004, **126**, 12586.

67. S. G. Telfa, R. Kuroda, J. Lefebvre and D. B. Leznoff, *Inorg. Chem.*, 2006, **45**, 4592.

68. P. W. Anderson, *Science*, 1987, **235**, 1196.

69. H. B. Gray and B. G. Malmstroem, *Biochemistry*, 1989, **28**, 7499.

70. A. Messerschmidt, R. Huber, K. Wieghardt and T. Poulos, *Handbook of Metalloproteins, Volume 1*; Wiley, New York, 2001.

71. J. A. Hatnean, R. Raturi, J. Lefebvre, D. B. Leznoff, G. Lawes and S. A. Johnson, *J. Am. Chem. Soc.*, 2006, **128**, 14992.

72. A. L. Keen, M. Duster, H. Han and S. A. Johnson, *Chem. Commun.*, 2006, 1221.

73. H. Han, M. Elsmaili and S. A. Johnson, *Inorg. Chem.*, 2006, **45**, 7435.

74. L. H. Gade, *Acc. Chem. Res.*, 2002, **35**, 575.

75. L. H. Gade, *J. Organomet. Chem.*, 2002, **661**, 85.

76. L. Jia, E. Ding, A. L. Rheingold and B. Rhatigan, *Organometallics*, 2000, **19**, 963.

77. B. Cornils and W. A. Herrmann, *Aqueos-Phase Organometallic Catalysis Concepts and Applications*, Wiley-VCH, Weinhein, 1998.

78. F. Joo, *Aqueous Organometallic Catalysis*, Kluver Academic Publishers, Dordrecht, 2001.

79. W. A. Herrmann and C. W. Kholpainter, *Angew. Chem. Int. Ed. Engl.*, 1993, **32**, 1524.

80. P. Kalck and A. Monteil, *Adv. Organomet. Chem.*, 1992, **34**, 219.

81. E. G. Kuntz, *CHEMTECH.*, 1987, **17**, 570.

82. J. C. Bailar, *Catal. Rev.*, 1974, **10**, 17.

83. W. H. Lang, A. T. Jurewicz, W. O. Haag, D. D. Whitehurst and L. D. Rollman, *J. Organomet. Chem.*, 1977, **85**, 134.

84. N. Pinault and D. W. Bruce, *Coord. Chem. Rev.*, 2003, **241**, 1.

85. D. V. Moiseev, B. R. James and T. Q. Hu, *Inorg. Chem.*, 2006, **45**, 10338

86. D. V. Moiseev, B. R. James and T. Q. Hu, *Inorg. Chem.*, 2007, **46**, 4704.

87. T. Q. Hu, B. R. James, D. Yawalata and M. B. Ezhova, *J. Pulp Pap. Sci.*, 2004, **30**, 233.

88. D. S. Bharathi, M. A. Sridhar, J. S. Prasad and A. G. Samuelson, *Inorg. Chem. Commun.*, 2001, **4**, 490.

89. F. Lorenzini, B. O. Patrick and B. R. James, *Dalton Trans.*, 2007, 3224.

90. A. García-Fernáandez, J. Díez, Á. Manteca, J. Sánchez, M. P. Gamasa and E. Lastra, *Polyhedron*, 2008, **27**, 1214.

91. J. G. Verkade, *Coord. Chem. Rev.*, 1994, **137**, 233.

92. S. Bolaño, A. Albinati, J. Bravo, L. Gonsalvi and M. Peruzizini, *Inorg. Chem. Commun.*, 2006, **9**, 360.

93. B. J. Frost, C. M. Bautista. R. Huang and J. Shearer, *Inorg. Chem.*, 2006, **45**, 3481.

94. D. J. Darensbourg, C. G. Ortiz and J. W. Kamplain, *Organometallics*, 2004, **23**, 1747.

95. D. A. Krogstad, G. S. Ellis, A. K. Gunderson, A. J. Hammrich, J. W. Rudolf and J. A. Halfen, *Polyhedron*, 2007, **26**, 4093.

96. P. Smolenski, F. P. Pruchnik, Z. Ciunik and T. Lis, *Inorg. Chem.*, 2003, **42**, 3318.

97. J. Navech, R. Kraimer and J. P. Majoral, *Tetrahedron Lett.*, 1980, **21**, 1449.

98. D. J. Darensbourg, J. C. Yarbrough and S. J. Lewis, *Organometallics*, 2003, **22**, 2050.

99. B. Assmann, K. Angermaier and H. Schmidbaur, *J. Chem. Soc., Chem. Commun.*, 1994, 941.

100. A. D. Philips, S. Bolaño, S. S. Bosquain, J.-C. Daran, R. Malacea, R. Peruzzini, R. Poli and L. Gonsalvi, *Organometallics*, 2006, **25**, 2189.

101. A. Mena-Cruz, P. Lorenzu- Luis, A. Romerosa, M. Saoud and M. Serrano-Ruiz, *Inorg. Chem.*, 2007, **46**, 6120.

102. M. Erlandsson, L. Gonsalvi, A. Ienco and M. Peruzzini, *Inorg. Chem.*, 2008, **47**, 8.

103. G. W. Wong, J. L. Harkreader, C. A. Mebi and B. J. Frost, *Inorg. Chem.*, 2006, **45**, 6748.

104. G. W. Wong, W-C. Lee and B. J. Frost, *Inorg. Chem.*, 2008, **47**, 612.

105. D. J. Darensbourg, F. Joo, M. Kannisto, A. Katho, J. H. Reibenspies and D. J. Daigle, *Inorg. Chem.*, 1994, **33**, 200.

106. D. J. Darensbourg, N. W. Stafford, F. Joo and J. H. Reibenspies, *J. Organomet. Chem.*, 1996, **448**, 99.

107. D. M. Saysell, C. D. Borman, C. H. Kwak and A. G. Sykes, *Inorg. Chem.*, 1996, **35**, 173.

108. B. E. Schultz, R. Hille and R. H. Holm, *J. Am. Chem. Soc.*, 1995, **117**, 827.

109. W. H. Ang, E. Daldini, C. Scolaro, R. Scopelliti, L. Juillerat-Jeannerat and P. J. Dyson, *Inorg. Chem.*, 2006, **45**, 9006.

110. C. S. Allardyce, P. J. Dyson, D. J. Ellis, S. L. Heath, *Chem. Commun.*, 2001, 1396.

111. C. Scolaro, A. Bergamo, L. Brescacin, R. Delfino, M. Cocchietto, G. Laurenczy, T. J. Geldbach, G. Sava and P. J. Dyson, *J. Med. Chem.*, 2005, **48**, 4161.

112. A. Dorcier, C. G. Hartinger, R. Scopelliti, R. H. Fish, B. K. Keppler and P. J. Dyson, *J. Inorg. Biochem.*, 2008, **102**, 1066.

113. D. N. Akbayeva, L. Gonsalvi, W. Oberhuser, M. Peruzzini, F. Vizza, P. Brueggeller, A. Romerosa, G. Sava and A. Bergamo, *Chem. Commun.*, 2003, 264.

114. S. Bolaño, L. Gonsalvi, F. Zanobini, F. Vizza, V. Bertolasi, A. Romerosa and M. Peruzzini, *J. Mol Catal. A*, 2004, **224**, 61.

115. B. J. Frost and C. A. Mebi, *Organometallics*, 2004, **23**, 5317.

116. Z. Assefa, B. G. McBurnett, R. J. Staples, J. P. Fackler, B. Assman, K. Angermaier and H. Schmidbaur, *Inorg. Chem.*, 1995, **34**, 2490.

117. Z. Assefa, B. G. McBurnett, R. J. Staples, J. P. Fackler and P. John, *Inorg. Chem.*, 1995, **34**, 4965.

118. J. M. Forward, D. Bohmann, J. P. Fackler and R. J. Staples, *Inorg. Chem.*, 1995, **34**, 6330.

119. C. Scolaro, A. B. Chaplin, C. G. Hartinger, A. Bergamo, M. Cocchietto, B. K. Keppler, G. Sava and P. J. Dyson, *Dalton Trans.*, 2007, 5065.

120. W. H. Ang, E. Daldini, L. Juillerat-Jeannerat and P. J. Dyson, *Inorg. Chem.*, 2007, **46**, 9048.

121. S. Bolaño, G. Ciancaleoni, J. Bravo, L. Gonsalvi, A. Macchioni and M. Peruzzini, *Organometallics*, 2008, **27**, 1649.

122. C. Lidrissi, A. Romerosa, M. Saoud, M. Serrano-Ruiz, L. Gonsalvi and M. Peruzzini, *Angew. Chem. Int. Ed.*, 2005, **44**, 2568.

123. F. Mohr, L. R. Falvello and M. Laguna, *Eur. J. Inorg. Chem.*, 2006, 3152.

124. H. Z. Sun, H. Y. Li and P. J. Sadler, *Chem. Rev.*, 1999, **99**, 2817 and the references therein.

125. C. S. Allardyce, P. J. Dyson, D. J. Ellis, P. A. Salter and R. Scopelliti, *J. Organomet. Chem.*, 2003, **668**, 35.

126. R. A. Sanchez-Delgado, M. Navarro, H. Perez and J. A. Urbina, *J. Med. Chem.*, 1996, **39**, 1095.

127. D. J. Darensbourg, F. Joo, M. Kannisto, A. Katho and J. H. Reibenspies, *Organometallics*, 1992, **11**, 1990.

128. P. J. Dyson, D. J. Ellis and G. Laurenczy, *Adv. Synth. Catal.*, 2003, **345**, 211.

129. L. Laurenczy, F. Joò and L. Ndasdi, Inorg. *Chem., 2000*, **39**, 5083.

130. N. Katsaros and A. Anagnostopoulou, *Crit. Rev. Oncol. Hematol.*, 2002, **42**, 297.

131. L. Nádasdi and F. Joó, *Inorg. Chim. Acta*, 1999, **293**, 218.

132. F. P. Pruchnik, P. Smoleński, E. Gałdecka and Z. Gałdecki, *New J. Chem.*, 1998, 1395.

133. P. Smoleński, C. Dinoi, M. F. C. Guedes da Silva and A. J. L. Pombeiro, *J. Organomet. Chem.*, 2008, **693**, 2338.

134. W. Kläui, D. Schramm, W. Peters, G. Rheinwald and H. Lang, *Eur. J. Inorg. Chem.*, 2001, 1415.

135. F. P. Pruchnik and P. Smoleński, *App. Organometal. Chem.*, 1999, **13**, 829.

136. F. P. Pruchnik, P. Smoleński and K. Wajda-Hermanowicz, *J. Organomet. Chem.*, 1998, **570**, 63.

137. F. P. Pruchnik, P. Smoleński, E. Gałdecka and Z. S. Gałdecki, *Inorg. Chim. Acta*, 1999, **293**, 110.

138. S. Bolaño, A. Albinati, J. Bravo, M. Caporali, L. Gonsalvi, L. Male, M. M. Rodríguez-Rocha, A. Rossin and M. Peruzzini, *J. Organomet. Chem.*, 2008, **693**, 2397.

139. D. A. Krogstad, J. A. Halfen, T. J. Ferry and V. G. Young, Jr., *Inorg. Chem.*, 2001, **40**, 463.

140. D. A. Krogstad, A. J. DeBoer, W. J. Ortmeier, J. W. Rudolf and J. A. Halfen, *Inorg. Chem. Commun.*, 2005, **8**, 1141.

141. D. J. Darensbourg, F. A. Beckford and J. H. Reibenspies, *J. Cluster Sci.*, 2000, **11**, 95.

142. D. J. Darensbourg, C. G. Ortiz and J. C. Yarbrough, *Inorg. Chem.*, 2003, **42**, 6915.

143. J. Ruiz, N. Cutillas, F. López, G. López and D. Bauststa, *Organometallics*, 2006, **25**, 5768.

144. G. Abjabeng, T. Brenstrum, C. Frampton, A. J. Robertson, J. Hilhouse, J. McNulty and A. J. Capretta, *J. Org. Chem.*, 2004, **69**, 5082.

145. E. C. Alyea, G. Ferguson and S. Kannan, *Polyhedron*, 1998, **17**, 2727.

146. D. J. Darensbourg, T. J. Decuir, N. W. Stafford, J. B. Robertson, J. D. Draper, J. H. Reibenspies, A. Kathó and F. Joó, *Inorg. Chem.*, 1997, **36**, 4218.

147. D. J. Darensbourg, J. B. Robertson, D. L. Larkins and J. H. Reibenspies, *Inorg. Chem.*, 1999, **38**, 2473.

148. E. C. Alyea, G. Ferguson and S. Kannan, *Polyhedron*, 1998, **17** 2231.

149. D. M. Saysell, G. J. Lamprecht, J. Darkwa and A. G. Sykes, *Inorg. Chem.*, 1996, **35**, 5531.

150. S. Otto, A. Roodt and W. Purcell, *Inorg. Chem. Commun.*, 1998, **1**, 415.

151. S. Otto and A. Roodt, *Inorg. Chem. Commun.*, 2001, **4**, 49.

152. S. Otto and A. Roodt, *Acta Crystallogr. C: Cryst. Struct. Commun.*, 2001, 540.

153. Z. Assefa, B. G. McBurnett, R. J. Staples and J. P. Fackler, *Acta Cryst.* 1995, **51C**, 1742.

154. L. J. McCaffrey, W. Henderson, B. K. Nicholson, J. E. Mackay and M. B. Dinger, *J. Chem. Soc., Dalton Trans.*, 1997, 2731.

155. U. Bierbach, Y. Qu, T. W. Hambley, J. Peroutka, H. L. Nguyen, M. Doedee and N. Farrel, *Inorg. Chem.*, 1999, **38**, 3535.

156. E. I. Montero, S. Diaz, A. M. González-Vadillo, J. M. Pérez, C. Alonso and C. Navarro-Ranninger, *J. Med. Chem.*,1999, **42**, 4264.

157. M. Coluccia, A. Nassi, A. Boccarelli, D. Giordano, N. Cardellicchio, D. Locker, M. Leng, M. Sivo, F. P. Intini and G. Natile, *Inorg. Biochem.*, 1999, **77**, 31.

158. U. Bierbach, M. Sabat and N. Farrel, *Inorg. Chem.*, 2000, **39**, 1882.

159. S. Miranda, E. Vergara, F. Mohr, D. de Vos, E. Cerrada, A. Mendía and M. Laguna, *Inorg. Chem.*, 2008, **47**, 5641.

160. A. Habtemariam, J. A. Parkinson, N. Margiotta, T. W. Hambley and S. P. J. Parsons, *J. Chem. Soc., Dalton Trans.*, 2001, **36**, 2.

161. N. Margiotta, A. Habtemariam and P. J. Sadler, *Angew. Chem., Int. Ed. Engl.*, 1997, **36**, 1185.

162. A. Habtemariam and P. J. Sadler, *Chem. Commun.*, 1996, 1785.

163. A. Romerosa, P. Bergamini, V. Bertolasi, A. Canella, M. Cattabriga, R. Gavioli, S. Mañas, N. Mantovani and L. Pellacani, *Inorg. Chem.*, 2004, **43**, 905.

164. P. Bergamini, V. Bertolasi, L. Marvelli, A. Canella, R. Gavioli, N. Mantovani, S. Mañas and A. Romerosa, *Inorg. Chem.*, 2007, **46**, 4267.

165. W. Henderson, L. J. McCaffrey and B. K. Nicholson, *J. Chem. Soc., Dalton Trans.*, 2000, 2753.

166. K. Angermaier, E. Zeller and H. Schmidbaur, *J. Organomet. Chem.*, 1994, **472**, 371.

167. E. Vergara, S. Miranda, F. Mohr, E. Cerrada, E. R. T. Tiekink, P. Romero, A. Mendía and M. Laguna, *Eur. J. Inorg. Chem.*, 2007, 2926.

168. Z. Assefa, B. G. McBurnett, R. J. Staples, J. P. Fackler Jr., B. Assmann, K. Angermaier and H. Schmidbaur, *Inorg. Chem.*, 1995, **34**, 75.

169. Z. Assefa, M. A. Omary, B. G. McBurnett, A. A. Mohamed, H. H. Patterson, R. J. Staples and J. P. Fackler, *Inorg. Chem.*, 2002, **41**, 6274.

170. Z. Assefa, J. M. Forward, T. A. Grant, R. J. Staples, B. E. Hanson, A. A. Mohamed and J. P. Fackler, *Inorg. Chim. Acta*, 2003, **352**, 31.

171. Z. Assefa, R. J. Staples and J. P. Fackler, *Acta Crystallogr.*, 1996, **C52**, 305.

172. J. M. Forward, R. J. Staples, C. W. Liu and J. P. Fackler, *Acta Crystallogr.*, 1997, **C53**, 195.

173. J. M. Forward, Z. Assefa, R. J. Staples and J. P. Fackler Jr., *Inorg. Chem.*, 1996, **35**, 16.

174. J. M. Forward, J. P. Fackler Jr. and R. J. Staples, *Organometallics*, 1995, **14**, 4194.

175. J. M. Forward, D. Bohmann, J. P. Fackler Jr. and R. J. Staples, *Inorg. Chem.*, 1995, **34**, 6330.

176. W. Lu, H. F. Xiang, N. Zhu and C. M. Che, *Organometallics*, 2002, **21**, 2343.

177. K. L. Cheung, S. K. Yip and V. W. W. Yam, *J. Organomet. Chem.*, 2004, **689**, 4451.

178. M. P. Cifuentes and M. A. Humphrey, *J. Organomet. Chem.*, 2004, **689**, 3968.

179. M. C. Irwin, J. J. Vittal and R. J. Puddephatt, *Organometallics*, 1997, **16**, 3541.

180. C. P. McArdle, M. C. Irwin, M. C. Jennings, J. J. Vittal and R. J. Puddephatt, *Chem. Eur. J.*, 2002, 723.

181. F. Mohr, M. C. Jennings and R. J. Puddephatt, *Eur. J. Inorg. Chem.*, 2003, 217.

182. F. Mohr, E. Cerrada and M. Laguna, *Organometallics*, 2006, **25**, 644.

183. A. Laguna and M. Laguna, *Coord. Chem. Rev.*, 1999, **193–195**, 837.

184. F. Mohr, S. Sanz, E. R. T. Tiekink and M. Laguna, *Organometallics*, 2006, **25**, 3084.

185. G. F. Nieckarz, T. J. R. Weakley, W. K. Miller, B. E. Miller, D. K. Lyon and D. R. Tyler, *Inorg. Chem.*, 1996, **35**, 1721.

186. J. Bruckmann and C. Kruger, *J. Organomet. Chem.*, 1997, **536**, 465.

187. R. Kalio, P. Lönnecke and E. Hey-Hawkins, *J. Organomet. Chem.*, 2008, **693**, 590.

188. G. A. Geoffrey, *An Introduction to Hydrogen bonding*; Oxford University Press, Oxford, UK, 1997.

189. F. Hibbert and J. Emsley, *Adv. Phys. Org. Chem.*, 1990, **26**, 255.

190. D. H. Williams and I. Fleming, *Spectroscopic Methods in Organic Chemistry*, 5th Ed., The McGraw-Hill Publishing Company, 1995.

191. A. H. Allen, *Acta Cryst.* 2002, **B58**, 380.

192. Chemical Database Service, *J. Chem. Inf. Comput. Sc.*, 1996, **36**, 746.

193. J. D. Dunitz and R. Taylor, *Chem. Eur. J.*, 1997, **3**, 89.

194. S. E. Dann, S. E. Durran, M. R. J. Elsegood, M. B. Smith, P. M. Staniland, S. Talib and S. H. Dale, *J. Organomet. Chem.*, 2006, **691**, 4829.

195. J. J. Daley, *J. Chem Soc. Chem. Commun.*, 1964, 3799.

196. S. K. Singh, M. Trevedi, M. Chandra and D. S. Pandey, *J. Organomet. Chem.*, 2005, **690**, 647.

197. P. Lalrempuia, P. J. Carroll and M. R. Kollipara, *J. Chem. Sci.*, 2004, **116**, 21.

198. A. Dorcier, P. J. Dyson, C. Gossens, U. Rothlisberger, R. Scopelliti and I. Tavernelli, *Organometallics*, 2005, **24**, 2114.

199. J. Čemák, J. Žádný, A. Krupková, K. Lopatová, A. Vlachová, T.H.N. Thi, J. Šauliová, J. Sýkora and I. Císařová, *J. Organomet. Chem.*, 2007, **692**, 1557.

200. S. J. Coles, S. E. Durran, M. B. Hursthouse, A. M. Z. Slawin and M. B. Smith, *New J. Chem.*, 2001, **25**, 416.

201. S. E. Durran, M. B. Smith, S. H. Dale, S. J. Coles, M. B. Hursthouse and M. E. Light, *Inorg. Chim. Acta*, 2006, **359**, 2980.

202. H.-P. Chen, Y.-H Liu, S.-M. Peng and S.-T. Liu, *Organometallics*, 2003, **22**, 4893.

203. D. L. Davies, J. Neild, L. J. S. Prouse and D. R. Russell, *Polyhedron*, 1993, **12**, 2121.

204. K. H. Jogun, J. J. Stezowski, E. Fluck and J. Weidlein, *Phosphorus Sulfur Relat. Elem.*, 1978, **4**, 199.

205. R. E. Marsh, M. Kapon, S. Hu and F. H. Herbstein, *Acta Crystallogr., Sect. B: Struct. Sci.*, 2002, **58**, 62.

206. N. N. Greenwood and A. Earnshaw, *Chemistry of the Elements*, 2nd Edition, Butterworth-Heinemann, 2001.

207. G. Sánchez, J. García, J. J. Ayllón, J. L. Serrano, L. García, J. Pérez and L. López, *Polyhedron*, 2007, **26**, 2911.

208 P. Govindaswamy, Y.A. Mozharivskyj and M. R. Kollipara, *Polyhedron*, 2004, **23**, 3115.

209. F. P. Pruchnik, P. Smoleński and I. Raska, *Polish J. Chem.*, 1995, **69**, 5.

210. R. Huang and B. J.Frost, *Inorg. Chem.*, 2007, **46**, 10962.

211. M. Erlandsson, V. R. Landaeta, L. Gonsalvi, M. Peruzzini, A. D. Philips, P. J. Dyson and G. Laurenczy, *Eur. J. Inorg. Chem.*, 2008, 620.

212. J. Ruiz, N. Cutillas, V. Rodriguez, J. Sampedro, G. López, P. A. Chaloner and P. Hitchcock, *J. Chem. Soc., Dalton Trans.*, 1999, 2939.

213. R. B. Bedford, C. S. J. Cazin, S. J. Coles, T. Gelbrich, P. N. Horton, M. B. Hursthouse and M. E. Light, *Organometallics*, 2003, **22**, 987.

214. J. Vicente, A. Arcas, D. Bautista and P. G. Jones, *Organometallics*, 1997, **16**, 2127.

215. Z.-W. Xi, N. Zhou, Y. Sun and K.-L. Li, *Science*, 2001, **292**, 1139.

216. P.-D. Stevens, G.-F. Li, J.-D. Fan, M. Yen and Y. Gao, *Chem. Commun.*, 2005, 4435.

217. I.-P. Beletskaya and A.-V. Cheprakov, *Chem. Rev.*, 2000, **100**, 3009.

218. F. Alonso, I.-P. Beletskaya and M. Yus, *Tetrahedron*, 2005, **61**, 11771.

219. N.-T.-S, M.-V.-D. Sluys and C.-W. Jones, *Adv. Synth. Catal.*, 2006, **348**, 609.

220. A. Biffis, M. Zecca and M. Basato, *Eur. J. Inorg. Chem.*, 2001, 1131.

221. F.-Y. Zhao, M. Shirai, Y. Ikushima and M. Arai, *J. Mol. Catal. A Chem.*, 2002, **180**, 211.

222. F.-Y. Zhao, K. Murakami, M. Shirai and M. Arai, *J. Mol. Catal. A Chem.*, 2000, **194**, 479.

223. J.-G. de Varies, *Dalton Trans.*, 2006, 421.

224. L. Djakovitch, M. Wagner, C.-G. Hartung, M. Beller and K. Koehler, *J. Mol. Catal. A Chem.*, 2004, **219**, 121.

225. N. Ren, Y.-H. Yang, Y.-H. Zhang, Q.-R. Wang and Y. Tang, *J. Catal.*, 2007, **246**, 215.

226. C. E. Housecroft and A. G. Sharpe, *Inorganic Chemistry*, 2nd Edition, Pearson Education Limited, 2005.

227. www.undp.org/seed/eap/montreal

228. M. C. van Engelen, H. T. Teunissen, J. G. de Vries and C. J. Elsevier, *J. Mol. Catal. A: Chemical,* 2003, **206**, 185.

229. B. Boardman, M. J. Hanton, H. van Rensurg and R. P. Tooze, *Chem Commun.*, 2006, 2289.

230. R. A. Grey, G. P. Pez and A. Wallo, *J. Am. Chem. Soc.*,1981, **103**, 7536.

231. U. Matteoli, G. Menchi, M. Bianchi and F. Piacenti, *J. Mol. Catal.*, 1988, **44**, 347.

232. U. Matteoli, G. Menchi, M. Bianchi and F. Piacenti, S. Ianelli and M. Nardelli, *J. Organomet. Chem.*, 1995, **498**, 177.

233. H. T. Teunissen and C. J. Elsevier, *Chem. Commun.*, 1997, 667.

234. J. R. Ruiz, C. Jimmẽnez-Sanchidrián and M. Mora, *Tetrahedron*, 2006, **62**, 2922.

235. M. M. Dell'Anna, A. Lofũ, P. Mastrorilli, V. Mucciante and C. F. Nobile, *J. Organomet. Chem.*, 2006, **691**, 131.

236. K. R. Reddy, N. S. Kumar, P. S. Reddy, B. Sreedhar and M. L. Kantam, *J. Mol. Catal. A: Chemical,* 2006, **252**, 12.

237. L. Djakovitch, H. Heise and K. Köhler, *J. Organomet. Chem.*, 1999, **584**, 16.

238. M. Beller, H. Fisher, K. Kuhlein, C.-P. Reisinger and W.-A. Herrmann, *J. Organomet. Chem.*, 1996, **520**, 257.

239. M. T. Reetz and E. Westermann, *Angew. Chem. Ind. Ed.*, 2000, **39**, 165.

240. F.-Y. Zhao, B.-M. Bhanage, M. Shirai and M. Arai, *Chem. Eur. J.*, 2000, **6**, 843.

241. K. Köhler, R.-G. Heidenreich, J. -G. -F. Krauter and J. Pietsch, *Chem. Eur. J.*, 2002, **8**, 622.

242. M. Gruber, S. Chouzier, K. Köhler and L. Djakovitch, *Appl. Catal. A. Gen.*, 2004, **265**, 161.

243. R.-G. Heidenreich, J. -G. -F. Krauter, J. Pietsch and K. Köhler, *J. Mol. Catal. A: Chemical,* 2002, **182–183**, 449.

244. K. Egeblad, C. H. Christensen, M. Kustova and C. H. Christensen, *Chem. Mater.*, 2008, **20**, 946.

245. K. S. W. Sing, D. H. Everett, R. A. W. Haul, L. Moscou, R. A. Pierotti, J. Rouquérol and T. Siemieniewska, *Pure Appl. Chem.*, 1985, **57**, 603.

246. A. Corma, *Chem. Rev.*, 1997, **97**, 2373.

247. A. Corma, *Chem. Rev.*, 1995, **95**, 559.

248. C. Mirodatos and D. Barthomeuf, *J. Catal.*, 1985, **93**, 246.

249. C. M. Zicovich-Wilson, A. Corma and P. Viruela, *J. Phys. Chem.*, 1994, **98**, 10863.

250. B. P. Moore and J. Shen, *Nature*, 1983, **306**, 356.

251. M. T. Weller and K. E. Haworth, *J. Chem. Soc. Chem. Commun.*, 1991, 734.

252. V. I. Srdanov, W. T. A. Harrison, T. E. Gier, G. D. Stucky, A. Popitsch, K. Gatterer, D. Markgraber and H. P. Fritzer, *J. Physical Chem.*, 1994, **98**, 4673.

253. M. A. Bennett and A. K. Smith, *J. Chem., Soc., Dalton Trans.*, 1974, 233.

254. C. White, A. Yates and P. M. Maitlis, *Inorg. Synth.*, 1992, **29**, 228.

255. D. Drew and J. R. Doyle, *Inorg. Synth.*, 1997, **31**, 281.

256. R. E. Rulke, J. M. Ersting, A. L. Spek, C. J. Elsevier, P. W. N. M. Van Leeuwen and K. Vrieze, *Inorg. Chem.*, 1993, **32**, 5769.

257. A. C. Cope and E. C. Friedrich, *J. Am. Chem. Soc.*, 1968, **90**, 909.

258. G. E. Hartwell, R. V. Lawrence and M. J. Smas, *J. Chem. Soc. D: Chem. Commun.*, 1970, 912.

259. J. X. McDermott, J. F. White and G. M. Whitesides, *J. Am. Chem. Soc.*, 1976, **98**, 6521.

260. R. Uson, A. Laguna and M. Laguna, *Inorg. Synth.*, 1989, **26**, 85.

261. COLLECT: Data Collection Software, R. Hooft, B.V. Nonius, 1998.

262. APEX 2: User Manual, Bruker AXS Inc., Madison, WI, 2005.

263. DENZO, Z. Otwinowski, W. Minor, in: C. W. Carter Jr. and R. M. Sweet (Eds.), *Methods in Enzymology, Macromolecular Crystallography, part A*.vol. **276**, Academic Press, 1997, 307.

264. SAINT: Software for CCD Diffractometers, Bruker AXS Inc., Madison, WI, 2001.

265. G. M. Sheldrick, *Acta Crystallogr., Sect. A.*, 2008, **64**, 112.

266. G. M. Sheldrick, *SHELXTL user Manual*, v.6.10, Bruker AXS Inc., Madison, WI, 2001.

8.0 APPENDICES

Appendix 8.1 Crystal data and structure refinement details for **129**.

Chemical formula	$C_{28}H_{28}ClF_4N_4P$	
Formula weight	562.96	
Temperature	150(2) K	
Radiation, wavelength	MoKα, 0.71073 Å	
Crystal system, space group	monoclinic, $P2_1/c$	
Unit cell parameters	a = 13.4680(13) Å	α = 90°
	b = 13.3815(13) Å	β = 105.268(2)°
	c = 15.1511(15) Å	γ = 90°
Cell volume	2634.2(4) $Å^3$	
Z	4	
Calculated density	1.420 g/cm^3	
Absorption coefficient μ	0.260 mm^{-1}	
F(000)	1168	
Crystal colour and size	colourless, 0.48 × 0.36 × 0.31 mm^3	
Reflections for cell refinement	9044 (θ range 2.19 to 28.10°)	
Data collection method	Bruker SMART 1000 CCD diffractometer	
	ω rotation with narrow frames	
θ range for data collection	2.06 to 25.00°	
Index ranges	h −15 to 16, k −15 to 15, l −18 to 18	
Completeness to θ = 25.00°	99.9 %	
Intensity decay	0%	
Reflections collected	18579	
Independent reflections	4628 (R_{int} = 0.0239)	
Reflections with $F^2>2\sigma$	3727	
Absorption correction	semi-empirical from equivalents	
Min. and max. transmission	0.885 and 0.924	
Structure solution	direct methods	
Refinement method	Full-matrix least-squares on F^2	
Weighting parameters a, b	0.0897, 6.0358	
Data / restraints / parameters	4628 / 4 / 355	
Final R indices [$F^2>2\sigma$]	R1 = 0.0607, wR2 = 0.1622	
R indices (all data)	R1 = 0.0755, wR2 = 0.1825	
Goodness-of-fit on F^2	1.061	
Largest and mean shift/su	0.000 and 0.000	
Largest diff. peak and hole	2.090 and −0.544 e $Å^{-3}$	

Appendix 8.2 Crystal data and structure refinement details for **147.**

Chemical formula	$C_{16}H_{20}ClN_4P \cdot C_6H_4(NH_2)_2$	
Formula weight	442.92	
Temperature	120(2) K	
Radiation, wavelength	MoKα, 0.71073 Å	
Crystal system, space group	triclinic, P $\bar{1}$	
Unit cell parameters	a = 9.189 Å	α = 70.61°
	b = 9.562 Å	β = 88.33°
	c = 13.865 Å	γ = 72.23°
Cell volume	1090.7 Å^3	
Z	2	
Calculated density	1.349 g/cm^3	
Absorption coefficient μ	0.271 mm^{-1}	
F(000)	468	
Crystal colour and size	colourless, 0.15 × 0.07 × 0.05 mm^3	
Reflections for cell refinement	4747 (θ range 2.91 to 27.48°)	
Data collection method	Bruker-Nonius 95mm CCD camera on κ-goniostat	
	φ & ω scans	
θ range for data collection	2.91 to 27.55°	
Index ranges	h −11 to 11, k −12 to 12, l −17 to 18	
Completeness to θ = 26.00°	99.6 %	
Intensity decay	0%	
Reflections collected	19502	
Independent reflections	4982 (R_{int} = 0.0411)	
Reflections with $F^2>2\sigma$	4295	
Absorption correction	semi-empirical from equivalents	
Min. and max. transmission	0.609 and 0.692	
Structure solution	Patterson synthesis	
Refinement method	Full-matrix least-squares on F^2	
Weighting parameters a, b	0.0280, 0.8902	
Data / restraints / parameters	4982 / 0 / 295	
Final R indices [$F^2>2\sigma$]	R1 = 0.0414, wR2 = 0.0930	
R indices (all data)	R1 = 0.0500, wR2 = 0.0975	
Goodness-of-fit on F^2	1.031	
Largest and mean shift/su	0.000 and 0.000	
Largest diff. peak and hole	0.515 and −0.392 e Å^{-3}	

Appendix 8.3 Crystal data and structure refinement details for **156.**

Chemical formula	$C_{22}H_{21}F_3N_3P$	
Formula weight	415.39	
Temperature	150(2) K	
Radiation, wavelength	MoKα, 0.71073 Å	
Crystal system, space group	triclinic, P $\bar{1}$	
Unit cell parameters	a = 6.7500(9) Å	α = 75.378(2)°
	b = 11.7122(15) Å	β = 82.034(2)°
	c = 13.2877(17) Å	γ = 74.291(2)°
Cell volume	975.7(2) Å^3	
Z	2	
Calculated density	1.414 g/cm^3	
Absorption coefficient μ	0.182 mm^{-1}	
F(000)	432	
Crystal colour and size	colourless, 0.22 × 0.18 × 0.10 mm^3	
Reflections for cell refinement	3767 (θ range 3.14 to 28.39°)	
Data collection method	Bruker SMART 1000 CCD diffractometer	
	ω rotation with narrow frames	
θ range for data collection	1.59 to 29.03°	
Index ranges	h −9 to 8, k −15 to 15, l −17 to 17	
Completeness to θ = 26.00°	99.2 %	
Intensity decay	0%	
Reflections collected	8736	
Independent reflections	4518 (R_{int} = 0.0151)	
Reflections with $F^2>2\sigma$	3520	
Absorption correction	semi-empirical from equivalents	
Min. and max. transmission	0.961 and 0.982	
Structure solution	direct methods	
Refinement method	Full-matrix least-squares on F^2	
Weighting parameters a, b	0.0732, 0.8641	
Data / restraints / parameters	4518 / 0 / 265	
Final R indices [$F^2>2\sigma$]	R1 = 0.0496, wR2 = 0.1333	
R indices (all data)	R1 = 0.0662, wR2 = 0.1476	
Goodness-of-fit on F^2	1.028	
Largest and mean shift/su	0.000 and 0.000	
Largest diff. peak and hole	1.647 and −0.415 e Å^{-3}	

Appendix 8.4 Crystal data and structure refinement details for **166**.

Chemical formula	$C_{32}H_{36}Cl_2F_3N_3PRh \cdot 0.5CH_2Cl_2$	
Formula weight	766.88	
Temperature	150(2) K	
Radiation, wavelength	MoKα, 0.71073 Å	
Crystal system, space group	triclinic, P $\bar{1}$	
Unit cell parameters	a = 13.6390(6) Å	α = 70.7159(7)°
	b = 14.9333(7) Å	β = 70.1652(7)°
	c = 18.4072(8) Å	γ = 83.2264(8)°
Cell volume	3328.7(3) Å^3	
Z	4	
Calculated density	1.530 g/cm^3	
Absorption coefficient μ	0.846 mm^{-1}	
F(000)	1564	
Crystal colour and size	orange, 0.19 × 0.12 × 0.09 mm^3	
Reflections for cell refinement	6504 (θ range 2.30 to 27.18°)	
Data collection method	Bruker APEX 2 CCD diffractometer	
	ω rotation with narrow frames	
θ range for data collection	1.58 to 27.50°	
Index ranges	h −17 to 17, k −19 to 19, l −23 to 23	
Completeness to θ = 27.50°	99.5 %	
Intensity decay	0%	
Reflections collected	32691	
Independent reflections	15243 (R_{int} = 0.0411)	
Reflections with $F^2>2\sigma$	10973	
Absorption correction	semi-empirical from equivalents	
Min. and max. transmission	0.856 and 0.928	
Structure solution	Patterson synthesis	
Refinement method	Full-matrix least-squares on F^2	
Weighting parameters a, b	0.0783, 9.4428	
Data / restraints / parameters	15243 / 235 / 854	
Final R indices [$F^2>2\sigma$]	R1 = 0.0613, wR2 = 0.1552	
R indices (all data)	R1 = 0.0910, wR2 = 0.1709	
Goodness-of-fit on F^2	1.053	
Largest and mean shift/su	0.002 and 0.000	
Largest diff. peak and hole	1.971 and −1.585 e Å^{-3}	

Appendix 8.5 Crystal data and structure refinement details for **168**.

Chemical formula	$C_{32}H_{36}Cl_2F_3IrN_3P{\cdot}0.5CH_2Cl_2$	
Formula weight	856.17	
Temperature	150(2) K	
Radiation, wavelength	MoKα, 0.71073 Å	
Crystal system, space group	triclinic, P $\bar{1}$	
Unit cell parameters	a = 13.6719(3) Å	α = 71.1172(3)°
	b = 14.9948(4) Å	β = 70.6050(3)°
	c = 18.3942(5) Å	γ = 83.5070(4)°
Cell volume	3365.46(15) Å^3	
Z	4	
Calculated density	1.690 g/cm^3	
Absorption coefficient μ	4.297 mm^{-1}	
F(000)	1692	
Crystal colour and size	yellow, 0.37 × 0.21 × 0.11 mm^3	
Reflections for cell refinement	15350 (θ range 2.29 to 31.03°)	
Data collection method	Bruker APEX 2 CCD diffractometer	
	ω rotation with narrow frames	
θ range for data collection	1.23 to 31.53°	
Index ranges	h −19 to 19, k −21 to 21, l −27 to 26	
Completeness to θ = 24.00°	99.9 %	
Intensity decay	0%	
Reflections collected	40668	
Independent reflections	20664 (R_{int} = 0.0273)	
Reflections with $F^2>2\sigma$	16864	
Absorption correction	semi-empirical from equivalents	
Min. and max. transmission	0.287 and 0.623	
Structure solution	Patterson synthesis	
Refinement method	Full-matrix least-squares on F^2	
Weighting parameters a, b	0.0514, 4.3636	
Data / restraints / parameters	20664 / 0 / 794	
Final R indices [$F^2>2\sigma$]	R1 = 0.0356, wR2 = 0.0942	
R indices (all data)	R1 = 0.0469, wR2 = 0.1017	
Goodness-of-fit on F^2	1.055	
Largest and mean shift/su	0.003 and 0.000	
Largest diff. peak and hole	1.966 and −2.108 e Å^{-3}	

Appendix 8.6 Crystal data and structure refinement details for **169**.

Chemical formula	$C_{44}H_{48}Cl_2N_6P_2Pd \cdot CH_2Cl_2$	
Formula weight	985.05	
Temperature	150(2) K	
Radiation, wavelength	MoKα, 0.71073 Å	
Crystal system, space group	triclinic, P $\bar{1}$	
Unit cell parameters	a = 9.4366(6) Å	α = 109.406(2)°
	b = 13.8183(8) Å	β = 94.723(2)°
	c = 18.3184(11) Å	γ = 93.855(2)°
Cell volume	2233.9(2) $Å^3$	
Z	2	
Calculated density	1.464 g/cm^3	
Absorption coefficient μ	0.766 mm^{-1}	
F(000)	1012	
Crystal colour and size	yellow, 0.42 × 0.08 × 0.03 mm^3	
Reflections for cell refinement	5148 (θ range 2.36 to 27.87°)	
Data collection method	Bruker APEX 2 CCD diffractometer	
	ω rotation with narrow frames	
θ range for data collection	1.57 to 27.49°	
Index ranges	h −12 to 12, k −17 to 17, l −23 to 23	
Completeness to θ = 26.00°	99.1 %	
Intensity decay	0%	
Reflections collected	19324	
Independent reflections	9932 (R_{int} = 0.0330)	
Reflections with $F^2>2\sigma$	7005	
Absorption correction	semi-empirical from equivalents	
Min. and max. transmission	0.739 and 0.977	
Structure solution	Patterson synthesis	
Refinement method	Full-matrix least-squares on F^2	
Weighting parameters a, b	0.0501, 2.6558	
Data / restraints / parameters	9932 / 0 / 529	
Final R indices [$F^2>2\sigma$]	R1 = 0.0467, wR2 = 0.1051	
R indices (all data)	R1 = 0.0782, wR2 = 0.1209	
Goodness-of-fit on F^2	1.025	
Largest and mean shift/su	0.001 and 0.000	
Largest diff. peak and hole	1.023 and −0.868 e $Å^{-3}$	

Appendix 8.7 Crystal data and structure refinement details for **170**.

Chemical formula	$C_{44}H_{42}Cl_2F_6N_6P_2Pd \cdot 2CH_2Cl_2$
Formula weight	1177.93
Temperature	150(2) K
Radiation, wavelength	MoKα, 0.71073 Å
Crystal system, space group	monoclinic, $P2_1/n$
Unit cell parameters	a = 15.2214(7) Å α = 90°
	b = 16.4673(8) Å β = 94.017(2)°
	c = 19.9932(10) Å γ = 90°
Cell volume	4999.1(4) $Å^3$
Z	4
Calculated density	1.565 g/cm^3
Absorption coefficient μ	0.819 mm^{-1}
F(000)	2384
Crystal colour and size	yellow, 0.18 × 0.14 × 0.06 mm^3
Reflections for cell refinement	7070 (θ range 2.39 to 24.97°)
Data collection method	Bruker APEX 2 CCD diffractometer
	ω rotation with narrow frames
θ range for data collection	1.63 to 25.00°
Index ranges	h −18 to 18, k −19 to 19, l −23 to 23
Completeness to θ = 25.00°	99.9 %
Intensity decay	0%
Reflections collected	35644
Independent reflections	8798 (R_{int} = 0.0539)
Reflections with $F^2>2\sigma$	6231
Absorption correction	semi-empirical from equivalents
Min. and max. transmission	0.867 and 0.953
Structure solution	direct methods
Refinement method	Full-matrix least-squares on F^2
Weighting parameters a, b	0.0311, 20.1343
Data / restraints / parameters	8798 / 53 / 638
Final R indices [$F^2>2\sigma$]	R1 = 0.0482, wR2 = 0.0998
R indices (all data)	R1 = 0.0810, wR2 = 0.1188
Goodness-of-fit on F^2	1.034
Largest and mean shift/su	0.000 and 0.000
Largest diff. peak and hole	1.282 and −1.137 e $Å^{-3}$

Appendix 8.8 Crystal data and structure refinement details for **178**.

Chemical formula	$C_{44}H_{42}Cl_2F_6N_6P_2Pt$	
Formula weight	1096.77	
Temperature	150(2) K	
Radiation, wavelength	MoKα, 0.71073 Å	
Crystal system, space group	triclinic, P $\bar{1}$	
Unit cell parameters	a = 9.5700(4) Å	α = 83.128(2)°
	b = 11.9806(5) Å	β = 83.843(2)°
	c = 19.6613(9) Å	γ = 71.815(2)°
Cell volume	2120.43(16) Å^3	
Z	2	
Calculated density	1.718 g/cm^3	
Absorption coefficient μ	3.578 mm^{-1}	
F(000)	1088	
Crystal colour and size	colourless, 0.51 × 0.37 × 0.21 mm^3	
Reflections for cell refinement	8719 (θ range 2.16 to 29.03°)	
Data collection method	Bruker APEX 2 CCD diffractometer	
	ω rotation with narrow frames	
θ range for data collection	1.80 to 30.55°	
Index ranges	h −13 to 13, k −17 to 17, l −28 to 28	
Completeness to θ = 26.00°	99.8 %	
Intensity decay	0%	
Reflections collected	25416	
Independent reflections	12692 (R_{int} = 0.0280)	
Reflections with $F^2>2\sigma$	10941	
Absorption correction	semi-empirical from equivalents	
Min. and max. transmission	0.263 and 0.520	
Structure solution	Patterson synthesis	
Refinement method	Full-matrix least-squares on F^2	
Weighting parameters a, b	0.0323, 0.0000	
Data / restraints / parameters	12692 / 252 / 614	
Final R indices [$F^2>2\sigma$]	R1 = 0.0310, wR2 = 0.0655	
R indices (all data)	R1 = 0.0396, wR2 = 0.0684	
Goodness-of-fit on F^2	1.013	
Largest and mean shift/su	0.001 and 0.000	
Largest diff. peak and hole	1.568 and −0.885 e Å^{-3}	

Appendix 8.9 Crystal data and structure refinement details for **181**.

Chemical formula	$C_{25}H_{28}ClF_3N_3P$	
Formula weight	493.92	
Temperature	150(2) K	
Radiation, wavelength	MoKα, 0.71073 Å	
Crystal system, space group	orthorhombic, Ama2	
Unit cell parameters	a = 13.7194(15) Å	α = 90°
	b = 18.513(2) Å	β = 90°
	c = 9.5476(10) Å	γ = 90°
Cell volume	2425.0(5) $Å^3$	
Z	4	
Calculated density	1.353 g/cm^3	
Absorption coefficient μ	0.265 mm^{-1}	
F(000)	1032	
Crystal colour and size	colourless, 0.40 × 0.34 × 0.23 mm^3	
Reflections for cell refinement	8376 (θ range 2.20 to 28.92°)	
Data collection method	Bruker SMART 1000 CCD diffractometer	
	ω rotation with narrow frames	
θ range for data collection	2.20 to 28.97°	
Index ranges	h −17 to 17, k −23 to 24, l −12 to 12	
Completeness to θ = 26.00°	100.0 %	
Intensity decay	0%	
Reflections collected	10554	
Independent reflections	2932 (R_{int} = 0.0216)	
Reflections with $F^2>2\sigma$	2902	
Absorption correction	semi-empirical from equivalents	
Min. and max. transmission	0.901 and 0.942	
Structure solution	direct methods	
Refinement method	Full-matrix least-squares on F^2	
Weighting parameters a, b	0.0000, 10.4569	
Data / restraints / parameters	2932 / 1 / 162	
Final R indices [$F^2>2\sigma$]	R1 = 0.0546, wR2 = 0.1278	
R indices (all data)	R1 = 0.0551, wR2 = 0.1281	
Goodness-of-fit on F^2	1.257	
Absolute structure parameter	0.08(14)	
Largest and mean shift/su	0.000 and 0.000	
Largest diff. peak and hole	0.388 and −0.621 e $Å^{-3}$	

Appendix 8.10 Crystal data and structure refinement details for **185**.

Chemical formula	$C_{49}H_{51}BN_3P$	
Formula weight	723.71	
Temperature	150(2) K	
Radiation, wavelength	MoKα, 0.71073 Å	
Crystal system, space group	monoclinic, $P2_1/c$	
Unit cell parameters	a = 12.9954(4) Å	α = 90°
	b = 19.7592(6) Å	β = 108.271(2)°
	c = 16.6069(5) Å	γ = 90°
Cell volume	4049.3(2) $Å^3$	
Z	4	
Calculated density	1.187 g/cm^3	
Absorption coefficient μ	0.106 mm^{-1}	
F(000)	1544	
Crystal colour and size	colourless, 0.36 × 0.35 × 0.18 mm^3	
Reflections for cell refinement	8685 (θ range 2.58 to 29.05°)	
Data collection method	Bruker APEX 2 CCD diffractometer	
	ω rotation with narrow frames	
θ range for data collection	1.65 to 30.55°	
Index ranges	h −18 to 18, k −28 to 27, l −23 to 22	
Completeness to θ = 26.00°	100.0 %	
Intensity decay	0%	
Reflections collected	48008	
Independent reflections	12372 (R_{int} = 0.0427)	
Reflections with $F^2>2\sigma$	8920	
Absorption correction	semi-empirical from equivalents	
Min. and max. transmission	0.963 and 0.981	
Structure solution	Patterson synthesis	
Refinement method	Full-matrix least-squares on F^2	
Weighting parameters a, b	0.0595, 0.9033	
Data / restraints / parameters	12372 / 0 / 493	
Final R indices [$F^2>2\sigma$]	R1 = 0.0508, wR2 = 0.1178	
R indices (all data)	R1 = 0.0765, wR2 = 0.1314	
Goodness-of-fit on F^2	1.028	
Largest and mean shift/su	0.019 and 0.000	
Largest diff. peak and hole	0.773 and −0.338 e $Å^{-3}$	

Appendix 8.11 Crystal data and structure refinement details for **190**.

Chemical formula	$C_{25}H_{28}F_9N_3PSb$	
Formula weight	694.22	
Temperature	150(2) K	
Radiation, wavelength	MoKα, 0.71073 Å	
Crystal system, space group	triclinic, P $\bar{1}$	
Unit cell parameters	a = 8.5038(12) Å	α = 77.019(2)°
	b = 8.8389(13) Å	β = 78.879(2)°
	c = 19.082(3) Å	γ = 84.880(2)°
Cell volume	1369.8(3) Å^3	
Z	2	
Calculated density	1.683 g/cm^3	
Absorption coefficient μ	1.147 mm^{-1}	
F(000)	692	
Crystal colour and size	colourless, 0.27 × 0.21 × 0.04 mm^3	
Reflections for cell refinement	451 (θ range 2.23 to 30.25°)	
Data collection method	Bruker APEX 2 CCD diffractometer	
	ω rotation with narrow frames	
θ range for data collection	2.23 to 24.76°	
Index ranges	h −10 to 10, k −10 to 10, l −22 to 22	
Completeness to θ = 24.76°	99.7 %	
Intensity decay	0%	
Reflections collected	10538	
Independent reflections	4663 (R_{int} = 0.0227)	
Reflections with $F^2>2\sigma$	4154	
Absorption correction	semi-empirical from equivalents	
Min. and max. transmission	0.747 and 0.956	
Structure solution	direct methods	
Refinement method	Full-matrix least-squares on F^2	
Weighting parameters a, b	0.0394, 0.2424	
Data / restraints / parameters	4663 / 0 / 358	
Final R indices [$F^2>2\sigma$]	R1 = 0.0259, wR2 = 0.0641	
R indices (all data)	R1 = 0.0318, wR2 = 0.0675	
Goodness-of-fit on F^2	1.059	
Largest and mean shift/su	0.001 and 0.000	
Largest diff. peak and hole	0.838 and −0.759 e Å^{-3}	

Appendix 8.12 Crystal data and structure refinement details for **193**.

Chemical formula	$C_{25}H_{31}F_6N_3P_2$	
Formula weight	549.47	
Temperature	150(2) K	
Radiation, wavelength	MoKα, 0.71073 Å	
Crystal system, space group	orthorhombic, Pbca	
Unit cell parameters	a = 17.9476(5) Å	α = 90°
	b = 15.8400(5) Å	β = 90°
	c = 19.1365(6) Å	γ = 90°
Cell volume	5440.3(3) $Å^3$	
Z	8	
Calculated density	1.342 g/cm^3	
Absorption coefficient μ	0.220 mm^{-1}	
F(000)	2288	
Crystal colour and size	colourless, 0.50 × 0.21 × 0.15 mm^3	
Reflections for cell refinement	17860 (θ range 2.27 to 30.44°)	
Data collection method	Bruker APEX 2 CCD diffractometer	
	ω rotation with narrow frames	
θ range for data collection	2.02 to 30.55°	
Index ranges	h –25 to 25, k –22 to 22, l –27 to 27	
Completeness to θ = 30.55°	99.9 %	
Intensity decay	0%	
Reflections collected	62276	
Independent reflections	8335 (R_{int} = 0.0291)	
Reflections with $F^2>2\sigma$	6759	
Absorption correction	semi-empirical from equivalents	
Min. and max. transmission	0.8980 and 0.9678	
Structure solution	direct methods	
Refinement method	Full-matrix least-squares on F^2	
Weighting parameters a, b	0.0589, 1.3791	
Data / restraints / parameters	8335 / 0 / 331	
Final R indices [$F^2>2\sigma$]	R1 = 0.0377, wR2 = 0.1000	
R indices (all data)	R1 = 0.0494, wR2 = 0.1091	
Goodness-of-fit on F^2	1.020	
Largest and mean shift/su	0.001 and 0.000	
Largest diff. peak and hole	0.408 and –0.316 e $Å^{-3}$	

Appendix 8.13 Crystal data and structure refinement details for **199**.

Chemical formula	$C_{35}H_{45}Cl_2F_6N_3PRuSb \cdot 1.67CH_2Cl_2$	
Formula weight	1087.65	
Temperature	150(2) K	
Radiation, wavelength	MoKα, 0.71073 Å	
Crystal system, space group	triclinic, P $\bar{1}$	
Unit cell parameters	a = 12.9426(5) Å	α = 65.2785(5)°
	b = 14.0425(5) Å	β = 70.5853(5)°
	c = 14.7175(6) Å	γ = 66.5392(5)°
Cell volume	2184.23(15) $Å^3$	
Z	2	
Calculated density	1.654 g/cm^3	
Absorption coefficient μ	1.383 mm^{-1}	
F(000)	1088	
Crystal colour and size	orange, 0.31 × 0.22 × 0.11 mm^3	
Reflections for cell refinement	12704 (θ range 2.56 to 30.54°)	
Data collection method	Bruker APEX 2 CCD diffractometer	
	ω rotation with narrow frames	
θ range for data collection	1.67 to 30.55°	
Index ranges	h −18 to 18, k −20 to 19, l −20 to 20	
Completeness to θ = 30.55°	97.5 %	
Intensity decay	0%	
Reflections collected	25887	
Independent reflections	13047 (R_{int} = 0.0183)	
Reflections with $F^2>2\sigma$	11295	
Absorption correction	semi-empirical from equivalents	
Min. and max. transmission	0.674 and 0.863	
Structure solution	Patterson synthesis	
Refinement method	Full-matrix least-squares on F^2	
Weighting parameters a, b	0.0510, 3.3546	
Data / restraints / parameters	13047 / 57 / 533	
Final R indices [$F^2>2\sigma$]	R1 = 0.0377, wR2 = 0.0991	
R indices (all data)	R1 = 0.0442, wR2 = 0.1033	
Goodness-of-fit on F^2	1.028	
Largest and mean shift/su	0.006 and 0.000	
Largest diff. peak and hole	1.863 and −1.184 e $Å^{-3}$	

Appendix 8.14 Crystal data and structure refinement details for **200**.

Chemical formula	$C_{35}H_{42}Cl_2F_9N_3PRuSb \cdot 0.33CH_2Cl_2$	
Formula weight	1028.19	
Temperature	150(2) K	
Radiation, wavelength	MoKα, 0.71073 Å	
Crystal system, space group	triclinic, P $\bar{1}$	
Unit cell parameters	a = 11.8041(10) Å	α = 85.3916(15)°
	b = 13.1776(12) Å	β = 73.4595(14)°
	c = 14.7273(13) Å	γ = 78.9597(15)°
Cell volume	2154.6(3) $Å^3$	
Z	2	
Calculated density	1.585 g/cm^3	
Absorption coefficient μ	1.246 mm^{-1}	
F(000)	1023	
Crystal colour and size	orange, 0.17 × 0.10 × 0.05 mm^3	
Reflections for cell refinement	3134 (θ range 2.31 to 22.25°)	
Data collection method	Bruker APEX 2 CCD diffractometer	
	ω rotation with narrow frames	
θ range for data collection	1.58 to 25.00°	
Index ranges	h −14 to 14, k −15 to 15, l −17 to 17	
Completeness to θ = 25.00°	99.9 %	
Intensity decay	0%	
Reflections collected	17336	
Independent reflections	7586 (R_{int} = 0.0409)	
Reflections with $F^2>2\sigma$	4833	
Absorption correction	semi-empirical from equivalents	
Min. and max. transmission	0.816 and 0.940	
Structure solution	Patterson synthesis	
Refinement method	Full-matrix least-squares on F^2	
Weighting parameters a, b	0.0648, 4.1883	
Data / restraints / parameters	7586 / 359 / 598	
Final R indices [$F^2>2\sigma$]	R1 = 0.0541, wR2 = 0.1256	
R indices (all data)	R1 = 0.0960, wR2 = 0.1482	
Goodness-of-fit on F^2	1.025	
Largest and mean shift/su	0.001 and 0.000	
Largest diff. peak and hole	0.923 and −0.601 e $Å^{-3}$	

Appendix 8.15 Crystal data and structure refinement details for **207.**

Chemical formula	$C_{35}H_{46}Cl_2F_6N_3PRhSb \cdot 2CH_2Cl_2$	
Formula weight	1119.13	
Temperature	153(2) K	
Radiation, wavelength	MoKα, 0.71073 Å	
Crystal system, space group	monoclinic, $P2_1/n$	
Unit cell parameters	a = 8.9106(3) Å	α = 90°
	b = 14.7367(4) Å	β = 95.887(2)°
	c = 30.8857(9) Å	γ = 90°
Cell volume	4034.3(2) $Å^3$	
Z	4	
Calculated density	1.843 g/cm^3	
Absorption coefficient μ	1.578 mm^{-1}	
F(000)	2240	
Crystal colour and size	orange, 0.16 × 0.10 × 0.04 mm^3	
Reflections for cell refinement	104486 (θ range 2.91 to 27.48°)	
Data collection method	Bruker-Nonius Roper 2 CCD camera on κ-gonios	
	φ & ω scans	
θ range for data collection	2.99 to 27.55°	
Index ranges	h −11 to 11, k −19 to 19, l −39 to 40	
Completeness to θ = 24.00°	99.4 %	
Intensity decay	0%	
Reflections collected	47660	
Independent reflections	9116 (R_{int} = 0.0658)	
Reflections with $F^2>2\sigma$	6545	
Absorption correction	semi-empirical from equivalents	
Min. and max. transmission	0.786 and 0.940	
Structure solution	direct methods	
Refinement method	Full-matrix least-squares on F^2	
Weighting parameters a, b	0.0639, 28.2608	
Data / restraints / parameters	9116 / 147 / 512	
Final R indices [$F^2>2\sigma$]	R1 = 0.0830, wR2 = 0.1891	
R indices (all data)	R1 = 0.1167, wR2 = 0.2031	
Goodness-of-fit on F^2	1.107	
Extinction coefficient	0.0028(3)	
Largest and mean shift/su	0.001 and 0.000	
Largest diff. peak and hole	1.389 and −0.648 e $Å^{-3}$	

Appendix 8.16 Crystal data and structure refinement details for **211'**.

Chemical formula	$C_{43}H_{51}Cl_2N_5P_2Pd$	
Formula weight	877.13	
Temperature	150(2) K	
Radiation, wavelength	MoKα, 0.71073 Å	
Crystal system, space group	triclinic, P $\bar{1}$	
Unit cell parameters	a = 11.8604(19) Å	α = 91.073(2)°
	b = 18.855(3) Å	β = 90.720(2)°
	c = 19.155(3) Å	γ = 99.569(2)°
Cell volume	4222.9(12) Å^3	
Z	4	
Calculated density	1.380 g/cm^3	
Absorption coefficient μ	0.678 mm^{-1}	
F(000)	1816	
Crystal colour and size	colourless, 0.19 × 0.17 × 0.07 mm^3	
Reflections for cell refinement	3033 (θ range 2.17 to 24.16°)	
Data collection method	Bruker APEX 2 CCD diffractometer	
	ω rotation with narrow frames	
θ range for data collection	1.51 to 25.00°	
Index ranges	h −14 to 14, k −22 to 22, l −22 to 22	
Completeness to θ = 25.00°	99.8 %	
Intensity decay	0%	
Reflections collected	33408	
Independent reflections	14844 (R_{int} = 0.0990)	
Reflections with $F^2>2\sigma$	7386	
Absorption correction	semi-empirical from equivalents	
Min. and max. transmission	0.882 and 0.954	
Structure solution	Patterson synthesis	
Refinement method	Full-matrix least-squares on F^2	
Weighting parameters a, b	0.0576, 0.0000	
Data / restraints / parameters	14844 / 48 / 955	
Final R indices [$F^2>2\sigma$]	R1 = 0.0585, wR2 = 0.1140	
R indices (all data)	R1 = 0.1514, wR2 = 0.1522	
Goodness-of-fit on F^2	0.957	
Largest and mean shift/su	0.001 and 0.000	
Largest diff. peak and hole	1.427 and −1.174 e Å^{-3}	

Appendix 8.17 Crystal data and structure refinement details for **218**.

Chemical formula	$C_{34}H_{40}Cl_2F_3N_4PPd$
Formula weight	769.97
Temperature	120(2) K
Radiation, wavelength	synchrotron, 0.6943 Å
Crystal system, space group	monoclinic, $P2_1/n$
Unit cell parameters	a = 16.3089(7) Å $\alpha = 90°$
	b = 9.5474(4) Å $\beta = 104.817(6)°$
	c = 23.2240(10) Å $\gamma = 90°$
Cell volume	3495.9(3) $Å^3$
Z	4
Calculated density	1.463 g/cm^3
Absorption coefficient μ	0.775 mm^{-1}
F(000)	1576
Crystal colour and size	colourless, 0.10 × 0.05 × 0.03 mm^3
Reflections for cell refinement	6696 (θ range 2.44 to 26.18°)
Data collection method	Bruker APEX 2 CCD diffractometer
	ω rotation with narrow frames
θ range for data collection	1.72 to 27.61°
Index ranges	h −21 to 21, k −12 to 12, l −30 to 30
Completeness to θ = 27.00°	99.6 %
Intensity decay	3%
Reflections collected	34142
Independent reflections	8666 (R_{int} = 0.0500)
Reflections with $F^2>2\sigma$	6710
Absorption correction	semi-empirical from equivalents
Min. and max. transmission	0.927 and 0.977
Structure solution	direct methods
Refinement method	Full-matrix least-squares on F^2
Weighting parameters a, b	0.0406, 0.6658
Data / restraints / parameters	8666 / 0 / 414
Final R indices [$F^2>2\sigma$]	R1 = 0.0349, wR2 = 0.0778
R indices (all data)	R1 = 0.0521, wR2 = 0.0843
Goodness-of-fit on F^2	1.010
Largest and mean shift/su	0.001 and 0.000
Largest diff. peak and hole	0.636 and −0.357 e $Å^{-3}$

Appendix 8.18 Crystal data and structure refinement details for **220**.

Chemical formula	$C_{37}H_{40}Cl_2F_3N_4PPd$
Formula weight	806.00
Temperature	150(2) K
Radiation, wavelength	synchrotron, 0.6939 Å
Crystal system, space group	monoclinic, C2/c
Unit cell parameters	a = 27.1389(9) Å $\alpha = 90°$
	b = 9.7892(3) Å $\beta = 104.8029(4)°$
	c = 28.2756(10) Å $\gamma = 90°$
Cell volume	7262.6(4) $Å^3$
Z	8
Calculated density	1.474 g/cm^3
Absorption coefficient μ	0.750 mm^{-1}
F(000)	3296
Crystal colour and size	pale yellow, 0.17 × 0.08 × 0.04 mm^3
Reflections for cell refinement	42091 (θ range 2.22 to 29.56°)
Data collection method	Bruker APEX 2 CCD diffractometer
	ω rotation with narrow frames
θ range for data collection	1.52 to 29.72°
Index ranges	h −37 to 38, k −13 to 13, l −39 to 40
Completeness to θ = 29.00°	99.6 %
Intensity decay	2.3%
Reflections collected	40865
Independent reflections	11033 (R_{int} = 0.0490)
Reflections with $F^2>2\sigma$	9335
Absorption correction	semi-empirical from equivalents
Min. and max. transmission	0.883 and 0.971
Structure solution	direct methods
Refinement method	Full-matrix least-squares on F^2
Weighting parameters a, b	0.0329, 4.1734
Data / restraints / parameters	11033 / 0 / 441
Final R indices [$F^2>2\sigma$]	R1 = 0.0337, wR2 = 0.0812
R indices (all data)	R1 = 0.0408, wR2 = 0.0860
Goodness-of-fit on F^2	1.040
Largest and mean shift/su	0.003 and 0.000
Largest diff. peak and hole	0.428 and −0.534 e $Å^{-3}$

Appendix 8.19 Crystal data and structure refinement details for **222'**.

Chemical formula	$C_{34}H_{34}Cl_4F_4N_4P_2Pd_2 \cdot (CH_3)_2SO$	
Formula weight	1069.32	
Temperature	150(2) K	
Radiation, wavelength	synchrotron, 0.6710 Å	
Crystal system, space group	orthorhombic, Pbcn	
Unit cell parameters	a = 16.980(3) Å	$\alpha = 90°$
	b = 19.430(4) Å	$\beta = 90°$
	c = 12.751(2) Å	$\gamma = 90°$
Cell volume	4206.7(14) $Å^3$	
Z	4	
Calculated density	1.688 g/cm^3	
Absorption coefficient μ	1.287 mm^{-1}	
F(000)	2136	
Crystal colour and size	yellow, 0.10 × 0.04 × 0.03 mm^3	
Reflections for cell refinement	38823 (θ range 2.49 to 24.03°)	
Data collection method	Bruker APEX 2 CCD diffractometer	
	ω rotation with narrow frames	
θ range for data collection	1.50 to 26.61°	
Index ranges	h −22 to 22, k −25 to 25, l −16 to 16	
Completeness to θ = 26.61°	99.6 %	
Intensity decay	3%	
Reflections collected	36669	
Independent reflections	5231 (R_{int} = 0.0895)	
Reflections with $F^2>2\sigma$	3877	
Absorption correction	semi-empirical from equivalents	
Min. and max. transmission	0.882 and 0.962	
Structure solution	direct methods	
Refinement method	Full-matrix least-squares on F^2	
Weighting parameters a, b	0.0913, 0.0000	
Data / restraints / parameters	5231 / 223 / 284	
Final R indices [$F^2>2\sigma$]	R1 = 0.0600, wR2 = 0.1423	
R indices (all data)	R1 = 0.0816, wR2 = 0.1535	
Goodness-of-fit on F^2	1.024	
Largest and mean shift/su	0.001 and 0.000	
Largest diff. peak and hole	2.704 and −1.178 e $Å^{-3}$	

Appendix 8.20 Crystal data and structure refinement details for **223'**.

Chemical formula	$C_{34}H_{38}Cl_4N_4P_2Pt_2 \cdot CH_2Cl_2$	
Formula weight	1181.53	
Temperature	150(2) K	
Radiation, wavelength	synchrotron, 0.6884 Å	
Crystal system, space group	triclinic, P $\bar{1}$	
Unit cell parameters	a = 12.5972(3) Å	α = 114.1393(2)°
	b = 17.1567(4) Å	β = 96.4836(2)°
	c = 20.8242(4) Å	γ = 90.2454(2)°
Cell volume	4074.50(16) Å^3	
Z	4	
Calculated density	1.926 g/cm^3	
Absorption coefficient μ	7.362 mm^{-1}	
F(000)	2264	
Crystal colour and size	colourless, 0.72 × 0.09 × 0.05 mm^3	
Reflections for cell refinement	13616 (θ range 2.38 to 30.78°)	
Data collection method	Bruker APEX 2 CCD diffractometer	
	ω rotation with narrow frames	
θ range for data collection	1.26 to 31.09°	
Index ranges	h −18 to 18, k −25 to 25, l −30 to 30	
Completeness to θ = 26.00°	99.3 %	
Intensity decay	3%	
Reflections collected	49750	
Independent reflections	25936 (R_{int} = 0.0319)	
Reflections with $F^2>2\sigma$	20263	
Absorption correction	semi-empirical from equivalents	
Min. and max. transmission	0.076 and 0.710	
Structure solution	direct methods	
Refinement method	Full-matrix least-squares on F^2	
Weighting parameters a, b	0.0371, 0.0000	
Data / restraints / parameters	25936 / 0 / 841	
Final R indices [$F^2>2\sigma$]	R1 = 0.0378, wR2 = 0.0884	
R indices (all data)	R1 = 0.0479, wR2 = 0.0932	
Goodness-of-fit on F^2	1.053	
Largest and mean shift/su	0.003 and 0.000	
Largest diff. peak and hole	2.198 and −1.147 e Å^{-3}	

Appendix 8.21 Crystal data and structure refinement details for **225**.

Chemical formula	$C_{25}H_{28}AuCl_2F_3N_3P$	
Formula weight	726.34	
Temperature	150(2) K	
Radiation, wavelength	MoKα, 0.71073 Å	
Crystal system, space group	monoclinic, $P2_1/c$	
Unit cell parameters	a = 18.6440(16) Å	α = 90°
	b = 8.6308(7) Å	β = 98.5448(12)°
	c = 16.4841(14) Å	γ = 90°
Cell volume	2623.1(4) $Å^3$	
Z	4	
Calculated density	1.839 g/cm^3	
Absorption coefficient μ	5.914 mm^{-1}	
F(000)	1416	
Crystal colour and size	colourless, 0.49 × 0.08 × 0.07 mm^3	
Reflections for cell refinement	12920 (θ range 2.50 to 31.54°)	
Data collection method	Bruker APEX 2 CCD diffractometer	
	ω rotation with narrow frames	
θ range for data collection	2.21 to 31.56°	
Index ranges	h −27 to 27, k −12 to 12, l −23 to 23	
Completeness to θ = 29.00°	100.0 %	
Intensity decay	0%	
Reflections collected	30352	
Independent reflections	8321 (R_{int} = 0.0295)	
Reflections with $F^2>2\sigma$	7193	
Absorption correction	semi-empirical from equivalents	
Min. and max. transmission	0.164 and 0.659	
Structure solution	Patterson synthesis	
Refinement method	Full-matrix least-squares on F^2	
Weighting parameters a, b	0.0269, 0.3372	
Data / restraints / parameters	8321 / 0 / 322	
Final R indices [$F^2>2\sigma$]	R1 = 0.0222, wR2 = 0.0511	
R indices (all data)	R1 = 0.0292, wR2 = 0.0534	
Goodness-of-fit on F^2	1.036	
Largest and mean shift/su	0.002 and 0.000	
Largest diff. peak and hole	1.388 and −0.515 e $Å^{-3}$	

Appendix 8.22 COURSES/CONFERENCES ATTENDED

1) Lecture on Fire and Safety Precautions, 18th April, 2005.
2) Postgraduate Research Students Induction, 12th May, 2005.
3) Research seminar: Why control the `color' in variable band gap conjugated polymers delivered in the Department by Prof. John R. Reynolds, University of Florida USA, 8th June, 2005.
4) Lecture: The ground and excited state double proton transfer in lumichrome/acetic acid system: theoretical and experimental approach delivered in the Department by Dr Marek Sikorski, Adam Mickiewicz University, Poznan, Poland, 27th July, 2005.
5) Training on NMR for new Postgraduate Students by Dr Mark Edgar, 7th October, 2005.
6) Teaching Skills: Preparing to Teach and Promoting Learning, 25th October, 2005.
7) Teaching Skills for Postgraduates and Research Assistants with Supervising Practical Activities, 3rd November, 2005.
8) Introduction to the job of a lecturer for Postgraduates and Research Assistants, 9th November, 2005.
9) Departmental talk on training in transferable skills for PhD students, 23rd November, 2005.
10) Database of the month - Oxford English Dictionary 15th November, 2005.
11) Power-point for Presentations 25th November, 2005.
12) Presentation of PhD work to the Inorganic Section, 14th December, 2005.
13) CSD searching workshop and seminar organised by Dr Mark Elsegood in the Department, 24th February, 2006.
14) Catalysis: Half Day Discussion Meeting, University of Leicester, 3rd April, 2006.
15) Poster Presentation at Dalton Symposium, "New Cyclic Tertiary Phosphines Derived from Tetrakis(hydroxymethyl)phosphonium Chloride", University of Birmingham, 14th September, 2006.
16) Designing and Producing Conference Posters, 13th October, 2006.
17) Getting Articles Published for Postgraduates and Research Assistants, 23rd October, 2006.

18) RSC Industrial Lecture: Process Understanding – Why it is important to Process R & D (PR&D) by Dr Steve Eyley, 24th October, 2006.

19) Report Writing, 1st November, 2006.

20) Keeping your Research Up-to-Date for Postgraduates, 1st February, 2007.

21) Plagiarism, Citation and Managing your References, 14th March, 2007.

22) Inorganic Seminar: "Fast Detectors and Bright Sources; Pushing the Limits of Lab Powder Diffraction" by Dr Caroline Kirk, 18th July, 2007.

23) Research Assistants and Postgraduates- Career Management, 27th February, 2008.

24) Research Assistants and Postgraduates- Successful Applications, 5th March, 2008.

25) Intellectual Property, 5th March, 2008.

26) Career Management for Postgraduate Researchers- Interviews, 12th March, 2008.

27) Poster Presentation at Dalton Division Midlands Postgraduate Symposium, "New Cationic Phosphorus(III) Compounds Derived from a Simple Phosphonium Chloride", University of Warwick, 27th March, 2008.

28) VIVA- What happens? 25th April, 2008.

29) Personal Organisation and Time Management for Postgraduate researchers, 28th April, 2008.

30) RSC Ronald Nyholm Lecture 2007-8: "Exploiting Knowledge-based Approaches to Chemistry" by Prof Guy Orpen, 30th April, 2008.

31) RSC Hugo Müller Lecture 2007-8: "Seeing Inspiration in Nature's Laboratory" by Prof. Mark Weller, 21st May, 2008.

Appendix 8.23 REFEREED JOURNAL PUBLICATION(S) FROM THIS RESEARCH

1. A.T. Ekubo, M. R. J. Elsegood, A. J. Lake and M. B. Smith, Intramolecular Hydrogen-Bonded Tertiary Phosphines as 1,3,5-Triaza-7-phosphaadamantane (PTA) Analogues. *Inorg. Chem.*, 2009, **48**, 2633.

Inorg. Chem. 2009, 48, 2633–2638

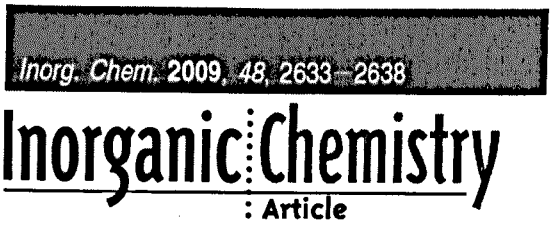

Intramolecular Hydrogen-Bonded Tertiary Phosphines as 1,3,5-Triaza-7-phosphaadamantane (PTA) Analogues

Allen T. Ekubo, Mark R. J. Elsegood, Andrew J. Lake, and Martin B. Smith*

Department of Chemistry, Loughborough University, Loughborough, Leics LE11 3TU, U.K.

Received September 5, 2008

New cationic trialkylphosphines $[P(CH_2NH_2R)\{CH_2N(R)CH_2N(R)CH_2\}]^+$ (R = $C_6H_5CH_2$, **a**; 4-$FC_6H_4CH_2$, **b**), as their Cl^- (**1a**, **1b**), SbF_6^- (**2a**, **2b**), and PF_6^- (**3a**, **3b**) salts, are described. The phosphine framework is conformationally locked, in the solid state, through pairs of intramolecular N−H···N hydrogen bonds which are maintained in the Ru^{II} and Rh^{III} complexes **4** and **5**. Phosphines **1a**−**3b** can be considered as charged variants of the well-known PTA ligand.

Introduction

The ability by which tertiary phosphines can be modified undoubtedly remains a major reason why this ligand class continues to find spectacular success in many branches of chemistry. Considerable recent interest has focused on the aliphatic caged tertiary phosphine 1,3,5-triaza-7-phosphaadamantane (hereafter abbreviated PTA), which has been shown to possess many desirable attributes including water solubility.[1] Synthetic routes for modifying the adamantanoid framework of PTA such as protonation or alkylation of the tertiary nitrogen atoms or upper or lower rim functionalization have been reported.[2,3] Consequently, numerous applications of PTA and their derivatives in biomedicine,[4] coordination and organometallic chemistry,[4,5] and catalysis,[6] especially in aqueous media, have been realized. One aspect of PTA not previously investigated is the ability to manipulate the nitrogen centers, for example, by changing the alkyl or aryl substituents yet *preserving* the tertiary amine character as opposed to quaternization[3b] or forming boronated species.[5c] One approach by which this could be accomplished is to envisage removal of two "upper-rim" methylene ($N-CH_2-N$) groups from PTA, thereby allowing different R groups on nitrogen to be incorporated. Using suitable noncovalent interactions, such as intramolecular H-bonding, would allow for retention of the adamantane core. As part of ongoing studies in our group, we have recently developed highly functionalized (di)tertiary phosphines with regiospecific H-bonding capabilities.[7] Herein a simple concept for the synthesis of novel cationic trialkylphosphines, with stereoelectronic properties similar to those of PTA, and a preliminary exploration of their late transition metal chemistries are reported. All new compounds have been character-

* To whom correspondence should be addressed. E-mail: m.b.smith@lboro.ac.uk. Tel: +44 (0)1509 222553. Fax: +44 (0)1509 223925.

(1) Daigle, D. J.; Pepperman, A. B.; Vail, S. L. *J. Heterocycl. Chem.* **1974**, *11*, 407–408.

(2) For recent examples of PTA functionalization, see: (a) Erlandsson, M.; Gonsalvi, L.; Lenco, A.; Peruzzini, M. *Inorg. Chem.* **2008**, *47*, 8–10. (b) Wong, G. W.; Lee, W.-C.; Frost, B. J. *Inorg. Chem.* **2008**, *47*, 612–620. (c) Huang, R.; Frost, B. J. *Inorg. Chem.* **2007**, *46*, 10962–10964. (d) Wong, G. W.; Harkreader, J. L.; Mebi, C. A.; Frost, B. J. *Inorg. Chem.* **2006**, *45*, 6748–6755. (e) Zablocka, M.; Duhayon, C. *Tetrahedron Lett.* **2006**, *47*, 2687–2690. (f) Darensbourg, D. J.; Yarbrough, J. C.; Lewis, S. J. *Organometallics* **2003**, *22*, 2050–2056.

(3) For the chemistry of open cage ligands related to PTA, see: (a) Mena-Cruz, A.; Lorenzo-Luis, P.; Romerosa, A.; Serrano-Ruiz, M. *Inorg. Chem.* **2008**, *47*, 2246–2248. (b) Mena-Cruz, A.; Lorenzo-Luis, P.; Romerosa, A.; Saoud, M.; Serrano-Ruiz, M. *Inorg. Chem.* **2007**, *46*, 6120–6128. (c) Krogstad, D. A.; Ellis, G. S.; Gunderson, A. K.; Hammrich, A. J.; Rudolf, J. W.; Halfen, J. A. *Polyhedron* **2007**, *26*, 4093–4100. (d) Phillips, A. D.; Bolaño, S.; Bosquain, S. S.; Daran, J.-C.; Malacea, R.; Peruzzini, M.; Poli, R.; Gonsalvi, L. *Organometallics* **2006**, *25*, 2189–2200. (e) Darensbourg, D. J.; Ortiz, C. G.; Kamplain, J. W. *Organometallics* **2004**, *23*, 1747–1754.

(4) For recent medicinal examples using PTA and related ligands, see: (a) Gossens, C.; Tavernelli, I.; Rothlisberger, U. *J. Am. Chem. Soc.* **2008**, *130*, 10921–10928. (b) Miranda, S.; Vergara, E.; Mohr, F.; de Vos, D.; Cerrada, E.; Mendía, A.; Laguna, M. *Inorg. Chem.* **2008**, *47*, 5641–5648. (c) Vock, C. A.; Renfrew, A. K.; Scopelliti, R.; Juillerat-Jeanneret, L.; Dyson, P. J. *Eur. J. Inorg. Chem.* **2008**, 1661–1671. (d) Dutta, B.; Scolaro, C.; Scopelliti, R.; Dyson, P. J.; Severin, K. *Organometallics* **2008**, *27*, 1355–1357. (e) Leyva, L.; Sirlin, C.; Rubio, L.; Franco, C.; Le Lagadec, R.; Spencer, J.; Bischoff, P.; Gaiddon, C.; Loeffler, J.-P.; Pfeffer, M. *Eur. J. Inorg. Chem.* **2007**, 3055–3066. (f) Dillinger, S. A. T.; Schmalle, H. W.; Fox, T.; Berke, H. *Dalton Trans.* **2007**, 3562–3571. (g) Bergamini, P.; Bertolasi, V.; Marvelli, L.; Canella, A.; Gavioli, R.; Mantovani, N.; Mañas, S.; Romerosa, A. *Inorg. Chem.* **2007**, *46*, 4267–4276. (h) Dorcier, A.; Ang, W. H.; Bolaño, S.; Gonsalvi, L.; Juillerat-Jeannerat, L.; Laurenczy, G.; Peruzzini, M.; Phillips, A. D.; Zanobini, F.; Dyson, P. J. *Organometallics* **2006**, *25*, 4090–4096. (i) Dorcier, A.; Dyson, P. J.; Gossens, C.; Rothlisberger, U.; Scopelliti, R.; Tavernelli, I. *Organometallics* **2005**, *24*, 2114–2123. (j) Allardyce, C. S.; Dyson, P. J.; Ellis, D. J.; Heath, S. L. *Chem. Commun.* **2001**, 1396–1397.

10.1021/ic801709z CCC: $40.75
Published on Web 02/11/2009

ized by a combination of spectroscopic and single crystal X-ray diffraction techniques.

Experimental Section

Materials. All manipulations and reactions were carried out under aerobic conditions. Dichloromethane was previously distilled over CaH_2 and diethyl ether over sodium/benzophenone, and tetrakis(hydroxymethyl)phosphonium chloride (THPC) was recrystallized from 2-propanol before use.[8] All other solvents and chemicals were obtained from commercial suppliers and used without further purification. The dinuclear metal compounds $\{RuCl_2(\eta^6\text{-}p\text{-cymene})\}_2$ and $\{RhCl_2(\eta^5\text{-Cp}^*)\}_2$ were prepared according to published procedures.[9,10]

Instrumentation. Fourier transform infrared (FT-IR) spectra were recorded within pressed KBr pellets over the range of 4000−200 cm^{-1} using a Perkin-Elmer system 2000 FT spectrometer. ^1H NMR and $^{31}P\{^1H\}$ NMR spectra were recorded on a Bruker DPX-400 FT spectrometer with chemical shifts (δ) reported relative to external tetramethylsilane (TMS) or 85% H_3PO_4. Coupling constants (J) were recorded in hertz. All NMR spectra were recorded in dmso-d^6 solutions at about 298 K. Elemental analyses (Perkin-Elmer 2400 CHN or Exeter Analytical, Inc., CE-440 Elemental Analyzers) were performed by the Loughborough University Analytical Service within the Department of Chemistry. Mass spectra for **1a**−**5** were analyzed (JEOL SX102 instrument) by fast atom bombardment (FAB) in a positive ionization mode using a 3-nitrobenzyl alcohol (NOBA) matrix. Compounds **6a** and **6b** were analyzed (Finnigan MAT 95XP) by low-resolution FAB (LSIMS) in positive ionization mode using CH_2Cl_2 as the solvent and a NOBA matrix.

Preparation of 1a. To a solution of THPC (3.83 g, 20.1 mmol) in EtOH (100%, 75 mL) was added dropwise $C_6H_5CH_2NH_2$ (8.94 g, 83.4 mmol). During the addition, heat was generated, and thick white fumes were observed. After about 5 min, the solution became clear. The mixture was stirred for 2 h at room temperature (frequently some unwanted "sticky" material was formed which was separated from the solution by decantation) and the volume reduced on a rotary evaporator to approximately a quarter of the original volume. The resulting crystalline solid was filtered and dried under vacuum. Yield: 7.60 g (86%). Selected data is as follows. $^{31}P\{^1H\}$ NMR: −55.0 ppm. ^1H NMR: 9.55 (br, NH_2, 2H), 7.59−7.01 (m, arom. H, 15H), 4.21 (s, CH_2, 2H), 3.42−3.38 (m, CH_2, 8H), 3.18 (d, $^2J_{PH}$ 13.6, CH_2, 2H), 2.65 (t, CH_2, 2H) ppm. FT-IR: 3028 and 2781 (br, NH and CH) cm^{-1}. FAB-MS: m/z 404 [M − Cl]. Anal. Calcd for $C_{25}H_{31}N_3PCl$: C, 68.24; H, 7.12; N, 9.55. Found: C, 68.25; H, 7.10; N, 9.58.

Preparation of 1b. To a solution of THPC (2.85 g, 14.9 mmol) in EtOH (100%, 55 mL) was added dropwise 4-$FC_6H_4CH_2NH_2$ (7.77 g, 62.0 mmol). The mixture was stirred for 2 h at room temperature and the volume reduced on a rotary evaporator to approximately a quarter of the original volume. The resulting crystalline solid was filtered and dried under vacuum. Additional crops of **1b** were obtained when the filtrate was allowed to stand for more than 24 h. Yield: 6.11 g (83%). Selected data is as follows. $^{31}P\{^1H\}$ NMR: −55.2 ppm. ^1H NMR: 7.62−6.93 (m, arom. H, 12H), 4.21 (s, CH_2, 2H), 3.29 (multiplicity could not fully be assigned as a result of overlap with residual solvent peaks, CH_2), 3.18 (d, $^2J_{PH}$ 13.8, CH_2, 2H), 2.67 (t, CH_2, 2H) ppm. FT-IR: 3044 and 2821 (br, NH and CH) cm^{-1}. FAB-MS: m/z 458 [M − Cl]. Anal. Calcd for $C_{25}H_{28}F_3N_3PCl$: C, 60.78; H, 5.73; N, 8.51. Found: C, 60.56; H, 5.58; N, 8.41.

Preparation of 2a. A solution of $Na(SbF_6)$ (0.18 g, 0.69 mmol) in the minimum volume of high performance liquid chromatography (HPLC) grade CH_3OH was added to a solution of **1a** (0.20 g, 0.45 mmol) in HPLC grade CH_3OH (10 mL). The solution was stirred at room temperature for 30 min. Concentration of the solution, under reduced pressure, and addition of distilled water afforded a colorless precipitate which was filtered and dried under vacuum. Yield: 0.28 g (97%). Selected data is as follows. $^{31}P\{^1H\}$ NMR: −55.2 ppm. ^1H NMR: 9.01 (br, NH_2, 2H), 7.49−6.92 (m, arom. H, 15H), 4.22 (s, CH_2, 2H), 3.57−3.41 (multiplicity could not fully be assigned as a result of overlap with residual solvent peaks, CH_2), 3.10 (d, $^2J_{PH}$ 12, CH_2, 2H), 2.66 (t, CH_2, 2H) ppm. FT-IR: 3064, 3031, and 2808 (s, NH and CH), 654 (vs, SbF) cm^{-1}. FAB-MS: m/z 404 [M − SbF_6]. Anal. Calcd for $C_{25}H_{31}N_3PSbF_6 \cdot 0.5H_2O$: C, 46.25; H, 4.98; N, 6.47. Found: C, 46.35; H, 4.80; N, 6.46.

Preparation of 2b. A solution of $Na(SbF_6)$ (0.16 g, 0.61 mmol) in the minimum volume of HPLC grade CH_3OH was added to a solution of **1b** (0.20 g, 0.40 mmol) in HPLC grade CH_3OH (10 mL). The solution was stirred at room temperature for 30 min. Concentration of the solution, under reduced pressure, and addition of distilled water afforded a colorless precipitate which was filtered and dried under vacuum. Yield: 0.21 g (73%). Selected data is as follows. $^{31}P\{^1H\}$ NMR: −55.0 ppm. ^1H NMR: 8.95 (br, NH_2, 2H), 7.57−6.98 (m, arom. H, 12H), 4.22 (s, CH_2, 2H), 3.84−3.50 (multiplicity could not fully be assigned as a result of overlap with residual solvent peaks, CH_2), 3.10 (d, $^2J_{PH}$ 13.6, CH_2, 2H), 2.67 (t, CH_2, 2H) ppm. FT-IR: 3052, 2953, 2830, 2799, and 2730 (m, NH

(5) For recent examples of PTA coordination complexes, see: (a) Serrano Ruiz, M.; Romerosa, A.; Sierra-Martin, B.; Fernandez-Barbero, A. *Angew. Chem., Int. Ed.* **2008**, *47*, 8665–8669. (b) Tu, X.; Nichol, G. S.; Wang, R.; Zheng, Z. *Dalton Trans.* **2008**, 6030–6038. (c) Bolaño, S.; Albinati, A.; Bravo, J.; Caporali, M.; Gonsalvi, L.; Male, L.; Rodríguez-Rocha, M. M.; Rossin, A.; Peruzzini, M. *J. Organomet. Chem.* **2008**, *693*, 2397–2406. (d) Jaremko, L.; Kirillov, A. M.; Smoleński, P.; Lis, T.; Pombeiro, A. J. L. *Inorg. Chem.* **2008**, *47*, 2922–2924. (e) Mena-Cruz, A.; Lorenzo-Luis, P.; Romerosa, A.; Serrano-Ruiz, M. *Inorg. Chem.* **2008**, *47*, 2246–2248. (f) Marchi, A.; Marchesi, E.; Marvelli, L.; Bergamini, P.; Bertolasi, V.; Ferretti, V. *Eur. J. Inorg. Chem.* **2008**, 2670–2679. (g) Smoleński, P.; Dinoi, C.; Guedes da Silva, M. F. C.; Pombeiro, A. J. L. *J. Organomet. Chem.* **2008**, *693*, 2338–2344. (h) Mebi, C. A.; Frost, B. J. *Inorg. Chem.* **2007**, *46*, 7115–7120. (i) Mohr, F.; Falvello, L. R.; Laguna, M. *Eur. J. Inorg. Chem.* **2006**, 3152–3154. (j) Wang, Z.; Liu, J.; He, C.; Jiang, S.; Åkermark, B.; Sun, L. *Inorg. Chim. Acta* **2007**, *360*, 2411–2419. (k) Frost, B. J.; Bautista, C. M.; Huang, R.; Shearer, J. *Inorg. Chem.* **2006**, *45*, 3481–3483. (l) Phillips, A. D.; Gonsalvi, L.; Romerosa, A.; Vizza, F.; Peruzzini, M. *Coord. Chem. Rev.* **2004**, *248*, 955–993. (m) Darensbourg, D. J.; Robertson, J. B.; Larkins, D. L.; Reibenspies, J. H. *Inorg. Chem.* **1999**, *38*, 2473–2481.

(6) (a) Erlandsson, M.; Landaeta, V. R.; Gonsalvi, L.; Peruzzini, M.; Phillips, A. D.; Dyson, P. J.; Laurenczy, G. *Eur. J. Inorg. Chem.* **2008**, 620–627. (b) Korthals, B.; Göttker-Schnetmann, I.; Mecking, S. *Organometallics* **2007**, *26*, 1311–1316. (c) Xu, X.; Wang, C.; Zhou, Z.; Tang, X.; He, Z.; Tang, C. *Eur. J. Org. Chem.* **2007**, 4487–4491. (d) Ruiz, J.; Cutillas, N.; López, F.; López, G.; Bautista, D. *Organometallics* **2006**, *25*, 5768–5773. (e) Krogstad, D. A.; DeBoer, A. J.; Ortmeier, W. J.; Rudolf, J. W.; Halfen, J. A. *Inorg. Chem. Commun.* **2005**, *8*, 1141–1144. (f) Mejia-Rodriguez, R.; Chong, D.; Reibenspies, J. H.; Soriaga, M. P.; Darensbourg, M. Y. *J. Am. Chem. Soc.* **2004**, *126*, 12004–12014. (g) Darensbourg, D. J.; Joó, F.; Kannisto, M.; Kathó, A.; Reibenspies, J. H.; Daigle, D. J. *Inorg. Chem.* **1994**, *33*, 200–208.

(7) (a) Smith, M. B.; Dale, S. H.; Coles, S. J.; Gelbrich, T.; Hursthouse, M. B.; Light, M. E.; Horton, P. N. *CrystEngComm* **2007**, *9*, 165–175. (b) Dann, S. E.; Durran, S. E.; Elsegood, M. R. J.; Smith, M. B.; Staniland, P. M.; Talib, S.; Dale, S. H. *J. Organomet. Chem.* **2006**, *691*, 4829–4842. (c) Elsegood, M. R. J.; Smith, M. B.; Staniland, P. M. *Inorg. Chem.* **2006**, *45*, 6761–6770. (d) Smith, M. B.; Dale, S. H.; Coles, S. J.; Gelbrich, T.; Hursthouse, M. B.; Light, M. E. *CrystEngComm* **2006**, *8*, 140–149.

(8) Frank, A. W.; Drake Jr., G. L. *J. Org. Chem.* **1972**, *37*, 2752–2755.

(9) Bennett, M. A.; Smith, A. K. *J. Chem. Soc., Dalton Trans.* **1974**, 233–241.

(10) White, C.; Yates, A.; Maitlis, P. M. *Inorg. Synth.* **1992**, *29*, 228–234.

and CH), 653 (vs, SbF) cm^{-1}. FAB-MS: *m/z* 458 [M − SbF_6]. Anal. Calcd for $C_{25}H_{28}N_3PSbF_9 \cdot 0.5H_2O$: C, 42.70; H, 4.16; N, 5.98. Found: C, 42.46; H, 3.90; N, 5.87.

Preparation of 3a. A solution of $K(PF_6)$ (0.13 g, 0.71 mmol) in the minimum volume of HPLC grade CH_3OH was added to a solution of **1a** (0.20 g, 0.45 mmol) in HPLC grade CH_3OH (10 mL). The solution was stirred at room temperature for 30 min. Concentration of the solution, under reduced pressure, and addition of distilled water afforded a colorless precipitate which was filtered and dried under vacuum. Yield: 0.18 g (72%). Selected data is as follows. $^{31}P\{^1H\}$ NMR: −54.6, −144.2 ppm, ($^1J_{PF}$ 711, PF_6^-). ^1H NMR: 9.02 (br, NH_2, 2H), 7.49−7.01 (m, arom. H, 15H), 4.23 (s, CH_2, 2H), 3.85−3.41 (multiplicity could not fully be assigned as a result of overlap with residual solvent peaks, CH_2), 3.10 (d, $^2J_{PH}$ 14, CH_2, 2H), 2.67 (t, CH_2, 2H) ppm. FT-IR: 3030 and 2809 (w, NH and CH), 842 (vs, PF) cm^{-1}. FAB-MS: *m/z* 404 [M − PF_6]. Anal. Calcd for $C_{25}H_{31}N_3P_2F_6$: C, 54.64; H, 5.70; N, 7.65. Found: C, 55.03; H, 5.61; N, 7.68.

Preparation of 3b. A solution of $K(PF_6)$ (0.11 g, 0.60 mmol) in the minimum volume of HPLC grade CH_3OH was added to a solution of **1b** (0.20 g, 0.40 mmol) in HPLC grade CH_3OH (10 mL). The solution was stirred at room temperature for 30 min. Concentration of the solution, under reduced pressure, and addition of distilled water afforded a colorless precipitate which was filtered and dried under vacuum. Yield: 0.20 g (83%). Selected data is as follows. $^{31}P\{^1H\}$ NMR: −54.4, −144.2 ppm, ($^1J_{PF}$ 714, PF_6^-). ^1H NMR: 9.00 (br, NH_2, 2H), 7.58−6.98 (m, arom. H, 12H), 4.22 (s, CH_2, 2H), 3.84−3.51 (multiplicity could not fully be assigned as a result of overlap with residual solvent peaks, CH_2), 3.12 (d, $^2J_{PH}$ 13.6, CH_2, 2H), 2.67 (t, CH_2, 2H) ppm. FT-IR: 3077, 3042, 3007, 2949, 2820 (m, NH and CH), 848 (vs, PF) cm^{-1}. FAB-MS: *m/z* 458 [M − PF_6]. Anal. Calcd for $C_{25}H_{28}N_3P_2F_9 \cdot H_2O$: C, 48.32; H, 4.88; N, 6.76. Found: C, 48.21; H, 4.51; N, 6.72.

Preparation of $RuCl_2(\eta^6$-*p*-Cymene)(2a) (4). To a stirred solution of $\{RuCl_2(\eta^6$-*p*-cymene)$\}_2$ (0.030 g, 0.049 mmol) in CH_2Cl_2 (10 mL) was added **2a** (0.063 g, 0.10 mmol) as a solid in one portion. The solution was stirred for 30 min, the volume reduced to about 1−2 mL under reduced pressure, and Et_2O (10 mL) added. The suspension was stirred for 30 min and the solid collected on a glass sinter and dried under vacuum. Yield: 0.080 g (91%). Selected data is as follows. $^{31}P\{^1H\}$ NMR: 7.3 ppm. ^1H NMR: 8.98 (br, NH_2, 2H), 7.53−6.99 (m, arom. H, 15H), 5.94 (dd, $^3J_{PH}$ 8, C_6H_4, 4H), 4.29 (s, CH_2, 2H), 4.02 (d, $^2J_{PH}$ 4.8, CH_2, 2H), 3.80−3.71 (m, CH_2, 4H), 3.45 (partially obscured by solvent, CH_2), 2.62 (sept, $^3J_{PH}$ 6.8, $CH(CH_3)_2$, 1H), 1.96 (CH_3, 3H), 1.14 (d, $^3J_{PH}$ 6.8, $CH(CH_3)_2$, 6H) ppm. FT-IR: 3060 and 2967 (w, NH and CH), 660 (vs, SbF) cm^{-1}. FAB-MS: *m/z* 710 [M − SbF_6]. Anal (bulk material). Calcd for $C_{35}H_{45}N_3PSbF_6RuCl_2 \cdot 3.5CH_2Cl_2$: C, 37.18; H, 4.22; N, 3.38. Found: C, 37.17; H, 4.00; N, 3.24. A single crystal X-ray determination of **4** showed 1.67 CH_2Cl_2 molecules present in the crystal lattice.

Preparation of $RhCl_2(\eta^5$-Cp*)(2a) (5). To a stirred solution of $\{RhCl_2(\eta^5$-Cp*)$\}_2$ (0.030 g, 0.050 mmol) in CH_2Cl_2 (10 mL) was added **2a** (0.062 g, 0.10 mmol) as a solid in one portion. The solution was stirred for 30 min, the volume reduced to about 1−2 mL under reduced pressure, and Et_2O (10 mL) added. The suspension was stirred for 30 min and the solid collected on a glass sinter and dried under vacuum. Yield: 0.090 g (98%). Selected data is as follows. $^{31}P\{^1H\}$ NMR: 4.6 ppm, $^1J_{RhP}$ 144. ^1H NMR: 7.51−6.91 (m, arom. H, 15H), 4.37 (s, CH_2, 2H), 4.10 (s, CH_2, 2H), 3.76 (d, $^2J_{PH}$ 12.4, CH_2, 4H), 3.22 (multiplicity could not fully be assigned as a result of overlap with residual solvent peaks, CH_2), 1.67 (s, η^5-Cp*, 15H) ppm. FT-IR: 3031 (br, NH and CH), 660 (vs, SbF) cm^{-1}. FAB-MS: *m/z* 712 [M − SbF_6]. Anal (bulk material). Calcd for $C_{35}H_{46}N_3PSbF_6RhCl_2 \cdot CH_2Cl_2$: C, 41.81; H, 4.68; N, 4.06. Found: C, 41.46; H, 4.50; N, 4.07. A single crystal X-ray determination of **5** showed two CH_2Cl_2 molecules present in the crystal lattice.

Preparation of *trans*-$RhCl(CO)(1a)_2$ (6a). To a stirred solution of $\{RhCl(CO)_2\}_2$ (0.030 g, 0.080 mmol) in CH_2Cl_2 (10 mL) was added **1a** (0.14 g, 0.32 mmol) as a solid in one portion. The dark orange solution immediately went pale yellow, and a yellow solid was deposited within about 10 min. The suspension was stirred for 30 min, the volume reduced to about 1−2 mL under reduced pressure, and Et_2O (10 mL) added. The solid was collected on a glass sinter and dried under vacuum. Yield: 0.14 g (88%). As a result of the extreme insolubility of **6a** in both nonpolar and polar solvents, no meaningful NMR (^1H, ^{31}P) data could be obtained for this compound. FT-IR: 1979 (CO) cm^{-1}. LSI-MS: *m/z* 1009 [M − 2H − Cl]. Anal. Calcd for $C_{51}H_{62}N_6OP_2RhCl_3 \cdot 1.25CH_2Cl_2$: C, 54.45; H, 5.65; N, 7.29. Found: C, 54.28; H, 5.40; N, 7.46.

Preparation of *trans*-$RhCl(CO)(1b)_2$ (6b). To a stirred solution of $\{RhCl(CO)_2\}_2$ (0.030 g, 0.080 mmol) in CH_2Cl_2 (10 mL) was added **1b** (0.15 g, 0.30 mmol) as a solid in one portion. The dark orange solution immediately went pale yellow, and a yellow solid was deposited within about 10 min. The suspension was stirred for 30 min, the volume reduced to about 1−2 mL under reduced pressure, and Et_2O (10 mL) added. The solid was collected on a glass sinter and dried under vacuum. Yield: 0.16 g (93%). As a result of the extreme insolubility of **6b** in both nonpolar and polar solvents, no meaningful NMR (^1H, ^{31}P) data could be obtained for this compound. FT-IR: 1979 (CO) cm^{-1}. LSI-MS: *m/z* 1117 [M − 2H − Cl]. Anal. Calcd for $C_{51}H_{56}N_6OP_2F_6RhCl_3 \cdot CH_2Cl_2$: C, 50.40; H, 4.72; N, 6.78. Found: C, 50.63; H, 4.70; N, 6.94.

X-ray Crystallography. Suitable crystals of **1b** were obtained by allowing an ethanol filtrate, obtained from the reaction of THPC with $4\text{-}FC_6H_4CH_2NH_2$, to stand for several days. Crystals of **2b** and **3a** were obtained upon layering CH_2Cl_2 solutions with petroleum ether (bp 40−60 °C) over several days. Slow diffusion of petroleum ether (bp 40−60 °C) into a $CDCl_3/CH_2Cl_2$ solution gave X-ray quality crystals of $4 \cdot 1.67CH_2Cl_2$. Vapor diffusion of Et_2O into a CH_2Cl_2 solution gave suitable crystals of $5 \cdot 2CH_2Cl_2$.

Measurements for **1b**, **2b**, **3a**, and $4 \cdot 1.67CH_2Cl_2$ were made on a Bruker Apex 2 CCD diffractometer, at 150 K, using graphite-monochromated radiation from a sealed tube Mo Kα source (λ = 0.71073 Å). Diffraction data for $5 \cdot 2CH_2Cl_2$ was collected, at 120 K, using a rotating anode source and a Bruker-Nonious Roper CCD camera. Narrow frame ω scans were employed for **1b**, **2b**, **3a**, and $4 \cdot 1.67CH_2Cl_2$, and ϕ and ω scans were used for $5 \cdot 2CH_2Cl_2$. Intensities were corrected semi-empirically for absorption on the basis of symmetry-equivalent and repeated reflections. The structures were solved by direct methods (Patterson synthesis for $4 \cdot 1.67CH_2Cl_2$) and refined on F^2 values for all unique data by full-matrix least-squares. Table 1 gives further details. All non-hydrogen atoms were refined anisotropically. N*H* hydrogens for **2b**, **3a**, and **4** had coordinates freely refined with U_{eq} set to $1.2U_{eq}$ of the carrier atom, while the remaining hydrogen coordinates were constrained using a riding model with U_{eq} set to $1.2U_{eq}$ of the carrier atom ($1.5U_{eq}$ for methyl hydrogen). In $4 \cdot 1.67CH_2Cl_2$, one of the CH_2Cl_2 molecules was modeled as disordered over two sets of positions. This disorder was refined with restraints on geometry and anisotropic displacement parameters. The major component was equal to 66.0(3)%. In $5 \cdot 2CH_2Cl_2$, the SbF_6^- counterion was found to be disordered over two sets of positions and was refined as above, the major component equal to 80.7(5)%. Programs used were COL-

Table 1. Details of the X-ray Data Collections and Refinements for Compounds **1b**, **2b**, **3a**, **4**·1.67CH_2Cl_2, and **5**·2CH_2Cl_2

	1b	**2b**	**3a**	**4**·1.67CH_2Cl_2	**5**·2CH_2Cl_2
formula	$C_{25}H_{28}ClF_3N_3P$	$C_{25}H_{28}F_9N_3PSb$	$C_{25}H_{31}F_6N_3P_2$	$C_{36.67}H_{48.33}Cl_{5.33}F_6N_3PRuSb$	$C_{37}H_{50}Cl_6F_6N_3PRhSb$
M	493.92	694.22	549.47	1087.65	1119.13
cryst dimens (mm³)	0.40 × 0.34 × 0.23	0.27 × 0.21 × 0.04	0.50 × 0.21 × 0.15	0.31 × 0.22 × 0.11	0.16 × 0.10 × 0.04
cryst morphology, color	block, colorless	plate, colorless	block, colorless	block, orange	plate, orange
cryst syst	orthorhombic	triclinic	orthorhombic	triclinic	monoclinic
space group	*Ama*2	$P\bar{1}$	*Pbca*	$P\bar{1}$	$P2_1/n$
a (Å)	13.7194(15)	8.5038(12)	17.9476(5)	12.9426(5)	8.9106(3)
b (Å)	18.513(2)	8.8389(13)	15.8400(5)	14.0425(5)	14.7367(4)
c (Å)	9.5476(10)	19.082(3)	19.1365(6)	14.7175(6)	30.8857(9)
α (deg)		77.019(2)		65.2785(5)	
β (deg)		78.879(2)		70.5853(5)	95.887(2)
γ (deg)		84.880(2)		66.5392(5)	
V (Å³)	2425.0(5)	1369.8(3)	5440.3(3)	2184.23(15)	4034.3(2)
Z	4	2	8	2	4
μ (mm⁻¹)	0.265	1.147	0.220	1.383	1.578
θ range (deg)	2.20–28.97	2.23–24.76	2.02–30.55	1.67–30.55	2.99–27.55
measured reflns	10554	10538	62276	25887	47660
independent reflns	2932	4663	8335	13047	9116
observed reflns ($F^2 > 2\sigma(F^2)$)	2902	4154	6759	11295	6545
R_{int}	0.0216	0.0227	0.0291	0.0183	0.0658
$R1$ [$F^2 > 2\sigma(F^2)$][a]	0.0546	0.0259	0.0377	0.0377	0.0830
$wR2$ [all data][b]	0.1281	0.0675	0.1091	0.1033	0.2031
largest difference map features (e·Å⁻³)	0.388, −0.621	0.838, −0.759	0.408, −0.316	1.863, −1.184	1.389, −0.648

[a] $R1 = \sum||F_o| - |F_c||/\sum|F_o|$. [b] $wR2 = [\sum[w(F_o^2 - F_c^2)^2]/\sum[w(F_o^2)^2]]^{1/2}$.

LECT[11] or Bruker AXS APEX 2[12] for diffractometer control, DENZO[13] or SAINT[14] for frame integration, Bruker SHELXTL[15,16] for structure solution, refinement, and molecular graphics, and local programs. Disordered molecules of CH_2Cl_2 (for **5**·2CH_2Cl_2) were modeled by the Platon Squeeze procedure.[17]

Results and Discussion

Commercially available THPC ([$P(CH_2OH)_4$]Cl) has previously been shown to react with primary aromatic amines, through a series of condensation and elimination steps, to give aniline based tertiary phosphines.[8,18] In contrast, we have found when more basic benzylic amines such as $C_6H_5CH_2NH_2$ and 4-$FC_6H_4CH_2NH_2$ are reacted with THPC (ca. 4:1 ratio), crystalline cationic chloride salts **1a** and **1b** are obtained in high yields (typical nonoptimized yields >80%, Scheme 1). Using this procedure we have successfully synthesized batches of **1a** at the 5−10 g scale. Anion metathesis of **1a** or **1b** with Na(SbF_6) or K(PF_6) in CH_3OH at room temperature gave the corresponding salts **2a**−**3b** in excellent yields (72−97%). Compounds **1a**−**3b** have been fully characterized by spectroscopic and analytical methods.

Scheme 1. Preparation of Salts **1a**−**3b**[a]

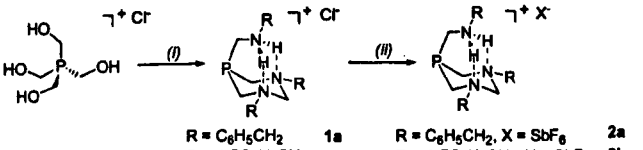

R = $C_6H_5CH_2$ **1a**
R = 4-$FC_6H_4CH_2$ **1b**

R = $C_6H_5CH_2$, X = SbF_6 **2a**
R = 4-$FC_6H_4CH_2$, X = SbF_6 **2b**
R = $C_6H_5CH_2$, X = PF_6 **3a**
R = 4-$FC_6H_4CH_2$, X = PF_6 **3b**

[a] Key, reagents and conditions: (i) 4.1 equiv of $C_6H_5CH_2NH_2$ or 4.2 equiv of 4-$FC_6H_4CH_2NH_2$, C_2H_5OH, and (ii) Na(SbF_6) or K(PF_6), CH_3OH.

In particular, the $^{31}P\{^1H\}$ NMR spectra (dmso-d^6) of **1a**−**3b** showed a single phosphorus resonance around δ_P −55 ppm, some 40 ppm downfield with respect to PTA [δ_P −96.2 ppm, D_2O].[2a] At ambient temperature, **1a**−**3b** possess good solubility in CH_2Cl_2, CH_3OH, and dmso but were found to be insoluble in H_2O. Furthermore, in the solid state, **1a**−**3b** are air stable but slowly oxidize in dmso-d^6 solution over about 24 h.

The X-ray structures of **1b** (Figure 1), **2b** (Supporting Information), and **3a** (Figure 2) have been determined. Compound **1b** was found to lie across a crystallographic mirror plane that bisects the ammonium group of the cation and the methylene diamine bridge (mirror plane runs through [P(1)/C(1)/N(1)/C(2)/C(3)/C(6)/F(1)/C(8)]. Inspection of the intracage P−C bond lengths and P−C−N bond angles reveals close similarities with those of PTA.[19] The C−P−C angles within the P−C−N−C−N−C ring in **1b**, **2b**, and **3a** are in the range of 97.78(5)−99.4(2)° and are slightly enlarged in comparison with PTA [C−P−C, 96.1(1)°].[19] The most significant structural

(11) Hooft, R. W. W. *COLLECT: Data Collection Software*; Nonius B. V., 1998.
(12) *APEX 2: User Manual*; Bruker AXS Inc.: Madison, WI, 2005.
(13) Otwinowski, Z.; Minor, W. DENZO. In *Methods in Enzymology, Macromolecular Crystallography, Part A*; Carter, C. W., Jr., Sweet, R. M., Eds.; Academic Press: New York, 1997; Vol. 276, pp 307−326.
(14) *SAINT: Software for CCD Diffractometers*; Bruker AXS Inc.: Madison, WI, 2001.
(15) Sheldrick, G. M. *Acta Crystallogr., Sect. A* **2008**, *64*, 112−122.
(16) Sheldrick, G. M. *SHELXTL User Manual*, v.6.10; Bruker AXS Inc.: Madison, WI, 2001.
(17) Spek, A. L. *Acta Crystallogr., Sect. A* **1990**, *46*, C34.
(18) (a) Hatnean, J. A.; Raturi, R.; Lefebvre, J.; Leznoff, D. B.; Lawes, G.; Johnson, S. A. *J. Am. Chem. Soc.* **2006**, *128*, 14992−14999. (b) Han, H.; Elsmaili, M.; Johnson, S. A. *Inorg. Chem.* **2006**, *45*, 7435−7445. (c) Keen, A. L.; Doster, M.; Han, H.; Johnson, S. A. *Chem. Commun.* **2006**, 1221−1223. (d) Han, H.; Johnson, S. A. *Organometallics* **2006**, *25*, 5594−5602.
(19) (a) Jogun, K. H.; Stezowski, J. J.; Fluck, E.; Weidlein, J. *Phosphorus Sulfur Relat. Elem.* **1978**, *4*, 199−204. (b) Marsh, R. E.; Kapon, M.; Hu, S.; Herbstein, F. H. *Acta Crystallogr., Sect. B: Struct. Sci.* **2002**, *58*, 62−77.

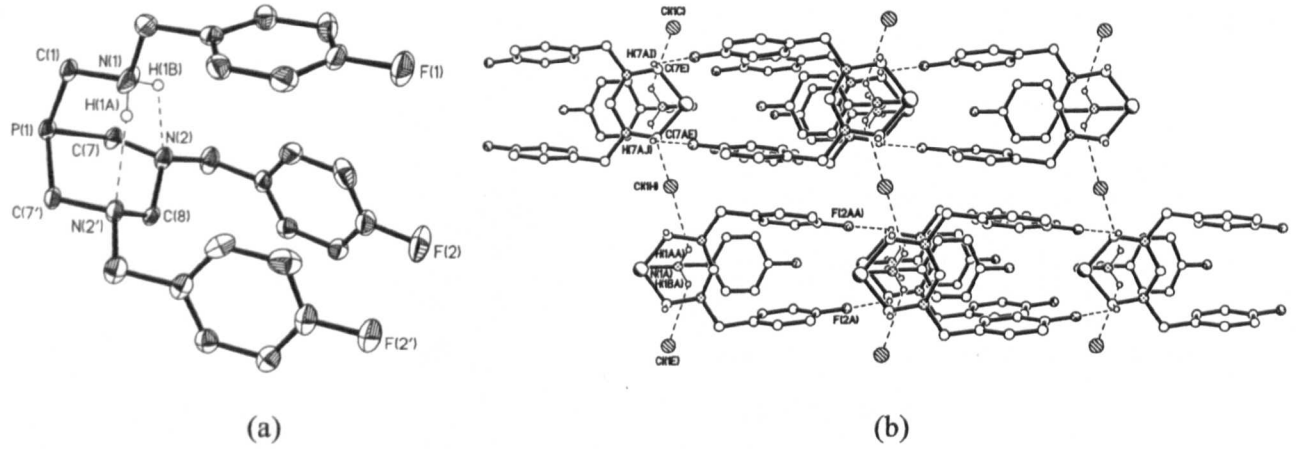

Figure 1. (a) Oak Ridge thermal ellipsoid plot (ORTEP) of the cation in **1b**. Selected bond lengths (Å) and angles (deg): P(1)−C(1) 1.841(5), P(1)−C(7) 1.847(3); P(1)−C(1)−N(1) 116.2(3), P(1)−C(7)−N(2) 113.8(2). Thermal ellipsoids are drawn at the 50% probability level. (b) Packing plot of **1b** viewed along the *c*-axis showing the H-bonded sheet pattern.

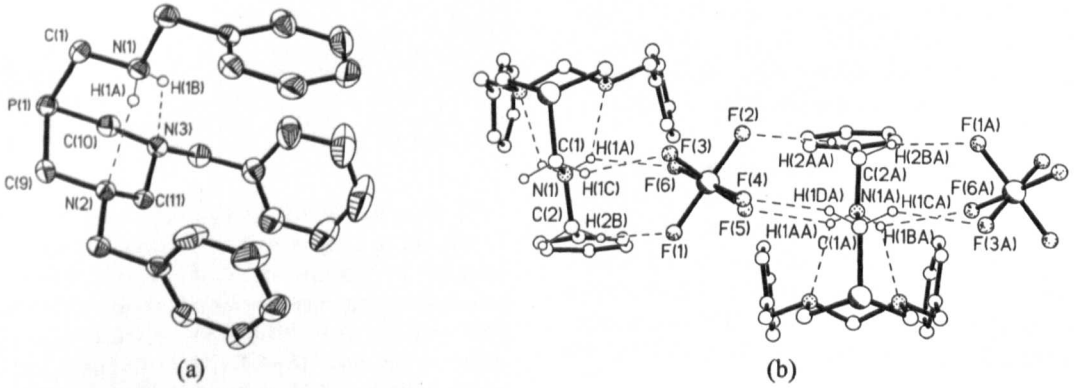

Figure 2. (a) ORTEP of the cation in **3a**. Selected bond lengths (Å) and angles (deg): P(1)−C(1) 1.8490(12), P(1)−C(9) 1.8359(12), P(1)−C(10) 1.8366(13); P(1)−C(1)−N(1) 116.70(7), P(1)−C(9)−N(2) 114.09(7), P(1)−C(10)−N(3) 113.53(7). Thermal ellipsoids are drawn at the 50% probability level. (b) Packing plot of **3a** viewed along the *c*-axis showing the 1-D chain pattern.

feature observed in **1b**, **2b**, and **3a** is the presence of a pair of intramolecular hydrogen bonds between N(1)−H(1A)···N(2 or 2′) and N(1)−H(1B)···N(2 or 3) [**1b**, N(1)···N(2) 2.915(5) Å, H(1B)···N(2) 2.27 Å, N(1)−H(1B)···N(2) 126°; **2b**, N(1)···N(2) 2.804(3) Å, H(1A)···N(2) 2.14(3) Å, N(1)−H(1A)···N(2) 138(3)° and N(1)···N(3) 2.841(3) Å, H(1B)···N(3) 2.20(3) Å, N(1)−H(1B)···N(3) 130(2)°; and **3a**, N(1)···N(2) 2.8506(13) Å, H(1A)···N(2) 2.241(15) Å, N(1)−H(1A)···N(2) 128.7(12)° and N(1)···N(3) 2.8234(13) Å, H(1B)···N(3) 2.154(15) Å, N(1)−H(1B)···N(3) 132.9(12)°]. Various additional weak intermolecular H-bonding contacts exist between the cations and the Cl^-, SbF_6^-, or PF_6^- counterions leading to infinite 1-D chains or 2-D sheet structures (see Supporting Information for further details).

The single crystal data highlight three key findings regarding the N−H···N hydrogen-bonded framework[20] in the cations of **1b**, **2b**, and **3a**, namely, (i) while all synthetic reactions were performed in alcohol solvents (CH_3OH or C_2H_5OH) or required water for precipitation, no disruption of the N−H···N intramolecular hydrogen-bonded motif was apparent under the experimental or crystallization conditions employed; (ii) the core structure of each cation is independent of the counteranion (Cl^-, SbF_6^-, or PF_6^-) even though the potential for alternate hydrogen-bonding arrangements involving these anions is possible; and (iii) the absence of N−H···F−C contacts, albeit rarely observed,[21] shows that the three electronegative fluorines in the 4-position (**1b** and **2b**) do not disrupt the N−H···N hydrogen-bonding array found here.

Dyson and co-workers[4h,j] have previously shown that half-sandwich organometallic Ru^{II} and Rh^{III} compounds of PTA can be synthesized. To assess whether **2a** could function as a similar *P*-monodentate ligand, the piano-stool complexes **4** and **5** were prepared in high yields. Reassuringly, the coordination chemical shifts for **4** ($\Delta\delta_P$ 62 ppm) and **5** ($\Delta\delta_P$ 60 ppm) were found to closely match those of $RuCl_2(\eta^6$-*p*-cymene)(PTA) ($\Delta\delta_P$ 60 ppm) and $RhCl_2(\eta^5$-Cp*)(PTA) ($\Delta\delta_P$ 65 ppm),[4h,j] suggesting comparable stereoelectronic properties.

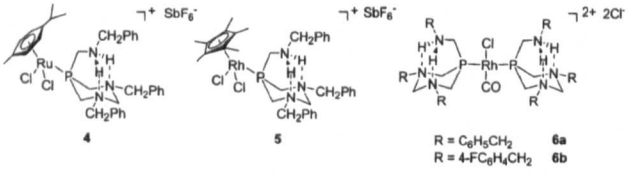

X-ray analyses of **4** and **5** have been performed (Figure 3). The M−P, M−Cl(1), and M−Cl(2) (M = Ru or Rh) parameters for **4** and **5** are similar to those of analogous complexes with PTA.[2b,4h,j] Moreover, upon coordination of

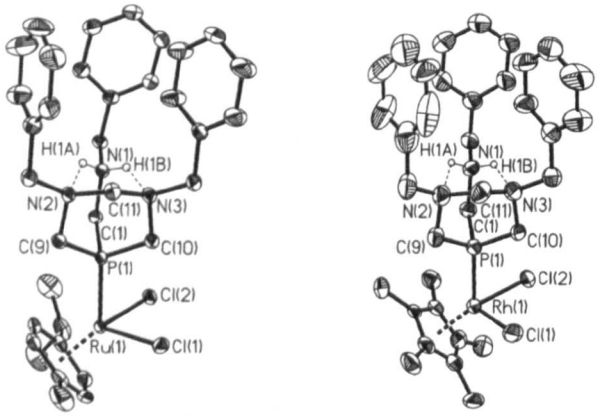

Figure 3. (a) ORTEP of the cation in **4**. Selected bond lengths (Å) and angles (deg): Ru(1)−Cl(1) 2.4064(7), Ru(1)−Cl(2) 2.4103(6), Ru(1)−P(1) 2.3293(6), Ru(1)−C_{av} 2.210(3), P(1)−C(1) 1.843(2), P(1)−C(9) 1.831(3), P(1)−C(10) 1.828(2); Cl(1)−Ru(1)−Cl(2) 88.00(2), Cl(1)−Ru(1)−P(1) 87.60(2), Cl(2)−Ru(1)−P(1) 83.75(2), P(1)−C(1)−N(1) 115.07(16), P(1)−C(9)−N(2) 110.35(16), P(1)−C(10)−N(3) 111.74(16). (b) ORTEP of the cation in **5**. Selected bond lengths (Å) and angles (deg): Rh(1)−Cl(1) 2.406(2), Rh(1)−Cl(2) 2.424(2), Rh(1)−P(1) 2.2851(19), Rh(1)−C_{av} 2.188(8), P(1)−C(1) 1.834(7), P(1)−C(9) 1.836(8), P(1)−C(10) 1.830(7); Cl(1)−Rh(1)−Cl(2) 92.67(8), Cl(1)−Rh(1)−P(1) 88.85(7), Cl(2)−Rh(1)−P(1) 83.37(7), P(1)−C(1)−N(1) 115.4(5), P(1)−C(9)−N(2) 110.1(5), P(1)−C(10)−N(3) 110.0(5).

the phosphine **2a**, there are minimal differences in the P−C and P−C−N metric parameters with respect to **1b**, **2b**, or **3a**. As seen previously for **1b**, **2b**, or **3a**, pairs of intramolecular N−H···N hydrogen bonds are once again maintained upon complexation [**4**, N(1)···N(2) 2.894(3) Å, H(1A)···N(2) 2.22(3) Å, N(1)−H(1A)···N(2) 130(3)° and N(1)···N(3) 2.840(3) Å, H(1B)···N(3) 2.24(3) Å, N(1)−H(1B)···N(3) 128(3)°; **5**, N(1)···N(2) 2.952(9) Å, H(1A)···N(2) 2.34 Å, N(1)−H(1A)···N(2) 124° and N(1)···N(3) 2.851(8) Å, H(1B)···N(3) 2.18 Å, N(1)−H(1B)···N(3) 129°]. Additional weak H-bonding interactions link molecules into dimer pairs (Supporting Information) and is a feature that has recently been observed in cationic dimeric Ru^{II} complexes of PTA.[22]

The electronic properties of **1a** and **1b** have been evaluated through preparation of the square-planar dicationic Rh^{I} carbonyl complexes **6a** (88%) and **6b** (93%) from $Rh_2(CO)_4(\mu-Cl)_2$ and the appropriate ligand. Both Rh^{I} compounds displayed poor solubility in common solvents preventing full characterization. However, FT-IR spectra of **6a** and **6b** were recorded as KBr pellets and showed, in each case, a single terminal carbonyl band at ν_{CO} 1979 cm^{-1}. These findings suggest the electronic properties of **1a** (R = $CH_2C_6H_5$) and **1b** (R = 4-$CH_2C_6H_4F$) are similar despite the different para substituents. Although no direct comparisons between the FT-IR data for **6a** and **6b** with the known neutral complexes *trans*-$RhCl(CO)(L)_2$ [L = PTA, ν_{CO} 1963 cm^{-1} (chloroform); L = "lower-rim" trisubstituted analogues of PTA, ν_{CO} 1978−1987 cm^{-1} (chloroform)][2c,23] can be drawn, **1a** and **1b** can be viewed as possessing similar electron donating properties to this series of PTA ligands.

Concluding Remarks

In summary, we have shown how simple modification of the PTA core can be achieved in which noncovalent interactions maintain the rigid cage structure in the solid state. Further studies are in progress and directed toward understanding the properties of this ligand family in aqueous and organic media, their coordination chemistry, and potential catalytic or medicinal applications.

Acknowledgment. We thank the EPSRC, Loughborough University, and Niger Delta University, Bayelsa State, Nigeria, for funding (A.T.E., A.J.L.). Rhodia UK Ltd. (Dr. Ranbir Padda) and Johnson Matthey are gratefully acknowledged for their kind donations of THPC and precious metal salts, respectively. We wish to acknowledge the use of the EPSRC Chemical Database Service at Daresbury.

Supporting Information Available: X-ray data for **1b**, **2b**, **3a**, **4**·1.67CH_2Cl_2, and **5**·2CH_2Cl_2 in CIF format and additional figures and details. This material is available free of charge via the Internet at http://pubs.acs.org.

IC801709Z

(20) (a) Allen, F. R. *Acta Crystallogr., Sect. B* **2002**, *58*, 380–388. (b) Fletcher, D. A.; McMeeking, R. F.; Parkin, D. *J. Chem. Inf. Comput. Sci.* **1996**, *36*, 746–749.
(21) Dunitz, J. D.; Taylor, R. *Chem.—Eur. J.* **1997**, *3*, 89–98.
(22) Bolaño, S.; Ciancaleoni, G.; Bravo, J.; Gonsalvi, L.; Macchioni, A.; Peruzzini, M. *Organometallics* **2008**, *27*, 1649–1652.
(23) Pruchnik, F. P.; Smoleński, P.; Raksa, I. *Pol. J. Chem.* **1995**, *69*, 5–8.